IRENE GKIOULEKA

THESIS

Assessment of Trends in Water Supply and Demand under Climate Change Conditions

for Three Cr(VI) Impacted Areas (Loutraki, Assopos and Central Euboea, Greece) with the Aid of Precipitation and Drought Analysis and Indices

NATIONAL AND KAPODISTRIAN UNIVERSITY OF ATHENS

NATIONAL AND KAPODISTRIAN UNIVERSITY OF ATHENS

DEPARTMENT OF GEOLOGY AND GEOENVIRONMENT

SECTOR OF ECONOMIC GEOLOGY AND GEOCHEMISTRY

MSc APPLIED ENVIRONMENTAL GEOLOGY

THESIS TITLE:

Assessment of Trends in Water Supply and Demand under Climate Change Conditions for Three Cr(VI) Impacted Areas (Loutraki, Assopos and Central Euboea, Greece) with the Aid of Precipitation and Drought Analysis and Indices

GKIOULEKA ELPIDA EIRINI (IRENE)

21318

SUPERVISOR:

Maria Hatzaki

Assistant Professor
National & Kapodistrian
University of Athens

ATHENS 2017

Table of Contents

Brief description

High concentrations of Cr(VI) were recorded in three areas located in central Greece: Euboea Island, the Asopos River Basin and the Loutraki Region (Fig. 1). An investigation of the hydrological characteristics of those areas was undertaken, in order for data regarding the current situation to be amassed and evaluated. In this manner, appropriate mitigation scenarios can be proposed for consideration. The subject of this thesis concerns the assessment of hydrological characteristics regarding the area of study, related climatology, average prevailing conditions, extreme values, and variability concerning the component responsible for surface water supply in the water balance equation, determining current and future climate conditions.

Drought is analyzed with the aid of the Standardized Precipitation Index (SPI), which utilizes precipitation data and was designed to quantify the precipitation deficit, by calculating the probability of precipitation for a selected time scale. The SPI index is widely used as a tool for the estimation of the intensity and duration of drought events. Here, the SPI is calculated for three different time scales (3-month SPI, 6-month SPI and 12 – month SPI).

Two types of data were employed: Gridded Observations aiming to assess the current hydrometeorological conditions prevalent in the three areas of study from the beginning of the previous century until today and Model Data corresponding to two RCP (Representative Concentration Pathways) scenarios in order to evaluate prevalent climatic conditions for the near and the remote future. Results are visually represented, so they will be easily accessible to decision makers. Data was incorporated in the study areas' map showcasing each area's special characteristics.

From this analysis, it can be deduced that mean precipitation and drought values show almost no change during the previous century. Variability on the other hand, displays a statistically significant rise, especially with respect to the wet period. Regarding the future climate, RCP4.5 shows a tendency towards drier conditions, while under RCP 8.5 it is clear that both short and long term drought conditions are expected to be extremely dry, affecting agricultural activities and underwater reservoirs respectively, especially towards the end of the century.

The current study is part of an integrated project comprised of various stages, ERANETMED CrITERIA. The project will deliver an optimization tool including documentation and a database to assist water resource management organizations and water users with decision making when coping with water scarcity, climate change and polluted water.

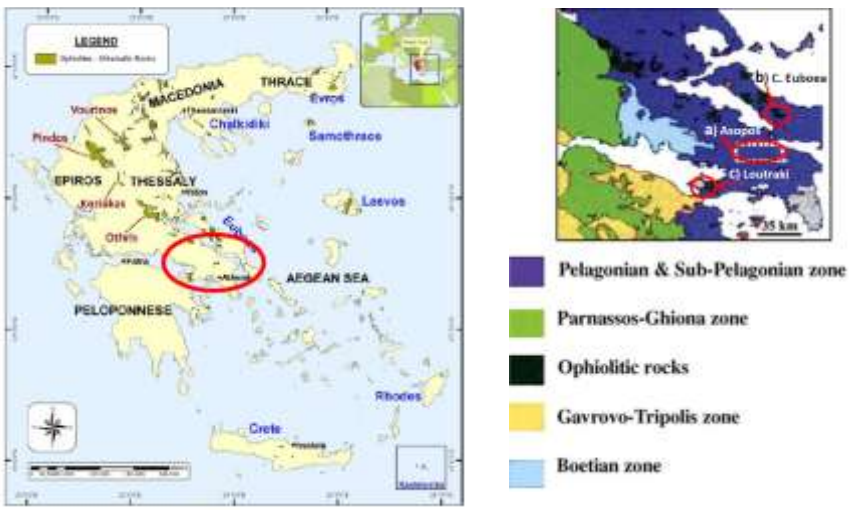

Figure 1. Three case study areas located in Central Greece

1 Introduction

1.1 Purpose And Objectives

The purpose of this Thesis is to define the occurrence and variability of drought in three study areas located in central Greece in order to inform decision and policy makers on the current prevalent situation regarding precipitation trends and the expected future changes. Those three areas show increased Cr(VI) concentrations as a special feature and will be studied in terms of hydrology. Analysis of dry and wet periods will take place at various time scales, showcasing their impact on the groundwater and surface stream flow systems.

The current study is part of an integrated, interdisciplinary collaborative research project comprised of various stages, named CrITERIA. The acronym stands for: Cr(VI) Impacted water bodies in the Mediterranean: Transposing management options for Efficient Water Resources use through an Interdisciplinary Approach. The project will be a product of various Research institutes in the Mediterranean and is financed by the European Commission. According to the CrITERIA project proposal, "The project will deliver an optimization tool including documentation and a database to assist water resource management organizations and water users on decision making when coping with water scarcity, climate change and polluted water, that takes into account the EU water framework directive ((WFD) 2000/60/EC). Pollution by Cr(VI) will be used as an example of additional water pressure problem that has to be tackled through integrated water resource management."

The project is multidisciplinary in nature bringing together specialists from the fields of geology, geochemistry, hydrogeology, civil and chemical engineering, plant physiology, climatology and environmental technology. Shortage of renewable water resources is being documented in the southern and eastern Mediterranean Countries (SEMCs) and intense agricultural (livestock practices, crops, etc.), industrial (food, textiles, tanning) and urban (urban development, tourism) activities intensify the problem.

The project consists of multiple working packages. Results derived from this thesis will be used as part of the WP3 whose purpose is to define the "estimates and costing of Cr(VI) contamination impact for various water uses under present and future climate change conditions", and more specifically on the third task of the work–package, aiming towards the "assessment of trends in supply and demand under climate change conditions."

Results derived from this thesis will be combined with other data for establishing future hydrological and hydrogeological balance conditions. The water system's hydrologic response will be calculated in accordance with climate change scenarios. To this end, additional data have to become employed – i.e. temperature, runoff and water storage data. Anticipated change projected in the future, has to be approached with the hydrological balance in mind.

Based on the water balance equation bellow Eq. (1),

$$P_m - ETa_m - R_m = \Delta W_m \qquad \textit{Eq. (1)}$$

where P_m stands for monthly precipitation (mm), ETa_m for monthly actual evapotranspiration (mm), R_m for monthly runoff depth (mm), and ΔW_m for monthly water storage change (mm), trends regarding evapotranspiration need to be calculated as the result of the analysis of future temperature time series. This in combination with runoff and underground reservoirs study will lead to a complete illustration of the future conditions dominant in the area of interest regarding water supply and demand.

The project intends to promote the sustainability of resources under the stress of climate change. Scarce water resources in the Mediterranean area will be used sparingly according to the prioritization of needs.

As main objectives of this Master Thesis are identified the following:

- To study the occurrence and variability of precipitation events in three study areas located in central Greece. Although similar research studies have been conducted before using the SPI Index for Europe (Lana et al., 2001; Lloyd-Hughes and Saunders, 2002; Kostopoulou and Jones, 2005; Blenkinsop and Fowler, 2007; Heinrich and Gobiet, 2012; and others) and Greece (Livada and Assimakopoulos, 2007; Tigkas, 2008; Koutroulis et al., 2010; Karavitis et al., 2011; Founda et al., 2013; Mimikou and Baltas, 2013 and others), this particular thesis aims to do the same at a local level for study areas with a special geochemical feature.

- To predict and assess future precipitation and drought conditions with the aid of model data, using statistical analysis and mapping techniques as a visual output. The purpose is to provide a clear understanding of possible dangers emerging from the future situation of those study areas.

- To inform decision makers about the current condition regarding precipitation trends, taking into account the vulnerability of those areas in regard to their exposure to Cr(VI). This study aims to be of service in matters regarding sustainability and water management issues; and

- To provide valuable information of climatological and hydrological nature for the initial stage of the CrITERIA project. This is a typical example of information gathered at the local level that is to be utilized for an international purpose. Comparative and collaborative research will take place using data from case study areas located in each of the countries participating in the project.

1.2 Study Area Description

The areas of our study consist of Euboea Island, Asopos River Basin and Loutraki Region and are all located in central Greece, displaying similar geological features. More specifically, site descriptions are as follows:

1.2.1. Euboea Island

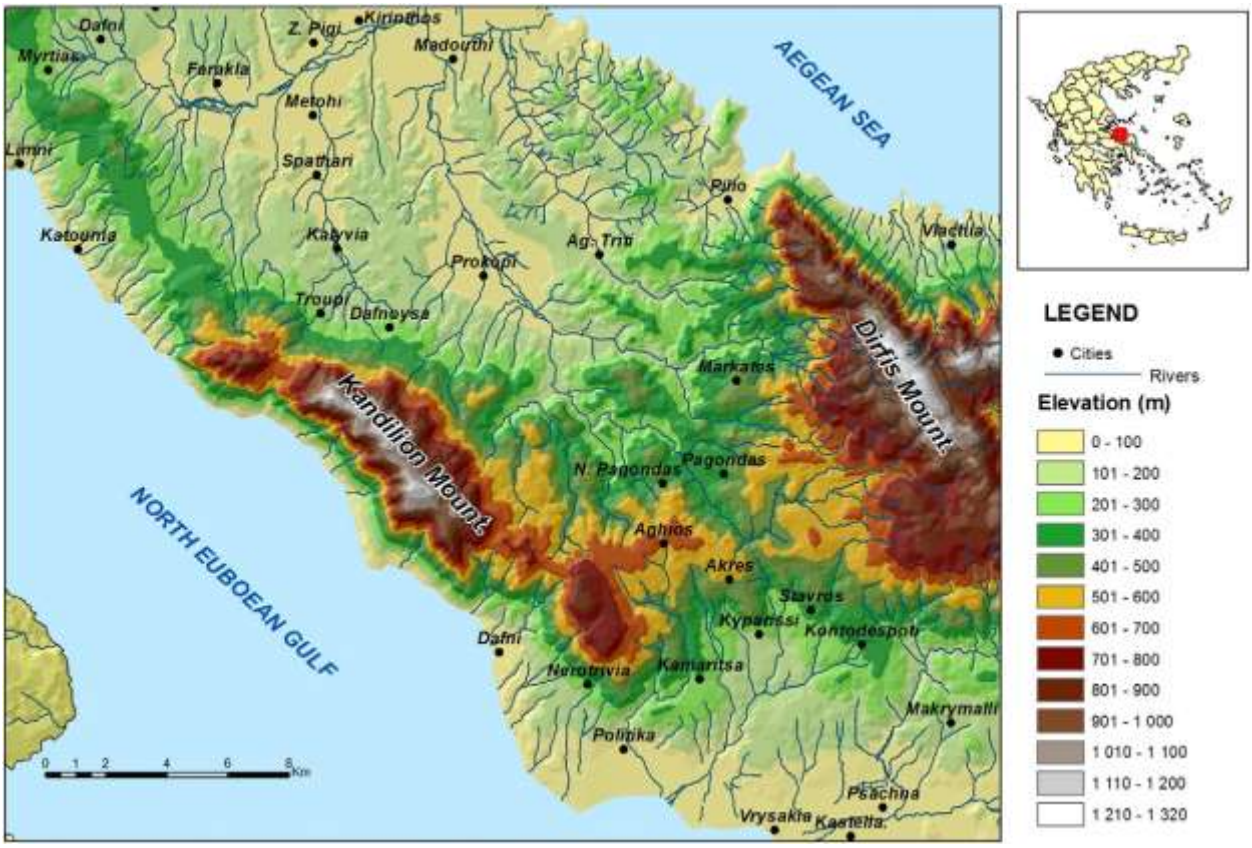

Figure 2. Topographical map of central Euboea (Voutsis et. al.,2015)

Euboea Island is the second largest island in Greece, covers a surface of 3,580 km^2, and bears a coastline 48 km long. The northern part is mostly occupied by forests, while agricultural activities dominate the southern part. In central Euboea, several mountainous regions are encountered, the occurrence of which is in close proximity to flat areas resulting in a diverse topographical relief that characterizes the island. Land use practices include agriculture, mineral extraction and residential use. In central Euboea, where the data source stations are located, the mean altitude is around 335m above sea level. (Voutsis et al.,2015).

Clastic metamorphic rocks of pre-alpine (Permian) age, comprise the substrate of the geological regime in central Euboea, and are followed by a series of dolomites, dolomitic limestones and limestones of Triassic – Jurassic age, in which intercalations are present. Those carbonate rocks slowly progress to silicified limestones. A mélange containing mudstones, schists and serpentinized ophiolithic fragments (Upper Jurassic) covers the clastic and carbonate formations. Subsequently, ophiolithic rocks become present in the sequence and constitute the source of the aforementioned ophiolithic fragments that bear the form of olistoliths. A sequence of partly karstified cretaceous limestones, together with Eocenic flysch completes the alpine facies, over which Post-Alpine formations are present (marls and sandstones of Neogene origin, Quaternary alluvial and colluvial deposits) (Katsikatsos et al., 1980; Katsikatsos et al., 1981).

The local ophiolithic occurrences have been studied extensively. Geochemical and mineralogical data suggest that they are classified as serpentinites, since serpentine minerals are dominant (antigorite and chrysotile) while some olivine (forsterite), with orthopyroxene (enstatite), clinopyroxene (diopside), talc,

clinochlore and amphibole (tremolite) are also present in various samples (Voutsis, 2011). High concentrations in Mg and low concentrations in Fe were documented during the analysis of the ophiolithic bedrock, while Al, Ca, Na and K concentrations were also reported but in significantly smaller amounts. Regarding trace elements, Ni, Co, Cr and Mn concentrations were recorded, as they occur naturally in ultramafic rocks (Voutsis, 2011). The ophiolithic bodies display the development of rich lateritic horizons that were eroded, forming weathered crusts on top of them, redepositing material rich in Fe, Ni, Co and Mn (Skarpelis, 2006).

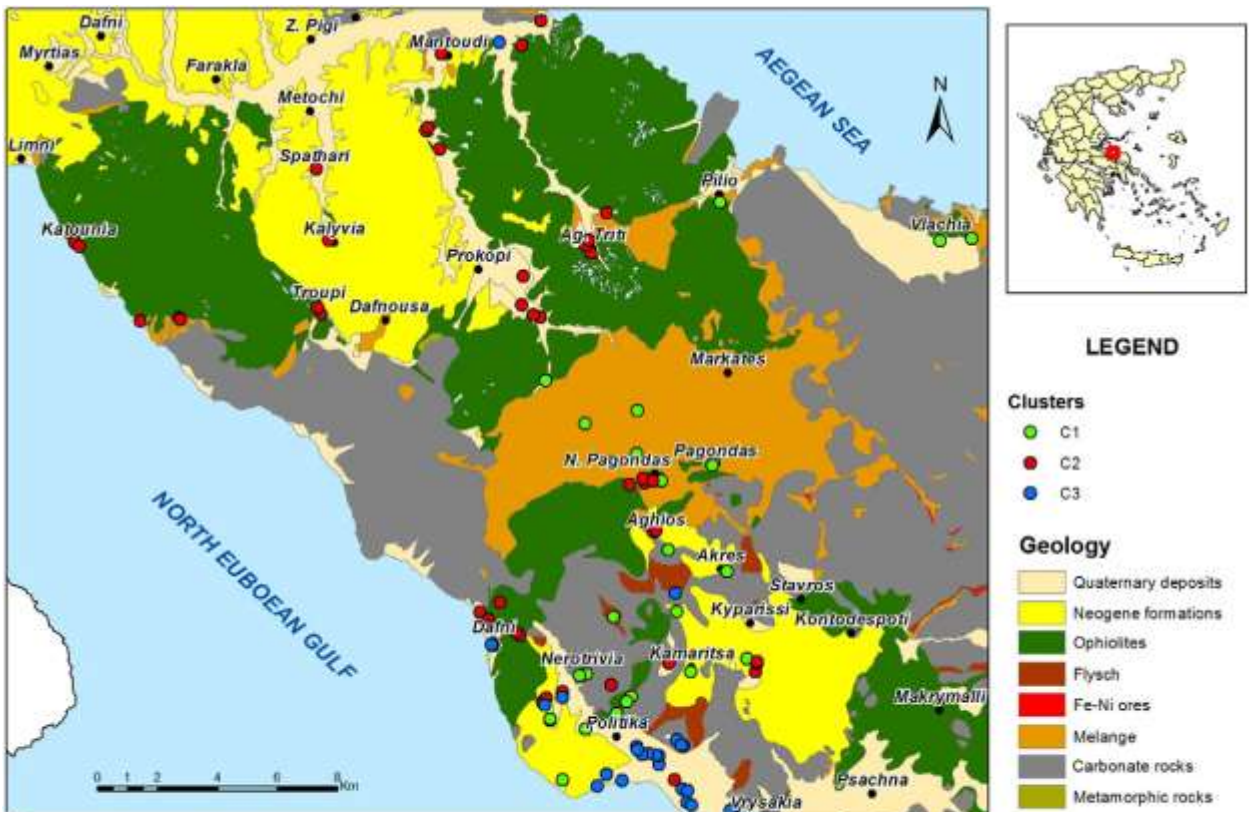

Figure 3. Simplified geological map of central Euboea (after Katsikatsos et al., 1981) with the results obtained by hierarchical cluster analysis.

The karstified formations host Euboea's most significant aquifers. Those are the northeastern and the central system. In the northeastern system, known as Mantoudi karstic system, aquifers are mostly of confined to semi-confined nature. Groundwater flow follows a direction towards west and southwest. In the central system, known as Dirfis karstic system, several individual aquifers have developed. Those aquifers show no hydraulic connections to other systems and are directly recharged by the surrounding mountains (Voutsis 2011). Less potent aquifer systems include the Psachna system, a system developed within Neogene formations (sandstones, marls, breccias etc.) characterized by lower yield, the same way alluvial aquifers in quaternary deposits do. The ophiolithic formations and the ophiolithic mélange also host some low potential aquifers, mainly due to tectonic-driven procedures and are developed across the highly fractured zones (Voutsis et al.,2015).

1.2.2. Asopos river basin

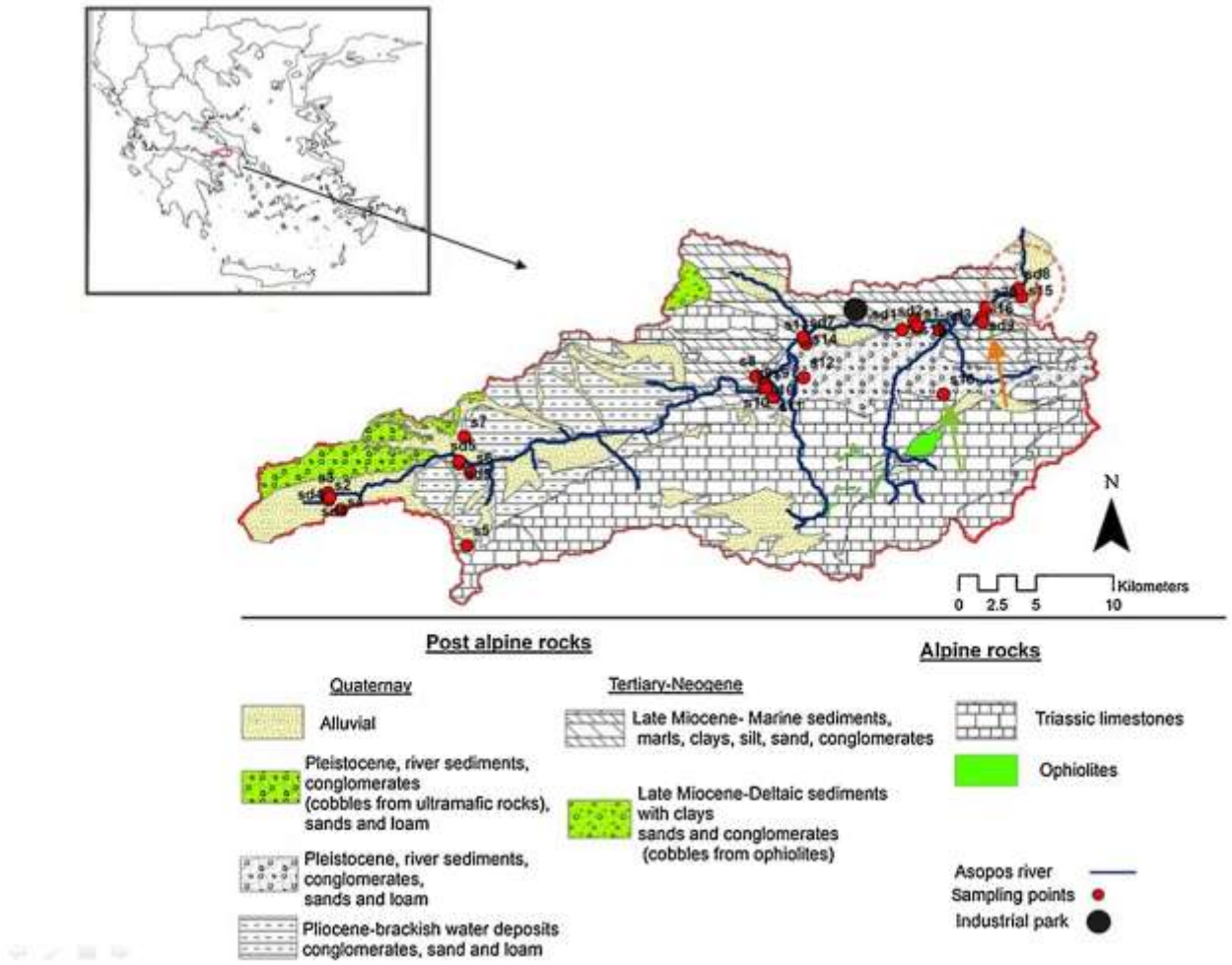

Figure 4. Geology map of the study area with the main lithological units (Lilli et. al.,2014).

Asopos river features a total length of 54 km. It runs through various areas including Thebes, Avlona, Tanagra etc. and finally discharges into Euboekos gulf. Its river basin covers a surface area of approximately 703 km^2. Within the industrial zone located in Oinofyta area, more than 450 industries are located. Industrialization of this area took place during the last three decades (Lilli et al.,2014). It's an area relatively close to the capital, Athens, located about 100km north of the city.

The area's geology can be divided into two major units, the alpine facies and the post-alpine facies. The alpine facies include limestones of Triassic age and ophiolite rocks, while the post-alpine formations that lay on top, comprise of Pliocene conglomerates, Pleistocene river sediments and alluvial sediments.

The alpine sediments belong to the Pelagonian nappe, which consists of thick bedded limestones and dolomites. They are mostly encountered in the southern parts of the watershed. Over the Pelagonia nappe, an ophiolithic nappe is documented. Just like in Euboea, these ophiolithic formations constitute the source of ophiolithic fragments that are found within Neogene and Pleistocene sediments (Moraetis et al.,2012). Ultramafic rocks appear in the south of the Asopos basin, but are rarely encountered in the remaining area. However, hornstones and serpentinized ophiolite occurrences are a usual phenomenon across the watershed. Field observations by Lilli et al.,(2014), revealed visible ophiolite fragments close to the ophiolite nappe.

Post-alpine sediments (30 – 150 m thick) are deposited over the river's watershed. On rare occasions, they reach a thickness of up to 300m. In the eastern part of the watershed, marine deposits of Tertiary

(Neogene) age, comprised of marl, clay, loam and sand, prevail. Lignite lenses and coarse unconsolidated material is found within these deposits (Papanikolaou et al.,1988; Stamatis et al.,2011).

In the Western parts of the basin, Pliocene deposits containing sand, loam clays and marls are observed, with a thickness of 30m. Along the river, Pleistocene fluvial deposits are encountered displaying a thickness of 120 – 150 m. Finally, the sequence becomes complete with alluvial fluvial sediments, mainly situated within the active riverbed (Lilli et al.,2014) .

1.2.3. Loutraki region

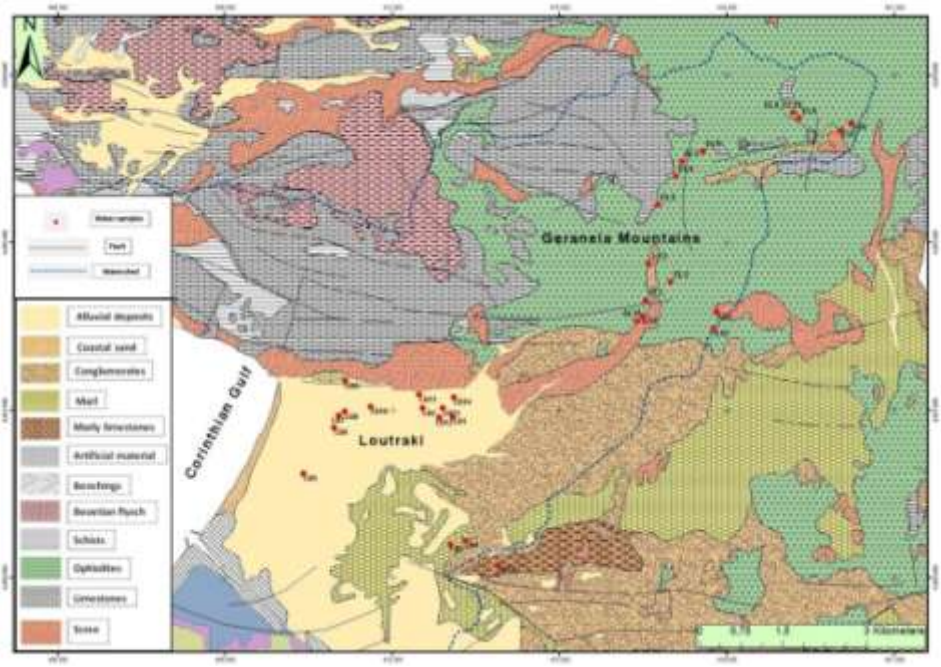

Figure 5. Geological map of Loutraki (Pyrgaki et. al.,2016)

The region of Loutraki is represented by a drainage basin with a surface area of about 53.27 km^2 and a perimeter of 35 km. It is located within the Corinthia region, Greece, 81 kilometers west of Athens, in the southern part of Perachora peninsula, and is noted for its natural springs. It's a coastal town, surrounded by the Gulf of Lechaio, that functions as a popular seaside resort. The region's mean altitude is approximately 470 m above sea level.

The geology is characterized by carbonate rocks, ophiolites, carbonate clay formations and alluvial deposits. The region is situated between the external and the internal Hellenides. (Dotsika et al., 2010). More specifically, the alpine sequence that lies underneath is made up of limestone and dolomitic limestone of Triassic age and ophiolites, mainly peridotite and serpentinite. The ophiolite complex forms the Geraneia mountains, which are subject to erosion and weathering processes resulting in ophiolite fragmentation. Clay formations of Neogene age, mainly consist of marl and are impermeable. They play a major role in the region's underwater flow system, as they constitute a barrier regulating the flow. The main aquifer is hosted within the alluvial deposits and conglomerates of Quaternary age. Within these deposits, ophiolite fragments typically occur, and are source to many metallic minerals present in the groundwater. The main streams in the watershed are Loumpiniaris and Agia Triada.

1.1 Chromium Geochemistry in the Study Areas

Chromium in nature is mainly encountered in two oxidation states, the immobile trivalent Cr(III) displaying low toxicity and the mobile hexavalent Cr(VI) being highly toxic and hard to remove (James, 1996). The maximum permitted content of total Chromium in drinking water is 50 μg/L as established by the European Commission and the World Health Organization. Chromium found in soil and water is the result of both anthropogenic (industry and agriculture i.e. phosphorus fertilizers) and natural procedures (ultramafic rocks weathering) (Molina et al.,2009; Fantoni et al.,2002). Those ultramafic rocks contain pyroxene, olivine and chromite, whose weathering can lead to transfer and integration of Chromium into minerals such as iron (hydroxi)oxides, smectites and other clay minerals (Oze et al.,2004). Cooper (2002) suggested a two stage mechanism regarding chromite weathering. A process of slow hydrolysis turns Cr(III) into $Cr(OH)_3$, followed by a slow oxidation phase by Mn oxides leading to Cr(VI). This is the mechanism according to which Chromium coming from weathering of ultramafic rocks is released into the groundwater. Regarding Greece, several cases of Cr(VI) water contamination are reported, with the majority of them taking place within aquifers related to ophiolitic lithologies (Kazakis et al., 2015; Kaprara et al.,2015; Dermatas et al., 2015). The Oinofyta - Asopos area represents a situation where both geogenic and anthropogenic sources of contamination are involved (Panagiotakis et al., 2015) and so does the case of Euboea where an area rich in ultramafic rocks suffers from the negative impacts of extensive agriculture.

The Loutraki area is part of the Aegean volcanic arc, a dormant but geodynamically and hydrothermally active volcanic system. It is related to the collision taking place between the Eurasian and the African plates and is known as the youngest example of volcanism in the region of the Aegean Sea (Mckenzie, 1970). Around the study area, several thermal springs are documented since antiquity. Mixing procedures between meteoric, magmatic and sea water take place in deep geothermal systems. Chemical and isotopic data in the area suggest that spring water's origin is purely meteoric. Furthermore, the existence of a deep geothermal reservoir of low enthalpy (80 °C) is proposed. Those temperatures are uncertain, this may be attributable to the contribution of marine solutions to the geothermal fluids (Dotsika et al., 2010). Besides, there's no actual industrial activity reported in the wider area, another indicator of the geogenic origin of Cr(VI) in water. It is suggested that Cr(VI) in groundwater is a product of oxidation of Cr bearing minerals in ophiolithic rocks found in the neighboring Geraneia Mountains (Pyrgaki et al., 2016).

The Asopos river basin consists of calcareous, siliceous and ultramafic lithologies characterized by high Chromium content. Field and laboratory studies (heavy metal analysis) conducted by Lilli et al. (2014), suggested that the elevated Chromium levels present in the area are of geogenic origin. More specifically, Chromium distribution occurs due to erosion procedures manifested in ultramafic rocks during the last 5 Ma. Moreover, the Asopos river suffered from industrial and metallurgical waste. Those activities, however, were discontinued during the last 5 years (Lilli et al., 2014). The weathering of ultramafic parent rocks located in higher elevations supply the topsoil covering the western part of the watershed with Cr and Ni (Kelepertzis et al., 2013).

Euboea Island displays diverse topographic relief in which mountainous regions intertwine with flat areas. High Cr concentrations are present in groundwater, due to its interaction with serpentinites. These concentrations reach as high as 71 μg/L raising environmental concerns. In the alluvial coastal area salinization by seawater intrusion is also documented. Intense agricultural activities take place in the area, intensifying the contamination phenomenon due to the extensive use of chemical fertilizers. Groundwater is primarily alkaline in nature. An ophiolithic bedrock is dominated by serpentine and olivine; it exhibits high concentrations in Mg, and low in Fe. In regard to trace element content, Ni, Cr, Co and Mn prevail (Voutsis et al., 2015).

2 Literature Review

2.1 General

A literature review comprised the initial stage of this research project. To this end, peer-reviewed material was extensively studied including academic publications and books, academic journals, conference outcomes, policy reports, previous research documents and outcomes relative to the main concepts of this study considering climate change, adaptation and mitigation strategies, statistical methods, climate modeling, environmental sciences and geology. This section represents the summary derived from this study and presents a short background note on relative subjects, essential to understanding the results obtained from the statistical analyses in the chapters to follow.

2.2 Climatic Conditions

2.2.1 Climate in the Mediterranean

According to the IPCC (2007), climate is defined "as the average weather, or more rigorously, as the statistical description in terms of the mean and variability of relevant quantities over a period of time ranging from months to thousands or millions of years."

The climate is determined by both external and internal factors of the earth system (Alverson et al.,2003). Internal factors include volcanic activity, processes taking place between the spheres of the earth, changes in circulation patterns of oceanic currents, the concentration of greenhouse gases in the atmosphere and anthropogenic impacts. External factors focus on the interaction between our planet and the sun (orbital parameters and solar activity).

The Mediterranean region due to its unique geographical setting displays specific climatic characteristics. It "lies in a transition zone between the arid climate of North Africa and the temperate and rainy climate of central Europe and is strongly affected by interactions between mid-latitude and tropical processes." (Giorgi and Lionello, 2008). The Mediterranean Sea is semi-enclosed, surrounded by Europe to the North, Africa to the South and Asia to the East (Fig. 6). It is connected to the Atlantic Ocean via the narrow Gibraltar Strait, with a depth less than 300m and width of 14.5 km. Twenty one countries in total, located in in Europe and Asia, surround the Mediterranean Sea.

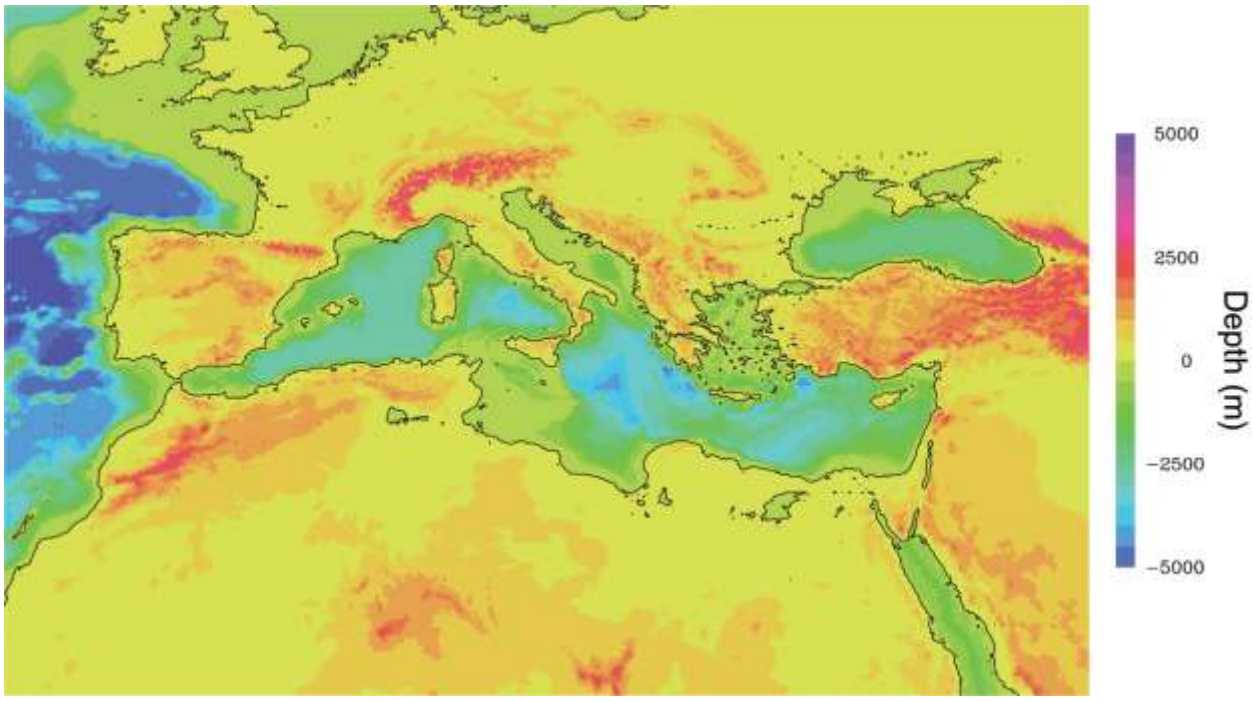

Figure 6. Orography and Sea-depth of the Mediterranean region. Source: Lionello et. al 2008

Generally, mild and wet winters are encountered, while summers tend to be hot and dry. The main factors that account for climate conditions in the area are atmospheric circulation, latitude, altitude, interaction between the land and the sea surface and various other small scale processes. Regional seas and basins, numerous islands and intricate coastlines compose a complex land-sea pattern, affecting sea and atmospheric circulation. Land topography also has an effect, due to the high relief and sharp orographic features.

As a result of the constant exchange of heat and moisture between the ocean and the atmosphere, oceans are a major source of influence regarding the Mediterranean climate type, equally affecting local and long-term weather conditions (IPCC, 2007). The Mediterranean displays different climatic sub-regions within itself, with the most notable being the distinction between eastern, central and western Mediterranean (Luterbacher and Xoplaki, 2003).

Precipitation patterns during winter are mainly affected by the North Atlantic Oscillation (NAO) in the western parts, and the East Atlantic (EA) pattern in the northern parts. Local phenomena such as internal storms can occur as well, as a product of cyclogenetic areas (the Alps, the Gulf of Lyon, Gulf of Genoa etc.) (Lionello et al., 2006). During summer, dry conditions prevail due to high pressure and descending motions, especially on the southern parts of the Mediterranean region (DRBG, 2011).

The most intense climate episodes taking place within the Mediterranean region during the last millennium are the Medieval Climate Anomaly that occurred during the period of 900-1350 A.D., and displayed unusually warm temperatures, and was followed by a cold period known as the Little Ice Age lasting from 1500 until 1850 A.D. This period included the Spörer (1460-1550 A.D.), and the Maunder Minima (1675-1715 A.D.), events associated with decreased solar activity, as sunspots during that period became extremely rare (Jansen et al., 2007). Between 1500 and 1900 AD intense volcanic activity was recorded in Europe, and in the Mediterranean region as well (DRBG, 2011).

2.2.2 Climate in Greece

Greece is geographically located in the southeastern part of Europe, on the eastern part of the Mediterranean Sea. The climate is of the Mediterranean type, a common type that characterizes regions around the Mediterranean Sea. It translates to mild wet winters and dry warm summers. However, various climatic subtypes are present throughout the country, due to its complex topography and altitude variability, including Alpine and continental types. Another important feature of the country that affects the climate is the vast coastline (16300 km), of which around 20% is ranked as moderate-high in the vulnerability scale (DRBG, 2011).

Due to its diverse topography and characteristic geography, Greece displays a variety of distinct climate subtypes. An interesting fact is that because of the interaction between these unique climatic conditions and the intense terrain changes, one climate type is very likely to transition to another in a relatively short distance.

The prevailing climate subtypes in Greece are the following (Mariolopoulos, 1938):

- **Maritime Mediterranean climate:** Characterized by cool summers and mild winters, it is present along the western coast of Greece and the Ionian islands
- **Lowland Mediterranean climate:** Characterized by dry summers and colder winters, it is often encountered in SE Greece, the eastern Peloponnese, the central Aegean Sea, Crete and the southern Ionian Sea.
- **Continental Mediterranean climate:** More typical of regions in the northern Balkans, it is found over the larger part of Thrace, Macedonia, Epirus and parts of Thessaly.
- **Highland Mediterranean climate:** Resembling the alpine climate type during the winter, it is encountered in mountainous zones across Greece.

Air mass movement over the southern Balkans and the eastern Mediterranean is determined by high (anticyclones) and low (depressions) pressure systems. Those act as centers of atmospheric activity and regulate weather patterns. It is notable that they are easily affected by local factors, while at the same time affecting the region they move over.

Since Greece is located in the Northern Hemisphere, it receives the maximum amount of solar radiation around the Summer Solstice (June 21st) and the minimum around the Winter Solstice (December 21st). Other atmospheric factors that affect the amount of solar radiation received include dust particles, cloud occurrences, absolute humidity etc. This is the reason why in Athens solar radiation is more intense during spring compared to the summer (DRBG, 2011).

Greece, in general, features a small number of overcast days, when cloud cover reaches above 80%, during the course of the year. Respectively, clear days (cloud cover under 20%) occur very often, with the highest average annual sunshine duration taking place in Southern Greece (southern Aegean, Crete and southern Dodecanese). The duration of clear days progressively decreases as the distance from the shoreline grows, reaching its minimum in the north-western mountainous regions (DRBG, 2011).

Topography and latitude severely affect air temperature in Greece. The coldest regions are located where cold air masses are allowed to flow unobstructed during winter, while the most temperate ones are protected by mountainous blocks. Distance from the coastline is a determining factor as well with coastal regions experiencing milder winters and cooler summers. Summer and winter isotherms run parallel to latitude. During July and August, air temperature reaches its maximum point, which usually varies among 32 and 35^{o}C, but in rare cases can climb above 40 ^{o}C. Minimum temperatures occur during January and

February, reaching as low as -20 ^{o}C in certain regions. The annual temperature range is usually above 20 ^{o}C. Air temperature is affected by altitude, displaying a decrease of 0.6 – 0.8 ^{o}C for every 100m (DRBG, 2011).

Regarding air humidity, the maximum values (11-12 mm Hg) are observed along the coast of western Greece, while a gradual decrease takes place towards the inland. Nearing the eastern coast and the Aegean Sea air humidity values increase again, but still remain lower than those observed in the west (DRBG, 2011).

The mean annual precipitation in Greece is documented around 900mm. Due to Greece's geography and morphology, the spatial distribution and the intensity of precipitation show intense spatial variation. (DRBG, 2011). Most rainfalls occur in Western Greece (over 1500 mm/year), compared to Eastern Greece, Crete and the Aegean Sea. The reason for this variation lies in the fact that warm and moist air masses moving from West and South encounter the occurrence of the mountainous chain of Pindos ridge and the mountains of Peloponnese, whose orientation is from NW to SE. This fact, results to the release of the air masses' water load in the form of precipitation. This phenomenon takes place in the Iberian and Italian peninsula as well, with precipitation values displaying a decrease from West to East and from North to South.

Whenever intense atmospheric instability is present, those meteorological conditions that generate rainfall, can lead to thunderstorm. In the Mediterranean region, thunderstorms are a product of collisions between warm tropical air masses, or the confrontation of cold polar air masses by the warm sea waters during the autumn season.

Winter winds in Greece show a variability in direction and intensity. This is the outcome of cyclogenesis centers generated by high pressure systems over Eurasia and the north Atlantic. High pressure systems originating from North Africa and the Atlantic and carrying warm moist air masses, develop warm dry winds when forced by the topography over a mountain range. This type of wind is known as "livas" and is observed from Autumn to Spring. Another type of wind, encountered mainly in Northern Greece is known as "Vardar" and is the result of the combination of a high pressure system emerging from the Balkans and a low pressure one over the Aegean. Another type of wind worth mentioning are the Etesians or Meltemia, strong seasonal winds mostly prevalent in Eastern Greece and the Aegean Sea. Typically, they're of moderate intensity and their peak hour is around midday, due to the mixing of upper and lower atmospheric layers. They are very rare during the night. They reach their maximum intensity during July and August preferably above open seas (DRBG, 2011).

During the winter months, precipitation shows maximum values, while summer is characterized as a dry season. Dry and hot summers, with high evapo-transpiration rates are common in "Meditarranean" climate types, and such is the climate in Greece, in regard to low altitude areas (Mariolopoulos, 1938).

Two seasons are observed in terms of climatology, a dry season lasting from April until September and a wet season, from October to March. At the end of Spring, around May, moisture loss increases due to the rise in air temperature and so does evapo-transpiration. Drought event duration is usually around 2 months in Northern Greece (Thrace and Macedonia), and 4-5 in SE Greece and the Aegean islands. (DRBG, 2011). Mild to moderate agricultural droughts can occur at any time of the year and show variability across the country (Kalamaras et al., 2010; Livada and Assimakopoulos, 2007).

2.3 The definition of Drought

Although a precise and objective definition is not available, drought can be roughly described as a complex phenomenon, according to which a temporary water supply reduction occurs, compared to the long term average water supply conditions for a specific geographical area. This phenomenon leads to water scarcity and is often the result of decreased rainfall and increased evapotranspiration. Drought severity depends on multiple factors including the duration, intensity and geographical extent of the event, human activity and vegetation. The environmental and economic impact of a drought event is undeniable.

Multiple classifications of drought have been suggested over time. According to Wilhite and Glantz (1985), drought could be categorized into four types: meteorological, agricultural, hydrologic, and socio-economic.

Meteorological drought is characterized by a temporary lower water supply to the environment compared to the mean value for a specific (longer) time period. This incident is called a drought event and is described by its intensity and duration. Definitions can vary among regions due to special characteristics prevalent on each.

An agricultural drought is outlined by the impact of meteorological drought on agricultural activities. Thus, it depends not only on meteorological factors (water deficit and evapotranspiration), but biological characteristics of the plants and soil as well. The development stage of the crop at the time of the drought is also a defining factor regarding yield loss. (Wilhite and Glantz, 1985).

Hydrological drought is defined as the kind of water deficiency that affects the hydrologic system in a geographical area and is of major concern to hydrologists. It takes time for a drought incident to affect the hydrological balance, therefore a deficiency in precipitation may affect immediately soil and plant conditions, but it will only show up in hydrologic storage systems after a long period of time. However, prolonged drought periods may have a severe impact on a basin level scale. The severity of hydrologic drought lays upon its influence on river basins. Depending on the river basin or stream, a hydrological drought can be identified according to the minimum period that has been specified for that particular basin, but can be of any specific length.

A socio-economic drought occurs whenever the effects of a long term drought are manifested in society. In this situation, water is considered an economic good and thus, economy-related scenarios apply. Therefore, socio-economic drought occurs when supply levels do not meet those of demand. Effects are linked to the supply and demand mechanism and can severely affect human activities (social, agricultural, economical etc.). Sometimes, it is possible that both water demand and supply increase, in which cases, the critical factor regarding the classification of a drought event occurrence is the relative change rate.

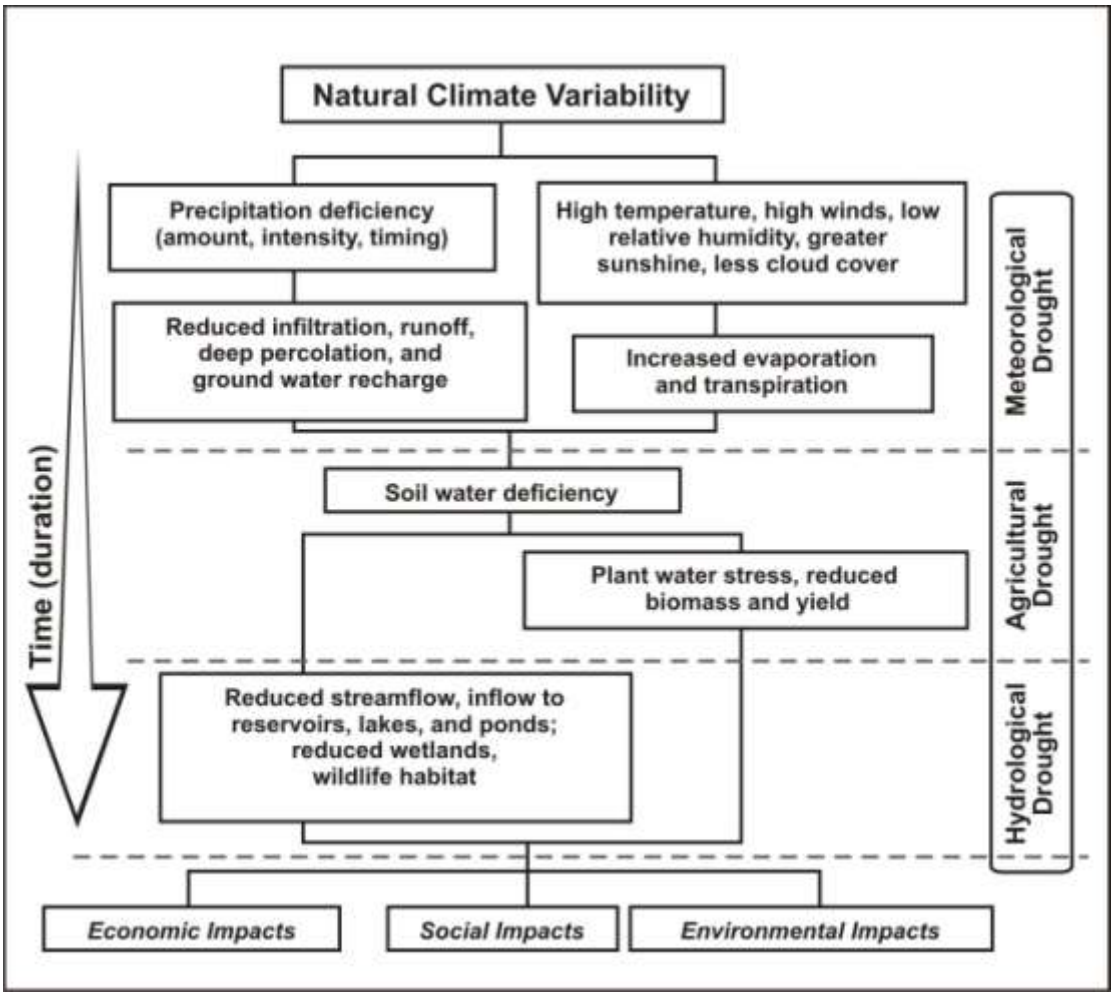

Figure 7. Accepted drought types and impacts (Source: National Drought Mitigation Center, University of Nebraska-Lincoln, USA).

It is important to monitor droughts. They are of major importance in the context of defining a region's climatic parameters and can occur globally. As described above, their impact can be widespread and affect a variety of socioeconomic sectors. However, they are easily monitored, since they can be identified by the study of changes in precipitation and temperature patterns. Droughts can be the result of a variety of factors and their impacts can be just as varied (WMO 2016). Drought indicators and indices are widely used to monitor drought. The indicator most suitable for each case study depends on the available data and the nature of the research taking place. To this regard, it is important that the selected indicator reflects the impacts occurring during the studied drought events.

According to the World Meteorological Organization (2016), "A drought impact is an observable loss or change at a specific time because of drought." The impacts depend on the season and the region the drought is taking place.

A drought early warning system (DEWS) is a tool aiming to "track, assess and deliver relevant information concerning climatic, hydrologic and water supply conditions and trends", including a monitoring and a forecast component (WMO 2016). Its purpose is to timely inform decision makers about a drought event and provide with a plan responding to the management of its impacts.

.

2.3.1 Recorded Drought Events in Greece

Greece is prone to drought events. Most studies regarding those events have been conducted using data from 1950 until today. For the time period from 1950 until 1956 wet conditions were prevalent and that is the time when the first significant drought events in the modern history of Greece took place. For the years 1985 until the early 2000s conditions became drier (Livada and Assimakopoulos, 2007). More specifically, drought events were present in the Athens area for the years 1956-57 and 1959-60, in the Cyclades during 1957-59 and Thessaly and E. Crete during 1958-59 (Tigkas, 2008). A drought event took place in Athens and the Cyclades islands during the period of 1965 – 1966. Another one occurred in Thessaly and eastern Crete during the years 1969–70 and 1973–74 (the latter in eastern Crete only). In the following years dry conditions were present in Crete and Thessaly. During 1977 a major drought event took place and affected a large area in Greece including regions in Western, Central and Northern Greece (Kalamaras et al., 2010). Many researchers classified the period of 1989 – 90 as one of the driest that ever occurred in the country, as many regions were affected during the time (Tigkas, 2008; Kalamaras et al., 2010; Karavitis et al., 2011). This was followed by severe drought events recorded in numerous stations during the year 1993 in Thessaly and eastern Crete (Tigkas, 2008; Karavitis, et al., 2011). During the early 2000s, various drought events continued to occur. In 2000, many regions suffered dry conditions, while a major dry period occurred between 2005 – 2009. The last recorded drought event took place in 2012 in the area of the Aegean Sea (Spinoni et al., 2015).

2.4 Climate Change

The IPCC (Intergovernmental Panel on Climate Change), defines climate change as "change in the state of the climate that can be identified (e.g., by using statistical tests) by changes in the mean and/or the variability of its properties and that persists for an extended period, typically decades or longer." This can occur due to natural internal processes or external forces. However, the United Nations Framework Convention on Climate Change (UNFCCC), makes a distinction between anthropogenic effects altering the composition of the atmosphere and climate variability, the process linked to natural causes (IPCC, 2014).

In the last 1400 years, the time period from 1983 until 2012 was the warmest 30-year period ever recorded for the Northern Hemisphere. Over the period of 1880 to 2012 ocean surface temperature data show a warming of 0.85 °C (IPCC, 2014).

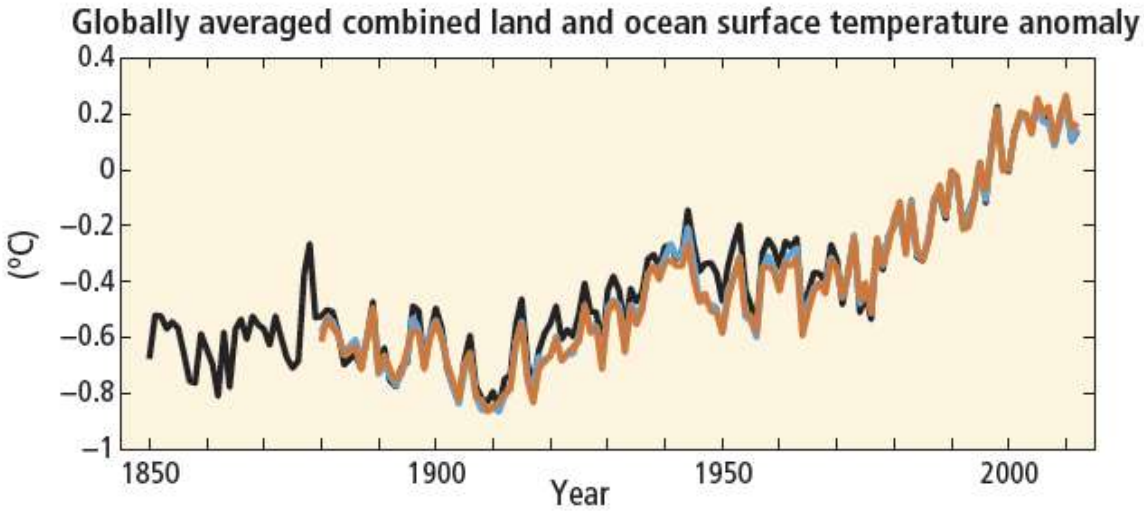

Figure 8. Annually and globally averaged combined land and ocean surface temperature anomalies relative to the average over the period 1986 to 2005. Colours indicate different data sets. Source: IPCC, 2014

Anthropogenic effects are mostly linked to altering the atmospheric consistency and more specifically the increase of the percentage of Greenhouse Gases (GHGs) in the atmosphere. The term Greenhouse Gases (GHG) refers to gases that occur in the atmosphere and absorb and emit radiation within the thermal infrared range. GHGs are an essential component of the Earth's atmosphere, as the current life forms on the planet would not have developed in their absence. Without the presence of GHGs in the Earth's atmosphere, the average temperature on its surface would be around 30°C lower than the current average. Therefore, the Earth's climate is severely dependent upon the balance resulting from the interaction between solar radiation and radiatively active trace gases, aerosols and clouds.

The process by which GHGs contribute to the current temperature of the earth's atmosphere is called "the greenhouse effect". Radiation emitted by the sun enters the earth's atmosphere. Short wave radiation passes through a greenhouse gas, but long wave radiation is absorbed by them; short wave radiation that strikes the surface of the Earth is re-emitted by the surface in the form of thermal infrared radiation.

GHG molecules re-emit long wave radiation in every direction. Radiation aimed towards the surface of the earth is reflected back into the atmosphere. As a result, a continuous exchange of long-wave radiation takes place between the surface of the Earth and the atmosphere. This procedure contributes to the increase of the Earth's average temperature. Although the surface of the earth emits radiation, only 10% of

this radiation escapes towards space filtered through the atmosphere, while the rest is absorbed by greenhouse gases and clouds. The most important and common GHG is CO_2, but CH_4 and N_2O contribute to the global warming effect as well. Although the atmospheric concentrations of CH_4 and N_2O are significantly lower, their effectiveness is much larger than that of CO_2.

The effect is named after the analogy of a greenhouse, because a greenhouse retains heat after being exposed to radiation that passes through its glass structure (although the mechanism through which heat is absorbed in a greenhouse is different from that which takes place in the atmosphere). The severity of the effect depends on the concentration of GHGs in the atmosphere and the proportion of every gas included, since each one of them is characterized by different reflective abilities.

The fact that this intense increase of CO_2 emissions during the recent past is a result of anthropogenic activity is undeniable. First of all, records from ice cores show small natural variability with regard to GHG values over the past millennium. At a specific point, however, the observed increased rate parallels the emission trends from fossil fuel combustion and land use practices.

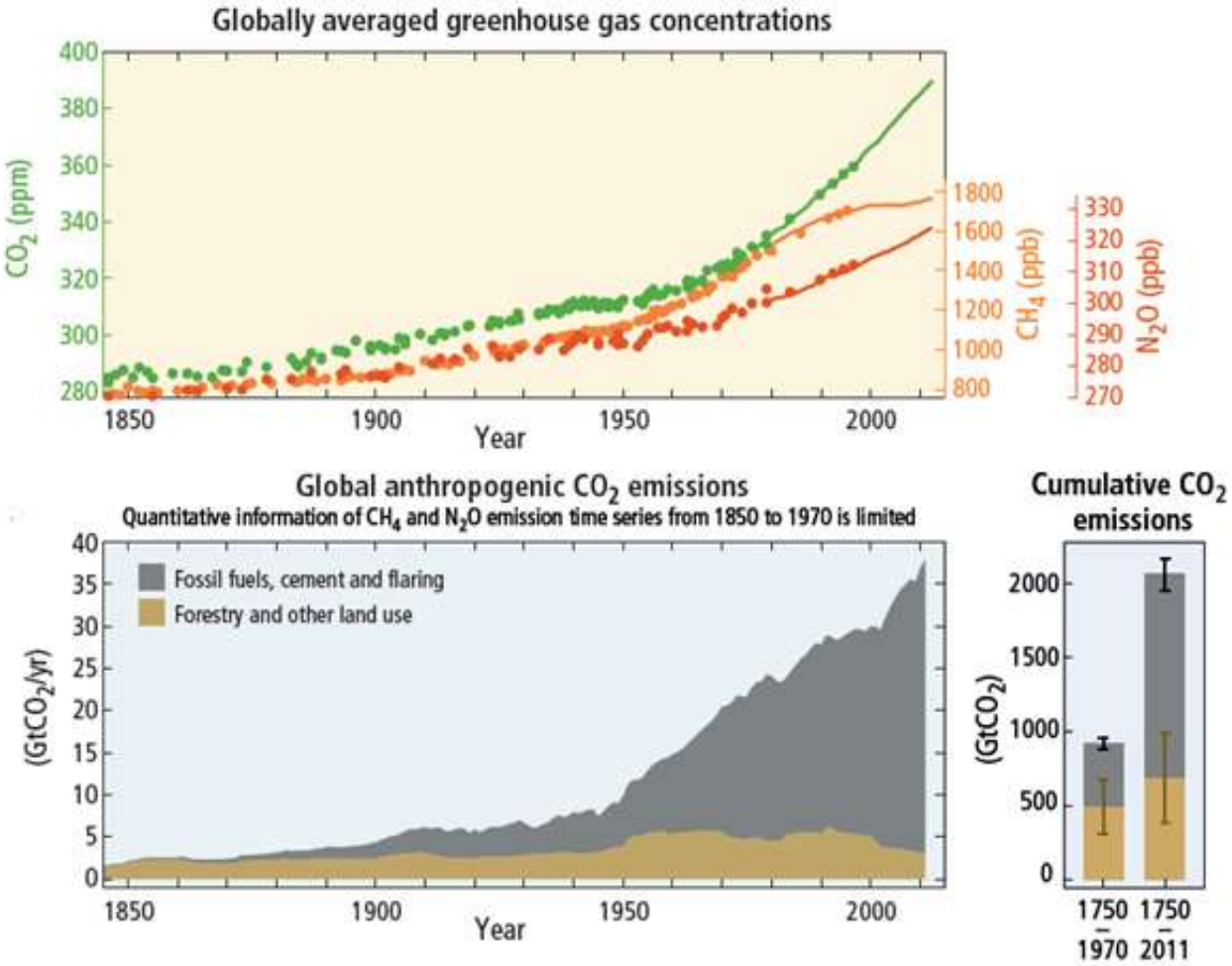

Figure 9. Upper Graph: Atmospheric concentrations of the greenhouse gases carbon dioxide (CO2, green), methane (CH4, orange) and nitrous oxide (N2O, red) determined from ice core data (dots) and from direct atmospheric measurements (lines). Lower Graph: Global anthropogenic CO2 emissions from forestry and other land use as well as from burning of fossil fuel, cement production and flaring. Cumulative emissions of CO2 from these sources and their uncertainties are shown as bars and whiskers, respectively, on the right hand side. Source: IPCC, 2014

Climate change impacts manifest themselves in a comprehensive way regarding natural systems. Changes in precipitation patterns or the melting of the ice sheets, affect the hydrological systems and water

resources. Due to climate change several species were forced to alter their activities and geographic ranges. Agricultural practices have also been affected, primarily in a negative way (IPCC, 2014). Extreme weather events have been modified compared to 1950, displaying increases in warm temperature extremes and decreases in cold temperature extremes. Heavy precipitation events are more prone to occur and sea level rise is considerable. Several ecosystems and human systems display significant vulnerability (IPCC, 2014).

In order to project future changes in the climate system, emission scenarios have been developed. All of them show that the Earth's surface temperature is expected to increase over the 21st century.

2.4.1 Emission Scenarios

In order to implement policy actions, it is important for reliable projections about the future of climate change to be established. In this respect, several factors need to be taken into account including greenhouse gas emissions, technological advancements, energy production, land-use activities, economic development and population growth.

Multiple scientific groups around the world are involved with climate modelling, using different metrics, starting points and methods. This situation results in difficulties regarding the process of comparing models generated by different groups with each other. In addition, running simulations from scratch for each and every experiment is costly and time consuming.

The chosen method for addressing this problem was the establishment of a standard set of climate change scenarios. These scenarios combined several aspects of the climate change science incorporating historical data and projections. Scenarios are defined as the alternative images according to which the future might unfold, while assessing associated uncertainties. Their main functionality is to aid in the analysis of possible climate change, its impacts, mitigation and adaptation options associated with it and climate modeling. They illustrate emission paths; however, the probability that a specific emission path will occur in the future is uncertain. All scenarios include subjective elements and are subject to various interpretations.

Scenarios are used by scientists, policy makers, and several groups including Climate Model (CM) groups, Integrated Assessment Model (IAM) groups and Impacts, Adaptation and Vulnerabilities (IAV) groups, in order to conduct research and communicate effectively in matters regarding climate change.

The reason why so many scenarios are established is simple. Man-made forces like greenhouse gas emissions, are external to the climate system; yet, they determine how that system reacts to them. Future climate projections are in fact assumptions made by scientific groups about the Earth's response to those forces, taking into account the internal variability of the climate system. Different models simulate alternative responses. Combinations of those models provide a variety of suggestions concerning possible futures. Models are primarily based on the physical principles dominant in our climate system, empirical comprehension and analogues from past observations. They are basically complex equations running using numerical algorithms through computer simulation. However, their ability to predict the future is somehow limited by the lack of computational ability to describe the system at a resolution high enough and the lack of complete understanding of all climatic parameters included in it (Collins et al., 2013).

Table 1. Scenarios developed by the IPCC through the years

Year	Name	Established in
1990	SA90	First Assessment Report
1992	IS92	Second Assessment Report
2000	SRES	Third & Fourth Assessment Report
2009	RCP	Fifth Assessment Report

Through the years, several scenarios have been developed by the IPCC. With every new scenario set, many parameters changed, such as titles, classification, assumptions and methods (Girod et al, 2009). As early as 1990, the IPCC established the first long term emission scenarios known as SA90 within the First Assessment Report (FAR), resulting in 4 scenarios in total.,Shortly after, the IS92 scenarios followed. They were six in number and included a wide array of assumptions reflecting how future greenhouse gas emissions might evolve in the absence of climate policies beyond those already adopted.

In 1996, the IPCC decided to develop a new set of scenarios, as significant changes in understanding of radiative forcing and methodologies took place after 1992. Thus, the Special Report on Emissions Scenarios (SRES) was published in 2000. According to the IPCC (2000), "the SRES scenarios covered a wide range of the main driving forces of future emissions, from demographic to technological and economic developments". They consisted of four narrative storylines, with each of them representing different demographic, social, economic, technological, and environmental developments. Each storyline comprised a scenario "family", and included various different scenarios. The SRES scenarios were 40 in total.

The latest set of scenarios was published in 2014 as part of the IPCC Fifth Assessment Report (AR5). Those new scenarios are called Representative Concentration Pathways (RCPs) and include four pathways: RCP8.5, RCP6, RCP4.5 and RCP2.6. Together they reflect the range of radiative forcing values for the year 2100 ranging from 2.6 to 8.5 W/m^2. Radiative forcing, is expressed as Watts per m^2 and represents the additional energy absorbed by the earth - atmosphere system as a result of the reinforced greenhouse effect. It is defined as the difference between the current energy balance in the earth's atmosphere and the one that was prevalent during the pre-industrial period. While radiative forcing increases, global temperature increases as well.

As suggested in the IPCC Expert Meeting Report (2007), "RCPs are referred to as pathways in order to emphasize that their primary purpose is to provide time-dependent projections of atmospheric greenhouse gas (GHG) concentrations." Each RCP includes a set of starting and estimated values for each emission category up to 2100, taking into account quite a few socio-economic factors. Each RCP reflects different socio-economic assumptions, resulting in different estimated values.

The RCPs include scenarios of low and greenhouse gas emissions and provide gridded information on land use. They also include extensions up to the year 2300 examining climate change impacts for the distant future. Each RCP scenario, reflects a different set of underlying socioeconomic assumptions and extend up to 2100. A short description of each one of the four scenarios follows.

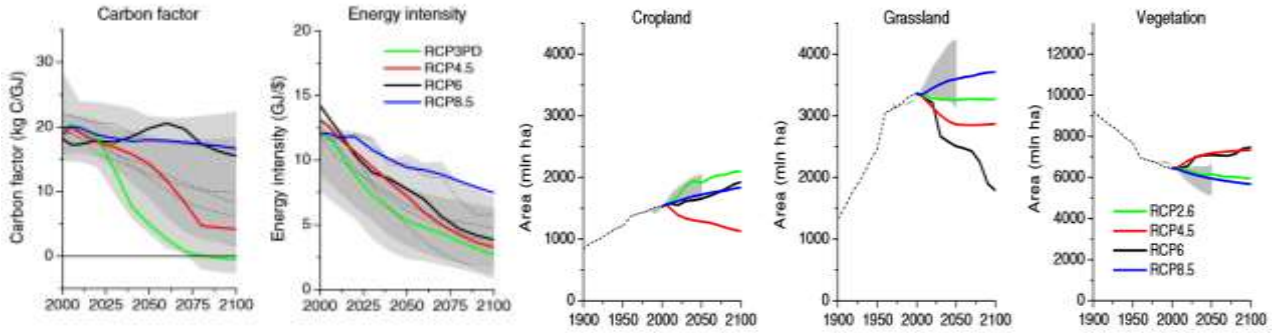

Figure 10. Graphs depicting carbon, energy intensity and land use (cropland, grassland and vegetation) for the 4 RCP scenarios. The dotted lines correspond to former SRES scenarios. (van Vuuren et al., 2011)

The RCP 2.6 scenario represents a low emission future situation. It was developed by the PBL Netherlands Environmental Assessment Agency and suggests a reduction in radiative forcing, reaching as low as 2.6 W/m^2 by 2100. This scenario requires several measures including a reduction in oil use, CH_4 emissions by 40%, as well as CO_2 by 2100 (van Vuuren et al., 2007).

The RCP 4.5 scenario assumes a stabilized and sustainable situation that is less extreme than the one presented by RCP 2.6. It is developed by the Pacific Northwest National Laboratory in the USA. This scenario also suggests that various climate policies are implemented (Thomson et al., 2011). It suggests the implementation of strong reforestation programs, an increase in crop yield and therefore a decrease in cropland and grassland use (van Vuuren et al., 2011). In addition, CH_4 emissions are expected to remain stable, while CO_2 emissions are allowed to increase slowly until 2040, when a decline starts taking place (Figure 11). Fossil fuel use will continue in moderation, while bioenergy and CCS will also be used as an energy source (Thomson et al., 2011). In fact, RCP 4.5 shows trends similar to RCP 2.6, but less extreme, with respect to energy intensity and reliance on fossil fuels (van Vuuren et al., 2011).

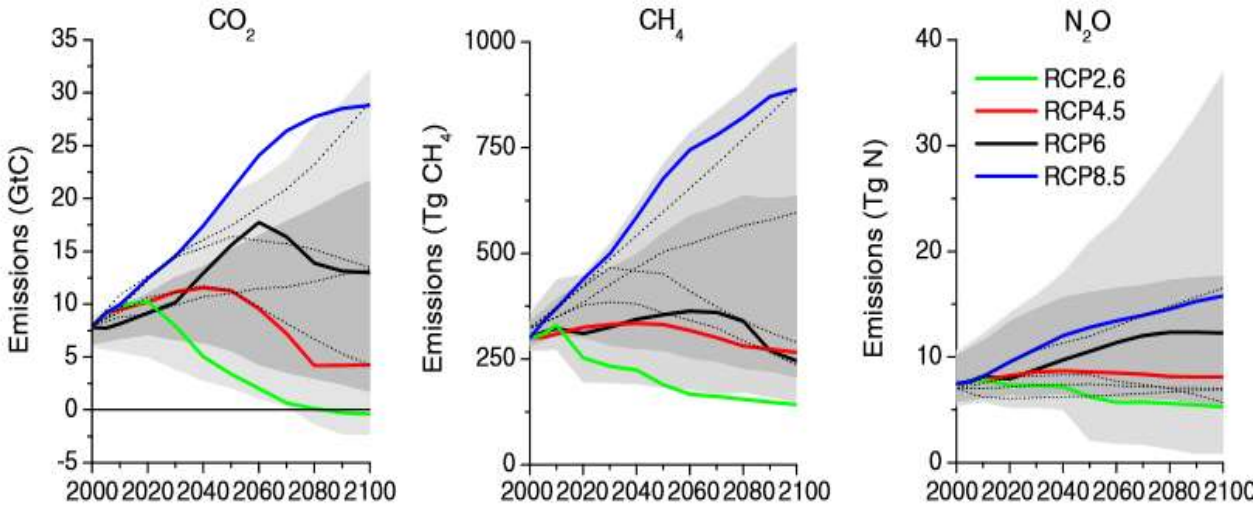

Figure 11. Emissions of main greenhouse gases across the RCPs. The dotted lines correspond to former SRES scenarios. (van Vuuren et al., 2011)

The RCP 6 is developed by the National Institute for Environmental Studies in Japan and represents a less sustainable future (Masui et al., 2011). It still however lies heavily on new technologies aiming at GHG emission reduction. In this scenario CH_4 emissions are reduced by around 40% (van Vuuren et al., 2011), while CO_2 emissions reach a peak level in 2060 (75% above current levels) and then start to decline (25% above current levels). Use of croplands is expected to increase, while reliance on fossil fuels will be heavy.

Finally, the RCP 8.5 scenario represents a future state where no climate policies aiming at the reduction of GHG emissions are implemented (van Vuuren et al., 2011). This leads to increased GHG emissions over time, reaching as high as 200% by 2050 and 300% of today's levels by 2100 (Riahi et al., 2011). CH_4 and N_2O emissions are expected to grow rapidly by the end of the century too (van Vuuren et al., 2011). Technology development is expected to be hindered and fossil fuels will constitute the main source of energy, while the world population increases up to 12 billion by 2100. More specifically, coal use increases tenfold by the end of the century, while the transportation sector mainly depends on oil (Riahi et al., 2011). As a result of the increased human population, cropland and grassland uses and intensity skyrocket (van Vuuren et al., 2011). This scenario was developed by the International Institute for Applied System Analysis in Austria.

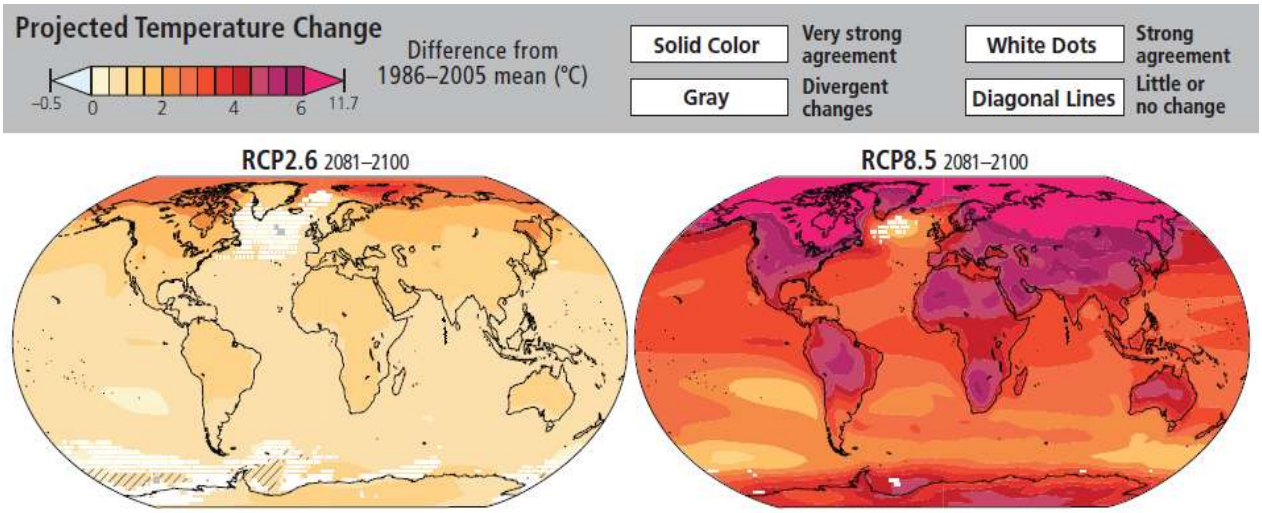

Figure 12. Observed and projected changes in annual average surface temperature under climate change scenarios, taking into account the most extreme ones (IPCC 2014).

2.4.2 Climate Change Impacts in the Mediterranean

The Mediterranean region is a region potentially vulnerable to climate change due to its geographic position. It is highly affected by modifications of circulation processes, due to its location within a transition zone between North Africa's arid climatic conditions and central Europe's rainy ones (Giorgi and Lionello, 2008).

During the warm season, model simulations suggest a significant decrease in precipitation and a mean temperature increase in the Mediterranean region. This fact is mainly associated with increasing anticyclonic circulation causing a northward shift of the mid-latitude storm track especially during the summer months (Giorgi and Lionello, 2008). In fact, annual mean temperatures in the Mediterranean region are likely to rise more compared to the global mean, especially during the summer (Christensen et al., 2007), inducing the risk of greater fire frequencies (Pausas and Abdel Malak, 2004). Crop - water efficiency will decrease due to a reduction in crops productivity while their water needs will increase (Abou-Hadid,2006). As a result, species currently residing in the Mediterranean region are in danger of extinction (Bakkenes et al., 2002).

The total number of precipitation days per year is expected to fall as well, while the risk of summer drought is awaited to rise. Limited precipitation and increased evapotransiparion caused by the expected temperature rise, will have a severe impact on soil moisture (Christensen et al., 2007), agricultural production and water supply for domestic and industrial purposes (Kundzewicz et al.,2007). During the winter, especially over some areas in the northern part, increased precipitation is likely to take place. (Giorgi & Lionello, 2008).

It is also suggested that the greenhouse gas forcing is causing large scale wave patterns to change, altering the anticyclonic circulations over the northeastern part of the Atlantic sea (Pal et al., 2004). Under global warming, sea levels are expected to rise; the Mediterranean region would be affected severely, especially its ecosystems, human health and activities and water resources. Salinization is awaited to spread while freshwater availability is likely to decline along the coastal areas (Klein & Nicholls, 1999).

Model projections also show that extreme heat and drought events are about to occur, resulting in increased inter-annual variability. The increased precipitation intensity combined with elevated temperatures are likely to lead to heightened levels of water pollution and water-borne diseases (Hunter, 2003).

2.4.3 Climate Change Impacts on Water Systems in Greece

Water balance is characterized by water demands and water resources. Water demands are defined as the total amount of water that's required for certain human activities. Water resources are water reserves or sources potentially exploitable and depend on location, quality and quantitative variability over time.

According to the report of the Bank of Greece (DBRG, 2011), Greece displays numerous special characteristics in regard to its water reserves. Precipitation patterns show a rather uneven distribution; 85% of total precipitation occurs during the wet season, while only 15% during the dry season. This fact

combined with extensive agricultural activities and a peak in tourism, contributes to great water demand imbalance. As indicated above, most rainfalls take place in Western Greece, more specifically west of the Pindus mountain range. Northern Greece is permeated by transboundary waters; its four major rivers originate from neighboring countries. Also, Greece shows an uneven population distribution, with most people residing in urban and coastal areas, allowing for overpumping and seawater intrusion in coastal aquifers. The islands of the Aegean Sea suffer mostly because of the low rainfall levels, intense topographic relief and surface runoff. Compared to the rest of the Mediterranean region, Greece can be considered a country rich in water reserves. This is thanks to the occurrence of the Pindus mountain range and its effects on precipitation patterns across the country.

A clear distinction needs to be made between the terms of water scarcity and aridity. Water scarcity is possible to occur as a result of a drought event, but also because of bad water management and planning even when a drought event is not experienced. Generally, it is defined as the decrease in available water potential compared to anticipated use. Aridity on the other hand is a term solely connected to deficiencies in water supply to the environment when compared to past time series.

Freshwater availability is critical for numerous sectors in economy. Thus, every negative consequence is expected to affect a variety of activities, including agriculture, industry, pisciculture etc. Risk of disasters is also anticipated, making the occurrence of fires and floods more likely. Costs from wastewater treatment and extraction of underground waters are due to inflate as well. Coastal aquifers will become more vulnerable. Overall, climate change will affect water use and human quality of life in a negative way.

Even though the islands in the Aegean Sea used to have sufficient water resources, this situation tends to change. Development in the tourism sector, changes in lifestyle and improved living standards will likely lead to water scarcity. The same problem is encountered in Attica basin, where intense urbanization took place during the past twenty years with 40% of the national population residing in that region.

Climate change in Greece is envisioned to result in several disadvantageous consequences. Decreased rainfall will contribute to an overall reduction in aquifer infiltration and recharge. Sea-water intrusion resulted by over pumping will evoke the decline of groundwater levels, which will respectively increase salinity in coastal aquifers. Pollution levels in water bodies will escalate due to pollutants diluted in smaller volumes of water compared to previous states. Coastal wetlands and deltaic regions will degrade with a faster rate and desertification will intensify.

Management and adaptation actions should be put into effect, but it’s crucial that they occur in a well-coordinated and planned manner, especially when taking into account that Greece as country already suffers from both deficient legislation and enforcement (DRBG , 2011). Therefore, a plan aiming at policy-led adaptation is necessary.

2.5 Adaptation & Mitigation Strategies for Water Systems Management

The consequences of climate change can be multiple. In order to deal with them, decision makers need to assess and analyze all possible impacts of human interference with the climate system. Human societies have always struggled to adjust to climate conditions throughout history. Today climate-change impacts are more comprehensive than ever. From 2005 until 2010 the number of available publications addressing this subject matter increased rapidly, especially regarding adaptation (IPCC 2014).

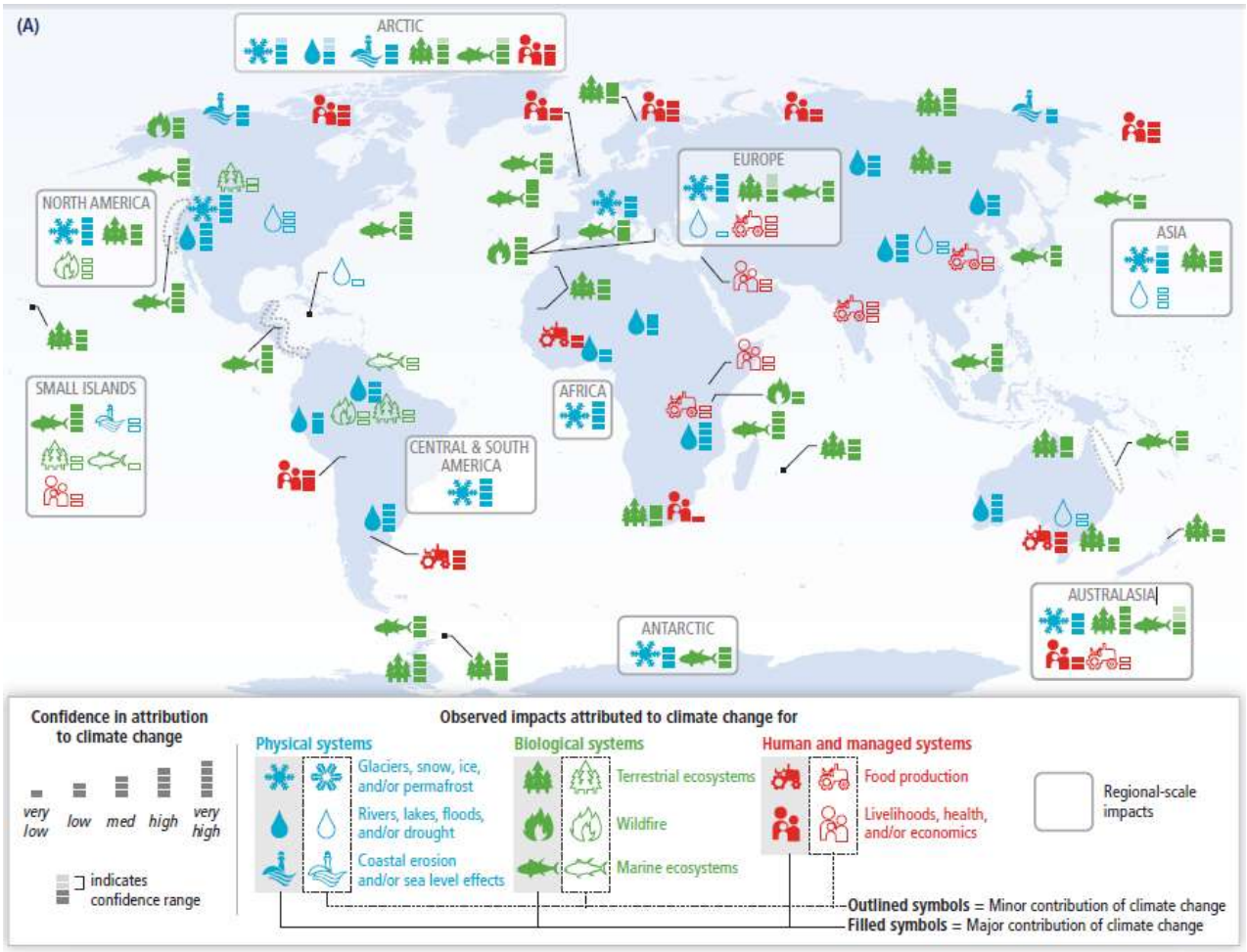

Figure 13. Global patterns of impacts in recent decades attributed to climate change at a range of geographic scales. Symbols indicate categories of attributed impacts, the relative contribution of climate change to the observed impact, and confidence in attribution (IPCC 2014).

Water moves through the hydrological cycle and is linked to many functions of human society, such as agriculture, transportation, health and energy. Climate change can induce a variety of impacts and changes to the hydrological cycle affecting all referenced functions, each one in a different way. The increasing water demand caused by population growth, urbanization and economic development further challenges resources sustainability. Apart from climate change itself, human activities contribute greatly to hydrological change (land use, water withdrawal and pollution) (IPCC 2014).

To this regard, adaptation and mitigation are crucial. According to the IPCC (2014), adaptation is defined as the "process of adjustment to actual or expected climate and its effects" and mitigation accordingly as "a human intervention to reduce the sources or enhance the sinks of greenhouse gases (GHGs)."

Concerning freshwater systems, observed and projected impacts originate from temperature and sea level rise, change in precipitation and increased variability of the aforementioned quantities. They manifest themselves mainly in semi-arid and arid climates. It is evident that climate change has an impact on water management infrastructure and many regions have developed adaptation and risk management practices regarding the water sector in order to tackle the anticipated threat (Jiménez et al., 2008). According to climate models, some regions, especially mid-latitude and dry subtropical, are likely to display a reduction in their renewable water resources, while humid mid-latitude and high latitude regions are about to witness an increase (Jiménez et al., 2008).

Elevated water supply in some regions is expected due to an anticipated increase in precipitation. For the most part however, climate change bears negative impacts on freshwater systems. In regions where large amounts of precipitation are envisioned, although water scarcity will reduce, flood risk will elevate. Another example of a negative impact associated with extreme precipitation is the extended salinization and infrastructure damage due to a raised groundwater table. Boosted storm runoff is likely to transfer nutrients causing eutrophication towards the sea, inducing further damage to marine ecosystems. It is therefore unquestionable that in cases where additional water supply is expected, infrastructure must be developed in a way that accommodates and handles this excess supply properly (Jiménez et al., 2008).

Long term planning is essential to tackle the diverse effects of climate change in water systems. Since climate change projections bear a high degree of uncertainty is it important that a flexible agenda is initiated, incorporating solutions that can be implemented step by step in an adaptive manner. Such an agenda would include adaptive techniques such as scenario planning and experimental approaches, allowing policies to advance gradually, constantly facing the challenges that may arise (Bates et al., 2008).

Rainwater harvesting, desalination, water reuse combined with efficient soil and irrigation water management could contribute to tackling water shortages. Maintaining the vegetation cover and planting trees in steeply sloping fields could alleviate the negative effects of excessive runoff caused by uncontrolled water bodies. It is also fundamental to restore and protect freshwater habitats (Jiménez et al., 2008) and aid wetland conservation, as it will improve water quality and biodiversity (House et al., 2010).

While planning adaptation for the water sector, other closely connected sectors should also be considered, those being forestry, agriculture and industry (Jiang et al., 2013). Controlled flooding in cropland can mitigate urban flooding and respectively, increased upstream irrigation may result in reduced water supplies downstream (World Bank, 2007). Erosion and sedimentation in river channels is moderated by improved agricultural land management practices (Lu et al., 2010). Afforestation is a highly recommended practice having a positive impact on water quality, soil erosion and local flood risk by decreasing total runoff (van Dijk and Keenan, 2007). Introducing green infrastructure, green roofs, porous pavements and urban parks, for instance, within the urban environment can benefit both mitigation and adaptation actions. It will moderate the heat-island effect, reduce flood risk and improve storm water management (Noble et al., 2014).

Change in precipitation patterns ought to influence freshwater input, output and sediment delivery. Those factors combined with high storm surges that move coastal sand away from the shore contribute to coastal erosion leading to sea level rise (Wong et al., 2014). Marine ecosystems highly depend on ocean temperature, ocean acidification and of course, sea level. A rise in sea level results in the alteration of a variety of parameters including available light, temperature and salinity resulting in the destabilization of the ecosystem's balance. The metabolism of species is modified affecting other species, and corals

undergo “coral bleaching”, a process that weakens them. Even worse, if animal and plant species fail to adjust to the altered situation they will likely become extinct. Organisms living in the ocean are not the only ones in danger; mangroves and coastal wetlands can be severely affected as well. Ocean acidification is the consequence of atmospheric CO_2 being absorbed into the ocean, the product of which is carbonic acid. The acidity in ocean water elevates, dissolving carbonate, the main structural element in shells, skeletons and corals (Wong et al., 2014).

Some adaptation measures to combat the negative impacts of climate change in coastal systems include the enhancement of coastal vegetation in order to reduce erosion and establish the coast as a barrier against storm surges. The building of artificial dunes or the nourishment of existing ones is also recommended. Sometimes the building of barriers such as seawalls is critical for the sake of protecting existing infrastructure. Infrastructure itself can be adapted too; buildings can be reinforced becoming more resistant against sea level rise and physical shelter capacity ought to be increased. If every other measure fails, moving away from the coast is the only option available (Wong et al., 2014).

Last but not least, terrestrial and inland freshwater ecosystems possess a vital role in the way human societies adapt to climate change, because they operate as a vast carbon sink. Although they function with no human intervention, a concerted effort to restore damage in ecosystems (management of forest fires and pest outbreaks, improvement of species migration corridors, assisted migration and reduced peatland drainage) could boost this attribute even further (Settele et al., 2014).

2.6 Drought in Europe and Greece

There are abundant examples in literature analyzing precipitation events in Europe with the aid of drought indices. Many of them utilize emission scenarios in order to assess future conditions. In general, they tend to agree that Southern Europe is more sensitive to extreme and prolonged dry events, while Northern Europe is at risk of extreme wet events. Below are some examples.

20th century drought in Europe was studied by Lloyd-Hughes and Saunders (2002) using the Standardized Precipitation Index (SPI) as well. They calculated the index at time scales of 3, 6, 9, 12, 18, and 24 months for the period 1901–99 using CRU gridded data. They found that SPI12 resembles the PDSI index closely. Significant spatial changes in the mean value of the studied indices haven't been reported during the whole century. Wetter conditions are mostly prevalent in northeastern Europe, while dry ones in central eastern Europe and western Russia. Those trends tend to be intense during the winter/spring seasons. The longest droughts are found in Italy, northwest France, and northwest Russia, reaching typical durations as long as 40 months.

Many similar studies have been conducted for the eastern Mediterranean and Greece in particular. Kostopoulou and Jones (2005) studied climate (precipitation and temperature) extremes in the eastern Mediterranean. They concluded that the western part of their study area (represented mostly by Italian stations), tends towards intense precipitation events, while the eastern half exhibited negative trends for all studied indices. Stations located towards the south, especially on islands, resulted in great numbers of consecutive dry days.

Livada and Assimakopoulos (2007) used the SPI index to classify drought in 23 stations all over Greece for a time period of 51 years. They found that most severe droughts take place in southern Greece; as one progresses towards the North, the intensity decreases. In fact 3 and 6 month SPIs showed that moderate droughts occur in Northern Greece for the most part. On the 12 month time-scale extreme droughts were found to be very rare.

Blenkinsop and Fowler (2007), studied 6 European regions, representing a variety of climatological and hydrological regimes using (CRU) CRS TS 2.0 datasets (1901 – 2000) and observational data (for a control period of 1961–1990). Those regions were the Eden in north-west England , a fine example of temperate maritime climate, the Meuse in France and the Dommel in Netherlands (lowland catchments less exposed to mid-latitude cyclones from the Atlantic), Ebro and the Gallego, in north-east Spain (Mediterranean climate) and Brenta in Italy, a topographically diverse region, among the Alps and the Po Valley. They concluded that precipitation increases are more likely to occur during the winter season in Northern Europe, extending towards northern Spain, Italy, northern Greece and southern France, with the exception of one model predicting drought over the Mediterranean. For the majority of southern European regions, precipitation during Summer is expected to decrease. Another finding was that, several of the RCMs project large precipitation variability especially during winter.

Koutroulis et al. (2010) conducted a hydrometeorological study at a more local level, for the island of Crete in Southern Greece. They used the SPI and the SN-SPI index (a spatially normalized–standardized precipitation variant of the SPI index) for the timescales of 12, 24, and 48 months. All those timescales

result to drier conditions towards the end of the 22nd century, with the longest timescale in particular, showing that the island of Crete is expected to witness prolonged and extended extreme droughts approaching 2100. The most severe manifestations of drought occur towards the southern and eastern parts of the island.

Karavitis et al. (2011) utilize the SPI index in order to provide a more appropriate understanding of drought characteristics (duration, magnitude and spatial extent) in semi-arid areas like Greece. They believe that Greece's hydrological conditions are ideal for the application of this index and suggest that a continuous temporal online SPI tool serving as a drought alert mechanism should become available to decision makers. Historical precipitation data were used and the SPI was applied in a variety of time scales (1, 3, 6, 12 and 24 months), for 46 precipitation stations, corresponding to the period of 1947–2004.

Heinrich and Gobiet (2012), studied dry and wet spells for 9 European subregions using the SPI index for various timescales. The southernmost (mainly France, Italy, and Spain) and northernmost (mainly Iceland and Scandinavia) European subregions, display greater changes in the mean with respect to both wet and dry events. This situation is also present in relation to event length, distance, magnitude, and area. Interannual variability is expected to increase in regions displaying changes in the mean towards both wetter and drier conditions. Their study agrees with other studies supporting the notion that southern Europe is more prone to increased risk of longer, more frequent, severe, and widespread droughts, while northern Europe to increased risk of extreme wet events.

Founda et al. (2013) used the 150-year historical record of the National Observatory of Athens (NOA)(from 1860 to 2008) and an ensemble of regional climate models, in order to assess precipitation variability in Athens for a 2.5 century period. The Mann-Kendall test was used with NOA datasets displaying negative trends without statistical significance. Their findings also suggested a future decrease of 35% in total annual precipitation and an increase in extreme precipitation as projected by the model ensemble up to 2100.

Mimikou and Baltas (2013) proved that Greece follows the general European climate change trends, that suggest temperature and evapotranspiration rise together with decreased precipitation and runoff. Dry summer periods are expected to last longer as well.

Finally, Anagnostopoulou (2016), studied model (statistically and dynamic downscaled) and observational data with the aid of the SPI index (3-, 6- and 12-month SPI). Her findings suggested that as drought intensity increases, event frequency decreases, especially regarding the 3-month SPI. The SPI index shows high variability among selected time scales. The 12-month SPI presented a period of intense drought lasting from 1989 until 1990 for Athens, and some years earlier, around 1984 for Thessaloniki.

Spain seems to face similar challenges as Greece. Lana et al. (2001) conducted a study regarding the Catalonia region, calculating SPI indices of various timescales utilizing data obtained from 99 rain gauges with monthly totals, from 1961 to 1990. The regions shares similar characteristics to our case study, with very dry spring and summer seasons and wet winters and autumns.

3 Materials And Methods

3.1 Methodology Overview

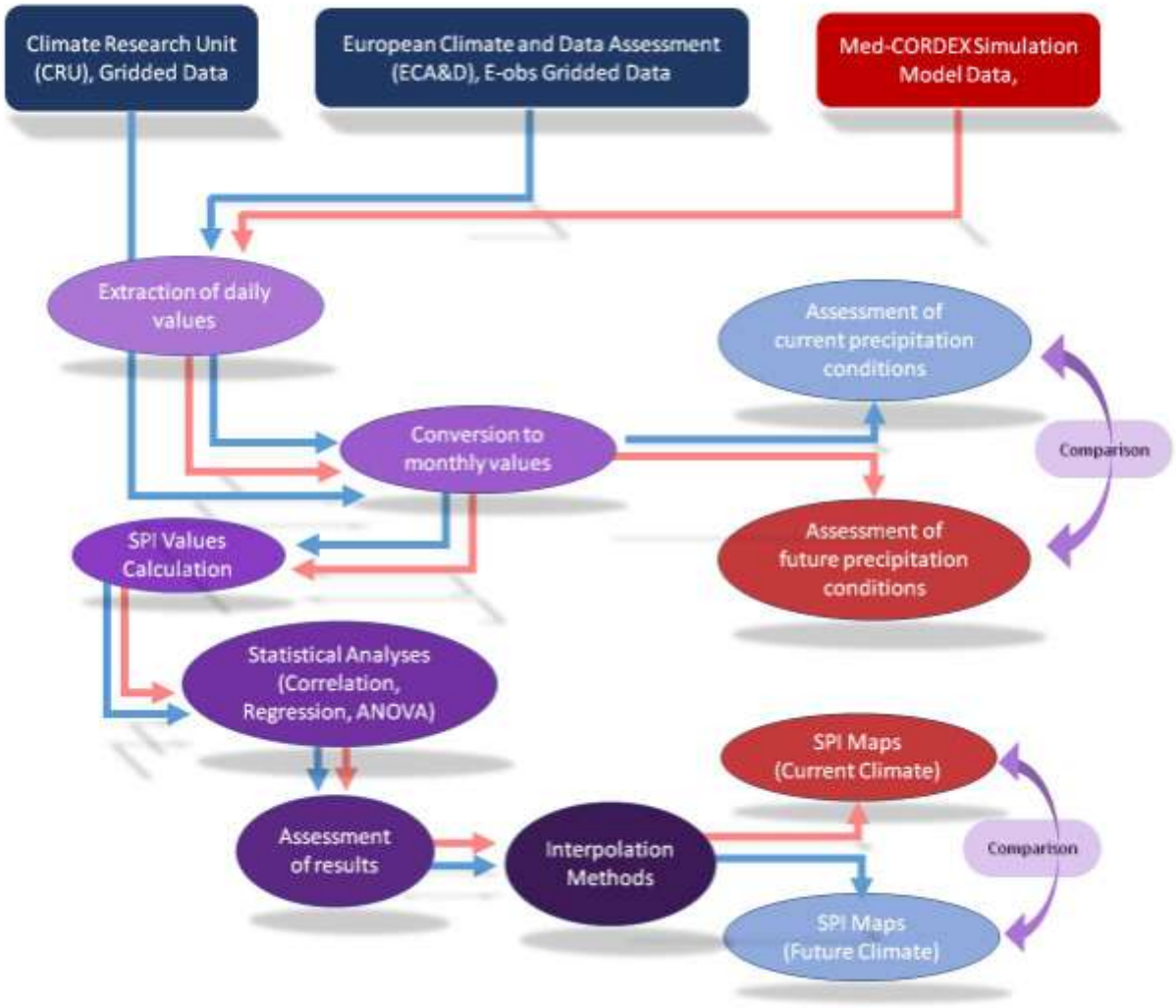

Figure 14. Visual representation of methodological steps used towards the completion of this Thesis

This case study utilized precipitation data from various sources available for climate studies of regional and global interest.

Gridded observational data were acquired from the Climate Research Unit (CRU) and the European Climate and Data Assessment (ECA&D). They were available in the form of daily or monthly precipitation values in NetCDF (Network Common Data Format) file format, a format commonly used for the storage of large volumes of data. The values of interest were extracted and daily values were then converted to monthly precipitation values using spreadsheet software.

CRU data correspond to nine grid points (GP1, GP2, GP3, GP4, GP5, GP6, GP7, GP8 and GP9) (Figure 15). However due to the inclusion of large periods containing lack of data, the grid points GP3 and GP9 were omitted from the study. The remaining grid points exhibited good data quality and coherence with minimal gaps. Those data sets are available for the time period from 1901 until 2014.

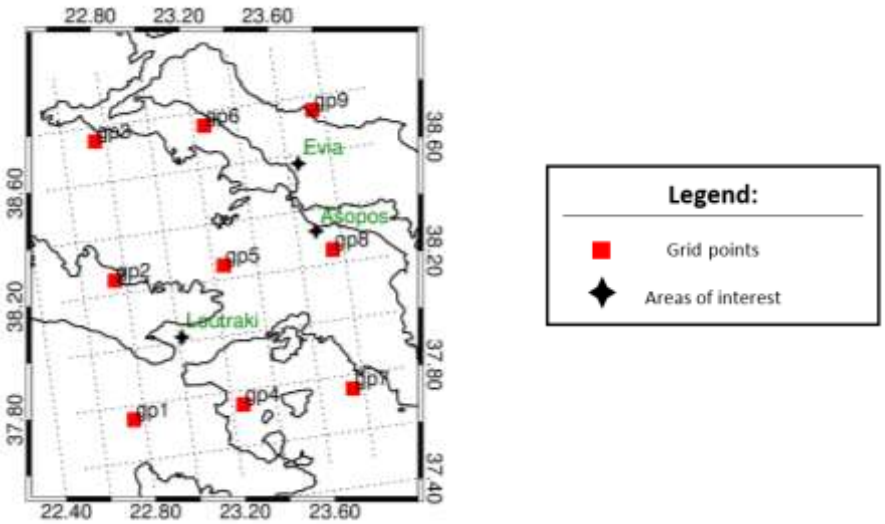

Figure 15. Grid Points around the study area from which Climate Research Unit (CRU) values were derived.

Data from the European Climate and Data Assessment (ECA&D), E-obs gridded data, were provided for the three input locations, that represent the centers of our study areas ([23.02,38.02], [23.65,38.57], [23.68,38.32]), with each of them containing six output locations, thus six (6) grid points. The time period between 1950 and 2014 is covered. However, some grid points display extended periods where lack of data is observed. Those grid points were completely omitted from the calculations. For the grid points that showed a continuous time series, SPI values for the period 1955 until 2014 were calculated (Figure 16).

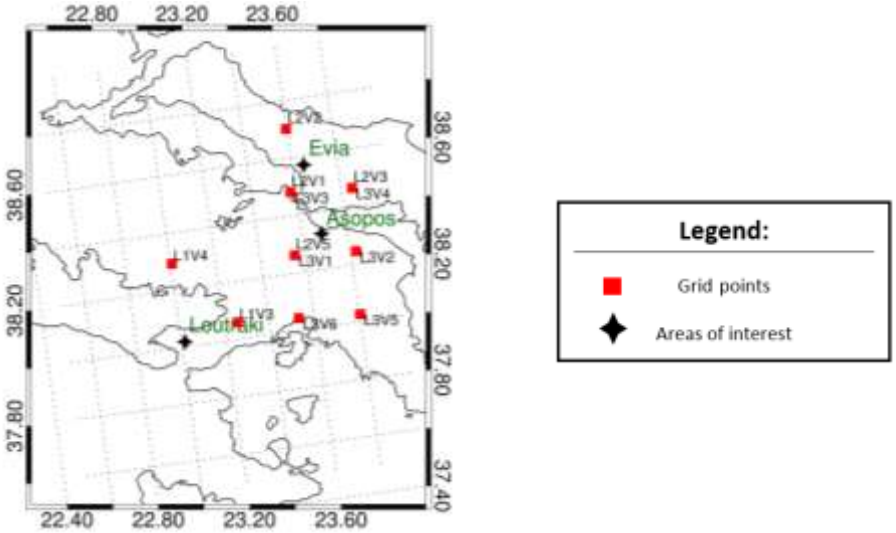

Figure 16. Grid Points around the study area from which, E-obs gridded data values were derived.

Model data were provided by the Med-CORDEX initiative in accordance with two emission scenarios (RCP 4.5 and RCP 8.5). This dataset included several grid points as well. For this thesis, we utilized the six closest ones to each area of interest and focused on the one approaching each area in the best possible way. In the case of Euboea two grid points that equally approach the area, were taken into account (Figure 17). The data used consist of daily precipitation values that were transformed to monthly ones. The model data ranged from 1971 until 2100 and included three distinct periods, a control period from 1971 until 2000, a near future period (from 2021 until 2050) and a remote future period (2071 – 2100). Both scenarios feature the same control period, but after 2006 develop in a diverse way, suggesting different outcomes with respect to the climatic evolution of the study areas.

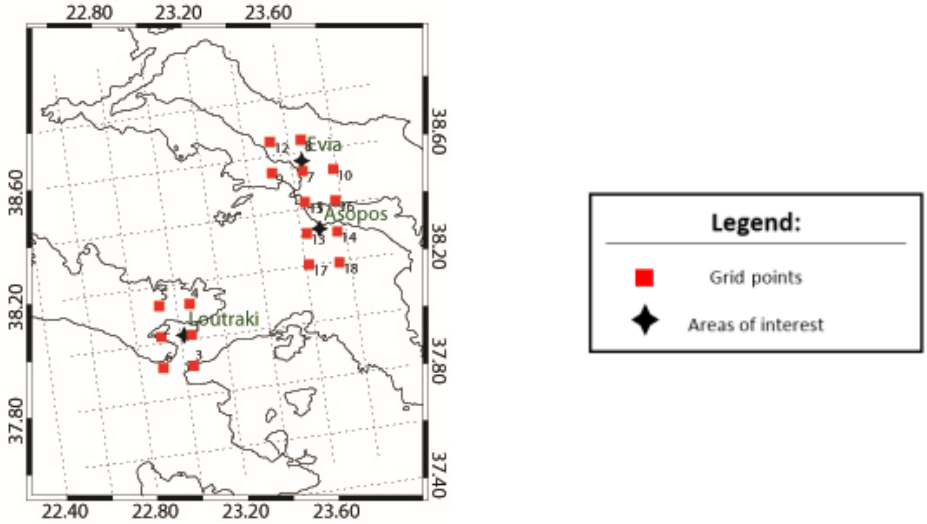

Figure 17. Grid Points of Model Data as provided by the SMHI, the Swedish Meteorological and Hydrological Institute

Regression and correlation statistical analysis were then applied on the index values, examining trends and variance. In order to define and comprehend the climatological background of the area of interest, apart from the SPI values, monthly precipitation values were also analyzed and plotted. Results were interpreted accordingly.

With respect to the monthly precipitation values the SPI index was calculated for the timescales of 3, 6, 9 and 12 months, using software provided by the WMO (SPI_SL_6.exe). The indices that were calculated are the following:

- SPI3 – Examining seasonal variation
  - February (02), corresponding to winter
  - May (05), corresponding to spring
  - August (08), corresponding to summer
  - November (11), corresponding to autumn
- SPI 6 – Partitions the annual circle into two seasons, a wet and a dry
  - March (03), corresponding to wet season
  - October (03), corresponding to dry season
- SPI 12 – Examining annual variation

3.2 Materials

Two sets of gridded observations and a model precipitation dataset were used for our calculations:

- Climate Research Unit (CRU) Data, Version: CRU TS 3.22
- European Climate and Data Assessment (ECA&D), E-OBS gridded dataset Version 14.0
- Med-CORDEX Simulation Model Data, SMHI

Software used for the extraction of indices and the statistical analysis of the datasets:

- SPI.exe developed by the World Meteorological Organization (WMO)
- R (programming language)
- Microsoft Office Excel – Data Analysis tool
- ESRI ArcGIS
- IBM SPSS
- IDL (programming language)

3.2.1. Climate Research Unit (CRU) Data, Version: CRU TS 3.22

CRU (Climatic Research Unit Data) datasets, refer to monthly precipitation values over the last century. They are produced by the University of East Anglia and are available for use in scientific research. They are calculated on high resolution latitude-longitude grids (0.5x0.5 degree) and include a variety of variables. There are more than 4000 individual weather stations worldwide (excluding Antarctica), whose records analysis results to the production of this dataset. For our case study, we used Precipitation data time series. The available time period for which data is available ranges from 1901 to 2014 (CRU TS Version 3.22). The precipitation data have been used to assess global precipitation variability.

This type of data features numerous advantages, with the most striking one being the compilation of station data from various sources into a consistent format. However, trends derived should be interpreted with caution since although most input data were homogenized, not all data sets are strictly homogenous.

Table 2. The sources of station records from which the database was constructed. The climate variables to which the sources contribute are temperature (tmp), DTR (dtr), precipitation (pre), vapour pressure (vap), cloud cover (cld), sunshine duration (spc), and wet days (wet). The dtr includes information from individual records of daily temperature minima (tmn) and maxima (tmx) (Mitchell & Jones 2005).

Label	Reference	Information	Period
Jones	Jones and Moberg (2003)	tmp	1701–2002
Hulme	Mike Hulme, personal communication	pre	1697–2001
GHCN v2	Peterson *et al.* (1998c)	tmp, dtr, pre	1702–2001
Mark New	New *et al.* (2000)	tmp, dtr, vap, cld, spc	1701–1999
Hahn	Hahn and Warren (1999)	tmp, vap, cld	1971–96
MCDW	William Angel, personal communication	tmp, pre, vap, spc, wet	1990–2002
CLIMAT	UK Met Office, personal communication	tmp, dtr, pre, vap, spc, wet	1994–2002

Mitchell and Jones (2005) created a global database of monthly climate observations that included six climatic elements. Various sources were used as station records, and in case of duplicate sources regarding

one station, the most likely to be reliable was prioritized. The station records are listed in Table 2, and are held in space-delimited fixed-format ASCII files.

The available databases were checked for homogeneity issues using a variation of the GHCN method (Peterson and Easterling, 1994; Easterling and Peterson, 1995). The original GHCN method used a reference series constructed by neighboring stations which are selected by a correlation method. This reference series was then compared with each candidate series. The GHCN method was designed for datasets that feature a continuous series of records for a fixed time period and used annual series in order to detect inhomogeneity. Since the method had to deal with datasets containing incomplete station records and neighboring stations that partly overlap in time, monthly series had to be used for the detection of inhomogeneity instead of annual, Mitchell and Jones (2005), modified it accordingly. The newly developed method offered the ability to utilize incomplete data records and records from neighboring stations that only partly overlap in time, create a reference series from the most highly correlated neighboring stations using multiple records, and check homogeneity for each monthly series by combining information from all 12 available sources. There are, however, several weaknesses to this method, with the most notable being its inability to detect gradual inhomogeneities, unless they are not widespread. As an automated method, it lacks all advantages of a manual one, but is capable of processing large quantities of data, and is sufficient in providing interannual variations.

A station was merged into the database, after all inhomogeneities were corrected, by using its WMO code when applicable. For all stations that didn't incorporate such a code into their data, information about the country and location was used instead. In order to achieve a complete record for each station and avoid duplicates, each additional station was compared with the ones already in the database. Any available overlap was utilized for this purpose and when none was available, a reference series was constructed. That way a longer series was produced for each station. This dataset was used in order to examine the long term trends in precipitation in the greater area covering the study areas in order to provide a wider understanding of the prevailing hydrologic conditions.

Finally, all station anomalies were adjusted and interpolated onto a grid, and 80-100% of the land surface was estimated for temperature and precipitation.

3.2.2. European Climate and Data Assessment (ECA&D), E-OBS gridded dataset Version 14.0

Haylock et al.,(2008), created a high-resolution land only daily gridded data set for precipitation and temperature. These datasets are generated through interpolation of station data and consist a daily gridded observational dataset for precipitation, temperature and sea level pressure in Europe based on ECA&D information for the time period between the years 1950 and 2016. It was originally developed as part of the ENSEMBLES (EU-FP6) and EURO4M (EU-FP7) projects and is currently maintained as part of the UERRA project (EU-FP7). The Royal Netherlands Meteorological Institute (KNMI) was initially responsible for the collection of data, and it also hosts the European Climate Assessment and Data set (ECA&D).

Data from 68 participants for 63 countries is collected. The ECA dataset of daily station series contains 43176 series of observations for 12 elements at 10576 meteorological stations throughout Europe and the

Mediterranean. Data was obtained from climatological divisions of National Meteorological and Hydrological Services and station series maintained by observatories and research centers.

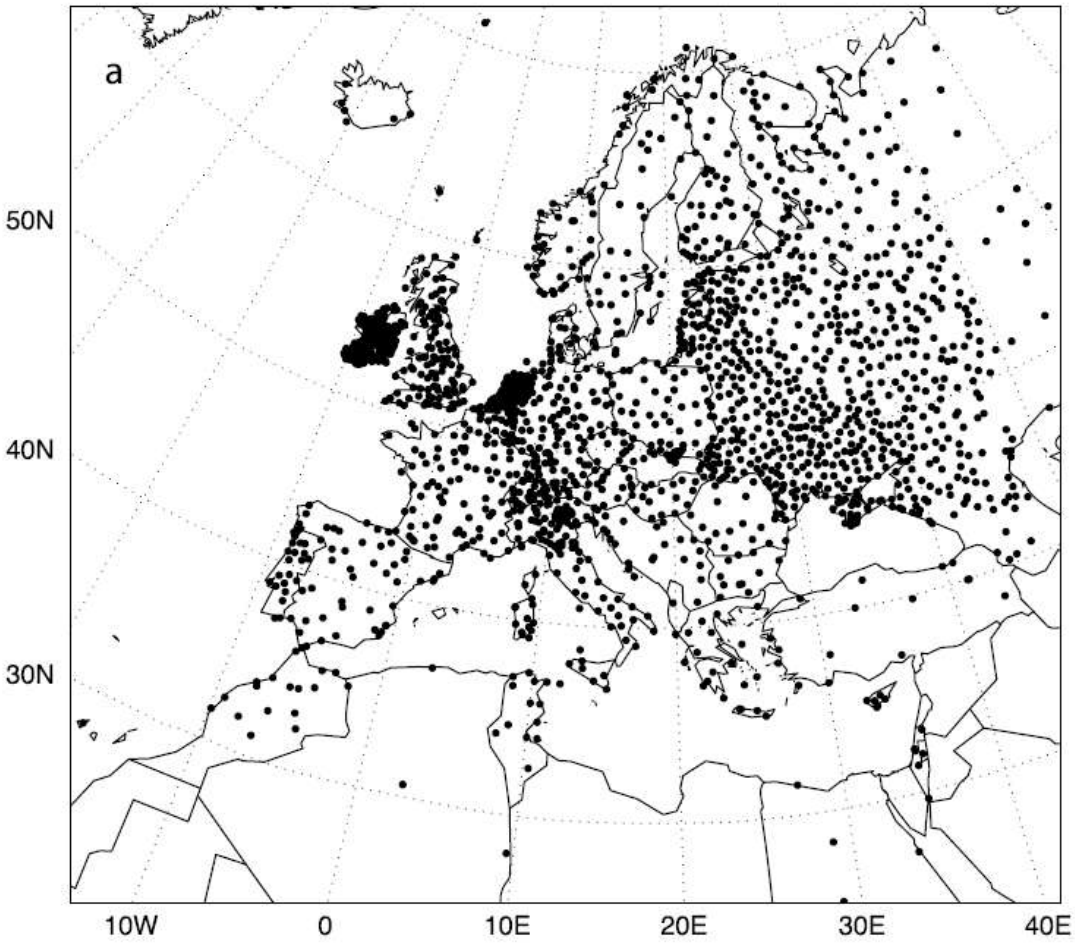

Figure 18. The complete gridding region (land-only),showing the station network for precipitation (Haylock et.al 2008)

In order for data density to be achieved in the construction of the desired high-resolution network, one station per 25km x 25 km was the minimum requirement. That would result in the establishment of 16,000 stations all across Europe, which was not feasible. Even though additional series were obtained from other research projects or with the help of National Meteorological Services, there was still need for interpolation estimates. After numerous cross validation exercises, Haylock et al.,(2008) decided upon the Kriging interpolation method, and more specifically the thin-plate-splines method. With respect to monthly precipitation and temperature, the three-dimensional splines method was used, since it was able to take the elevation in each station into account.

According to stochastic methods, probability theory is preferred for modeling the observations as random functions. The Kriging method is one of those methods. Interpolation methods are used to estimate an expected mean value of a random function for a location that features no sampling capabilities, by producing a surface that fits to that expected mean.

Numerous Kriging methods exist and are all based on the solution of multiple linear equations in order to minimize the variance in observations around the interpolation surface. Since Europe is a region that contains a wide array of different climate zones and topography, solving the least squares problem,

requires that all daily data be homogenized. To this end, a method similar to Universal Kriging was the solution to this problem. This method comprised of three stages: the definition of the underlying spatial data trend using thin-plate splines, kriging the anomalies while taking into account the monthly mean, and towards the production of the final result, the application of the interpolated anomaly to the interpolated monthly mean. More specifically, the resulted temperature anomalies were defined as the difference between the daily observation and the monthly mean, while for precipitation, the daily anomaly was equal to the quotient of the daily precipitation value and the monthly total (proportion of the monthly total that corresponds to a day) (Haylock et al., 2008).

The main purpose of this dataset in regard to this thesis was to assist in the evaluation of climatic conditions prevalent in the study areas at a more refined scale, since the provided spatial resolution allows for such a task. However, due to the inconvenient spatial distribution of grid points, results extracted from the analysis of this dataset will only function as additional verification of the findings coming from the use of other datasets and as further evaluation regarding model data.

3.2.3. Med-CORDEX Simulation Model Data

2. Model data used were derived from the Med-CORDEX initiative, which has been proposed by the Mediterranean climate research community. The initiative follows previous existing initiatives and utilizes new fully coupled Regional Climate System Models (RCSMs) and Regional Climate models (RCMs) of very high resolution, up to 10 km. This way, the scientific community can benefit by the use of regional atmospheric, land surface, river and oceanic climate models and coupled regional climate system models, with the purpose of increasing reliability of past and future regional information, while at the same time comprehending the procedures responsible for the distinct characteristics that define the Mediterranean climate type. Twenty (20) modeling groups from nine (9) countries in Europe, Middle-East and North-Africa (France, Italy, Spain, Serbia, Turkey, Israel, Tunisia, Germany, and Hungary) constitute Med-CORDEX's source of input. More precisely, nine (9) atmosphere RCMs, eight (8) regional ocean models and twelve (12) Regional Climate System Models are included. The community meets regularly in dedicated workshops that take place in the participating countries. Med-CORDEX is a coordinated contribution to CORDEX, a World Climate Research Programme (WCRP), whose purpose as stated by its creators is to "advance and coordinate the science and application of regional climate downscaling through global partnerships."
3. The term Regional Climate Downscaling (RCD) refers to a process according to which Regional Climate Models (RCM) and Empirical Statistical Downscaling (ESD), applied over a limited area and driven by Global Climate Models (GCMs), can provide information at much smaller scales. RCMs provide prediction information for areas sized around 1000 x 1000 km. For many vulnerable regions across the world, especially for the ones featuring intense topographic variation such as the Mediterranean region, the aforementioned procedure can contribute towards supporting more detailed impact and adaptation assessment.
4. GCM models provide the scientific community with projections illustrating future climate change, with the purpose of aiding the international community to coordinate climate change mitigation actions. For regional adaptation actions, information aimed at the local level is crucial for tackling the consequences of climate change locally. For that purpose, RCD was

developed and addressed using both statistical and dynamic approaches. Statistical approaches are primarily based on statistical relationships developed between large-scale and regional-scale projections, and then applied to the output derived from climate model simulations. Dynamical approaches consider physically-based models, such as high-resolution and variable - resolution global atmospheric models (Giorgi et al., 2009).

5. Simulations taking place within the Med-CORDEX initiative gather three kinds of runs (evaluation, historical and scenario) and four kinds of regional models (atmosphere, land-surface, ocean and coupled RCSM) that are classified in two categories: CORE simulations and TIER1 simulations. Evaluation runs use the ERA-Interim reanalysis, a global atmospheric reanalysis from 1979, continuously updated in real time (Uppala et al., 2008), as lateral boundary conditions. Historical and scenario runs use six different GCMs from Coupled Model Intercomparison Project Phase 5 (CMIP5), a framework that provides a set of coordinated climate model experiments aimed towards addressing several scientific questions raised during the preparation of the Intergovernmental Panel on Climate Change (IPCC) Fourth Assessment Report (AR4). (Taylor et al., 2012)
6. CORE simulations follow the CORDEX frame over the Mediterranean domain and include Atmosphere-Land only simulations, simulations 50 km over the MED-44 CORDEX domain, evaluation run (89-2008 minimum), historical (1981-2005 minimum, 1950-2005 advised) and scenario runs (2011-2040 or 2041-2070 minimum, 2006-2100 advised).
7. Tier 1 simulations include the extension of the ERA-Interim evaluation CORDEX runs to the longest possible period extending to the present using: the most recent evaluation data available and field campaign results for the advised period ranging from 1979 until 2013; the production of an ensemble of higher-resolution atmosphere RCM with a target resolution of 0.11°, about 12 km; the production of an ensemble of simulations with coupled Regional Climate System Models (RCSM), with fully interactive Atmosphere-Land surface-River-Ocean components, covering the whole Mediterranean basin at high resolution; and the production of stand-alone simulations for all the components of the RCSM.

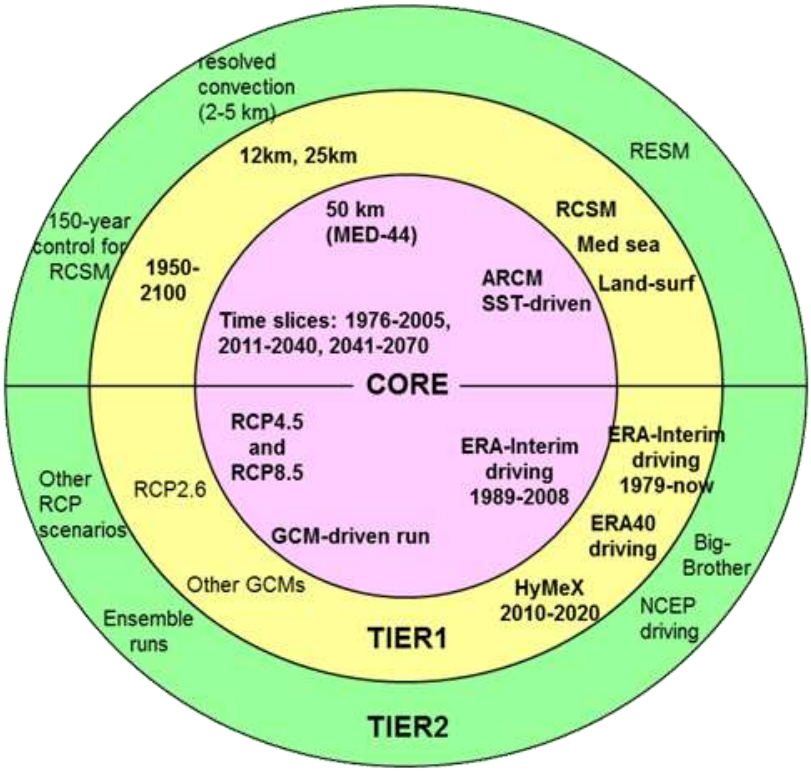

Figure 19. Infographic describing Med-CORDEX simulation types. Source: www.medcordex.eu

Registered modeling groups include: ENEA, CNRM, LMD, MPI, IPSL, Univ. Belgrade, UCLM, UPM, INSTM, KIT, GUF, UAH, IC3, CMCC, ENSTA, MERCATOR, TAU, ITU, IIBR, Eotvos Lorand U and the participating models are the following: nine Atmosphere-only 50-25 km RCM (RegCM3, RegCM4, ALADIN, REMO, LMDZ, EBU, WRF, COSMO-CLM, PROMES), four Atmosphere-only 10-20 km RCM (RegCM4, ALADIN, WRF, COSMO-CLM), eight Ocean-only regional models (MITgcm, NEMOMED8, MPIOM, NEMOMED12, MOSLEF, POM, INSTM-MED, NEMO-MFS), twelve fully coupled RCSM (at least ocean-atmosphere) (ENEA, MPI, CNRM, LMD, Univ. Belgrade, MORCE-MED, UCLM/UPM, INSTM, COSMO-CLM, UAH, IC3, CMCC) and six GCMs used for the scenario runs (CNRM-CM5, IPSL-CM5, HadGEM, MPI, CMCC, EC-Earth).

For this study, we made use of the SMHI datasets for a time period ranging from 1971 until 2100. A control period from 1971 until 2000 was considered for the sake of comparison between those values and the ones derived by observational data. Other options regarding the optimal choice of the control period were initially considered, such as the most commonly used ranging from 1981 to 2010. This option was rejected because the current CORDEX model ends in 2005 and scenarios are applied starting from the year 2006. Another option would be the period from 1986 until 2005, which was also used the latest IPCC report, but this period would not have been statistically reliable regarding the datasets that are available to us for our study areas.

3.2.1. Software

For the evaluation of the present precipitation conditions we used the .exe program made available by the WMO in order to calculate the SPI values. This software takes into account the whole time series for the calculation of values. However, in order to evaluate the models, we need to only consider the timeframe between 1971 and 2000 as the control period. Such a task cannot be completed using the WMO's software. To this regard, R was used. R is a programming language and statistical computing environment widely used among statisticians and data analysts. It provides a wide variety of statistical and graphical techniques; many extension packages are available via the CRAN family of internet sites covering many diverse fields in modern statistics. R is available as free software. It was developed by John Chambers and colleagues. As R is widely used in the analysis of a variety of scientific subjects, several packages have been created. In this case, we used the package SPEI (Calculation of the Standardized Precipitation-Evapotranspiration Index) (https://cran.r-project.org/web/packages/SPEI/index.html).

This package allows for the computation of both SPEI and SPI indices, with the SPI index, that is of interest to this thesis, being a wrapper for SPEI. The functions standardize a variable following a log-Logistic distribution function, with the input variable being a time ordered series of precipitation values for SPI (Vicente-Serrano et al.,2010). This package offers a great degree of parameterization contrary to the software provided by the WMO. Although the function by default uses the whole data series for parameter fitting, it is possible to be modified in a way that takes into account a specific reference period with a well defined beginning and an end within the time series provided. Nonetheless, the desired index values will be calculated for the entire dataset.

For the statistical analysis of values MS Excel was used, a popular Spreadsheet software developed by Microsoft for the Windows Operating System, and more specifically the Data Analysis tool (Regression Statistics, Correlation, f-test and T-test). In addition, SPSS a popular predictive analytics software developed by IBM, was also used for the computation of large volumes of data. Plotted maps were created with the ArcGIS and IDL (Interactive Data Language) software. The interpolation method used in both cases was Kringing.

3.3 The Standardized Precipitation Index (SPI) Index

For the purpose of studying drought conditions, numerous drought indices were developed. Those indices are able to effectively illustrate large volumes of precipitation data in a comprehensive format. They provide a quantitative method for determining the beginning and the end of a drought event and its severity level. Over the past 20 years, various indicators and indices have been developed, suitable for several scales and applications, in order to supply decision and policy makers with options for tackling the challenge of addressing the public when facing environmental problems (WMO, 2016). It is important that the selected index allows for the timely detection of a drought event successfully leading to mitigation actions through communication and coordination. Moreover, it's crucial that they supply with reliable results taking into account the available historic record.

In this case, the SPI index was selected because it successfully exposes climate change effects and comprises a starting point for meteorological drought monitoring. The index is based upon the relationships of drought to frequency, duration and timescales and was recommended by the World Meteorological Organization as the "main meteorological drought index that countries should use to monitor and follow drought conditions". It can be calculated for multiple timescales and the only input data required is monthly precipitation values. Contrary to most indices whose calculation solely depends on station-based data, the SPI can be also calculated for gridded precipitation datasets. Since gridded datasets are utilized for our case study, SPI provides us with the ability to successfully work with them, using the same method as we would facing observational data. Another characteristic of the SPI index that's of great importance is the fact that the program used for the calculation of values can compute for short periods of record for which data is missing.

McKee, Doesken and Kleist designed the Standardized Precipitation Index (SPI) in 1993 in order to quantify the precipitation deficit for multiple time scales. Various indices of several complexity levels have been developed over the years aiming to quantify drought, the Palmer Drought Severity Index (PDSI) being the most prevalent. It is however essential that a drought index is flexible and simple and the PDSI is not. The reason for this is that the PDSI is strongly driven by the variation in precipitation. According to McKee *et al.,*(1993) it "correlates highest to an SPI with a 10- to 14- month time scale". Also, compared to the PDSI the SPI responds better to agricultural stress stemming from short-term drought events. The calculation of the SPI is solely based on precipitation data and is fairly easy. This asset combined with the ability of the Index to adapt to different conditions and time-scales consisted the SPI a powerful tool. It is extensively used for drought monitoring across the United States with The Colorado Climate Center, the Western Regional Climate Center and the National Drought Mitigation Center being the most notable examples. Apart from the US, the SPI is used in research (institutions, universities) or operational mode (National Meteorological and Hydrological Services) in more than 70 countries. It's a powerful tool for decision makers, due to its nature which relies on probability.

The SPI can be calculated for any location, being a normalized index that provides reliable results for both wet and dry climates. However, it is not suitable for climate change analysis on its own, since temperature values are not considered input data for the calculation of the index. Evapotranspiration data is addressed in a new variation of the Index developed by Vicente-Serrano *et al.,*in 2010, the Standardized Precipitation and Evapotranspiration Index (SPEI). SPI's initial purpose was to determine the impact of drought on the available water resources.

SPI uses a probability distribution function on which a long-term precipitation record for a desired period of time is fitted. It is then normalized so that SPI values are depicted as standard deviations from the median. This is the reason why SPI can deliver results regardless the climate conditions prevalent in the area of study. For a specific location and time period the mean SPI equals to zero (Edwards & McKee, 1997).

More specifically, the SPI value is based on cumulative probability of a given rainfall event occurring at a station. The probability distribution function is a Gamma distribution, which according to Thom (1966), fits precipitation time series quite well. The rainfall distribution at a specific station is successfully represented by a cumulative probability function. A drought event likely occurs whenever the probability of a rainfall event is low on the probability cumulative function at a specific station. Therefore, rainfall functions as the variate in a Gamma distribution function as seen below (Eq. (2)):

$$g(x) = \frac{1}{\beta^{\alpha}\Gamma(\alpha)} x^{\alpha-1} e^{-x/\beta} \qquad \text{for } x>0$$

where: *Eq. (2)*

$\alpha > 0$	α is a shape parameter
$\beta > 0$	β is a scale parameter
$x > 0$	x is the precipitation amount
$\Gamma(\alpha) = \int_0^{\infty} y^{\alpha-1} e^{-y} dy$	$\Gamma(\alpha)$ is the gamma function

The standard deviation and the mean utilized by the Gamma distribution function depend on the specific characteristics of each station. Therefore, it's not possible to compare data derived from different stations with each other. For this reason, this cumulative probability Gamma distribution is transformed into a normal distribution with a mean of zero and a standard deviation equal to one. Each rainfall amount in the Gamma distribution corresponds to an amount in the normal distribution. This results to a uniform set of values with respect to data from multiple stations.

The SPI is essentially a z-score, the number of standard deviations an event distances itself from the mean. Standard deviation can be considered as the unit in which the SPI is measured and is defined as the value along a distribution at which the cumulative probability of an event occurring is 0.1587.

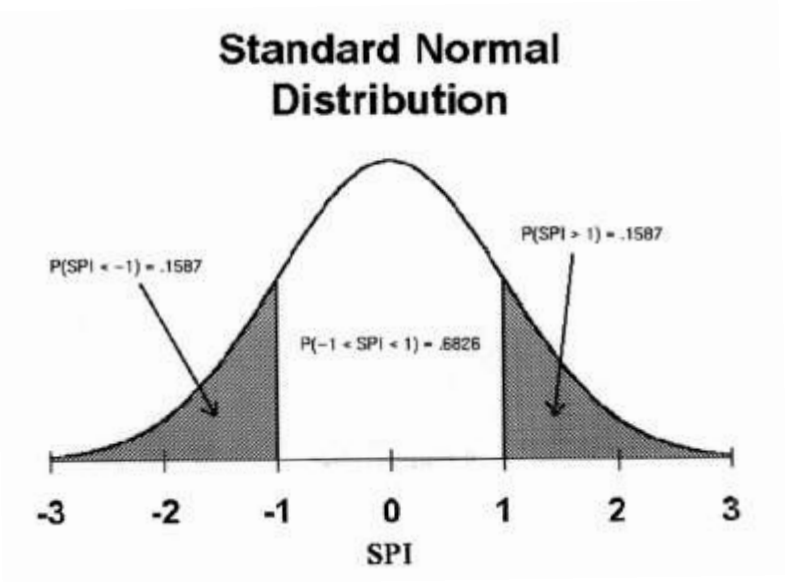

Figure 20. Standard normal distribution with the SPI having a mean of zero and a variance of one. Around 16% of the time, the SPI values under -1.0, indicating drought conditions, 68% of the time between -1.0 and +1.0 indicating normal precipitation conditions, and around 16% of the time over +1.0 indicating anomalously wet conditions (Edwards & McKee, 1997).

Table 3. and Corresponding Cumulative Probability in Relation to the Base Period (Edwards & McKee, 1997)

SPI	Cumulative Probability
-3,0	0,0014
-2,5	0,0062
-2,0	0,0228
-1,5	0,0668
-1,0	0,1587
-0,5	0,3085
0,0	0,5000
+0,5	0,6915
+1,0	0,8413
+1,5	0,9332
+2,0	0,9772
+2,5	0,9938
+3,0	0,9986

A positive SPI indicates precipitation that's greater than the median, while a negative one, signifies a drought event. The severity of a precipitation event, is classified according to Table 3, established by McKee and others in 1993. Whenever the SPI values are continuously negative and their cumulative intensity reaches at least -1.0, a drought event is reported. Respectively, whenever a continuous positive SPI is witnessed with an intensity of at least +1, an extreme precipitation event occurs. In both cases, the end of any precipitation event is signified by the change in value sign.

3.4 Statistical Analysis

All the necessary calculations regarding the statistical analysis of the time series will take place using appropriate software (MS Office, Excel 2016, Data Analysis Tool).

ANOVA stands for Analysis of variance and comprises of a variety of statistical models whose aim is to analyze the differences among group means and procedures associated with them. For this thesis, the regression, correlation, f-test and t-test operations were used.

3.4.1 Regression analysis

A fundamental statistical method for the calculation of relationships among variables. In particular, it's a method according to which, the manner and severity of the impact one variable inflicts to another is defined. In other words, how the value of the dependent variable changes whenever any one of the independent variables is varied, while the other independent variables are held fixed. In every occasion where two variables connect with a functional relationship Y = f (X), for every X value a Y value can be calculated. Regression analysis aims at defining such a relationship between two sets of values, whenever one exists, utilizing the smallest possible error. This function (model) can be linear or have any other form.

Simple linear regression is explained as an approach for modeling the relationship between a dependent **Y** variable and an independent **X** using a linear function that takes the general form:

$$y_i = a + bx_i \qquad \textit{Eq. (3)}$$

Where **a** and **b** stand for the constants that define the function.

The method of least squares is a standard approach in regression analysis to the approximate solution of systems in which the number of unknown factors exceeds the number of equations. Such a situation is usually encountered whenever a system is constructed using random coefficients. In order to avoid subjective solutions when determining a function that describes the relationship between two data sets, we utilize this method. Out of all the available solutions, for a specific number of values the one compliant with the following property is considered ideal:

$$D_1^2 + D_2^2 + \ldots + D_n^2 = minimum \qquad \textit{Eq. (4)}$$

That means that the solution minimizes the squares of errors in the results of every single equation. The most commonly used method, is the linear least squares method, from which a linear function is derived. In order to define the **a** and **b** constants of the function, the following forms are followed, where **a** equals the **Y -** intercept and **b** equals the slope of the line:

$$a = \frac{\sum_{i=1}^{n} y_i \cdot \sum_{i=1}^{n} x_i^2 - \sum_{i=1}^{n} x_i \cdot \sum_{i=1}^{n} x_i y_i}{n \cdot \sum_{i=1}^{n} x_i^2 - \left(\sum_{i=1}^{n} x_i\right)^2}$$

$$b = \frac{n \sum_{i=1}^{n} x_i y_i - \sum_{i=1}^{n} x_i \cdot \sum_{i=1}^{n} y_i}{n \sum_{i=1}^{n} x_i^2 - \left(\sum_{i=1}^{n} x_i\right)^2}$$

$$b = \frac{\sum_{i=1}^{n} (x_i - \bar{x})(y_i - \bar{y})}{\sum_{i=1}^{n} (x_i - \bar{x})^2}$$

Eq. (5)

The aforementioned equation refers to the available samples. There are problems however, that require the definition of the function that describes the statistical population from which the sample is collected. Constant **b**, displays the quantitative manner according to which the **Y** variable is affected by changes applied on the **X** with respect to the available samples, but cannot supply with reliable information regarding the statistical population. To this end, we need to define the limits within which the **B** constant referring to the population is most likely to occur, using the form: $\boldsymbol{t = \frac{\beta - b}{s_b}}$ *Eq. (6)*, following Student's t-test (***n-2*** degrees of freedom) where $\mathbf{S_b}$ equals to the typical error of six (6).

Confidence levels for **B**, are calculated using the following formula:

$$\boldsymbol{b - t_{a/2} \times S_b \leq \beta \leq b + t_{a/2} \times S_b}$$ *Eq. (7)*

$\boldsymbol{t_{\alpha/2}}$ equals to the critical values regarding significance levels and is calculated using the t-table. Confidence level ***(p)*** and Significance level ***(α)*** are two different notions.

They relate to each other with the formula: $\boldsymbol{p = 1 - \alpha}$. *Eq. (8)*

For example, if $\boldsymbol{\alpha = 0,05\ (or\ 5\%)}$ then $\boldsymbol{p = 95\%}$

Statistical significance is crucial when it comes to statistical hypothesis testing. Its functionality is to determine whether the null hypothesis $\mathbf{H_0}$ (the hypothesis assuming that no change has occurred) should be rejected or retained (Meier et al.,2009). In order for it to be rejected, a statistically significant result needs to be detected. To this regard, a p-value is calculated. The **p -value** responds to the probability of an event's observance assuming the null hypothesis is true. The null hypothesis is rejected if the p-value is less than a level determined by the **t-table** (significance level).

This in fact means that we're falling under a type I error (the incorrect rejection of a true null hypothesis; the assumption that a supposed effect or relationship exists when indeed it doesn't). The significance level is usually set at 5%, which means that a statistical significant result is observed in case the **p-value** is less than 5% and the rejection region comprises 5% of the sampling distribution (McKillup, 2006). In case this 5% is allocated towards one side of the sampling distribution we are referring to a one-tailed test, accordingly, if it's partitioned to both sides, to a two-tailed, with each tail enclosing 2,5%. Whether to use a one-tailed or a two-tailed test depends on the type of survey taking place and the type of available data.

3.4.2 Correlation analysis

This type of analysis indicates the general relationship between two variables, without considering the magnitude of this relationship. This occurs via the **r** coefficient, which does not evaluate a quantitative change a variable experiences in relation to another variable, but the strength of the "link" between those two variables. The correlation coefficient **(r)** is determined using the following formulas in which the denominator is always positive while the coefficient's sign depends on the sign of the numerator:

$$r = \frac{\sum_{i=1}^{n}(x_i-\bar{x})(y_i-\bar{y})}{\sqrt{\sum_{i=1}^{n}(x_i-\bar{x})^2 \cdot \sum_{i=1}^{n}(y_i-\bar{y})^2}}$$

$$r = \frac{n\sum_{i=1}^{n} x_i y_i - \sum_{i=1}^{n} x_i \cdot \sum_{i=1}^{n} y_i}{\sqrt{\left[n\sum_{i=1}^{n} x_i^2 - \left(\sum_{i=1}^{n} x_i\right)^2\right] \cdot \left[n\sum_{i=1}^{n} y_i^2 - \left(\sum_{i=1}^{n} y_i\right)^2\right]}} \quad \text{Eq. (9)}$$

If **r > 0** whenever one variable increases, the other one increases as well
If **r < 0** whenever one variable increases, the other one decreases
If **r = 0** no linear relationship between the two variables is observed

R coefficient is a net number within the numerical region **-1 ≤ r ≤ 1** and its sign is the same as **b**. $\mathbf{r^2}$ signifies the Coefficient of determination and indicates the amount of **Y** variance (dependable variable) from **X** (independent variable), explained by the form **Y = f (X).**

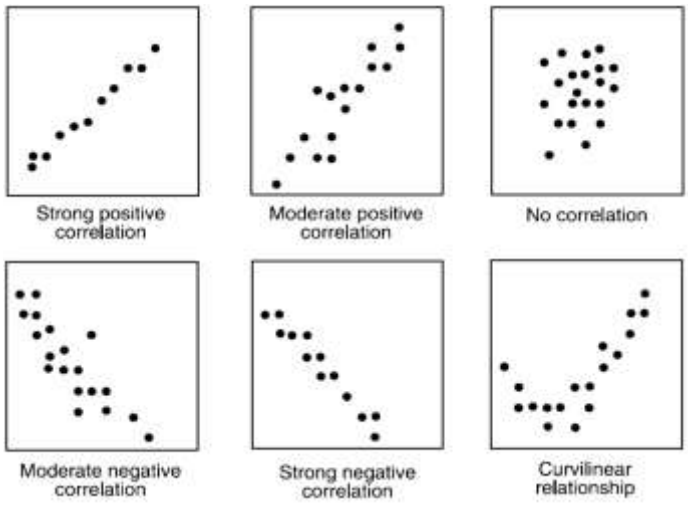

Figure 21. Scatter diagrams displaying various correlation types.

In climatology time series are studied extensively. A time series is a sequence of variable values reported at successive equally spaced points in time and can be stationary or non-stationary. A non-stationary times series displays a trend (slow variance in its mean value over time), periodicity or seasonality (variance occurring due to season change) and abrupt change, due to random external factors.

For our case study, linear trends corresponding to the evolution of values of the studied indices over time were computed. The variable's variance remains constant throughout the whole time series length. Linear trends can be calculated using regression analysis methods. More specifically, the linear regression is defined where the b coefficient equals to the time series trend. Statistical significance is analyzed using the **t-test** while accepting as the null hypothesis $\mathbf{H_0}$, the fact that time series displays no trend.

In order to investigate the dependence between multiple variables at the same time, a correlation matrix is created; a table containing the correlation coefficients between each variable and the others. The diagonal elements of the correlation matrix correspond to the correlation of a column with itself and therefore

equal to 1. A correlation matrix is always symmetric since e.g. the correlation of column a with column b is the same as the correlation of column b with column a. To this end, it is usual that the upper right half of the table is completely omitted.

3.4.3 Variance analysis

An F-test tests if the variances of two examined populations are equal and can be a one-tailed or a two-tailed test (Snedecor and Cochran, 1983). The preferred version of the test is determined by the problem that is addressed. A one-tailed test examines whether the variance of the first population is either greater or smaller than that of the second population; therefore it tests in one direction. Respectively, a two-tailed test examines whether the variance of the first population is greater or less than that of the second population examining in both directions.

Variance is defined as the square of the standard deviation and is used as a measure of dispersion, meaning the larger the value corresponding to Variance is, the further away data values are scattered from the mean value. An F-test is practically a ratio of Variances of the two populations involved.

$\boldsymbol{F} = \frac{S_1^2}{S_2^2}$, where $\boldsymbol{S_1^2}$ and $\boldsymbol{S_2^2}$ are the Variances of those populations *Eq. (10)*

The null hypothesis ***(H_0)*** states that the two variances are equal: $\boldsymbol{S_1^2 = S_2^2}$

Therefore the further away this ratio is from 1, the larger the difference between the variances. The test is defined as:

$\boldsymbol{\sigma_1^2 < \sigma_2^2}$ (lower one-tailed test)

$\boldsymbol{\sigma_1^2 > \sigma_2^2}$ (upper one-tailed test)

$\boldsymbol{\sigma_1^2 \neq \sigma_2^2}$ (two-tailed test)

The null hypothesis ***(H_0)*** is rejected, and therefore the difference in variance between the populations is statistically significant, if the following is true:

For a one-tailed test:

$\boldsymbol{F > F_{critical}}$ (upper one-tailed test) and $\boldsymbol{F < F_{critical}}$ (lower one-tailed test)

For a two-tailed test:

$\boldsymbol{F < F_{critical}}$ or $\boldsymbol{F > F_{critical}}$

The $\boldsymbol{F_{critical}}$ value is defined by preexisting tables and takes into account the degrees of freedom.

The significance level (α) is defined as the probability of rejecting the null hypothesis when it's true. By the commonly used ***α = 0,05*** (Figure 23), there's a possibility of 5% spotting a difference between Variances, when in fact, there is none. In statistics a sample is analyzed in order to conclude for the population this

sample originates from, it is therefore impossible to imply that the two are the same no matter how closely the sample resembles the entire population. For a one-tailed test this fact is visualized by the 5% of values towards the selected tail of the distribution. For a two-tailed test however, the 5% is distributed between the two tails, resulting to 2,5% for each tail.

A two-sample t-test determines whether the means of two populations are equal (Snedecor and Cochran, 1989). It's possible that the data is paired or not paired. In paired samples there's a one to one correspondence between the values, in other words both samples include the same number of values. In order for this correspondence to make sense the two populations need to be related and represent the same subject. This type of test is usually used to assess "before" and "after" conditions. This is the case encountered in this thesis. The reason why a paired t-test was used to analyze Model Data, is because time periods of the same duration are tested and a change is in fact tracked. The objective is to determine whether precipitation conditions will change in the future for a period lasting as long as the control period for the same location.

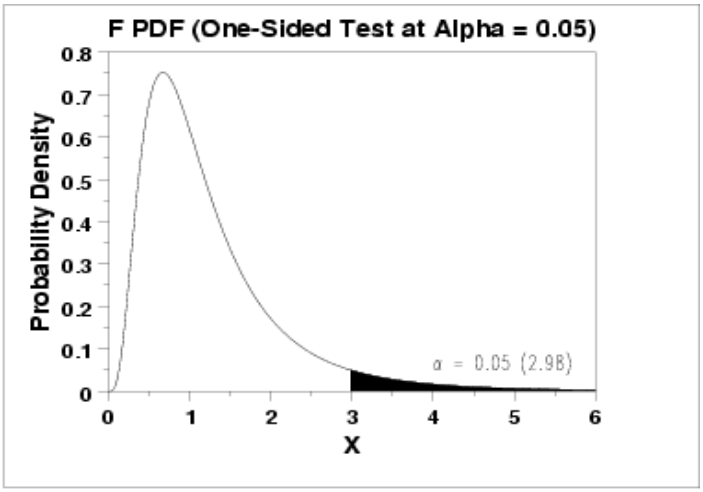

Figure 22 Graph demonstrating a significance level of α = 0,05 in a one-tailed test (Source: http://www.itl.nist.gov)

The null hypothesis ***(H_0)*** assumes that the difference between means equals to zero: $H_0: \mu_1 = \mu_2$ and in order for a difference between means to take place the alternative hypothesis ***(H_1)*** needs to be true:

$$H_1: \mu_1 \neq \mu_2$$

This test is illustrated as a ratio, which for unpaired data equals to:

$$T = \frac{\overline{Y_1} - \overline{Y_2}}{\sqrt{\frac{s_1^2}{N_1} + \frac{s_2^2}{N_2}}}$$

where N_1 and N_2 are the sample sizes, $\overline{Y_1}$ and $\overline{Y_2}$ are the sample means, and S_1^2 and S_2^2 are the sample variances. *Eq. (11)*

The null hypothesis is rejected if the following is true:

$|T| > t_{critical}$, where $t_{critical}$ is the critical value of Student's t-distribution and can be accessed through the respective tables .

4 Results And Discussion

4.1 Current Climate Analysis

4.1.1. Precipitation Analysis

CRU (Climatic Research Unit Data) dataset is available for a time period of over 100 years, thus, it allows for the assessment of the current interannual climate conditions regarding precipitation for the three study areas. Using monthly values, trends were calculated for wet and dry season, respectively. This section is vital to our study in order to provide a wide overview of the areas' hydrological conditions. The SPI index assesses trends in precipitation without, however, evaluating actual precipitation values. Therefore, in order to understand the study areas' climatic background, it is essential to statistically analyze the precipitation values first.

Total annual precipitation values were analyzed for 7 CRU grid points (GP1, GP2, GP4, GP5, GP6, GP7, GP8) that are the same grid points used for drought analysis presented in the following chapters. Trendlines show negative trends for all grid points, however regression statistics analyses show that none of them is statistically significant. The average precipitation for a period of 114 years ranges between 500 and 680 mm. The total average is around 605 mm (Figure 23).

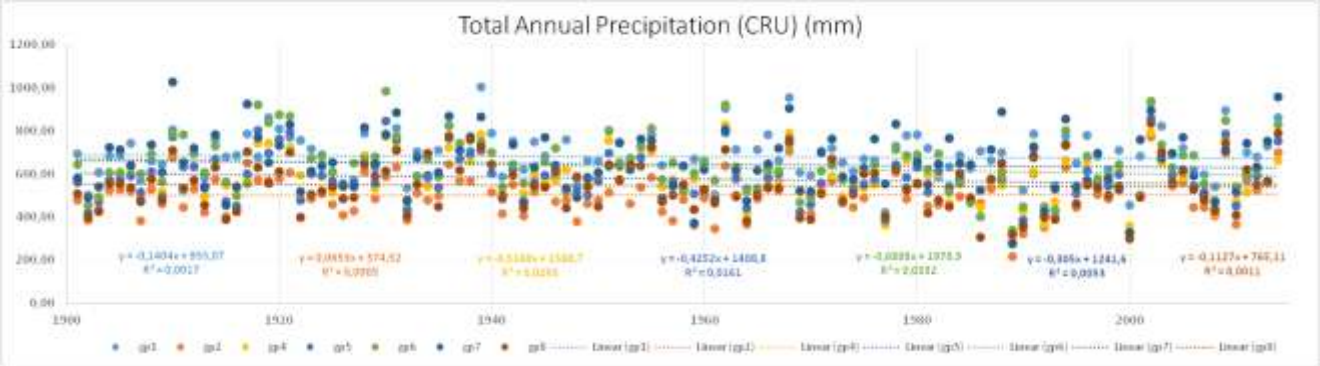

Figure 23. Total Annual Precipitation resulting from CRU datasets. Each grid point of interest is depicted in a different color

Seasonal analysis for winter shows that winter is the wettest season of all with respect to our study area. Total average precipitation for a period of 114 years for all grid points is 272,09 mm. Trendlines resulting from all grid points show non statistically significant negative trends. Two sample F-test analysis shows that during the second half of the century (1958 – 2014) compared to the first half (1901 – 1957) precipitation variability increases, this increase however is not statistically significant (Figure 24).

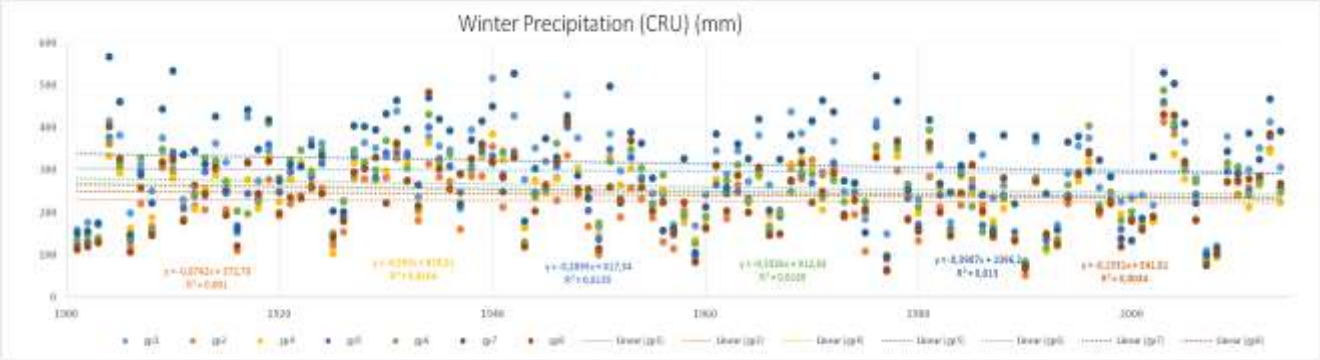

Figure 24. Total Precipitation for the winter season resulting from CRU datasets. Each grid point of interest is depicted in a different color

Regarding spring average total precipitation is much lower than what was witnessed for Winter, just around 120 mm. Trendlines associated with springtime, show both positive and negative trends, however none of them is statistically significant. In most cases precipitation variability is increased for the second half of the century (GP2, GP5, GP7, GP8), but only GP7 (located on the southeast of Loutraki area) is statistically significant (Figure 25).

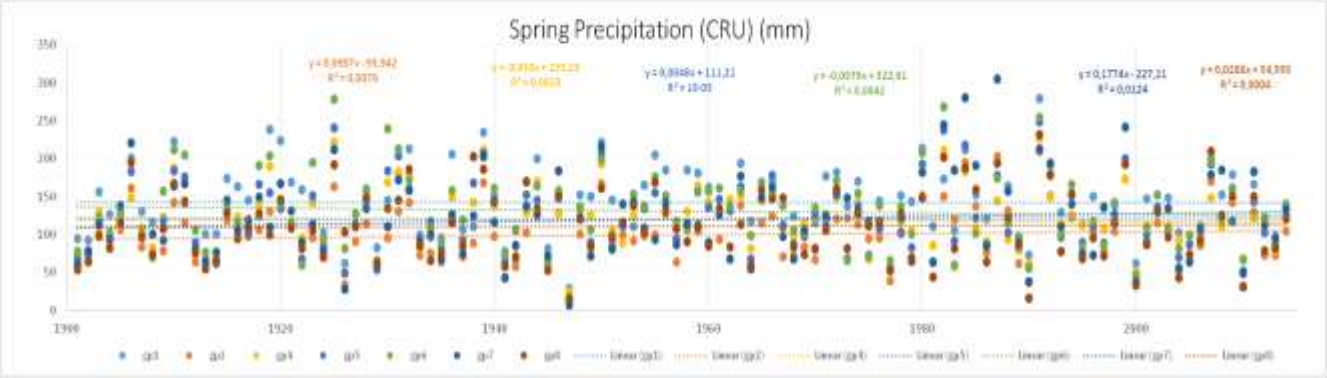

Figure 25. Total Precipitation for the spring season resulting from CRU datasets. Each grid point of interest is depicted in a different color

Summer is the driest season in Greece. Total average is just 34 mm for all studied grid points for a total of 114 years. All trendlines show negative trends, with none of them being statistically significant. This fact verifies that no actual reduction in precipitation has been witnessed during the last 114 years in the areas of interest. Precipitation variability is slightly decreased during summer, but none of the grid points shows a statistically significant result (Figure 26).

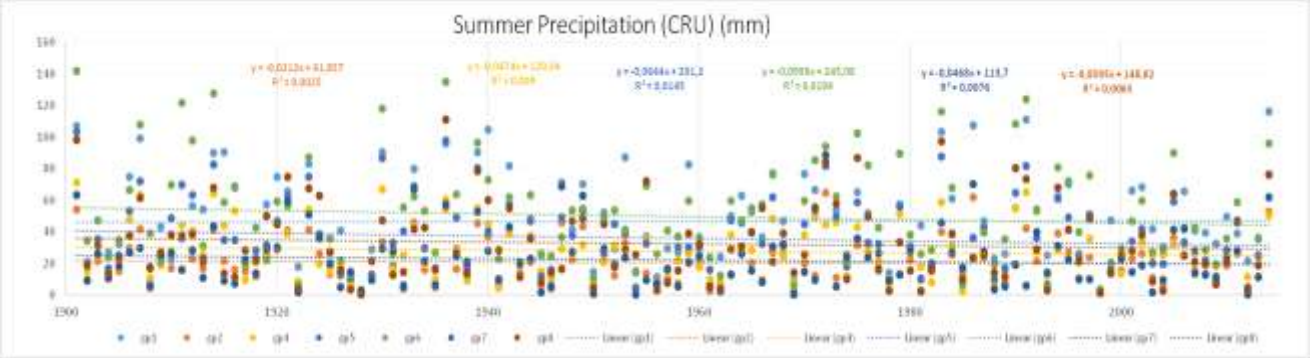

Figure 26. Total Precipitation for the summer season resulting from CRU datasets. Each grid point of interest is depicted in a different color

Finally, Autumn is the second wettest season for Greece. Average precipitation equals to 176.64 mm. Trendlines show both positive and negative trends and none of them is statistically significant. Regarding precipitation variability some grid points witness a slight increase, while some others a decrease, in both cases no statistical significance is observed (Figure 27).

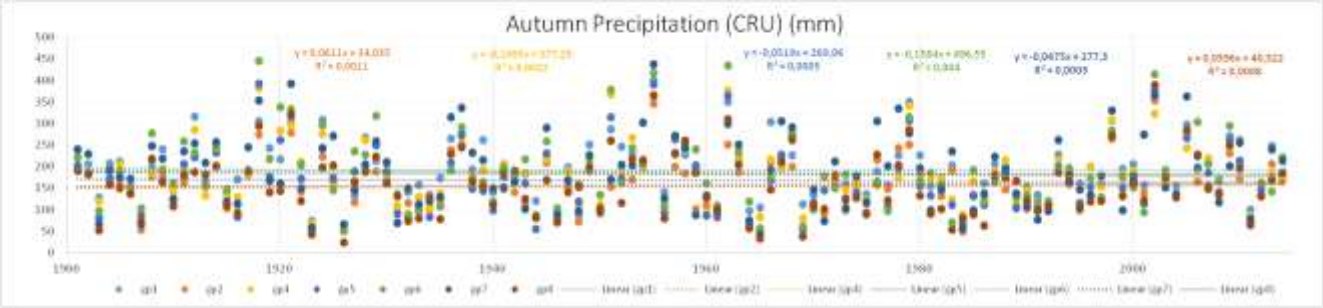

Figure 27. Total Precipitation for the autumn season resulting from CRU datasets. Each grid point of interest is depicted in a different color

All the above findings agree with studies performed with the National Observatory of Athens (NOA). observational data from 1860 to 2008 for the area of Athens, that in close proximity to the areas of interest to this Thesis. Trend and variability analyses applied on those datasets annual and seasonal precipitation displayed no statistical significant long term trend (Founda et al., 2012).

4.1.2. Drought Analysis

4.1.2.1. Dry and Wet Conditions During the 20th Century (CRU SPI)

CRU (Climatic Research Unit Data) provide monthly precipitation values over the last century. They are calculated on high resolution latitude by longitude grids of 0.5 x 0.5 degrees, or 50 x 50 km. They provide a complete image of precipitation trends that took place during the entire 20st century, allowing climate change observations.

The data sets are available for the time period from 1901 until 2014, a timeframe long enough to provide us with the appropriate information on precipitation and drought variability of the examined study areas. For the monthly precipitation values the SPI index was calculated for the timescales of 3, 6 and 12 months, using software provided by the WMO (SPI_SL_6.exe). Specifically, the indices that were calculated are the following:

- **SPI 3** - Displaying seasonal variations
  - February (02), corresponding to winter
  - May (05), corresponding to spring
  - August (08), corresponding to summer
  - November (11), corresponding to autumn
- **SPI 6** - Partitions the annual circle into two seasons; wet and dry
  - March (03), corresponding to wet season
  - October (03), corresponding to dry season
- **SPI 12** - Assessing annual variation

Precipitation and drought trends for the 20th century have been calculated. For each index, a comparative table including all grid points that were studied was created. Each cell represents a specific SPI value for the respective year and grid point; in order to mark the duration and intensity of each extreme precipitation or drought event, a variety of colors is used. Drought events are marked in shades of red; lighter shades respond to lower intensity, while darker shades represent events of higher intensity. Respectively, blue shades are used in order to display extreme precipitation events. Trendline sign is indicated in the first row of each table; positive trends are marked in orange, while negative ones are marked in green.

Statistical significance was studied as well. No statistically significant trends were reported with only one exception (12-month SPI in GP6, approaching Euboea).

4.1.2.2. 3 Month SPI for February

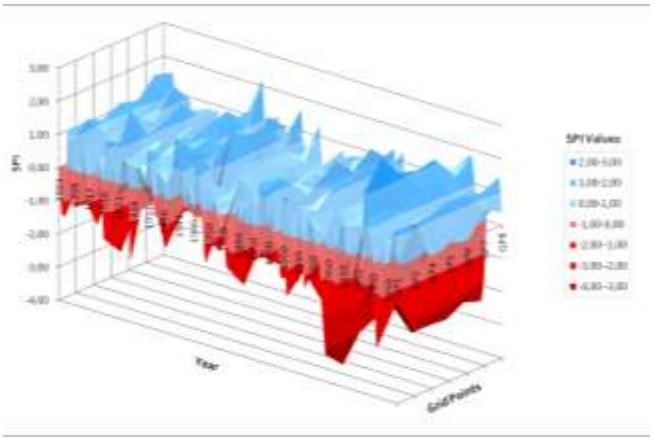

Figure 28 3D Plot showing the SPI 3 for February for all CRU data Grid points Consistency between grid points is obvious.

The 3-month SPI at the end of February compares the precipitation total for the December - February period with all the past totals for that same period. The 3-month SPI by the end of February gives a very good indication of the amount of precipitation that has fallen during the winter season. 3-month SPIs correspond to short to medium- term moisture conditions, estimating seasonal trends in precipitation. It is important to compare the 3-month SPI indices with the ones referring to longer time scales. It's a short term index providing early warning of drought while helping in assessing drought severity (WMO, 2012).

According to the following table (Table 4) compiling SPI index information for all the grid points of interest to our study, several extreme precipitation events were observed. From 1902 until 1903, the first drought event in this time series was encountered, classified as extremely dry for almost every grid point. It was succeeded right after by a two-year extreme precipitation event from 1904 until 1905. In 1906, a short drought made its appearance. From 1909 to 1910 some stations (GP2, GP5, GP6, GP7 and GP8) display a mildly wet incident. Around 1916, a short drought was documented for most stations. Four long wet periods followed, from around 1919 until 1924, 1927 - 1932, 1934-1942 and 1946-1948 marking the first half of the 20th century. The second half of the century began with a mild wet event, that was followed by a severe drought lasting for around 5 years for most of the grid points involved (1955 – 1960). In 1977 an intense short drought occurred, present in all stations. The end of the century was characterized by a variety of events of great intensity. From 1985 until 1990 and 1992-1993 very dry conditions dominated across the whole region. From 1994 to 1996 a three year long wet event took place in most grid points, just to be followed by another long and extremely intense dry period. From 2003 until 2005, extreme precipitation occured. The last drought documented in this time-series, took place from around 2006 until 2008 and was of extreme intensity. From 2014 until the end of the series wet conditions appeared at most.

Trendlines resulting from the statistical analysis of time-series for all grid points, show a negative trend, indicating a slight decrease in precipitation during the winter season taking place during the last 100 years. However, no trend seems to be statistically significant, meaning that although drier conditions seem to appear, the change is so minor that poses no real threat of aridity for the study areas.

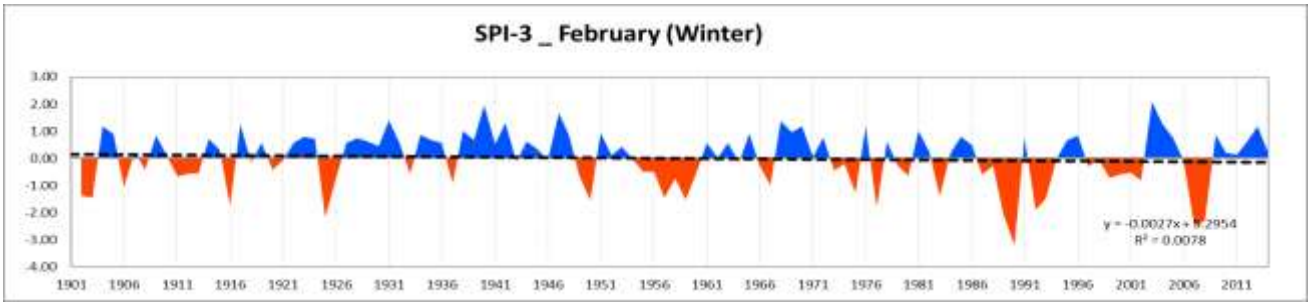

Figure 29 SPI Graph for the GP1 grid point. The negative trendline is typical for all seven grid points that were studied. Graphs available in the Appendix.

Table 4. SPI3 for February - Cumulative Table for CRU data

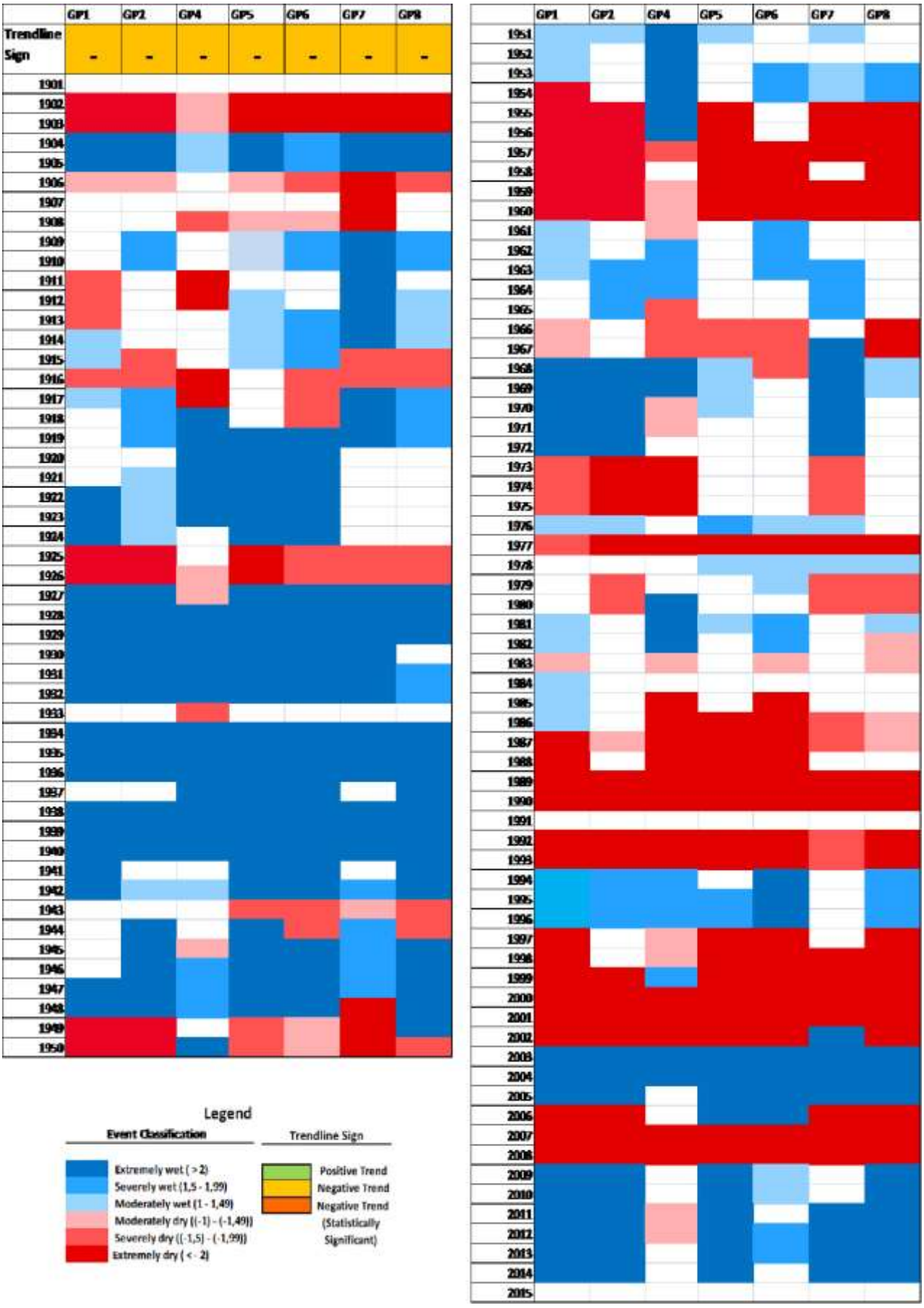

4.1.2.3. 3 Month SPI for May

Precipitation taking place during the spring season is estimated by the 3-month SPI at the end of May. The precipitation total for the period from March until May of each year is compared with all the past totals referring to the same period from the historic record. This particular index is of major importance to agriculture since it estimates precipitation trends and soil moisture conditions during the period where the growing season begins (WMO, 2012).

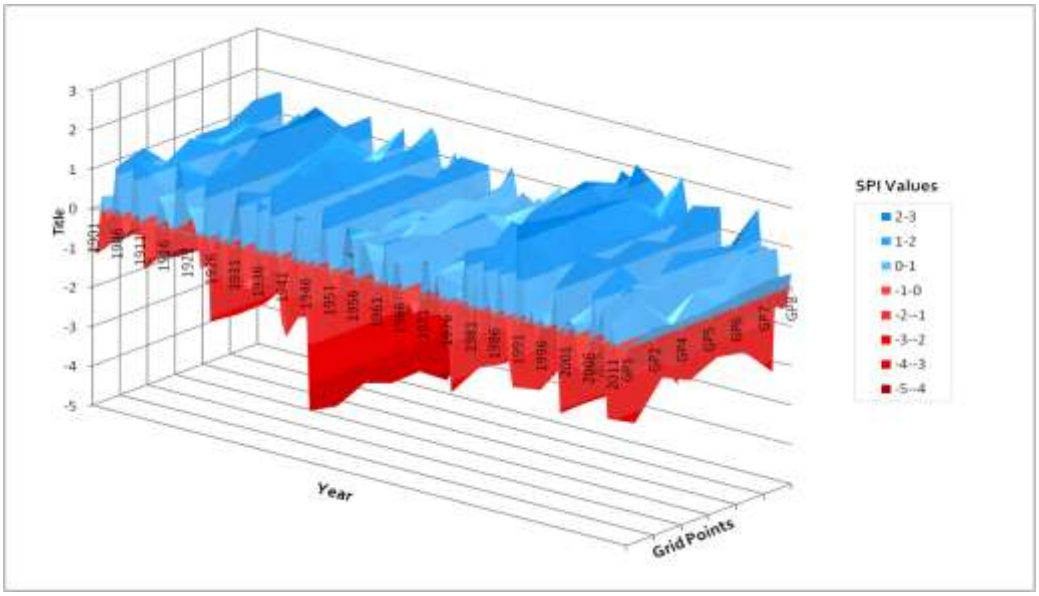

Figure 30. 3D Plot showing the SPI 3 for May for all CRU data Grid point. Consistency between grid points is obvious.

The century begun with dry conditions, with the first severe drought taking place from 1901 until 1904. A mild wet event followed during the years 1905-1906, which was then succeeded by a severe one from 1909-1911. From 1912 until 1914 an extreme drought was recorded. The years to follow displayed relatively wet conditions for most grid points and the year 1925 was characterized by a severe to extreme wet event for all grid points involved. During the years 1926 -1927 and 1929 drought events were documented for the majority of grid points. From 1930 until 1932 extremely wet conditions prevailed. From 1933 until 1935 another extreme drought was witnessed for all grid points except GP5, approaching the Loutraki area. An extremely wet event followed lasting from 1938 until 1940, that was succeeded by an extreme drought lasting two years (1941 - 1942). Wet and dry incidents of moderate importance followed; in 1947 a short extreme drought took place. The beginning of the second half of the century was marked by wet conditions (1948-1966) signifying increased precipitation. For a couple of years (1967-1970) a drought took place in some grid points. In 1977 another drought took place, this time apparent in all grid points. In the following years mainly wet conditions prevailed until in 1989 another extreme drought was encountered lasting for two years, being succeeded by an extreme dry event in the years 1991 to 1992. Mild wet conditions were present for the years 1998-1999, followed by a short but intense drought lasting 1-2 years in the year 2000. From 2003 until 2006 a prolonged extreme event took place. From 2007 to 2009, extremely wet conditions prevailed for most grid points. In 2010 a short drought event was witnessed. The century ends with mild dry conditions (Table 5).

For this index most trendlines show a slight positive trend, but it has to be made clear, that none of them was of statistical significance.

Table 5. SPI3 for May - Cumulative Table for CRU data

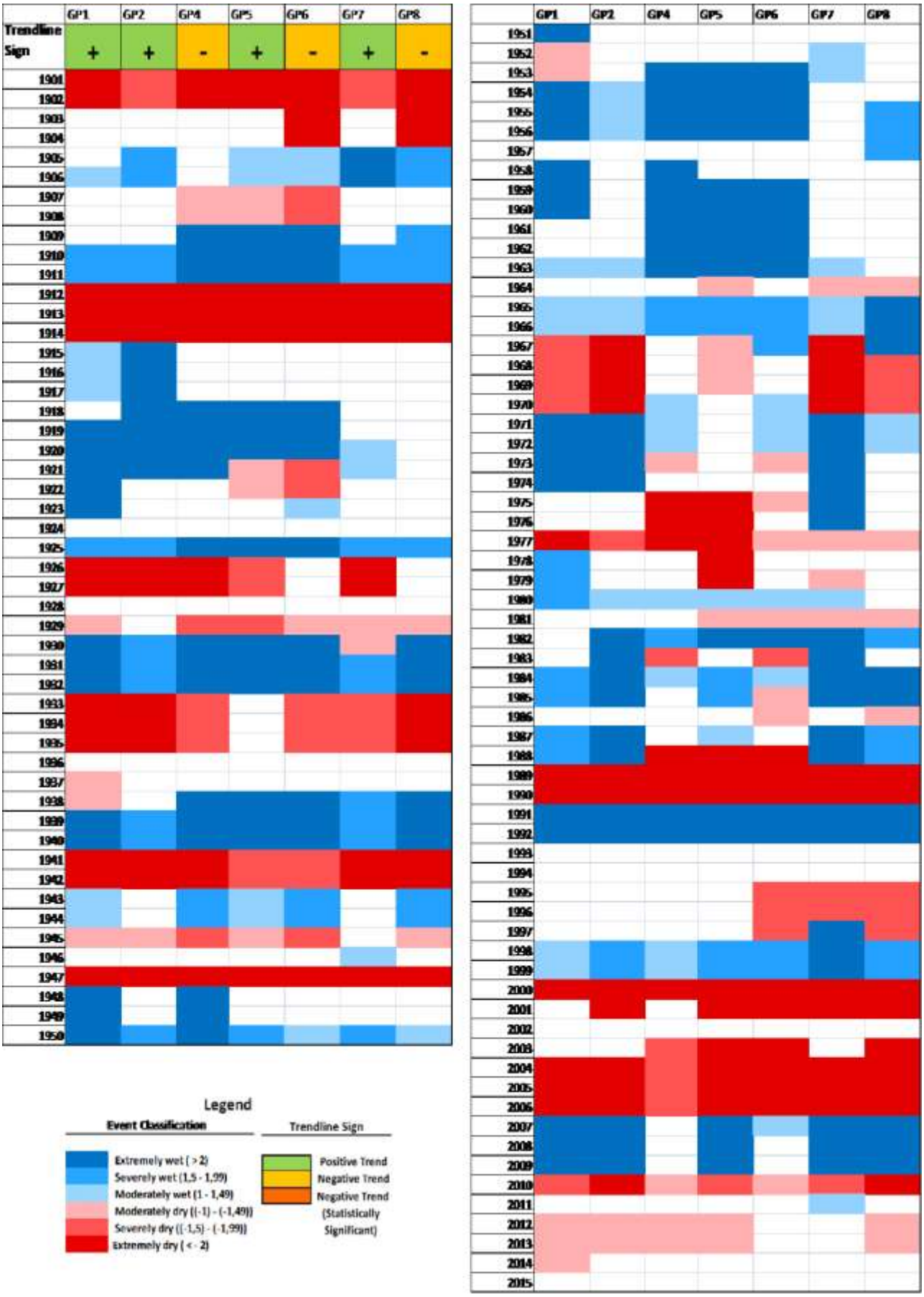

4.1.2.4. 3 Month SPI for August

Respectively, the 3-month SPI at the end of August compares the precipitation total for the summer season lasting from June until the end of August with all the past totals of that same period for the three areas of study. The summer season is recorded to be the driest of all seasons regarding Greece.

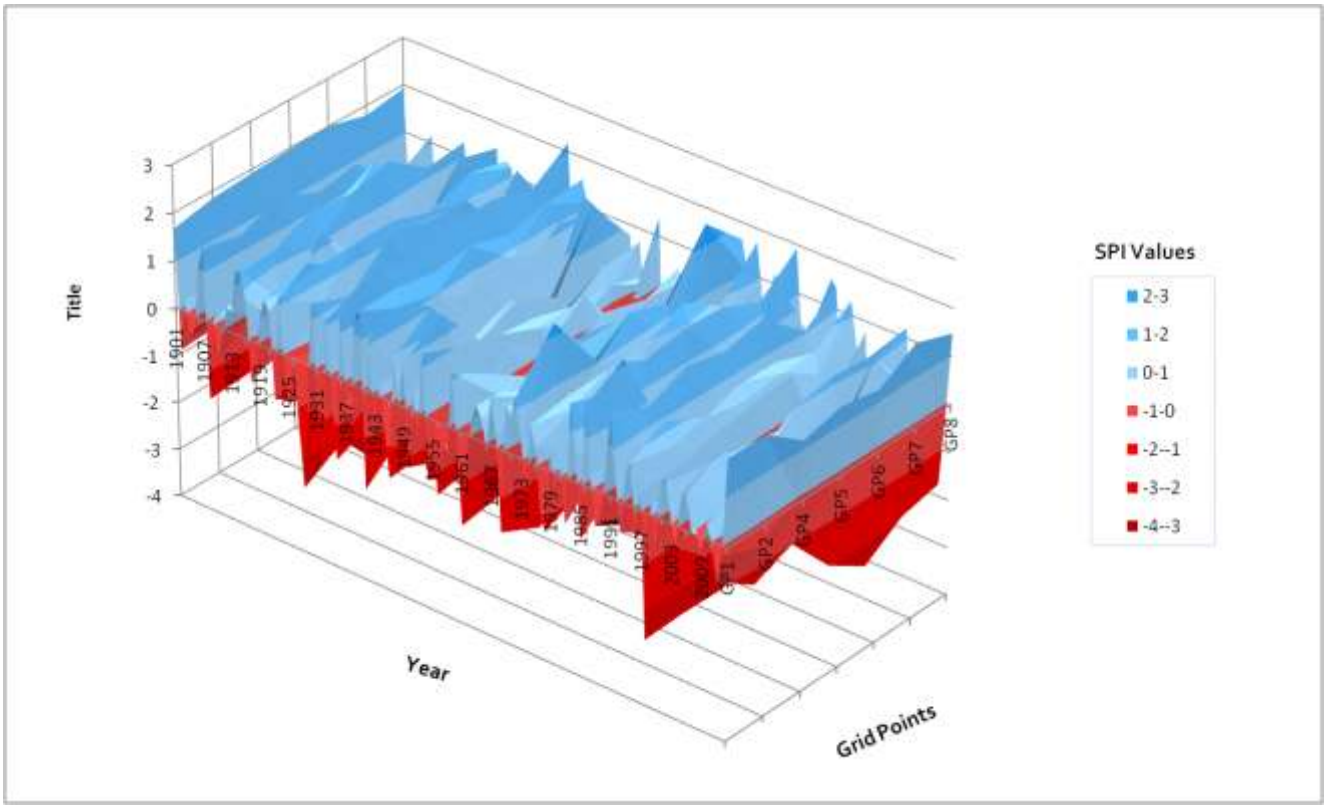

Figure 31. 3D Plot showing the SPI 3 for August for all CRU data Grid points. Consistency between grid points is prevalent.

The beginning of the century shows relatively wet conditions. Around 1925 an extreme drought began, lasting until 1929. A wet event lasting two years took place from 1939 until 1940, a drought event of varied intensity among the grid points was recorded from 1948 until 1949 followed by a mild short drought in 1950. The second half of the century displays dry periods of longer duration. From 1954 until 1962 roughly, extreme drought events were manifested. Until 1976 wet conditions followed, occasionally interrupted by short dry events. 1983 – 1984 was a short wet period for all grid points and respectively, 1988-1989 a short dry one. From 1990 until 1992 wet conditions prevailed. Around the end of the decade (1998), another extreme drought was documented. From 2010 and onwards, dry conditions of varied intensity were present for the most part (Table 6).

Table 6. SPI3 for August - Cumulative Table for CRU data

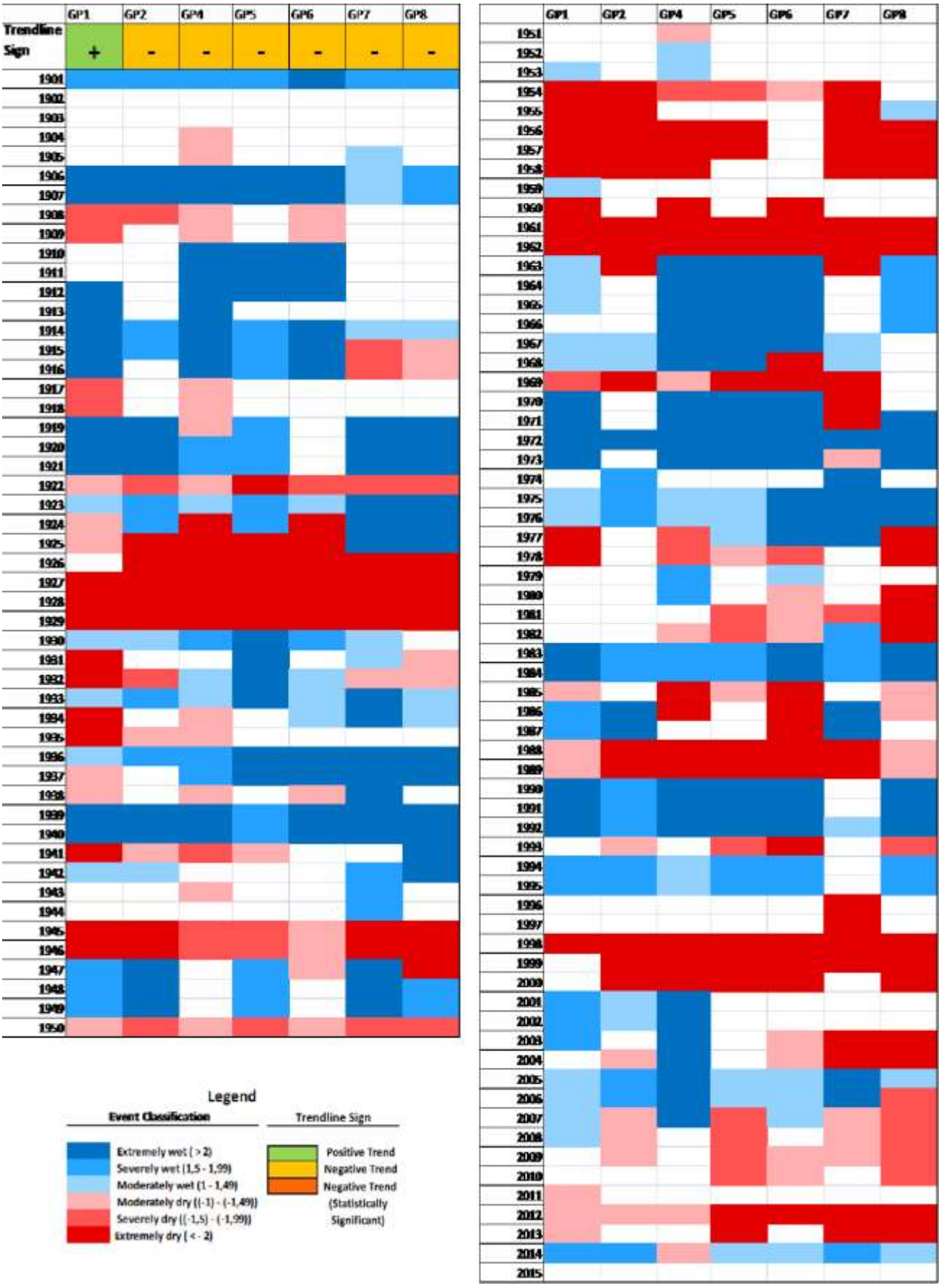

4.1.2.5. 3 Month SPI for November

Finally, the 3-month SPI for November provides a comparison between the precipitation total for the September - November period with all the past totals for that same period, estimating the trends taking place for the autumn season.

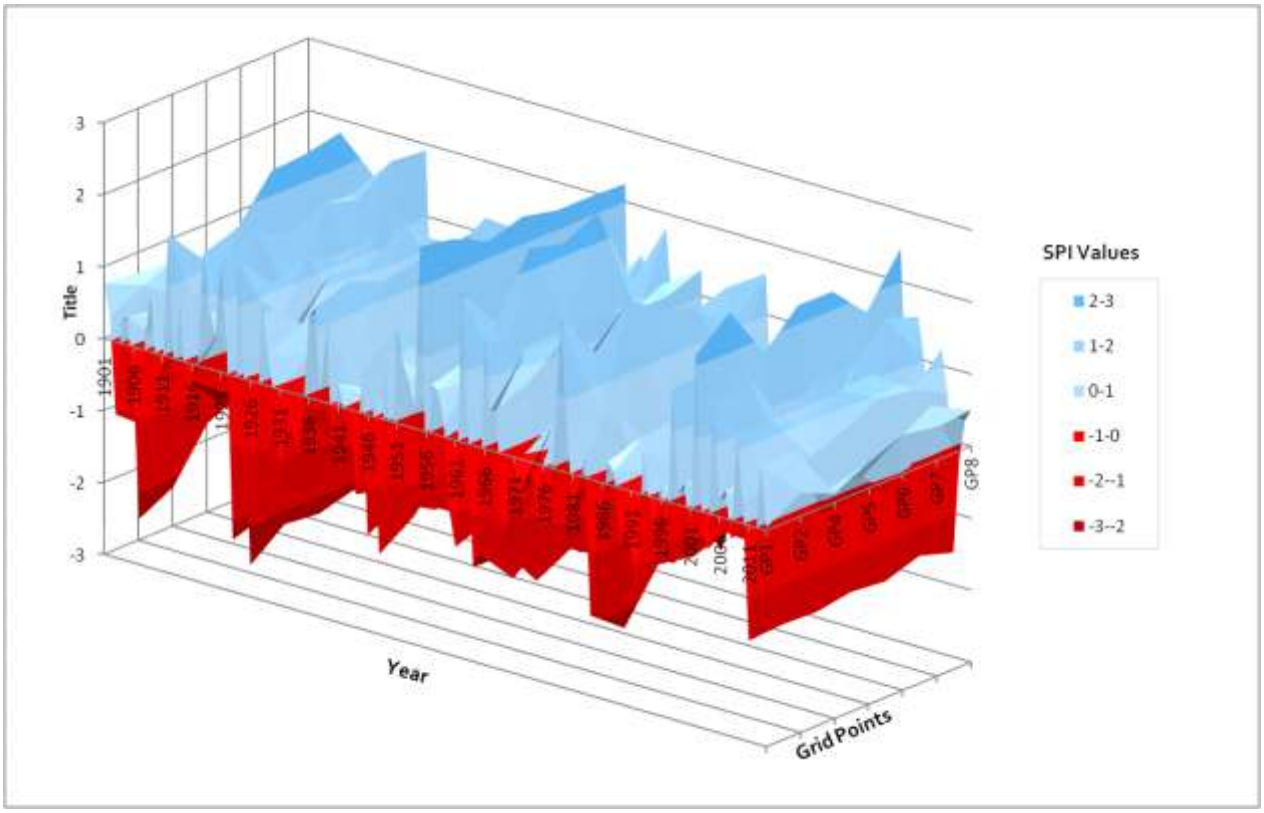

Figure 32 3D Plot showing the SPI 3 for November for all CRU data Grid points. Consistency between grid points is as well observed.

The first drought was encountered from 1906 until 1907 ranging from severe to mild across grid points. Until 1921 wet conditions prevailed with the exception of a mild drought lasting two years (1915 – 1916). In 1923 and 1926 short but intense drought events were manifested in all grid points, followed by extremely wet conditions during the years 1928 until 1930. For 5 years (1931 – 1932) an excessive drought took place that was followed by 2 very wet years (1936 – 1937). The first half of the century demonstrated sparse dry incidents.

From 1951 until 1958 extreme precipitation prevailed. An intense wet event lasting two years followed (1962 – 1963), a short intense drought (1964-1965) and another wet event from 1966 until 1968. For a long period extending from 1969 until 1992 extremely dry conditions dominated, with the exception of a small but intense wet event taking place from 1978 until 1979. The end of the century shows primarily wet conditions. The last drought took place during the years 2011 and 2012 (Table 7).

Generally, 3-month SPIs for Winter and Spring seem to agree, as well as those for Summer and Autumn. There were however some periods when all 3-month SPIs coincide: Dry conditions: Beginning of the century (around 1902-1903),1977, 1989-1990 and wet conditions: 1930 and around 1939.

Table 7. SPI3 for November - Cumulative Table for CRU data

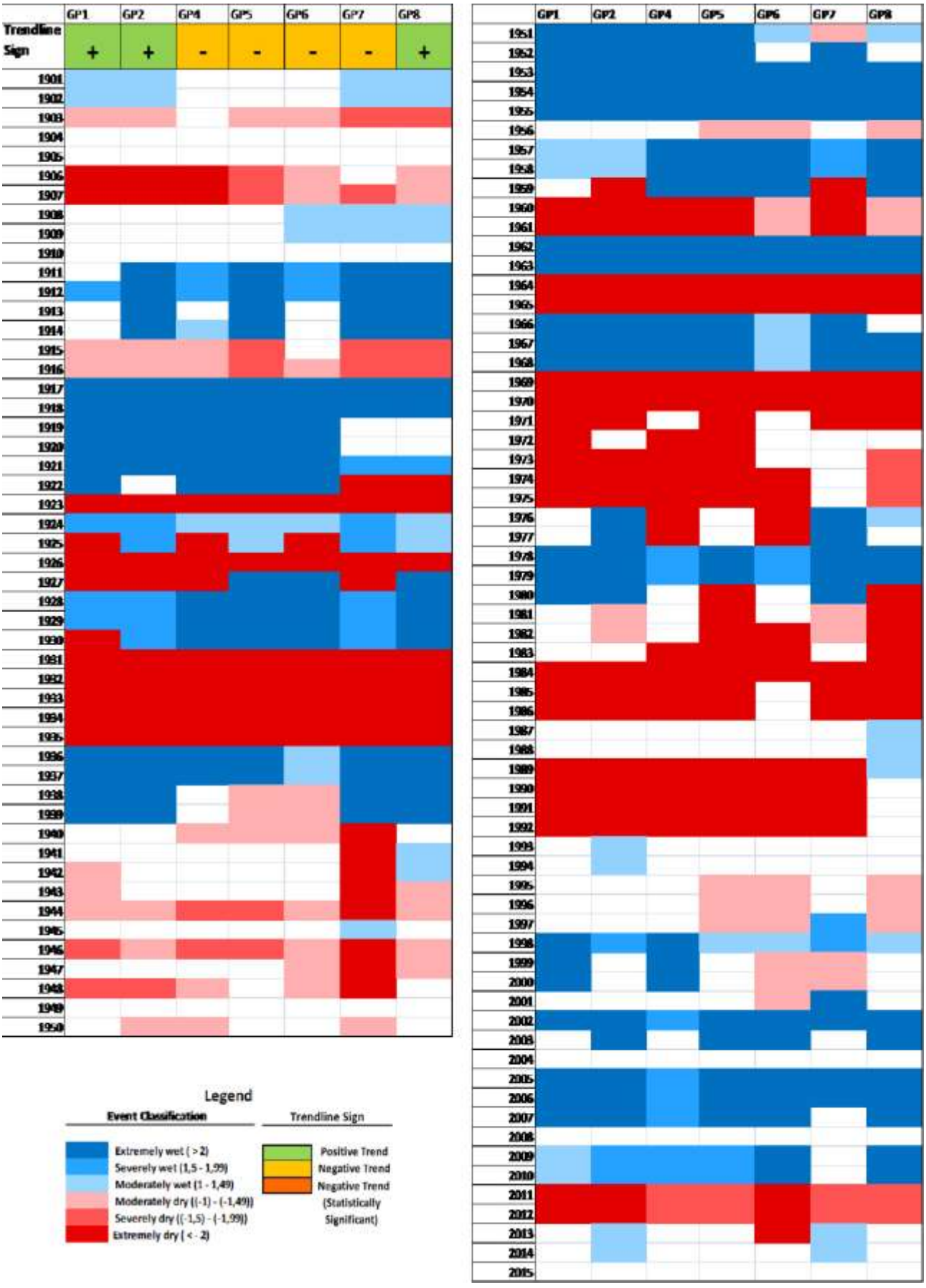

4.1.2.6. 6 Month SPI for March

A 6-month SPI showcases seasonal to medium- term precipitation trends. The 6-month SPI at the end of March provides a very strong indication of the precipitation conditions that took place during the wet period lasting from November until March. This is really important for the Mediterranean region and especially Greece, where a clear distinction between wet and dry periods is present (WMO, 2012).

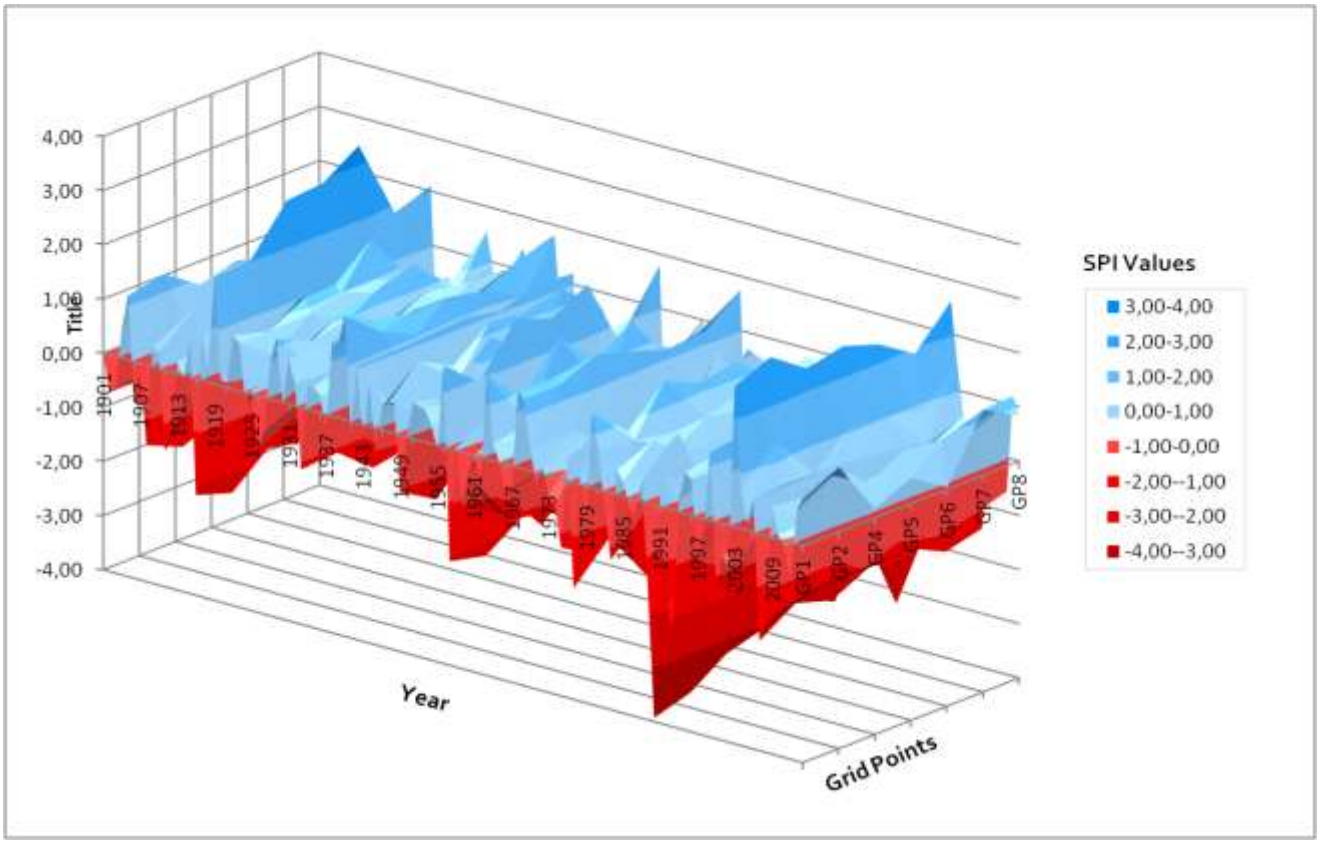

Figure 33. SPI 6 3D plot for March for all CRU data Grid points displaying consistency among them.

The first extremely dry events occurred during 1907 – 1908 and 1916. From 1918 until 1940 extreme precipitation periods were documented. From 1951 until 1956 another very wet period was manifested. In 1957 a short extreme drought took place and from 1959 until 1960 another one. For two years (1963 – 1964) precipitation of varying intensity was present in all stations, followed by a moderate drought (1966 – 1967). From 1973 to 1975, 1986 – 1990 and 1992-1993, extreme droughts were recorded. Mild wet conditions prevailed from 1994 until 1996. The last droughts of the century took place from 2000 until 2002 and from 2007 until 2008. They were interrupted by a period of extreme precipitation totals (2003 – 2006) (Table 8).

Table 8. SP6 for March - Cumulative Table for CRU data

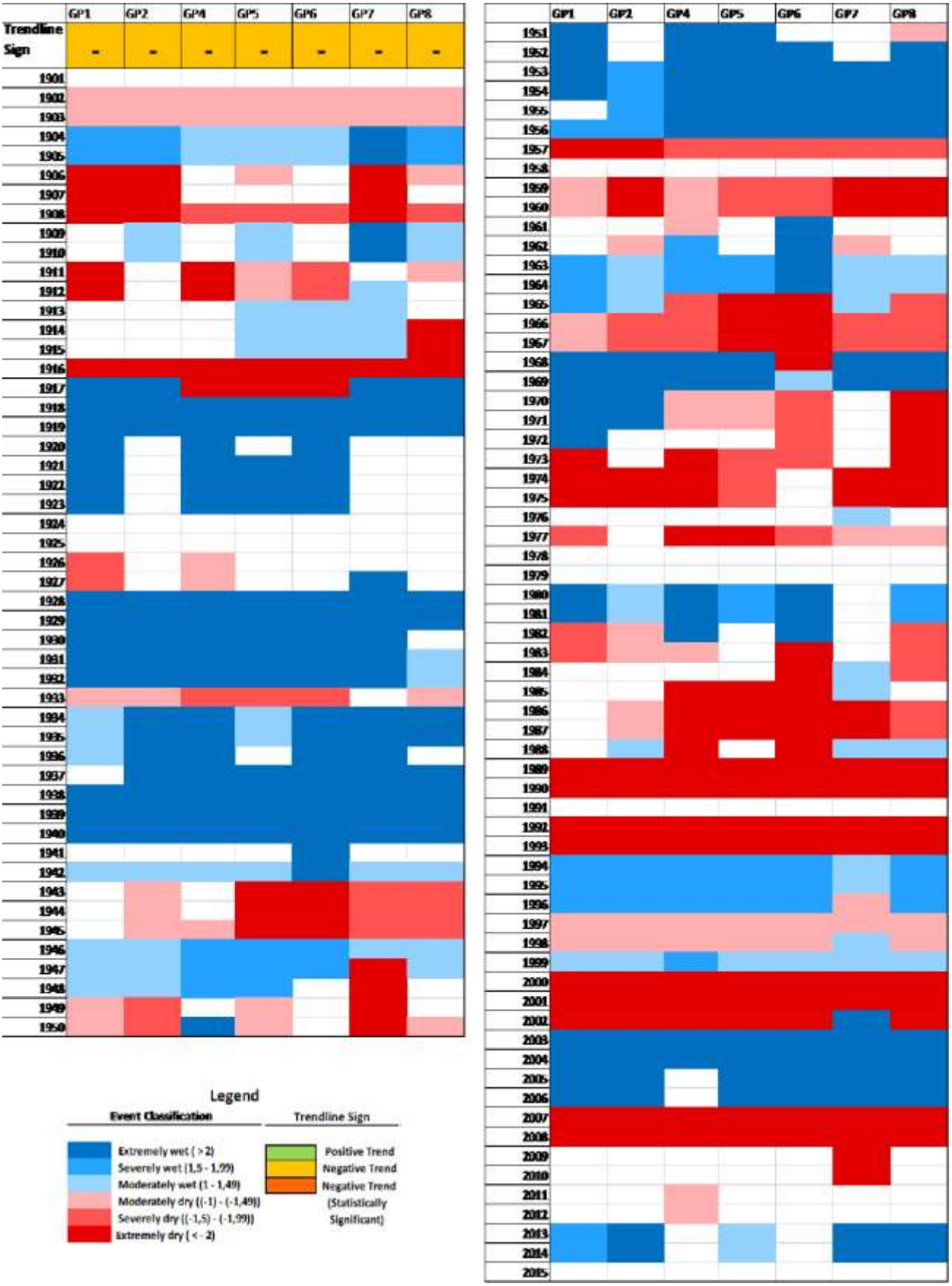

4.1.2.7. 6 Month SPI for October

The 6-month SPI at the end of October, reflects the precipitation conditions that prevailed during the dry period lasting from April until the end of October. This timescale is crucial for Mediterranean locales that tend to suffer from drought conditions during the very well defined dry period and can be associated with changes taking place in reservoir levels and streamflows (WMO, 2012).

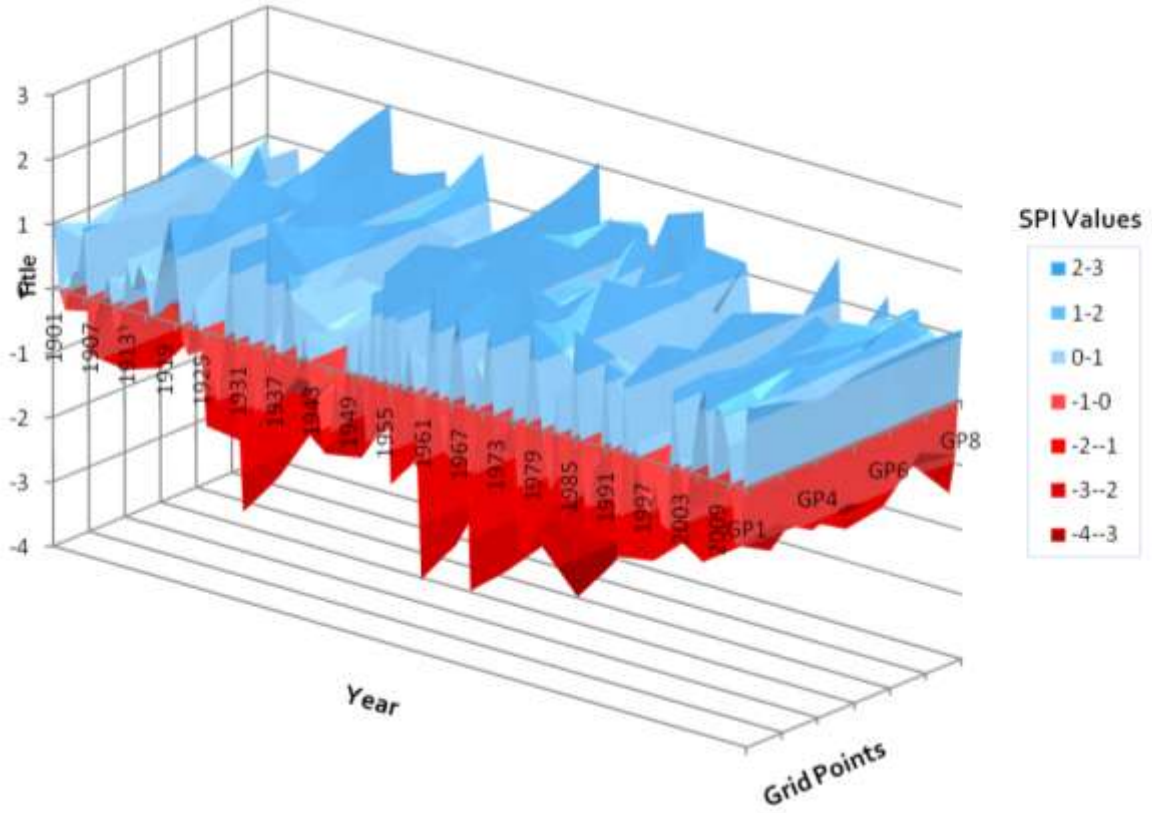

Figure 34. SPI 6 3D plot for October for all CRU data Grid point. Consistency is obvious

The century began with extensive wet conditions, especially from 1918 until 1921 severe precipitation was present. From 1925 until 1928 a drought event of varying intensity among grid points was documented. In 1929 – 1930, a wet event took place that was followed by a dry one from 1931 until 1935. From 1936 another wet period began, that was terminated in 1943 by severely dry conditions that lasted until 1948. Conditions varied during the beginning of the second half of the century. The most notable events from that period were some short but intense wet events (1962 – 1963, 1967 – 1968, 1970 – 1972 and 1978 until 1980), and respectively short intense droughts (1956, 1960 – 1961, 1969 and around 1973). From 1981 until 2000 extremely dry conditions dominated. This extensive drought was followed by extreme precipitation events (2005 – 2007 and 2009 – 2010). The last severe drought of the century took place from 2012 until 2013 (Table 9).

Common trend periods between the two 6-month SPIs include the years 1904-1905 (wet conditions), 1907 (short drought), 1918-1924, 1929-1930, 1936-1940, 1953-1955, 1963, 1980 (wet conditions), and from 1984 until 1993 and 1997-2001 long extreme droughts took place. Finally, from 2005 until 2006, heavy precipitation occurred in both cases.

Table 9. SP6 for October - Cumulative Table for CRU data

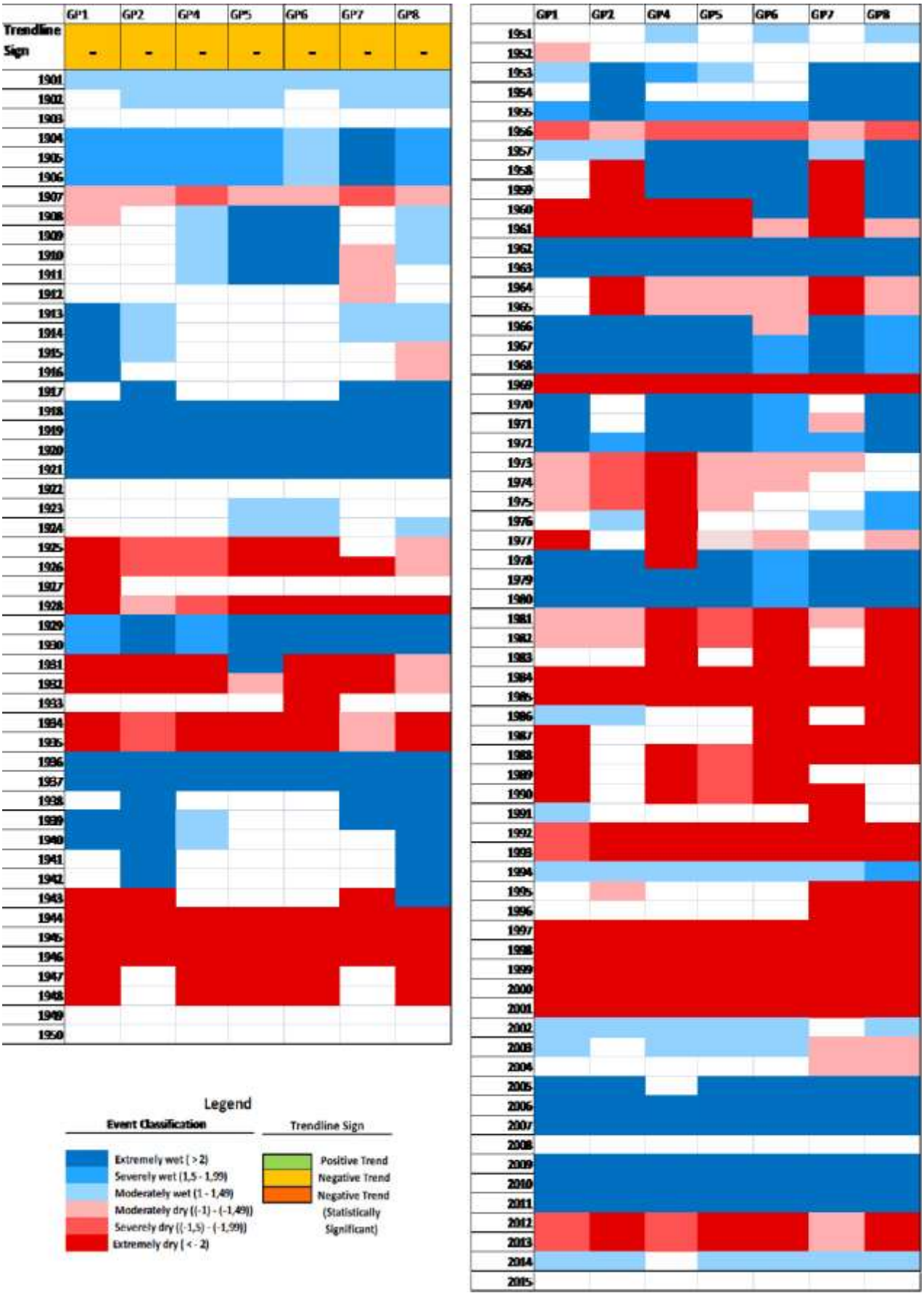

4.1.2.8. 12 Month SPI (Inter-Annual)

A 12-month SPI can suggest long term precipitation patterns. This index compares the precipitation for 12 consecutive months during the course of a whole year, with the same recorded period of 12 months contained in the historical record. In case where no distinctive dry or wet trend is taking place these SPIs tend to gravitate towards zero (WMO, 2012).

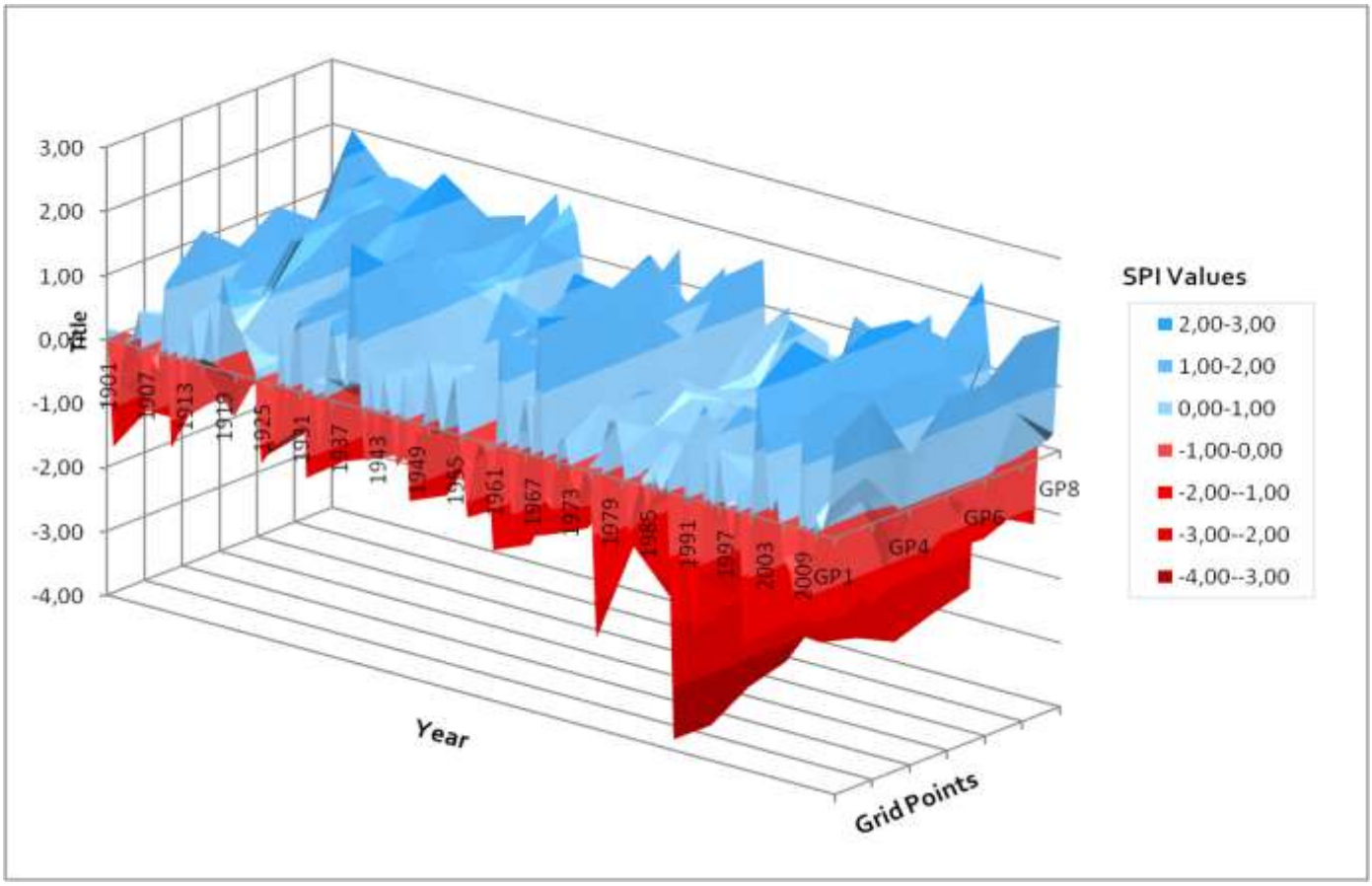

Figure 35 SPI12 3D plot showing inter-annual trends for all CRU data Grid points.

The century begins with a severe drought (1901 – 1903). Extreme precipitation prevailed from 1917 until 1921 in every grid point. Wet conditions continued to dominate the first half of the century (1930 – 1931 and 1935 – 1940). However, the situation changes during the second half. Although some wet periods made their appearance (1955, 1957, 1962 – 1963, 1966 – 1968, 1970 – 1972) the majority of extreme incidents is negative (1956, 1961, 1969, 1973, and a very severe large scale drought ranging from 1981 until 2001). In 2005 the situation seems to be stabilized again with extreme precipitation taking place (2005 – 2007, 2009 – 2011). The last drought of the century took place from 2012 until 2013, as documented by many of the indices examined above (Table 10).

Table 10. SP12 - Cumulative Table for CRU data

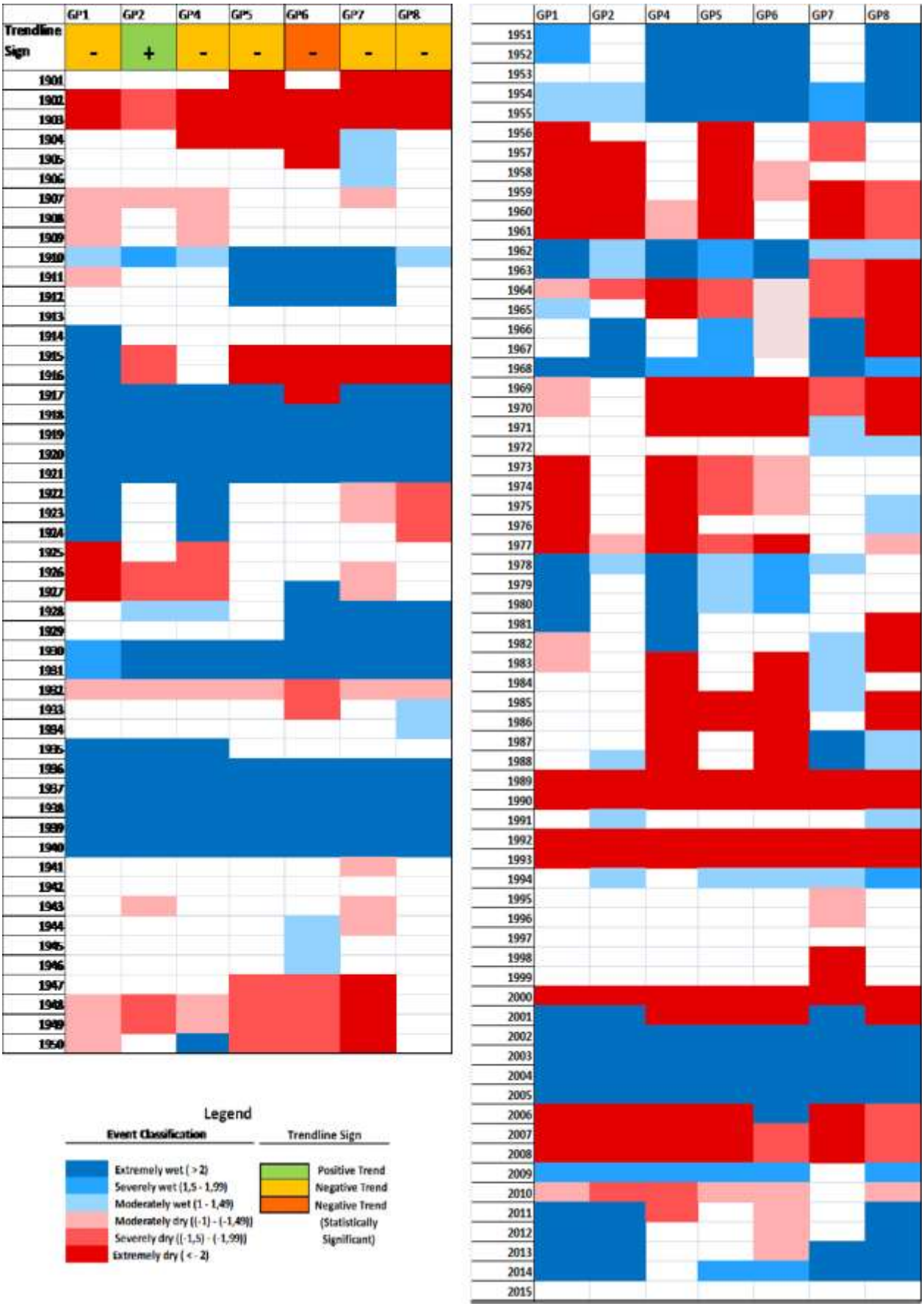

4.1.2.9. Trend Analysis

It is useful to display all trends resulting from the SPI graphs in one comparative table. It is obvious that the majority of them display a negative trend. However, there's only one case (SPI12 for GP6) where this trend is statistically significant. Although there's a trend towards drier conditions, the results of this study show that no actual threat for the 20 th century was posed (Table 11).

Table 11. Table displaying all trnedline signs from SPI indices for all CRU datasets

	GP1	GP2	GP4	GP5	GP6	GP7	GP8
SPI3 - February	-	-	-	-	-	-	-
SPI3 - May	+	+	-	+	-	+	-
SPI3 - August	+	-	-	-	-	-	-
SPI3 - November	+	+	-	-	-	-	+
SPI6 - March	-	-	-	-	-	-	-
SPI6 - October	-	-	-	-	-	-	-
SPI12 - Annual	-	+	-	-	-	-	-

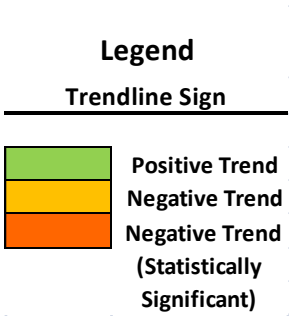

4.1.3. Dry And Wet Conditions In High Resolution (E-obs SPI)

Data from the European Climate and Data Assessment (ECA&D), E-obs gridded data, was provided for three input locations, (Loutraki [23.02,38.02], EUboea [23.65,38.57], Asopos [23.68,38.32]), with each of them displaying six output locations, that represent the studied grid points. E-obs data show better spatial resolution compared to CRU data, with a grid cell size of 22 x 22 km and are suitable for comparison with model data.

E-obs data was provided for the time period between 1950 and 2014. However, some grid points display extended periods where lack of data is observed. Those grid points were completely omitted. For the grid points that showed a continuous time series of precipitation values, SPI values for the period 1955 until 2014 were calculated. Since the control period in model data (1971 – 2000) is included in the entire E-obs time-series (1955 – 2014), E-Obs SPI values were calculated by simply using the Software provided by the World Meteorological Organization, which takes into account the entire length of the time-series in question.

Output locations (grid points) taken into account are 12 in total, as follows:

From Input location 1 corresponding to Loutraki [23.02,38.02]:

- V3 [23.25912,38.05930]
- V4 [23.00636,38.29399]

From Input location 2 corresponding to Euboea [23.65,38.57]:

- V1 [23.57405,38.48198]
- V2 [23.59573,38.70132]
- V3 [23.84797,38.46503]
- V5 [23.55250,38.26263]

From Input location 3 corresponding to Asopos [23.68,38.32]:

- V1 [23.55250,38.26263]
- V2 [23.82536,38.24575]
- V3 [23.57405,38.48198]
- V4 [23.84797,38.46503]
- V5 [23.80289,38.02646]
- V6 [23.53107,38.04328]

This dataset was mainly used in order to verify the findings suggested by the CRU dataset. They both represent gridded observations provided by different sources. Although E-obs data offer improved spatial definition compared to the CRU ones, they don't represent the study area in a satisfactory way due to the fact that the available grid points seem to only vaguely approach the area of interest. Thus, they are used as an additional clue to support the aforementioned results derived from the study of CRU data.

The study of the E-obs datasets suggests findings similar to the CRU ones. Mainly negative trends are prevalent displaying no statistical significance whatsoever. For example, the analysis of the SPI - 3 for February, results to conclusions similar to the SPI - 3 analysis for CRU as follows:

The time series begins with a long and extremely intense drought from 1956 until 1959, which is followed by extremely wet conditions for another 5 years, from 1961 until 1965 and then again from 1968 until 1974. In 1976 a mild short wet event took place. It was succeeded by a short moderate drought that lasted one year in 1976. In 1978 – 1979 and 1981 – 1982 moderate wet events occurred. For the time period from 1986 until 1990 a prolonged extreme drought was documented; it became paused in 1991, continued in 1992 - 1993 and then again from 1997 to 2002. An extreme wet event took place from 2003 until 2006 and then in 2007 – 2008 an extreme drought one followed. From 2010 until present, wet conditions prevailed for most grid points. 9 out of 12 grid points involved display negative trendlines. This fact signifies the shift towards drier precipitation conditions towards the end of the time-series.

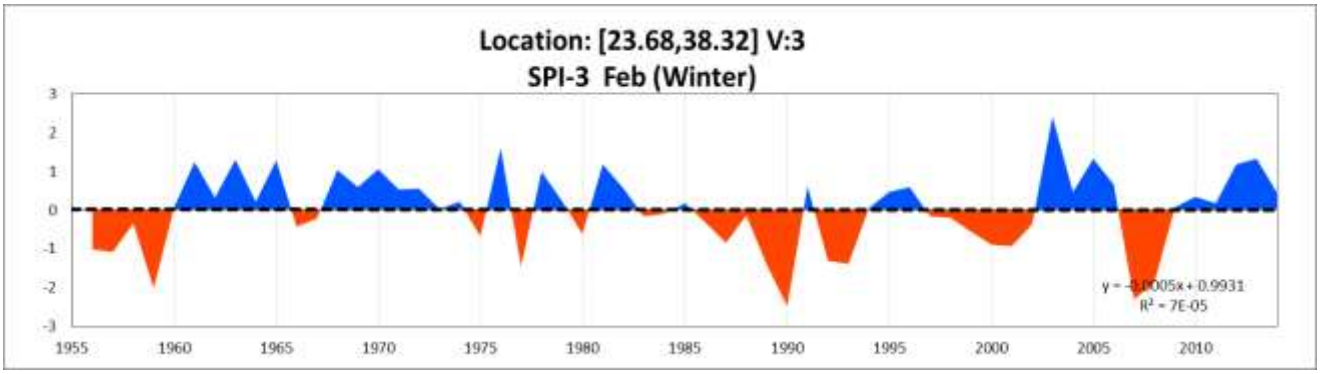

Figure 36. SPI Graph for the grid point In the location [23.68, 38.32], V3 approaching both Euboea and Asopos. The negative trendline is typical for most grid points that were studied. Graphs for all grid points involved in this study are available in the Appendix.

Respectively, the analysis of all other SPIs corresponds closely to the respective CRU analysis. E-obs graphs and tables are available in the appendix. The resemblance between datasets is clearly visible in the next chapter regarding correlation between them (Table 12).

Table 12. Table displaying all trnedline signs from SPI indices for all E-Obs dataset. No statistical significance trends are reported. Consistency between grid points is obvious.Generally L1 correspond to Loutraki, L2 to Euboea and L3 locations to Asopos

	L1V3	L1V4	L2V1	L2V2	L2V3	L2V5	L3V1	L3V2	L3V3	L3V4	L3V5	L3V6
SPI3 - February	-	-	+	-	-	-	-	+	+	-	-	-
SPI3 - May	-	-	+	+	+	-	-	+	+	+	-	-
SPI3 - August	-	-	-	-	-	-	-	-	-	-	-	-
SPI3 - November	-	-	-	-	-	-	-	-	-	-	-	-
SPI6 - March	-	-	-	-	-	-	-	-	-	-	-	-
SPI6 - October	-	-	-	-	-	-	-	-	-	-	-	-
SPI12 - Annual	-	-	-	-	-	-	-	-	-	-	-	-

Table 13. SPI3 for February - Cumulative Table for E-obs data

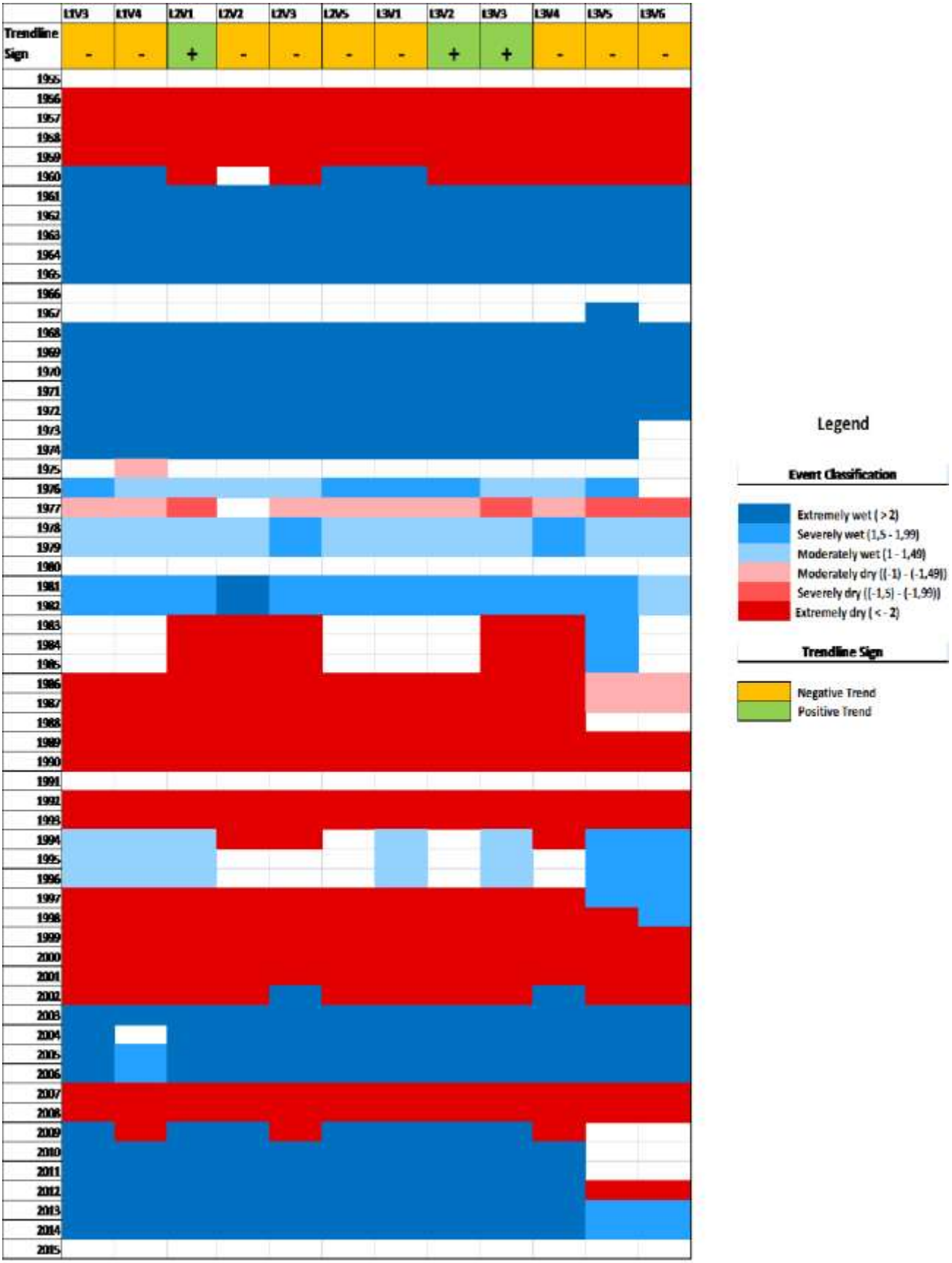

4.1.4. Comparison between gridded datasets

In order to examine the dependence between multiple variables at the same time, in this case the SPI values for a specific scale and period regarding all available datasets, a correlation matrix was computed. Correlation can be considered statistically significant when the correlation coefficient is larger than 0.3 or lower than -0.3, according to the Student's t-test.

For each SPI index that was calculated a correlation table examining the correlation between time-series for all grid points for all available data sets regardless the type of data provided, was created. Two additional correlation tables were calculated; one corresponding to all stations providing CRU data, and another one to the ones providing E-obs data. The tables dispayed coefficient values reaching as high as 1 for grid points belonging to the same dataset. As displayed below, all correlation tables show great statistical significance, even between grid points that don't belong in the same dataset. The coefficient values exceeded 0,8 for most cases. This fact indicates homogeneity between datasets and verifies their reliability. Those tables can be found in the Appendix.

A notable example is the Inter-annual SPI12 correlation table that follows below and shows great statistical significance among the examined grid points (Table 14). Those values correspond to the intercorrelation between the two gridded datasets that were analyzed and show that those two datasets are highly correlated, especially E-obs data with GP5 CRU grid point that approaches the middle of the whole study area.

Table 14. SPI 12 – Correlation table (all available datasets)

	GP1	GP2	GP4	GP5	GP6	GP7	GP8	L3V6	L3V4	L3V5	L3V3	L3V2	L3V1	L2V5	L2V3	L2V2	L2V1	L1V4	L1V3
GP1	1																		
GP2	0.915684	1																	
GP4	0.914134	0.830291	1																
GP5	0.88396	0.910037	0.936585	1															
GP6	0.812207	0.7864	0.923438	0.947236	1														
GP7	0.759057	0.91079	0.692396	0.82552	0.694344	1													
GP8	0.799025	0.886361	0.828817	0.937938	0.87322	0.842399	1												
L3V6	0.760233	0.819551	0.775536	0.824148	0.778899	0.810223	0.802726	1											
L3V4	0.718957	0.759076	0.775608	0.809204	0.820403	0.764264	0.780297	0.824048	1										
L3V5	0.712752	0.797135	0.742221	0.814856	0.775987	0.801086	0.815898	0.988733	0.838257	1									
L3V3	0.752269	0.803836	0.802852	0.840406	0.832628	0.8008	0.806153	0.875005	0.984815	0.878167	1								
L3V2	0.764993	0.814531	0.807379	0.850703	0.832322	0.804785	0.824501	0.90149	0.976784	0.912019	0.986889	1							
L3V1	0.799698	0.825134	0.832534	0.857142	0.838751	0.798197	0.817077	0.923946	0.960042	0.919744	0.980072	0.992348	1						
L2V5	0.799698	0.825134	0.832534	0.857142	0.838751	0.798197	0.817077	0.923946	0.960042	0.919744	0.980072	0.992348	1	1					
L2V3	0.718957	0.759076	0.775608	0.809204	0.820403	0.764264	0.780297	0.824048	1	0.838257	0.984815	0.976784	0.960042	0.960042	1				
L2V2	0.724004	0.745201	0.794254	0.808678	0.834319	0.750842	0.76084	0.821772	0.990507	0.828231	0.979213	0.96373	0.953992	0.953992	0.990507	1			
L2V1	0.752269	0.803836	0.802852	0.840406	0.832628	0.8008	0.806153	0.875005	0.984815	0.878167	1	0.986889	0.980072	0.980072	0.984815	0.979213	1		
L1V4	0.828259	0.780313	0.831301	0.795568	0.783363	0.739591	0.713909	0.876864	0.876841	0.8313	0.907566	0.907448	0.944399	0.944399	0.876841	0.892704	0.907566	1	
L1V3	0.799698	0.825134	0.832534	0.857142	0.838751	0.798197	0.817077	0.923946	0.960042	0.919744	0.980072	0.992348	1	1	0.960042	0.953992	0.980072	0.944399	1

4.1.5. Discussion

CRU data suggest that the driest of the three case studies is the Asopos area, while Loutraki and Euboea display the largest precipitation values. CRU data generally show average annual values between 500 and 700 mm of precipitation per year.

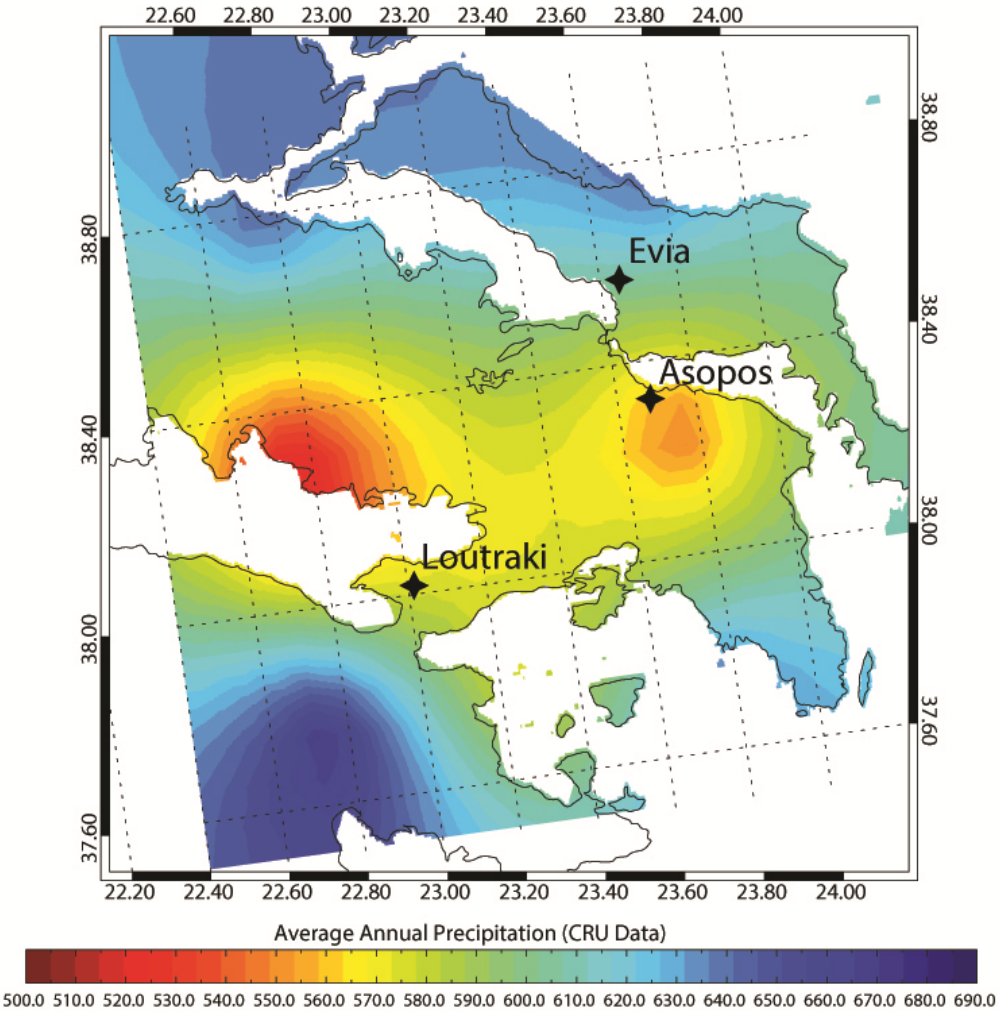

Figure 37. Interpolation maps displaying spatial distribution of annual precipitation as suggested by CRU data (1901 – 2014)

E-Obs data generally suggest lower precipitation values compared to CRU data (values lower than 500 mm for most cases annually). Although both datasets refer to the same geographical area, grid point distribution varies. CRU gridpoints are equally distanced from each other covering the three study areas as a whole. On the contrary, E-Obs gridpoints are concentrated around each one of the study areas, therefore spatial distribution between the two datasets differs. It is possible that annual precipitation totals are influenced by this fact. E-Obs dataset suggests that Euboea receives the least amount of precipitation. However, Asopos area is still pretty dry, while Loutraki area seems to be the one least in danger of drought.

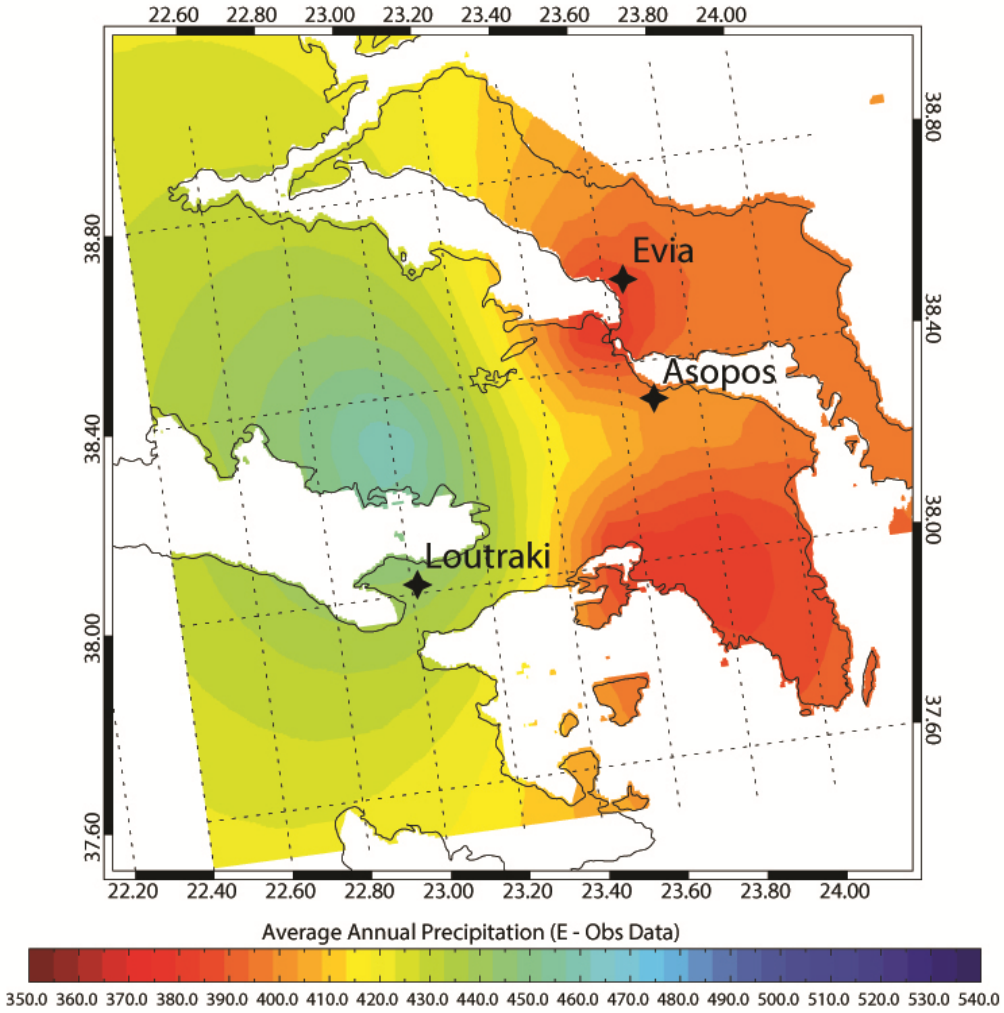

Figure 38. Interpolation maps displaying spatial distribution of annual precipitation as suggested by E-Obs data (1950 – 2014)

Generally, both datasets agree on Asopos and Loutraki areas. Euboea is a location displaying diverse topographic relief and is therefore harder to determine. Climatic and precipitation conditions are ought to change in relatively short distances. Whatever the case is, all studied SPI indices in addition to the precipitation analysis that took place in previous chapters indicate no reason for concern due to the lack of statistically significant negative trends.

Asopos river basin seems to receive the least of precipitation so far, this fact combined with the intense industrial and agricultural activity prevalent in the area could be a source of concern. However, as witnessed above, no actual statistically significant trend is documented signifying actual danger. The Loutraki area due to its proximity to the sea, could be classified as a rather vulnerable area. However, its underground water reservoirs, its natural springs and the vast amount of precipitation it receives, secure the area's well being in terms of water scarcity. This conclusion is further verified by the 12 month SPI index that displayed no significant trend. The only grid point that showed a statistically significant negative trend for this index is GP6 for CRU datasets, which corresponds to Northern Euboekos Gulf and seems to be rather far from our areas of interest. Besides, 12 month SPIs correspond to reservoir levels and a grid point located in the sea, serves no other purpose than to assist in the extraction of more accurate interpolation patterns.

4.2 Future Climate Analysis

Future Climate Analysis assesses model data acquired by the Swedish Meteorological and Hydrological Institute (SMHI) corresponding to two RCP scenarios (RCP 4.5 and RCP 8.5). Model data was provided for a time range from 1971 until 2100. The datasets were divided into three sections of thirty years each, the current section (1971 – 2000), near future (2021 – 2050) and remote future (2071 – 2100). The current section represents present conditions in the model simulations, while the future ones utilized the respective scenarios.

Four grid points were studied in total.,GP1 is used in order to assess the future situation for Loutraki, GP7 for Asopos and GP8 and GP13 for Euboea.

4.2.1. Precipitation Analysis

The goal of this analysis is to suggest the possible evolution of the hydrological conditions characterizing the areas of interest.

Paired two sample t-test analysis suggests that under RCP 4.5 scenario, the expected change regarding annual average precipitation, although negative is not going to be statistically significant concerning the near future. However, for grid points GP1 (Loutraki) and GP7 (Euboea) models show that in the distant future this trend is awaited to become statistically significant, a fact signifying danger. For the near future variability is expected to grow in all studied grid points and that growth is statistically significant. For the distant future, the situation is stabilized, with the only grid point displaying a statistically significant increase being GP13 (Asopos).

Contrary to the mildly upsetting RCP 4.5 scenario, RCP 8.5 suggests a situation much less pleasant. Even projections aiming at the near future for GP1 (Loutraki) and GP7 (Euboea) show a statistically significant decrease in expected annual precipitation. Regarding the distant future, t-test results in values far greater than the critical ones, for all grid points involved, suggesting that a severe reduction in precipitation is anticipated. Regarding variability in most cases (GP8 (Euboea), GP13 (Asopos) for the near future and GP7, GP8 (Euboea), GP13 (Asopos) for the distant future) a statistically significant increase is expected.

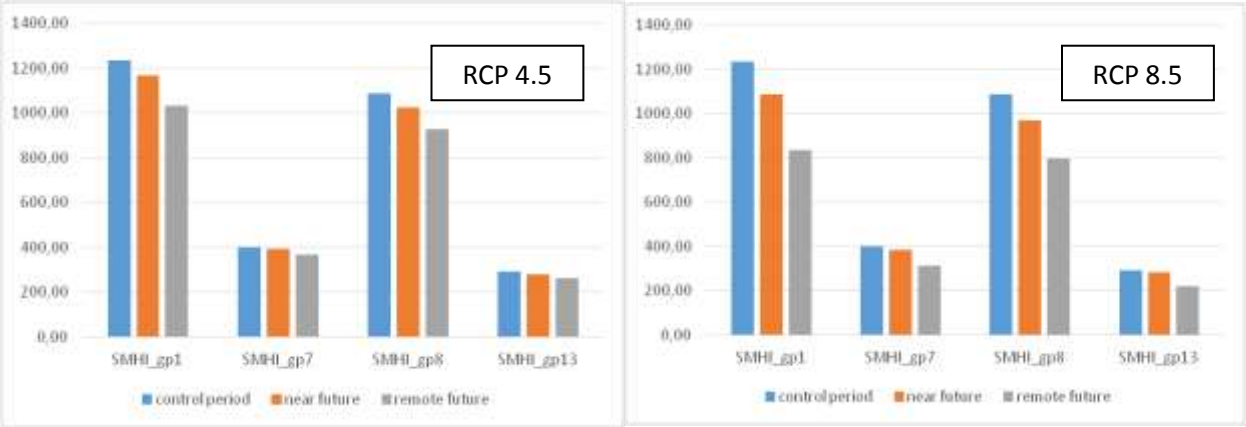

Figure 39. Projected annual average precipitation under the RCP 4.5 (left) and RCP 8.5 (right) scenario regarding current (control period) and future (near and remote) state.:

Seasonal analysis for RCP 4.5 generally shows a mild reduction in average precipitation for all seasons. Projections aiming at wet season (October – March) only display statistical significance for GP1 (Loutraki) and GP8 (Euboea) (distant future projections). It is interesting to notice that regarding the dry season (April – September) and most notably Summer, the distant future projections show a rise in precipitation average. Variability seems to increase towards the end of the century rapidly; statistically significant results correspond to GP1 (Loutraki), GP7 and GP8 (Euboea) for near future projections, and GP1 (Loutraki), GP7 (Euboea) and GP13 (Asopos) for remote regarding the wet season, GP1 (near future) and GP1 (Loutraki), GP7, GP8 (distant future) for the dry season, for winter season all grid points regarding the near future while for the distant future variability seems to decrease in a non statistically significant rate, and finally, projections for summer suggest that variability decreases for grid points GP1 (Loutraki),, GP7, GP8 (near future), while for GP13 (near future) and GP1 (distant future) increases.

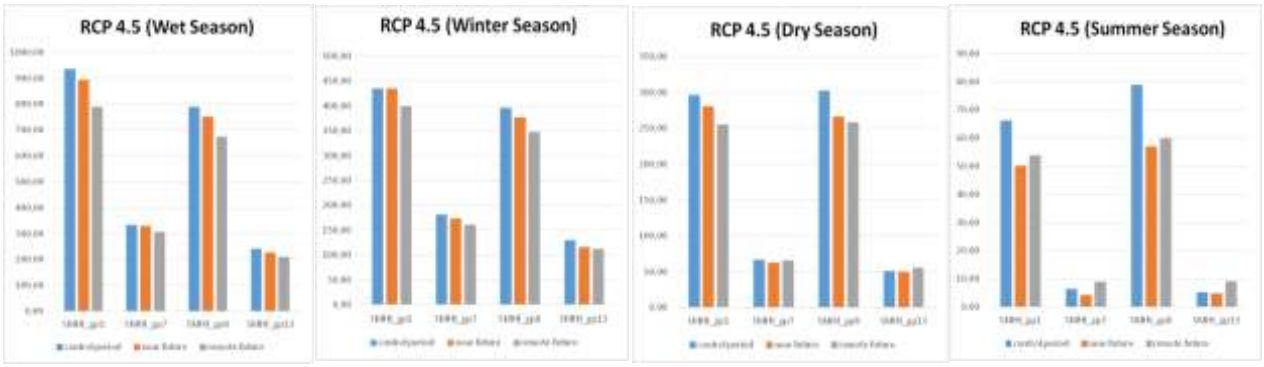

Figure 40. Projected average precipitation under the RCP4.5 scenario (wet, dry, winter and summer seasons), comparing current and future conditions.

As expected, RCP 8.5 projections are more extreme. A statistically significant decline in precipitation average is witnessed in regard to Wet season in GP1 (near future) and GP1, GP7, GP8, GP13 (remote future). Projections aiming at dry season show similar results; statistically significant reductions are present in GP8 (near future) and GP1, GP7, GP8, GP13 (remote future). For summer and winter statistical significance is displayed only in the remote future. Variability study shows very interesting results. During the wet season a statistically significant rise is witnessed in GP7, GP13 (near future) and GP1, GP7, GP8 (remote future), during the dry season in GP7 (near and remote future) and during winter in GP1, GP7 (near future) and GP1, GP13 (remote future). What is really interesting is that summer projections (both near and remote future) show a decrease instead of an increase that is actually statistically significant. The most possible explanation for this is that precipitation average is decreased to a point that variability doesn't even make sense. GP7 remote future projections for example, show an average as low as 3 mm.

Figure 41. Projected average precipitation under the RCP 8.5 scenario (wet, dry, winter and summer seasons), comparing current and future conditions.

4.2.2. Drought Analysis

For the evaluation of future precipitation conditions the SPI index was calculated for various timescales using model data acquired by the Swedish Meteorological and Hydrological Institute (SMHI), implementing the same methods as with gridded observations. Results between the two studied scenarios vary, therefore the analysis corresponding to each scenario is displayed in its respective subchapter. The SPI indices were calculated taking into account the control period from 1971 until 2000 and are the following:

- **SPI 3** - Displaying seasonal variations
  - February (02), corresponding to winter
  - May (05), corresponding to spring
  - August (08), corresponding to summer
  - November (11), corresponding to autumn
- **SPI 6** - Partitions the annual circle into two seasons; wet and dry
  - March (03), corresponding to wet season
  - October (03), corresponding to dry season
- **SPI 12** - Assessing annual variation

Just like with gridded observations, for each index, a table including all grid points that were studied is created. Each cell represents a specific SPI value for the respective year and grid point; in order to mark the duration and intensity of each extreme precipitation or drought event, a variety of colors is used. Drought events are marked in shades of red; lighter shades respond to lower intensity, while darker shades represent events of higher intensity. Respectively, blue shades are used in order to display extreme precipitation events. Although long periods of drought are present in both scenarios, quantitative differences between the two are obvious. To this regard, apart from the color code, numerical values are also included in the tables as a display of magnitude. 12 month SPIs with respect to both climate change scenarios are included with the description. The remaining tables can be found in the Appendix.

4.2.2.1. RCP 4.5 Projection Analysis

4.2.2.1.1. SPI12 - Inter-Annual

Table 15. SPI 12– Tables displaying model data values (RCP 4.5)

	GP1 rcp45	GP7 rcp45	GP8 rcp45	GP13 rcp45		GP1 rcp45	GP7 rcp45	GP8 rcp45	GP13 rcp45
1971	-0,46	-0,63	-0,95	-0,45	2034	-1,48	0,85	0,13	0,96
1972	-2,35	-1,38	-2,05	-1,02	2035	-0,15	1,27	-0,06	1,13
1973	0,64	-0,07	0,40	0,16	2036	-0,91	-1,46	-1,36	-0,74
1974	0,11	1,76	1,24	1,31	2037	-1,67	-4,44	-2,20	-2,90
1975	1,18	0,97	0,56	1,41	2038	-1,45	-0,62	-2,17	-1,71
1976	0,69	0,01	-0,21	0,43	2039	-1,04	-0,63	-1,21	-1,36
1977	-0,09	-0,28	-0,66	-0,37	2040	-1,46	-1,32	-1,21	-0,97
1978	1,50	1,01	1,59	0,95	2041	1,38	-0,16	0,09	0,10
1979	-0,20	0,66	0,64	0,60	2042	-0,10	-1,26	-0,61	-0,84
1980	1,22	1,01	0,80	0,80	2043	-0,54	0,46	-1,15	0,31
1981	-0,68	0,88	-0,45	0,29	2044	-1,29	-0,34	-0,68	-1,11
1982	0,33	0,89	-0,21	0,86	2045	1,16	2,04	1,44	2,27
1983	1,17	-0,93	0,41	-0,72	2046	1,24	1,02	0,91	1,17
1984	1,01	0,25	0,26	0,57	2047	0,67	0,23	-0,25	0,38
1985	1,11	0,18	0,97	-0,14	2048	-0,27	-1,74	-1,41	-1,72
1986	-2,03	-0,94	-1,05	-0,77	2049	-1,15	0,36	0,28	-0,63
1987	-0,07	0,84	0,30	-0,16	2050	-0,89	-0,16	0,27	-0,27
1988	0,36	-0,66	-0,01	-0,90	2051	-0,79	0,27	-0,74	-0,12
1989	0,30	-1,51	-0,06	-1,88	2052	-1,73	-0,99	-1,90	-0,92
1990	0,44	-0,01	0,38	0,36	2053	-0,84	-1,68	-1,09	-0,67
1991	0,15	-0,40	-0,61	0,82	2054	-0,34	0,77	0,76	1,33
1992	-0,97	-1,03	-0,10	-1,13	2055	-0,79	-0,16	-1,29	-0,43
1993	-0,25	0,44	-0,09	0,21	2056	-1,07	-1,11	-1,13	-1,36
1994	-2,02	-2,23	-2,40	-2,07	2057	-0,92	0,29	-0,43	-0,18
1995	-1,35	-0,83	-1,27	-1,57	2058	0,11	0,22	0,65	0,43
1996	0,18	-0,40	0,64	-0,62	2059	0,15	0,20	-0,11	-0,15
1997	-0,34	1,61	0,00	1,47	2060	-1,32	-0,59	-1,57	-0,32
1998	1,47	1,18	2,57	1,63	2061	0,11	-0,57	-0,57	-0,06
1999	-0,50	0,63	0,47	0,56	2062	-1,40	-1,26	-1,46	-1,44
2000	-0,55	-0,83	-1,15	-0,50	2063	0,72	-0,30	0,34	0,33
2001	0,40	-1,20	0,05	-0,72	2064	-0,26	1,02	-0,18	0,25
2002	0,38	0,14	0,98	0,27	2065	-1,61	-1,70	-0,86	-1,07
2003	-0,32	-1,61	0,27	-0,29	2066	-1,20	-1,81	-1,44	-1,76
2004	-0,52	-0,94	-0,43	-0,83	2067	-0,71	-0,67	-1,36	0,08
2005	-0,40	0,32	-0,42	0,57	2068	-0,48	-0,60	-0,36	0,62
2006	-0,72	-1,96	-1,48	-0,62	2069	0,42	0,20	0,38	1,08
2007	-0,70	1,89	1,14	2,64	2070	0,60	0,60	0,90	0,88
2008	-1,61	-0,22	-1,27	-0,48	2071	-0,28	0,28	0,30	0,83
2009	-0,35	-1,15	0,00	-0,79	2072	0,28	3,50	1,42	2,64
2010	0,19	-0,32	0,06	-0,70	2073	-0,22	0,22	-0,55	-0,46
2011	0,34	0,93	0,03	-0,06	2074	-1,86	-1,19	-1,66	-1,64
2012	-0,13	-1,36	-0,05	-1,19	2075	-0,92	-1,99	-1,36	-0,87
2013	-0,76	-0,80	-0,97	-0,73	2076	-0,25	-1,43	-0,47	-1,15
2014	1,18	0,73	1,01	0,72	2077	-2,59	-1,58	-2,86	-1,93
2015	1,77	2,28	1,87	1,64	2078	-0,95	-2,33	-1,38	-1,27
2016	-1,71	-1,31	-1,89	-0,60	2079	-0,70	0,03	-1,04	-0,22
2017	-2,22	-1,57	-2,64	-2,38	2080	-1,47	-1,38	-1,92	-0,74
2018	-1,32	-0,09	-0,61	-0,55	2081	-0,15	1,51	0,52	0,96
2019	0,05	-2,43	-1,39	-0,52	2082	-0,10	-0,11	-0,49	0,69
2020	0,38	0,65	-0,01	0,17	2083	-1,58	0,33	-0,26	-0,58
2021	0,46	-0,40	-0,03	-0,88	2084	-1,53	-1,20	-1,61	-1,24
2022	-3,01	-1,08	-1,86	-0,85	2085	0,91	0,95	-0,76	1,43
2023	-1,53	-0,22	-0,99	0,21	2086	0,19	0,04	-0,54	-0,06
2024	-1,06	0,99	-0,24	-0,12	2087	-0,98	-0,50	-1,24	-1,19
2025	-2,39	-1,39	-2,97	-0,54	2088	-0,98	-0,22	-0,50	-0,55
2026	1,14	1,54	1,65	1,52	2089	-1,29	-2,31	-2,13	-1,24
2027	0,14	0,12	-0,97	0,03	2090	-1,63	-1,25	-1,49	-1,05
2028	0,90	0,84	1,17	0,31	2091	-2,14	-1,31	-1,16	-0,94
2029	1,06	0,21	0,42	0,28	2092	-1,39	-0,74	-0,87	-0,47
2030	-0,57	-1,52	-0,42	-1,13	2093	-0,74	0,23	-1,09	-0,45
2031	0,64	0,45	0,44	0,23	2094	-0,12	0,74	0,65	0,30
2032	1,68	2,02	2,37	0,32	2095	-0,02	-0,61	-0,01	-0,67
2033	1,43	0,91	0,85	0,80	2096	-2,76	-2,43	-3,03	-1,60
					2097	-0,26	1,48	0,81	0,65
					2098	0,34	-0,75	-0,89	-0,52
					2099	-1,25	-0,25	-0,39	-0,83
					2100	0,43	0,01	0,21	1,03

Control period begins with a short drought (1971 – 1972), continues with wetter conditions (1974 – 1984) and finishes with dry conditions (1992 – 1996).

The first half of the century is characterized by periods of long drought (2016 – 2025, 2035 – 2040,) and extreme precipitation (2026 – 2033, 2045 – 2047), while the second half is mostly dry (2048 – 2068, 2073 – 2096) (Table 15; Table A XVIII, Appendix II).

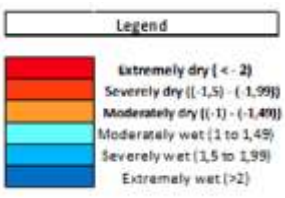

4.2.2.1.2. SPI3 - February (Winter Season)

During the period when models run using current conditions (1971 – 2000), not many distinct events took place. From 1982 until 1986, wet condition were prevalent in all stations, followed by drier conditions from 1989 until 1996, and then again wet (1997 – 1999), (2005 – 2007) with varying intensity among the stations. From 2011 until 2016 and 2026 - 2029, wet conditions are present. From 2034 until 2045 a prolonged extreme drought is expected to occur present in all stations. Dry and wet conditions intertwine until the end of the century. Generally, drier conditions seem to dominate, especially regarding the distant future (2071 – 2100) (Table A XII, Appendix II).

4.2.2.1.3. SPI3 - May (Spring Season)

During the control period several wet (1974 – 1976, 1982 – 1985, 1996 – 1998) and dry (1977-1980, 1994 – 1995) events took place. The beginning of the century is projected as a prolonged drought starting from around 2008 until 2028, when it gets interrupted, just to begin again in 2033 until 2044 (with a small wet event taking place in 2035).

Apart from some wet incidents (2045 – 2047, 2070 – 2072, 2081-2082 and 2098 – 2100), remote future can be described as a long sequence of extreme drought events (Table A XIII, Appendix II).

4.2.2.1.4. SPI3 - August (Summer Season)

During the control period some droughts (1983 – 1984, 1987) and wet events (1989-1990, 1993 – 1998) were witnessed.

Near future projections begin with an extensive drought (2019 – 2026), it is followed by a wet period (2031 – 2033). Until 2069 (remote future), dry and wet periods intertwine. In 2069 an extremely dry event takes place, lasting until 2075. Until the end of the century a couple more droughts make their appearance (2083 – 2086 and 2095 – 2096) (Table A XIV, Appendix II).

4.2.2.1.5. SPI3 - November (Autumn Season)

The control period starts with a moderately dry incident (1971 – 1972), from 1978 until 1981 wet conditions dominate, from 1984 until 1987 and 1993 – 1994, dry ones. This period ends with wet conditions (1998 – 2000). During the period 2004 until 2006 an extremely dry incident took place.

Generally, near future projections show a balance between dry (2016 – 2018, 2023 – 2025, 2051 – 2052) and wet events (2013 – 2015, 2029 – 2033, 2040 – 2041). Remote future projections pretty much follow the same principle, although incidents seem to appear more clearly defined and of greater intensity (wet events: 2057 – 2059, 2069 – 2071, 2082 – 2086, dry events: 2062 – 2066, 2073 – 2080, 2089 – 2096) (Table A XV,Appendix II).

4.2.2.1.6. SPI6 - March (Wet Season)

The beginning of the control period displays a moderate drought (1972 – 1973). Wet conditions dominate for the next decade (1974 – 1985), and are followed by dry ones (1987 – 1995). Wet (2015 – 2016, 2027 – 2029, 2033 – 2035, 2045 – 2047) and dry (2017 – 2018, 2036 – 2044) conditions are equally present during the first half of the century.

During the second half (including the remote future period), apart from the period of 2069 – 2073, when wet conditions are prevalent, extremely dry conditions are the norm (Table A XVI, Appendix II).

4.2.2.1.7. SPI6 - October (Dry Season)

During the control period, two major droughts took place (1983 – 1987, 1991 – 1997), this period however starts with wet conditions. In the beginning of the century a long drought of varying intensity is encountered from 2016 until 2025. Near future projections consist of interchanging wet (2027 – 2033, 2041 – 2047) and dry (2054 – 2054, 2059 – 2040, 2048 – 2056) incidents.

During the second half of the century half of the century, the same situation is present, beginning with mostly dry conditions 2072 – 2080 and 2088 – 2092, and ending with wetter ones (2083 – 2086, 2097 – 2100) (Table A XVII, Appendix II).

4.2.2.2. RCP 8.5 Projection Analysis

4.2.2.2.1. SPI12 Inter-Annual

Table 16. SPI 12– Tables displaying model data values (RCP 8.5)

	GP1 rcp85	GP7 rcp85	GP8 rcp85	GP13 rcp85
1971	-0,46	-0,63	-0,95	-0,45
1972	-2,35	-1,38	-2,05	-1,02
1973	0,64	-0,07	0,40	0,16
1974	0,11	1,76	1,24	1,31
1975	1,18	0,97	0,56	1,41
1976	0,69	0,01	-0,21	0,43
1977	-0,09	-0,28	-0,66	-0,37
1978	1,50	1,01	1,59	0,95
1979	-0,20	0,66	0,64	0,60
1980	1,22	1,01	0,80	0,80
1981	-0,68	0,88	-0,45	0,29
1982	0,33	0,89	-0,21	0,86
1983	1,17	-0,93	0,41	-0,72
1984	1,01	0,25	0,26	0,57
1985	1,11	0,18	0,97	-0,14
1986	-2,03	-0,94	-1,05	-0,77
1987	-0,07	0,84	0,30	-0,16
1988	0,36	-0,66	-0,01	-0,90
1989	0,30	-1,51	-0,06	-1,88
1990	0,44	-0,01	0,38	0,36
1991	0,15	-0,40	-0,61	0,82
1992	-0,97	-1,03	-0,10	-1,13
1993	-0,25	0,44	-0,09	0,21
1994	-2,02	-2,23	-2,40	-2,07
1995	-1,35	-0,83	-1,27	-1,57
1996	0,18	-0,40	0,64	-0,62
1997	-0,34	1,61	0,00	1,47
1998	1,47	1,18	2,57	1,63
1999	-0,50	0,63	0,47	0,56
2000	-0,55	-0,83	-1,15	-0,50
2001	0,40	-1,20	0,05	-0,72
2002	0,38	0,14	0,98	0,27
2003	-0,32	-1,61	0,27	-0,29
2004	-0,52	-0,94	-0,43	-0,83
2005	-0,40	0,32	-0,42	0,57
2006	0,22	-0,89	-0,52	0,01
2007	1,09	0,12	0,56	0,28
2008	-0,58	0,91	0,01	0,25
2009	0,08	1,08	0,26	-0,12
2010	0,32	1,27	0,71	0,21
2011	1,17	1,69	1,53	1,36
2012	-0,06	-0,71	-1,02	-0,40
2013	-1,58	-1,22	-1,10	-1,26
2014	-1,18	-0,91	-1,22	-0,48
2015	-1,01	0,27	-0,22	-0,39
2016	-1,53	-1,68	-1,63	-2,01
2017	-0,96	-1,54	-1,95	-0,70
2018	-0,81	-1,48	-1,21	-1,73
2019	0,27	-0,25	0,94	-0,57
2020	1,00	1,11	1,85	1,06
2021	1,10	0,81	0,91	0,90
2022	1,14	3,47	2,28	2,54
2023	-0,16	0,38	0,12	-0,40
2024	0,87	1,34	0,37	1,14
2025	-1,38	-1,11	-0,45	-0,72
2026	-0,08	1,55	0,68	-0,20
2027	-0,11	-1,25	-0,28	-0,03
2028	-2,87	0,88	-1,75	-0,49
2029	-0,44	-1,93	-1,76	-1,38
2030	-1,02	0,70	0,08	1,94
2031	1,40	0,38	0,60	0,92
2032	-1,12	-1,42	-1,39	-0,65
2033	0,54	-0,03	0,54	0,15

	GP1 rcp85	GP7 rcp85	GP8 rcp85	GP13 rcp85
2034	-2,10	-1,30	-2,18	-1,40
2035	-0,90	-0,34	-0,51	0,09
2036	-1,04	-0,64	-1,16	-0,03
2037	-0,97	-2,01	-0,93	-1,76
2038	-1,08	-0,94	-0,73	-0,14
2039	-0,49	-1,21	-1,09	-0,37
2040	0,53	1,49	0,20	0,57
2041	-0,26	0,01	0,01	0,05
2042	0,34	0,54	0,30	0,29
2043	-2,22	-1,92	-2,95	-1,69
2044	-2,68	-2,48	-3,16	-1,59
2045	-3,43	-4,04	-4,49	-3,63
2046	0,72	0,01	0,01	0,73
2047	-1,66	0,15	-1,18	-0,06
2048	-1,11	-1,68	-1,56	-1,01
2049	-0,29	1,06	0,12	0,41
2050	-0,04	1,07	0,22	0,83
2051	0,93	0,04	0,38	0,46
2052	-1,86	-1,77	-2,33	-0,89
2053	-0,95	-1,06	-1,21	0,05
2054	-0,40	0,72	-0,66	0,71
2055	-0,85	-1,27	-1,54	-0,56
2056	0,03	-0,82	-0,91	-0,63
2057	0,19	-0,70	0,40	-0,73
2058	-1,74	-0,18	-0,44	0,05
2059	0,11	0,27	0,72	0,56
2060	-3,85	-2,15	-3,55	-2,86
2061	-1,97	-1,18	-1,45	-1,25
2062	0,40	1,85	1,07	1,60
2063	1,02	2,17	0,45	0,77
2064	-1,28	-0,61	-0,74	-0,92
2065	-0,62	0,55	-0,98	-0,41
2066	0,79	2,20	1,27	1,87
2067	-0,43	-0,14	-1,02	-0,33
2068	0,37	1,30	0,94	1,15
2069	-1,27	-1,09	-1,08	-0,84
2070	-0,05	0,66	-0,42	0,01
2071	-1,61	-0,33	-0,16	-1,30
2072	-1,15	-0,63	-1,53	-1,07
2073	-1,59	-0,27	-0,91	-0,21
2074	-1,84	-3,22	-0,60	-3,14
2075	-1,05	-2,46	-1,74	-2,26
2076	1,71	1,38	1,67	2,21
2077	-1,76	-0,98	-1,51	-0,79
2078	-1,80	-0,04	-1,26	-0,24
2079	-3,26	-2,22	-3,09	-2,80
2080	-2,52	-2,33	-2,69	-1,86
2081	-2,73	-2,83	-2,64	-2,34
2082	-1,00	-0,02	-0,85	-0,29
2083	-1,64	-0,26	-2,25	0,25
2084	0,45	1,74	1,20	1,62
2085	-3,77	-3,83	-3,35	-2,88
2086	-3,43	-1,46	-3,32	-1,52
2087	-3,62	-3,17	-3,89	-3,43
2088	-1,22	0,56	-1,05	0,01
2089	-1,97	-2,14	-2,80	-1,75
2090	-1,63	0,14	-1,89	0,44
2091	-2,71	-1,26	-2,28	-1,54
2092	-1,23	0,47	-0,23	-0,34
2093	-2,96	-3,21	-3,91	-2,81
2094	0,47	-0,03	0,91	0,85
2095	-4,29	-3,64	-4,53	-2,88
2096	-1,34	-1,24	-0,65	-1,41
2097	-1,04	1,01	0,36	0,99
2098	-0,30	0,12	-0,55	0,33
2099	-0,83	-0,84	-1,35	-0,90
2100	-4,93	-3,30	-4,08	-3,66

The century begins with wet conditions (2007 – 2011), followed by a long extreme drought (2012 – 2018). Extreme precipitation takes place from 2020 until 2024. Until the end of the near future period long extreme droughts occur (2034 – 2039, 2043 – 2045).

Remote future projections result in almost entirely dry conditions of great magnitude (2052 – 2058, 2060 – 2061, 2069 – 2083, 2085 – 2100), and only a couple of moderately wet incidents interfere (2062 – 2063, 2084) (Table 16; Table A XXV, Appendix II).

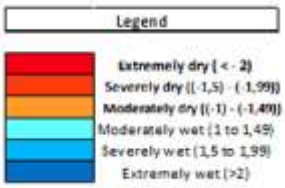

4.2.2.2.2. SPI3 - February (Winter Season)

The control period is obviously the same as in RCP 4.5 projections. For the near future, from 2007 until 2011, 2020 – 2025, 2030 – 2032, 1949 – 1954 wet conditions are going to take place, while for the periods 2013 – 2015, 2033 – 2037, 2044 – 2047 dry conditions prevail.

Regarding the remote future conditions, extremely dry conditions prevail, especially towards the end of the century (Table A XIX, Appendix II).

4.2.2.2.3. SPI3 - May (Spring Season)

The beginning of the century begins with moderately wet conditions (2011 – 2012, 2019 – 2024) but shortly after conditions become severely dry, especially aiming at the distant future (for example during the period of 2083 until 2096 values as high as 30) (Table A XX, Appendix II).

4.2.2.2.4. SPI3 - August (Summer Season)

In the beginning of the century a clear trend cannot be identified, since there don't seem to be a correlation between the grid points. However, after around 2040 and until the end of the century very long dry periods emerge. Especially from 2080 until 2100 in GP1, GP8 and GP13 droughts look extensive and extreme (Table A XXI, Appendix II).

4.2.2.2.5. SPI3 - November (Autumn Season)

From 2004 until 2019, an extreme dry event takes place, interrupted by a 2-year wet period taking place in 2010 – 2011. From 2043 until 2045 another intense drought occurs. It isn't until the end of the century (remote future), when extreme dry events occur again (2077 – 2081, 2095 – 2097) (Table A XXII, Appendix II).

4.2.2.2.6. SPI6 - March (Wet Season)

Near future projections show extended extreme drought events (2002 – 2006, 2013 – 2019, 2024 – 2029, 2032 – 2039, 2043 – 2047), interrupted by less extreme, and not equally long wet incidents (2011 – 2012, 2020 – 2023, around 1950). From 2065 until 2067 a wet conditions prevailed. Distant future projections show extremely dry conditions (2068 – 2076, 2078 – 2083, 2086 – 2088, 2090 – 2094, 2096 – 2097, 2099 – 2100) (Table A XXIII, Appendix II).

4.2.2.2.7. SPI6 - October (Dry Season)

From 202 until 2022 an extreme and prolonged drought takes place. From 2024 until 2028, extreme precipitation occurs, followed by generally dry conditions from 2030 until 2049.

Remote future seems even drier. Apart from some sparse wet incidents showing no consistency among stations, dry conditions dominate almost entirely (2058 – 2061, 2070 – 2071, 2077 – 2081, 2089 – 2093, 2095 – 2100) (Table A XXIV, Appendix II).

4.2.3. Discussion

Contrary to the situation witnessed in the case of gridded observations referring to the past, future projections display statistically significant trends. Regarding RCP4.5 scenario, most trends are negative and some of them (GP1: SPI6 – March, SPI12, GP8: SPI3 – February, SPI6 – March, SPI12, GP13: SPI3 – February) are statistically significant. Some positive trends are also present, with no significance whatsoever. The indices that seem to be affected the most, are the SPI3 corresponding to February, evaluating short-term precipitation trends for the winter season (the wettest season in Greece), the SPI6 at the end of March (mid-term precipitation trends), and the inter-annual 12 month SPI, corresponding to reservoir and groundwater levels (Figure 43).

As expected under RCP 8.5 statistically negative trends are mostly present, some of them exceeding the critical value by far. The indices that seem to be affected the most, are the 3-month SPIs corresponding to February and May evaluating short-term precipitation trends for winter and spring respectively, and the inter-annual 12-month SPI. These findings signify danger concerning agricultural issues since those particular short term SPIs refer to the wettest seasons in Greece when all precipitation takes place providing for streamflows and reservoir levels as well. A severe reduction in groundwater levels is expected to occur far more extreme than what was witnessed in RCP 4.5 (Table 17).

Table 17. Tables showing trendline signs. Left: RCP 4.5 scenario, Right: RCP 8.5 sc

	GP1 rcp45	GP7 rcp45	GP8 rcp45	GP13 rcp45
SPI3 February	-	-	-	-
SPI3 May	-	-	-	-
SPI3 August	-	-	-	-
SPI3 November	-	+	-	+
SPI6 March	-	-	-	-
SPI6 October	-	+	-	+
SPI12 Annual	-	-	-	-

	GP1 rcp85	GP7 rcp85	GP8 rcp85	GP13 rcp85
SPI3 February	-	-	-	-
SPI3 May	-	-	-	-
SPI3 August	-	-	-	-
SPI3 November	-	-	-	+
SPI6 March	-	-	-	-
SPI6 October	-	-	-	-
SPI12 Annual	-	-	-	-

Legend

Trendline Sign

Positive Trend
Negative Trend
Negative Trend (Statistically Significant)

Since agriculture is one of the primal sectors to be affected, several measures have to take place. Efficient soil and irrigation management would greatly assist groundwater storage. New crop varieties demanding less water, producing greater crop yield could also be introduced (Ahmed, 2010). Hazard and vulnerability mapping is essential, especially regarding areas with special characteristics (areas in close proximity to the coastline, or in danger due to certain elements' abundance such as the areas of our study).

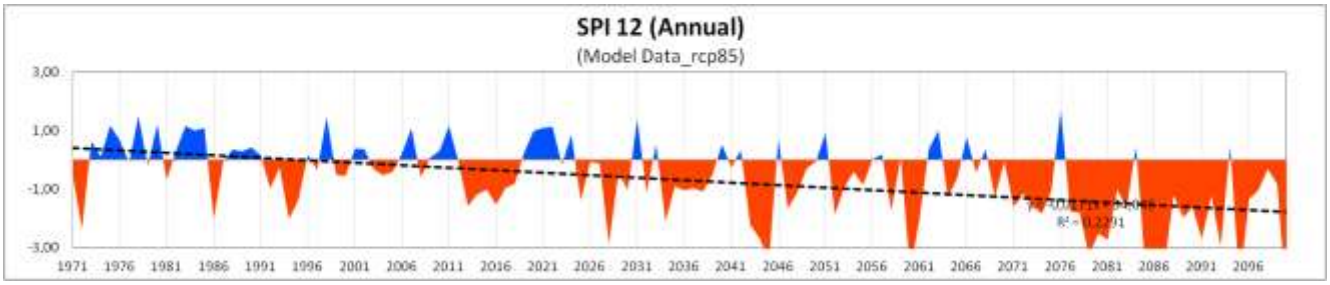

Figure 42. Graph displaying extremely dry conditions towards the end of the century under the RCP 8.5 scenario. (SPI12, grid point GP1)

Variability increases for the most part (Table 18). Regarding RCP 4.5 a positive change is witnessed for the near future but only in two cases it is statistically significant (GP8 (Euboea): SPI3-May, GP13 (Asopos): SPI3-May). Remote future projections show more statistically significant variances, but many negative ones as well. It should be noted that all negative changes are statistically significant. This might be due to the fact that RCP4.5 suggests a stabilization of conditions towards the end of the century (van Vuuren et al., 2011).

RCP 8.5 scenario brings events of higher severity resulting in increased variance in most cases. The second table below (Table 18), shows a rise in variance that is statistically significant, especially concerning remote future projections. Increased variability is likely to affect freshwater systems and water quality by intensifying surface runoff. Ecosystems are in danger as well since flood risk is awaited to elevate.

Table 18. Tables displaying variance changes between current and future (near, remote) conditions

	GP1 RCP4.5 (near future)	GP1 RCP4.5 (remote future)	GP7 RCP4.5 (near future)	GP7 RCP4.5 (remote future)	GP8 RCP4.5 (near future)	GP8 RCP4.5 (remote future)	GP13 RCP4.5 (near future)	GP13 RCP4.5 (remote future)
SPI3 February	+	+	+	+	+	-	+	+
SPI3 May	+	+	+	+	+	+	+	+
SPI3 August	+	-	-	+	-	+	+	+
SPI3 November	+	-	+	-	+	-	+	+
SPI6 March	+	+	+	+	+	+	+	+
SPI6 October	+	-	+	-	+	+	+	+
SPI12 Annual	+	-	+	+	+	-	+	+

	GP1 RCP8.5 (near future)	GP1 RCP8.5 (remote future)	GP7 RCP8.5 (near future)	GP7 RCP8.5 (remote future)	GP8 RCP8.5 (near future)	GP8 RCP8.5 (remote future)	GP13 RCP8.5 (near future)	GP13 RCP8.5 (remote future)
SPI3 February	+	+	+	+	+	+	+	+
SPI3 May	+	+	+	+	+	+	+	+
SPI3 August	+	+	-	-	-	+	+	+
SPI3 November	-	+	+	+	-	+	-	+
SPI6 March	+	+	+	+	+	+	+	+
SPI6 October	+	+	+	+	+	+	+	+
SPI12 Annual	+	+	+	+	+	+	+	+

Legend

Variability Change

- Negative Change
- Positive Change
- Positive Change (Statistically Significant)

For each scenario, correlation between datasets seems to be statistically significant as witnessed in the tables below (Table 19, Table 20). However, correlation between the two scenarios in as expected non-existent (Table 21).

Table 19. RCP 4.5 Correlation tables (all available model datasets and studied indices)

SPI3-February

	GP1 rcp45	*GP7 rcp45*	*GP8 rcp45*	*GP13 rcp45*
GP1 rcp45	1,0000			
GP7 rcp45	0,5402	1,0000		
GP8 rcp45	0,8001	0,8334	1,0000	
GP13 rcp45	0,6911	0,8198	0,8263	1,0000

SPI6-March

	GP1 rcp45	*GP7 rcp45*	*GP8 rcp45*	*GP13 rcp45*
GP1 rcp45	1,0000			
GP7 rcp45	0,6288	1,0000		
GP8 rcp45	0,8029	0,8415	1,0000	
GP13 rcp45	0,6977	0,8693	0,8006	1,0000

SPI3-May

	GP1 rcp45	*GP7 rcp45*	*GP8 rcp45*	*GP13 rcp45*
GP1 rcp45	1,0000			
GP7 rcp45	0,7100	1,0000		
GP8 rcp45	0,8704	0,8073	1,0000	
GP13 rcp45	0,7402	0,9011	0,7854	1,0000

SPI6-October

	GP1 rcp45	*GP7 rcp45*	*GP8 rcp45*	*GP13 rcp45*
GP1 rcp45	1,0000			
GP7 rcp45	0,6077	1,0000		
GP8 rcp45	0,7862	0,7100	1,0000	
GP13 rcp45	0,6931	0,8922	0,7493	1,0000

SPI3-August

	GP1 rcp45	*GP7 rcp45*	*GP8 rcp45*	*GP13 rcp45*
GP1 rcp45	1,0000			
GP7 rcp45	0,4893	1,0000		
GP8 rcp45	0,7749	0,5897	1,0000	
GP13 rcp45	0,6322	0,6993	0,7219	1,0000

SPI12

	GP1 rcp45	*GP7 rcp45*	*GP8 rcp45*	*GP13 rcp45*
GP1 rcp45	1,0000			
GP7 rcp45	0,5680	1,0000		
GP8 rcp45	0,8078	0,7566	1,0000	
GP13 rcp45	0,6205	0,8536	0,7332	1,0000

SPI3-November

	GP1 rcp45	*GP7 rcp45*	*GP8 rcp45*	*GP13 rcp45*
GP1 rcp45	1,0000			
GP7 rcp45	0,5401	1,0000		
GP8 rcp45	0,7800	0,6992	1,0000	
GP13 rcp45	0,6899	0,8460	0,7263	1,0000

Table 20. RCP 8.5 Correlation tables (all available model datasets and studied indices)

SPI3-February

	GP1 rcp85	*GP7 rcp85*	*GP8 rcp85*	*GP13 rcp85*
GP1 rcp85	1,0000			
GP7 rcp85	0,6865	1,0000		
GP8 rcp85	0,8583	0,8726	1,0000	
GP13 rcp85	0,7732	0,8672	0,8430	1,0000

SPI6-March

	GP1 rcp85	*GP7 rcp85*	*GP8 rcp85*	*GP13 rcp85*
GP1 rcp85	1,0000			
GP7 rcp85	0,6858	1,0000		
GP8 rcp85	0,8549	0,8403	1,0000	
GP13 rcp85	0,7544	0,8723	0,7901	1,0000

SPI3-May

	GP1 rcp85	*GP7 rcp85*	*GP8 rcp85*	*GP13 rcp85*
GP1 rcp85	1,0000			
GP7 rcp85	0,7619	1,0000		
GP8 rcp85	0,9099	0,8302	1,0000	
GP13 rcp85	0,8375	0,9324	0,8500	1,0000

SPI6-October

	GP1 rcp85	*GP7 rcp85*	*GP8 rcp85*	*GP13 rcp85*
GP1 rcp85	1,0000			
GP7 rcp85	0,7160	1,0000		
GP8 rcp85	0,8875	0,7307	1,0000	
GP13 rcp85	0,7669	0,9089	0,7419	1,0000

SPI3-August

	GP1 rcp85	*GP7 rcp85*	*GP8 rcp85*	*GP13 rcp85*
GP1 rcp85	1,0000			
GP7 rcp85	0,0572	1,0000		
GP8 rcp85	0,2078	0,4823	1,0000	
GP13 rcp85	0,2882	0,6423	0,6992	1,0000

SPI12

	GP1 rcp85	*GP7 rcp85*	*GP8 rcp85*	*GP13 rcp85*
GP1 rcp85	1,0000			
GP7 rcp85	0,7260	1,0000		
GP8 rcp85	0,9009	0,8204	1,0000	
GP13 rcp85	0,7844	0,9079	0,8207	1,0000

SPI3-November

	GP1 rcp85	*GP7 rcp85*	*GP8 rcp85*	*GP13 rcp85*
GP1 rcp85	1,0000			
GP7 rcp85	0,6064	1,0000		
GP8 rcp85	0,8485	0,7287	1,0000	
GP13 rcp85	0,6944	0,8935	0,7264	1,0000

Table 21. RCP 4.5 and RCP 8.5 Correlation table for SPI3 at the end of February (all available model datasets and studied indices). No correlation is witnessed between scenarios. Other indices suggest similar findings.

	GP1 rcp45	*GP1 rcp85*	*GP7 rcp45*	*GP7 rcp85*	*GP8 rcp45*	*GP8 rcp85*	*GP13 rcp45*	*GP13 rcp85*
GP1 rcp45	1							
GP1 rcp85	0,274351	1						
GP7 rcp45	0,540248	0,155414	1					
GP7 rcp85	0,062893	0,6865	0,152385	1				
GP8 rcp45	0,800077	0,281467	0,833354	0,173635	1			
GP8 rcp85	0,192515	0,858342	0,170919	0,872646	0,302311	1		
GP13 rcp45	0,691096	0,16508	0,819817	0,072854	0,826277	0,134489	1	
GP13 rcp85	0,1179	0,773156	0,082997	0,867249	0,167189	0,842953	0,08006	1

In order to visualize the expected change in precipitation under certain climate change scenarios more effectively, we plotted the mean difference between the control period (1971 – 2000) and the near future period (2021 – 2050) and respectively, between the control and the remote future period (2071 – 2100), concerning precipitation values. Five composites were created, corresponding to annual precipitation, dry and wet six month periods, summer and winter 3-month periods. Each composite consists of four interpolated maps, each of which corresponds to a different scenario output as described above.

In general, the future is projected drier compared to the present. RCP 4.5 scenario shows a mild decrease in precipitation that in most cases becomes more severe towards the end of the century. What's also made obvious in the maps (Figures A I to V, Appendix I) is greater anticipated difference between the lowest and highest value in remote future projections compared to near.

As expected, under the RCP 8.5 scenario the future looks more ominous. Especially regarding remote future projections, intense drought is explicit in most timescales. During the wet period, the RCP 4.5 scenario shows a slight decrease in precipitation, with Asopos area being mostly affected by this change. RCP 8.5 especially in regard to remote future projections shows extreme reductions in the amount of water received, Loutraki area in particular. Projections relating to dry season don't seem to agree. A slight decrease is also obvious, although under the RCP 4.5 scenario precipitation in Loutraki for the near future is expected to be the same, while in Asopos and Euboea precipitation is expected to slightly rise during remote future. However, the maps suggest greater spatial variability towards the end of the century, a finding consistent to IPCC's predictions. RCP 8.5 especially after 2071 shows an intense tendency towards drier conditions. Asopos and Loutraki seem to be influenced the most.

The projections for winter show almost no change for the near future under the RCP 4.5 scenario, while for the remote future, Euboea and Asopos are about to experience less precipitation in total, with Loutraki not being affected at all. RCP 8.5 on the other hand, although it indicates no change for the near future, regarding the remote, dry conditions prevail, most notably in Asopos basin.

It is to be noted that plots displaying the anticipated situation for the 3-month summer season, show increased precipitation towards the end of the century under RCP 4.5 scenario, while the near future experiences slightly drier conditions (Figure 45). It's known that, although not too severe, temperature rise is projected under the RCP 4.5 for the distant future. This fact can be interpreted in two ways. Summer is the driest season in Greece; therefore precipitation values are rather low. It is possible that the suggested increase is but a fluctuation of the model and does not correspond to any real possibility. However, this doesn't seem to be the case for RCP 8.5, where dry conditions prevail towards the end of the century.

Another explanation for this differentiation could be that fact that slightly elevated temperatures could potentially lead to increased convection. Convective rainfall usually occurs due to the vertical growth of air-mass storms with limited horizontal extend. For the ground gets intensely heated by the sun, the warm air rises as a result of evaporation. As it elevates towards the sky, it eventually cools down and the water vapor condenses giving birth to clouds that generate precipitation.

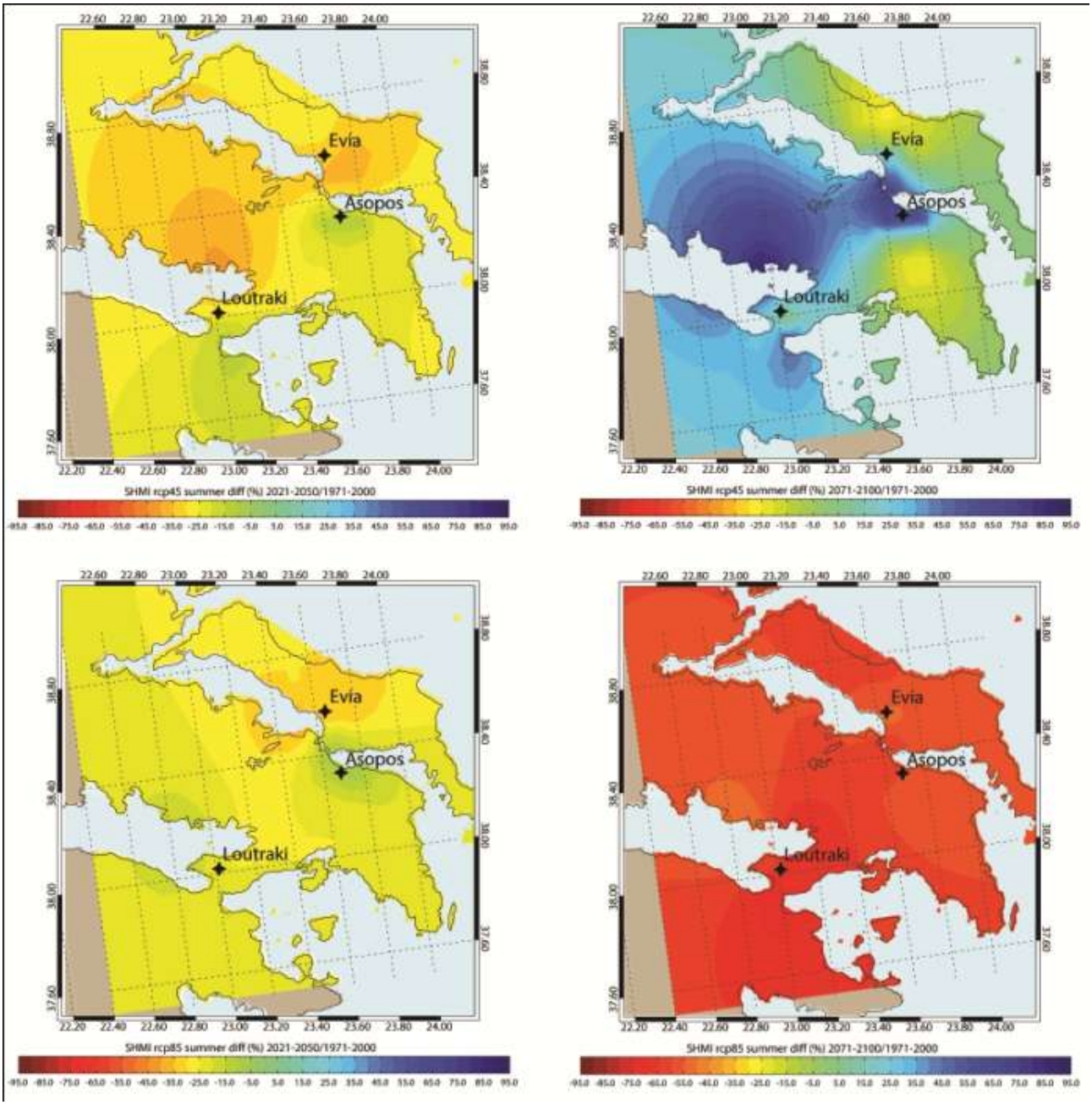

Figure 43. Interpolation maps comparingthe mean's difference from the control period for the near future (upper left) and the remote (upper right) during the summer season for the RCP 4.5 scenario, and the RCP 8.5 (lower left and right), respectively.

For the most part, the area affected by this change is the Asopos basin. Gridded Observational Data (CRU and E-Obs) classified the area as being the driest of all three. This would have important implications on the hydrogeological regime of the area in terms of aquifer recharge and possibly water residence time. Further research should focus in defining these feedbacks on groundwater recharge that subsequently might affect the release of Cr(VI) and other pollutants into the water.

Changes expected for the mean annual precipitation show a slight decrease in precipitation that only becomes more severe towards the end of the century under the RCP 4.5. Under the RCP 8.5, near future will be drier compared to the present. The remote future shows some really low precipitation values, with reductions reaching as much as -40mm.

SPI indices were plotted taking the mean values into account, segmenting the dataset into two periods for each scenario, near (2021 – 2050) and remote future period (2071 – 2100).

In general, near future analysis under the RCP 4.5 scenario, shows no statistically significant trends (Table A VIII, Appendix II), while after 2071 few statistically significant trends occur (Table A IX, Appendix II). RCP 8.5 scenario shows more statistically significant negative changes compared to RCP 4.5 as a whole. Near future projections display some statistical significant trends (Table A X, Appendix II) whose frequency increases dramatically towards the end of the century (Table A XI, Appendix II).

3-month SPIs generally respond to short to medium- term moisture conditions, estimating seasonal trends in precipitation. 3-month SPI for February shows some slight increase in Loutraki region for the near and remote future, while Euboea and Asopos tend to become drier, especially with respect to remote future, under the RCP 4.5 (Figure A VI, Appendix I).Most grid points show statistically significant reductions in mean values referring to remote future projections, corresponding to Euboea and Asopos respectively, while for Loutraki region no statistical significance is reported. RCP 8.5 suggests an overall slight decrease for the near future, while remote future looks significantly drier, under the RCP 8.5 scenario, with all grid points displaying statistically significant negative trends (Table A XI, Appendix II).

The same situation is encountered regarding the 3-month SPI for May (Figure A VII, Appendix I). However, the intensity of drier events is more severe, especially with respect to future projections under RCP 8.5, according to which, most negative changes are statistically significant even in the near future becoming entirely significant in the remote (Table A X, Appendix II and Table A XI, Appendix II). In this case, Euboea region is the one affected the most. It has to be noted that remote future projections show statistically significant reductions even for RCP 4.5.

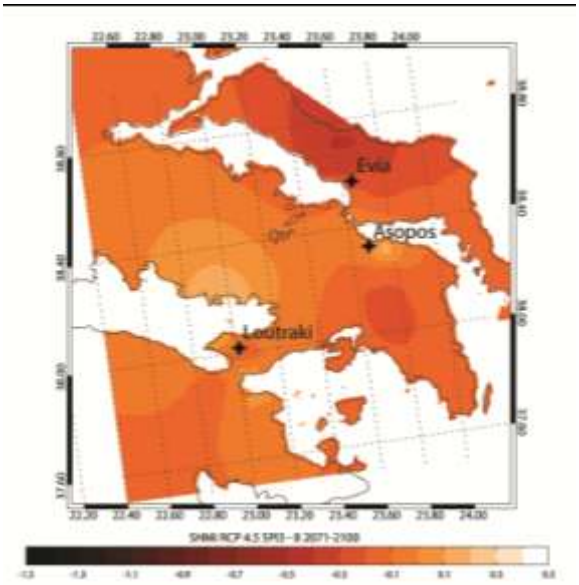

Figure 44. Interpolation map showing average values for the 3-month SPI for August under RCP 4.5 scenario

The same index calculated for August, shows a tendency towards drier conditions (Figure 45). However, the findings are similar to the ones derived from precipitation analysis (Figure A VIII, Appendix I). Under RCP 4.5 remote future projections show less intense drought compared to the near future. This fact might be a result of convective rainfalls manifested during the hot summer months. GP8, a grid point close to Euboea region shows statistically significant decreases concerning remote future (Table A IX, Appendix II). The fact also supports the assumptions about heightened variability towards the end of 2100. RCP 8.5 as expected, suggests further reductions regarding remote future, with all changes being statistically significant (Table A XI, Appendix II).

Finally, 3-month SPI interpolation maps for November verify anticipated trends (Figure A IX, Appendix I); a slight decrease during the near future under the RCP 4.5 scenario for all three study cases, that gets more severe towards the end of the century, with statistical significance being present in GP1 (Loutraki), GP7 (Euboea), and 16,17,18 (Asopos) (Table A IX, Appendix II). RCP 8.5 suggests similar findings, slightly more extreme for both near and remote future projections. Statistical significance is only reported in GP1

(Loutraki) and GP17, 18 (Asopos) regarding near future (Table A X, Appendix II) and GP15, 16 (Asopos) regarding remote (Table A XI, Appendix II).

3-month SPIs correlate with streamflow conditions and indicate meteorological and agricultural droughts. Especially the winter (February) and spring (May) 3-month SPI is strongly associated with soil moisture conditions that could have a severe impact on the beginning of the growing season. Euboea in particular, is largely affected since its economy is primarily based on agricultural activities and the 3-month SPI for May under RCP 8.5 scenario shows extremely negative changes.

6-month SPIs showcase seasonal to medium- term precipitation trends. The 6-month SPI for March does not display any major reductions under RCP 4.5 (Figure A X, Appendix I). Under RCP 8.5 however, even in the near future some grid points (GP1 corresponding to Loutraki area, and GP 17, 18 being closer to Asopos basin) show statistical significance (Table A X, Appendix II). In the remote future all reductions become statistically significant (Table A XI, Appendix II). The same index calculated for October (Figure A XI, Appendix I), shows a slight decrease during the near future, which becomes even less severe regarding remote future under RCP 4.5 (Table A IX, Appendix II). RCP 8.5 shows statistically significant negative changes in some grid points (GP1,2,8,10,12,17 and 18) for near future, while for remote, most reductions display statistical significance, affecting all areas of study (Table A XI, Appendix II).

Conclusions derived from 6-month SPI studies could function as a tool for early warning of hydrological drought. Soil and plant conditions will be severely affected, inducing negative impacts on agriculture in Euboea and river flow in Asopos basin. The aftermath of hydrological droughts can even include reduction in crop yield and produce quality. As a result, the use of chemical fertilizers is expected to increase even more. This will lead to the worsening of the eutrophication phenomenon and will further aggravate the Chromiun problem since concentrations in the ground will increase. 6-month SPIs seem to affect all three areas equally though.

The 12-month SPI suggests mild reductions in precipitation for the near future under both climate change scenarios (Figure 45; Figure A XII, Appendix I), although under RCP 8.5 some statistical significance is observed especially around Asopos basin (Table A IX, Appendix II), while the interpolation maps show a precipitation minimum around the area of Loutraki. Towards the end of the century RCP 4.5 suggests some statistically significant negative values, while RCP 8.5 foretells a future that is significantly drier with all negative changes being statistically significant (Table A XI, Appendix II). This index is closely associated to hydrological and socioeconomic droughts. The Loutraki region is known for its thermal springs and its deep geothermal reservoir. It takes time for a drought incident to affect the hydrological balance, but prolonged droughts can lead to that. The statistically significant changes suggested by the study of the 12-month SPI show that those reservoirs are in danger under both scenarios. Especially under RCP 8.5 the consequences seem to be terrifying. As the underground reservoir becomes empty sea water intrusion is awaited to occur. Generalized water deficiency will elevate Chromium concentrations in the ground in all study areas. As the effect of a long term drought is manifested in society, a socio-economic drought is unavoidable.

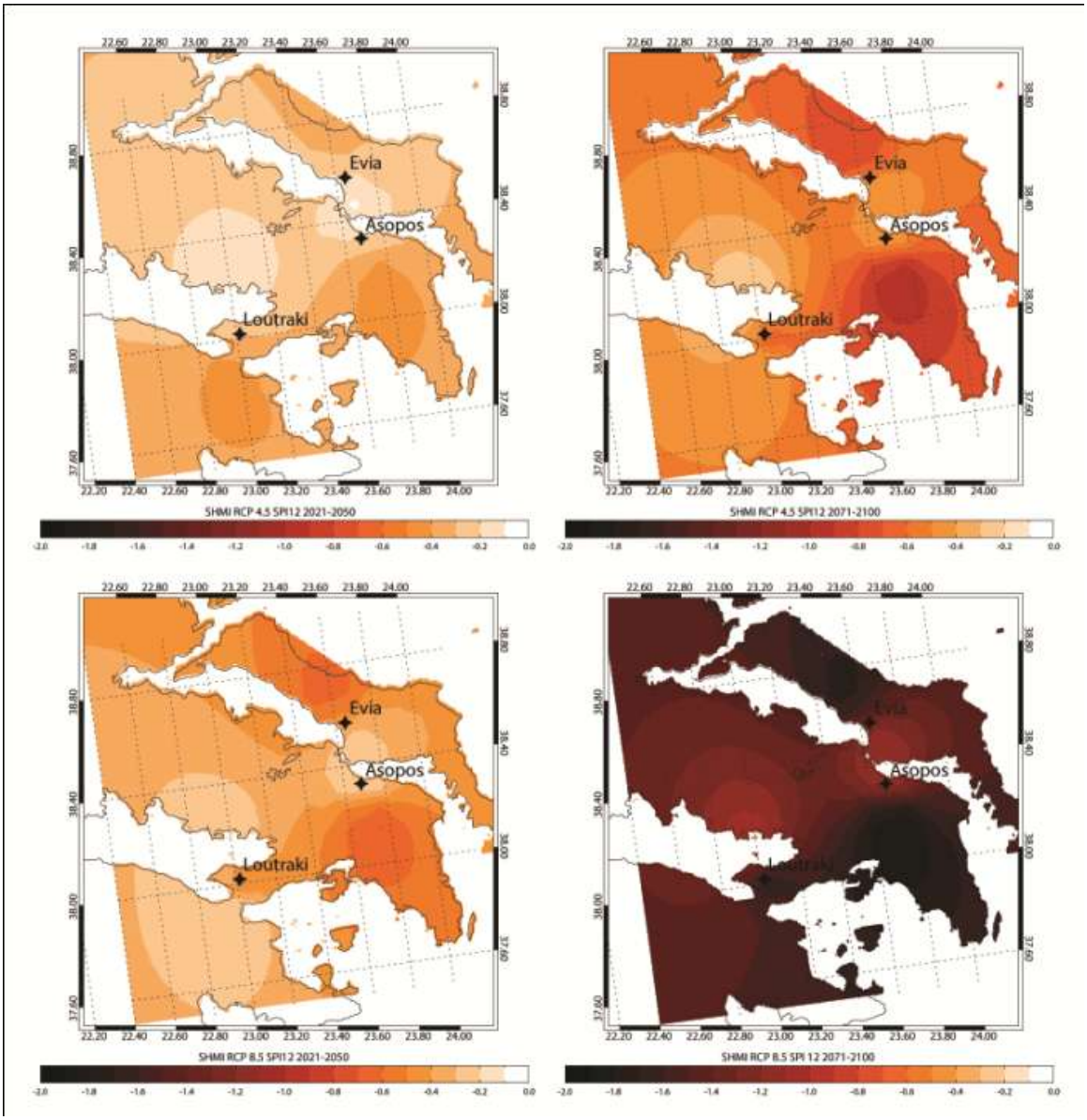

Figure 45. Interpolation maps displaying 12-month SPI values derived from Model data for RCP 4.5 for the near (upper left) and the remote (upper right) future and the RCP 8.5 (lower left and right) respectively.

A comparison was performed between model projections and gridded observations using the timeframe of the control period for model data, since it's the only window in time, for which values are provided by all datasets. This comparison shows that the correlation coefficient value among datasets hardly exceeds 0,4 signifying weak linear relationships, while in most cases, values are much lower than that. This factor suggests model projections should be handled carefully in regard to actual future events.

Of the gridded datasets, the ones displaying stronger linear relationships to the model data are the E-obs datasets. The calculation of SPI indices performed on CRU data took into account the entire time series (114 years), therefore this dataset cannot be directly compared to model and E-Obs data. CRU data was primarily used for the purpose of studying the inter-annual variability corresponding to precipitation patterns and assess the study area's climate conditions. They provide much coarser definition and characterize the area as a whole; the three study areas are not easily distinguishable.

Regarding Model and E-Obs data, it is obvious that certain stations correspond to certain areas. Loutraki is mainly described by GP1 (Model Data) and L1V3, L1V4 (E-Obs Data), Euboea by GP7, GP8 (Model Data), L2V1, L2V2, L2V3 (E-Obs Data), and finally Asopos by GP13 (Model Data) and L3V1 , L3V2 (E-Obs Data)(**Σφάλμα! Το αρχείο προέλευσης της αναφοράς δεν βρέθηκε.**).

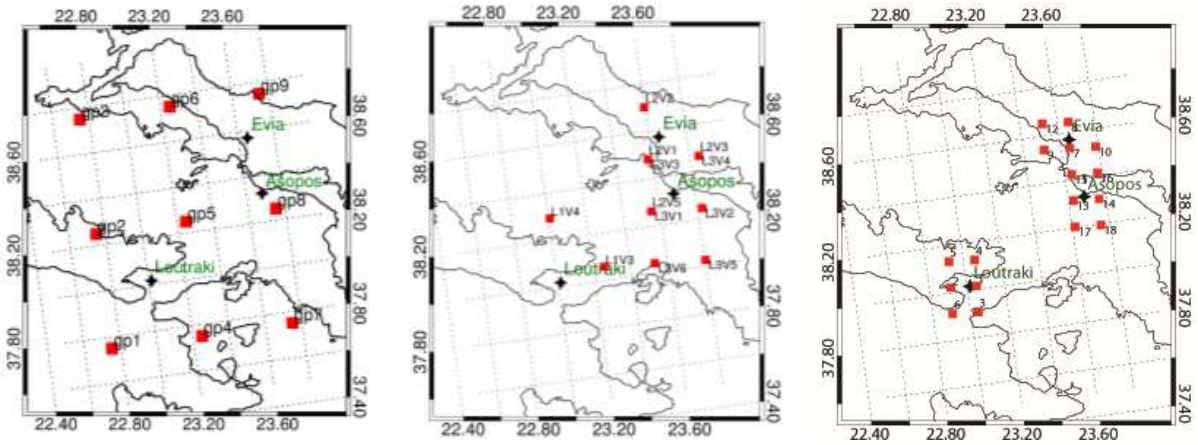

Figure 46. Maps showing CRU, E-Obs and SHMI (Model) data grid points

Regarding Asopos and Euboea, E-obs and model data show acceptable correlation. Loutraki stations don't seem to be closely correlated, due to the area's complicated topography.

5 Conclusions

Current climate precipitation and drought analysis shows that no major threat is posed in terms of water deficit. The majority of studied trends, both regarding precipitation values analysis and indices indicate mostly negative trends. Nevertheless, the statistical significant trends are few and always negative. A slow decrease in precipitation is witnessed, however the lack of statistically significant trends indicates that the current situation doesn't signify serious danger for the study areas, as the precipitation amount is maintained at the same levels since the beginning of the previous century.

Precipitation analysis performed on 20th century data suggested that the driest of the three case studies is the Asopos river basin, while Loutraki displays the highest precipitation values. Drought analysis displayed no statistical significance

Two sample F-test analysis was performed on gridded observational (CRU) data regarding SPI indices and precipitation values in order to determine changes in variability. Contrary to precipitation analysis, in most cases, variability is evidently increased towards the end of the previous century with statistical significance being present. Seasonal precipitation analysis, suggested statistically significant increased variability in some cases especially regarding the wet seasons, winter and spring. Variance analysis performed on SPI indices, displayed statistically significant increases towards the second half of the century as well.

Future climate precipitation analysis was performed in order to suggest the possible evolution of the hydrological conditions characterizing the areas of interest. RCP4.5 shows an overall tendency towards drier conditions with many trends displaying statistically significant results. RCP 8.5 on the other hand looks terrifying (Fig. 47). According to this scenario, extreme and prolonged droughts are anticipated and severe mitigation and adaptation strategies need to be implemented. Almost all trends are negative and statistically significant. The SPI graphs show great negative values almost entirely. Especially during dry seasons, precipitation is non-existent.

Specifically, annual and seasonal analysis showed that under the relatively mild RCP 4.5 scenario, precipitation is expected to slightly decrease in the near future without the occurrence of statistically significant trends. However, with respect to the remote future, negative trends corresponding to Euboea and Loutraki become statistically significant. RCP 8.5 scenario foretells statistically significant precipitation decreases facing the near future for Loutraki and Euboea. Towards the end of the century, all grid points display statistically significant negative trends.

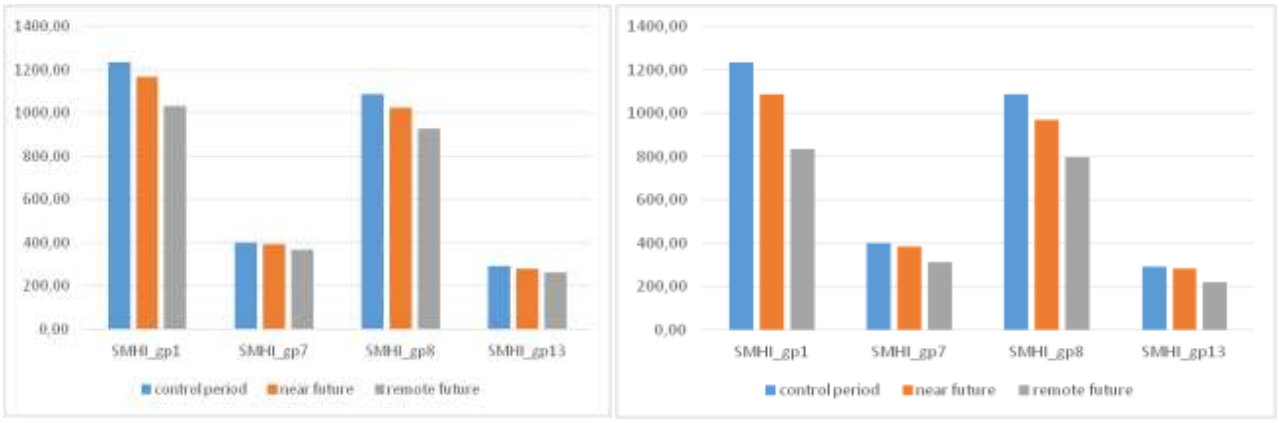

Figure 47. Expected Annual precipitation change under climate change scenarios (left: RCP4.5, right: RCP8.5)

Wet season analysis resulted in decreased precipitation in the future, more intensely towards the end of the century, for both climate change scenarios. However, this is not the case regarding the dry season. Interpolation maps and especially the 3-month summer period, illustrate an increase in precipitation in the remote future, although the near future is expected to be drier compared to the present condition. There are two possible explanations for this phenomenon. We are either witnessing a fluctuation of the model, since during the summer precipitation values are extremely low and therefore the models cannot compute values correctly, or an increase of convective rainfall events due to the expected temperature increase foretold by RCP 4.5. The area that seems to be affected the most from this phenomenon is the Asopos river basin.

Drought analysis performed for both climate change scenarios resulted in similar findings. In the near future, under RCP 4.5 a tendency towards drier conditions appears. In the case of indices linked to the wet season, the SPI3 of February and the SPI6 of March, statistically significant reductions were witnessed, especially regarding Euboea. In addition, all trends referring to the inter-annual SPI 12 are negative and in Euboea and Loutraki statistically significant. Under RCP 8.5 almost all trends are negative and statistically significant, especially with respect to the aforementioned indices.

Three- and six-month SPIs account for short term precipitation trends and are closely related to agricultural drought. Since the largest part of Greece's precipitation total takes place during the wet season, which is affected the most, agricultural practices are likely to suffer, especially in Euboea Island where the economy relies heavily on agriculture. Twelve-month SPIs show statistically significant negative trends under both climate change scenarios, especially RCP 8.5, signifying reductions in groundwater and reservoir levels. Loutraki area, known for its natural springs, will be severely affected.

Variability analysis performed on future precipitation values, suggested that under RCP 4.5 no statistically significant change is expected to occur and facing the remote future, only Asopos will display a statistically significant rise. Under RCP 8.5 variability is projected to increase, and all trends are statistically significant from the beginning until the end of the century.

A rise in variability is also present in the study of drought indices. Under RCP 4.5 most trends referring to the near future are positive, but only some of them are statistically significant. In the remote future, some positive trends become statistically significant (Euboea and Asopos), while others become negative. This is more obvious in Loutraki. It should be noted that all negative changes are statistically significant. This might be due to the fact that RCP4.5 suggests a stabilization of conditions towards the end of the century. RCP 8.5

foretells a statistically significance rise in variance, especially concerning remote future projections. This is likely to affect freshwater systems and water quality by intensifying surface runoff.

A comparison was performed between model projections and gridded observations using the timeframe of the control period for model data, since it's the only window in time, for which values are provided by all datasets. This comparison shows that the correlation coefficient value among datasets hardly exceeds 0,4 signifying weak linear relationships, while in most cases, values are much lower than that. This factor suggests model projections should be handled carefully in regard to actual future events.

It is known that all climate change scenarios show increased temperatures. Nevertheless, changes in precipitation display profound spatial variation. In the Mediterranean basin, and Greece in particular, low precipitation is expected to occur. In general, the future is projected to be drier compared to the present.

From this analysis, it can be deduced that any potential future state between the two studied scenarios is possible in the three case areas. The best way to tackle the adverse effects of climate change regardless of their magnitude is to develop adaptive solutions while building a portfolio of appropriate measures. That way, policies can be developed progressively taking into account the initial agenda, making use of all previous investments, while at the same time considering possible climate change outcomes. Forming water utility network working teams where improvement and sharing of information takes place will aid both mitigation and adaptation actions. The legal framework could be adapted in a way that addresses climate change impacts over the years (Jiménez et al., 2014).

Monitoring and early warning systems may assist in the prevention of disasters. The design and application of decision-making tools that consider uncertainty and fulfill multiple objectives is essential. The CrITERIA project aims at the development of such a tool (Jiménez et al., 2014).

Results derived from this thesis will be combined with other data for establishing future hydrological and hydrogeological balance conditions. The water system's hydrologic response will be calculated in accordance with climate change scenarios.

To this end, additional data have to become employed, for instance temperature, responsible for the evapotranspiration factor, runoff and water storage data. Anticipated change projected in the future, has to be approached with the hydrological balance in mind.

6 Bibliography

1. Abou-Hadid, A.F., (2006). Assessment of impacts, adaptation and vulnerability to climate change in North Africa: food production and water resources. A Final Report Submitted to Assessments of Impacts and Adaptations to Climate Change (AIACC), Project No. AF 90 (Washington, D.C.: International START Secretariat, 2006).
2. Ahmed, A.U. (ed.) (2010). Reducing Vulnerability to Climate Change: The Pioneering Example of Community Based Adaptation in Bangladesh. Centre for Global Change (CGC) and CARE Bangladesh, Dhaka, Bangladesh, 23 pp
3. Alverson, K.D., R.S. Bradley and T.F. Pedersen (eds) (2003), "Paleoclimate, Global Change and the Future", The IGBP Series, Springer-Verlag, New York
4. Bakkenes, M., R.M. Alkemade, F. Ihle, R. Leemans, & J.B. Latour (2002). Assessing effects of forecasted climate change on the diversity and distribution of European higher plants for 2050. Glob. Change Biol., 8, 390-407.
5. Bates, B.C., Z.W. Kundzewicz, S. Wu, & J.P. Palutikof (eds.), (2008). Climate Change and Water. Intergovernmental Panel on Climate Change (IPCC) Technical Paper VI, IPCC Secretariat, Geneva, Switzerland, 210 pp.
6. Bornovas, J.,Lalechos, N.& Filippakis N. (1969). Map of IGME Korinthos.
7. Blenkinsop, S., & H. J. Fowler, (2007). Changes in European drought characteristics projected by the PRUDENCE regional climate models, International Journal Of Climatology, 27, 1595–1610, Wiley InterScience, DOI: 10.1002/joc.1538
8. Botsou, F., Poulos, S.E., Dassenakis, M., & Scoullos, M., (2008). Estimation of surface runoff of Asopos River to the S. Evoikos Gulf, in: International Hydrogeological Congress of Greece, (in Greek with abstract in English).
9. Chatfield, C., (2004). The Analysis of Time Series-An Introduction. 6th Ed., CRC Press, Boca Raton.
10. Christensen, J.H., B. Hewitson, A. Busuioc, A. Chen, X. Gao, I. Held, R. Jones, R.K. Kolli, W.-T. Kwon, R. Laprise, V. Magaña Rueda, L. Mearns, C.G. Menéndez, J. Räisänen, A. Rinke, A. Sarr and P. Whetton, 2007: Regional Climate Projections. In: Climate Change 2007: The Physical Science Basis. Contribution of Working Group I to the Fourth Assessment Report of the Intergovernmental Panel on Climate Change [Solomon, S., D. Qin, M. Manning, Z. Chen, M. Marquis, K.B. Averyt, M. Tignor and H.L. Miller (eds.)]. Cambridge University Press, Cambridge, United Kingdom and New York, NY, USA
11. Collins, M., R. Knutti, J. Arblaster, J.-L. Dufresne, T. Fichefet, P. Friedlingstein, X. Gao, W.J. Gutowski, T. Johns, G. Krinner, M. Shongwe, C. Tebaldi, A.J. Weaver and M. Wehner, 2013: Long-term Climate Change: Projections, Commitments and Irreversibility. In: Climate Change 2013: The Physical Science Basis. Contribution of Working Group I to the Fifth Assessment Report of the Intergovernmental Panel on Climate Change [Stocker, T.F., D. Qin, G.-K. Plattner, M. Tignor, S.K. Allen, J. Boschung, A. Nauels, Y. Xia, V. Bex and P.M. Midgley (eds.)]. Cambridge University Press, Cambridge, United Kingdom and New York, NY, USA.
12. Cooper, G.R.C. (2002). Oxidation and toxicity of chromium in ultramafic soils inZimbabwe, Appl. Geochem., 17, 981–986.
13. Dermatas, D., Mpouras, T., Chrysochoou, M., Panagiotakis, I., Vatseris, C., Linardos, N.& Sakellariou, L. (2015). Origin and concentration profile of chromium in a Greek aquifer. Journal of Hazardous Materials, 281, 35-46.
14. Dotsika, E., Poutoukis, D., & Raco, B., (2010), Fluid geochemistry of the Methana Peninsula and Loutraki geothermal area, Greece, Journal of Geochemical Exploration 104,97–104, Elsevier B.V.

15. DRBG (2011), Zerefos, C., Repapis, C., Giannakopoulos, C., Kapsomenakis, J., Papanikolaou, D., Papanikolaou, M., Poulos, S., Vrekoussis, M., Philandras, C., Tselioudis, G. , Gerasopoulos, E., Douvis, C., Nastos, P., Diakakis, M., Hadjinicolaou, P. , Xoplaki, E. , Luterbacher, J. , Zanis, P., Tzedakis, C., Founda, D., Eleftheratos, & K., Repapis, K., The Environmental, economic and social impacts of climate change in Greece, Climate Change Impacts Study Committee, Bank of Greece, ISBN 978-960-7032-49-2.

16. Easterling, D.R., & Peterson, T.C. (1995). A new method for detecting undocumented discontinuities in climatological time series, International Journal of Climatology 15, 369–377, Elsevier B.V.

17. Edwards, D. C. , & McKee, T. B. .(1997). Characteristics of 20th century drought in the United States at multiple time scales. Climatology Report 97-2, Department of Atmospheric Science, Colorado State University, Fort Collins, Colorado.

18. Founda D., Giannakopoulos C., Pierros F., Kalimeris A., & Petrakis M. (2013), Observed and projected precipitation variability in Athens over a 2.5 century period, Atmos. Sci. Let. 14: 72–78, DOI: 10.1002/asl2.419

19. Fantoni, D., Canepa, Z.M., Cipolli, Z.F., Marini, Z.L., Ottonello, G. , & Zuccolini, Z.M.V. (2002). Natural hexavalent chromium in groundwaters interacting with ophioliticrocks, Environ. Geol. 42 871–882.

20. Founda, D., & Giannakopoulos, C. (2009). The exceptionally hot summer of 2007 in Athens, Greece — A typical summer in the future climate? Glob. Planet. Change 67, 227–236.

21. Giorgi, F. & P. Lionello (2008). “Climate change projections for the Mediterranean region”, Global and Planetary Change, 63, Elsevier , 90–104

22. Giorgi F., Jones C., & Asrar G., (2009). Addressing climate information needs at the regional level: The CORDEX framework. WMO Bulletin, Vol. 58, No. 3. , 175-183

23. Girod B., Wiek A., Mieg H., Hulme M. (2009). The evolution of the IPCC’s emissions scenarios, Environmental Science And Policy 12: 103 - 118, Elsevier

24. Harris, I., Jones, P.D., Osborn, T.J. & Lister, D.H. (2014). Updated high-resolution grids of monthly climatic observations - the CRU TS3.10 Dataset. International Journal of Climatology 34, 623-642

25. Hayes, M. (2003). "Drought indices." National Drought Mitigation Center, University of Nebraska-Lincoln

26. Hoerling, M., Eischeid, J., Perlwitz, J., Quan, X., Zhang, T., & Pegion, P. (2012). On the increased frequency of Mediterranean drought.J. Clim. 25 (6), 2146–2161.

27. Haylock, M.R., Hofstra, N. , Klein Tank, A.M.G., Klok, E.J., Jones, P.D., & New , M.. (2008). A European daily high-resolution gridded dataset of surface temperature and precipitation. J. Geophys. Res (Atmospheres), 113, D20119, doi:10.1029/2008JD10201"

28. Heinrich, G., & Gobiet, A. (2012). The future of dry and wet spells in Europe: a comprehensive study based on the ENSEMBLES regional climate models, International Journal Of Climatology, Volume 32, 1951–1970, Wiley InterScience, DOI: 10.1002/joc.2421

29. Houghton J.T., Jenkins G.J., Ephraums J.J., and IPCC , (1990).CLIMATE CHANGE The IPCC Scientific Assessment, (Cambridge, New York, Port CHester, Melbourne, Sydney: Cambridge University Press

30. House, J.I., Orr, H.G. , Clark, J.M., Gallego-Sala, A.V., Freeman, C., Prentice, I.C., & Smith, P. (2010). Climate change and the British Uplands: evidence for decision-making. Climate Research, 45(1), 3-12.

31. Hulme, M., (1992). A 1951-80 global land precipitation climatology for the evaluation of General Circulation Models. Climate Dynamics, 7, 57-72.

32. Hulme M, Osborn TJ & Johns TC (1998) Precipitation sensitivity to global warming: comparison of observations with HadCM2 simulations. Geophys. Res. Lett., 25, 3379-3382.

33. Hunter, P., (2003). Climate change and waterborne and vector borne disease. J. Appl. Microbiol., 94, 37-46

34. IPCC Special Report on Emissions Scenarios (SRES) (2000) by N. Nakićenović, J. Alcamo, G. Davis, et al.,edited by N. Nakićenović, R. Swart

35. IPCC, (2007). The Physical Science Basis. Contribution of Working Group I to the Fourth Assessment Report of the Intergovernmental Panel on Climate Change, edited by: Solomon, S., Qin, D., Manning, M., Chen, Z.,

Marquis, M., Averyt, K. B., Tignor, M., and Miller, H. L., Cambridge University Press, Cambridge, United Kingdom and New York, NY, USA, 996 pp.

36. IPCC, (2013), Summary for Policymakers. In: Climate Change 2013: The Physical Science Basis. Contribution of Working Group I to the Fifth Assessment Report of the Intergovernmental Panel on Climate Change [Stocker, T.F., D. Qin, G.-K. Plattner, M. Tignor, S.K. Allen, J. Boschung, A. Nauels, Y. Xia, V. Bex and P.M. Midgley (eds.)]. Cambridge University Press, Cambridge, United Kingdom and New York, NY, USA.
37. IPCC, (2014), Annex II: Glossary [Mach, K.J., S. Planton and C. von Stechow (eds.)]. In: Cli¬mate Change 2014: Synthesis Report. Contribution of Working Groups I, II and III to the Fifth Assessment Report of the Intergovernmental Panel on Climate Change [Core Writing Team, R.K. Pachauri and L.A. Meyer (eds.)]. IPCC, Geneva, Switzerland, pp. 117-130.
38. IPCC, (2014). Summary for policymakers. In: Climate Change 2014: Impacts, Adaptation, and Vulnerability. Part A: Global and Sectoral Aspects. Contribution of Working Group II to the Fifth Assessment Report of the Intergovernmental Panel on Climate Change [Field, C.B., V.R. Barros, D.J. Dokken, K.J. Mach, M.D. Mastrandrea, T.E. Bilir, M. Chatterjee, K.L. Ebi, Y.O. Estrada, R.C. Genova, B. Girma, E.S. Kissel, A.N. Levy, S. MacCracken, P.R. Mastrandrea, and L.L. White (eds.)]. Cambridge University Press, Cambridge, United Kingdom and New York, NY, USA, 1-32.
39. James, B.R., (1996). The challenge of remediating chromium-contaminated soil, J. Env-iron. Sci. Technol., 30 248–251.
40. Jansen, E., J. Overpeck, K.R. Briffa, J.-C. Duplessy, F. Joos, V. Masson-Delmotte, D. Olago, B. Otto-Bliesner, W.R. Peltier, S. Rahmstorf, R. Ramesh, D. Raynaud, D. Rind, O. Solomina, R. Villalba & D. Zhang. (2007). “Palaeoclimate”, in Solomon, S., D. Qin, M. Manning, Z. Chen, M. Marquis, K.B. Averyt, M. Tignor and H.L. Miller (eds), “Climate Change 2007: The Physical Science Basis”, Contribution ofWorking Group I to the Fourth Assessment Report of the Intergovernmental Panel on Climate Change, Cambridge University Press, Cambridge, United Kingdom, and New York, NY, USA.
41. Jiang, X.Y., Niu, G.Y., & Yang, Z.L. (2009). Impacts of vegetation and groundwater dynamics on warm season precipitation over the Central United States. Journal of Geophysical Research: Atmospheres, 114, D06109, doi:10.1029/ 2008JD010756.
42. Jiménez Cisneros, B.E., Oki, T.,. Arnell, N.W., Benito, G., Cogley, J.G. , Dφll, P., Jiang, T., & Mwakalila, S.S. (2014). Freshwater resources. In: Climate Change 2014: Impacts, Adaptation, and Vulnerability. Part A: Global and Sectoral Aspects. Contribution of Working Group II to the Fifth Assessment Report of the Intergovernmental Panel on Climate Change [Field, C.B., V.R. Barros, D.J. Dokken, K.J. Mach, M.D. Mastrandrea, T.E. Bilir, M. Chatterjee, K.L. Ebi, Y.O. Estrada, R.C. Genova, B. Girma, E.S. Kissel, A.N. Levy, S. MacCracken, P.R. Mastrandrea, and L.L. White (eds.)]. Cambridge University Press, Cambridge, United Kingdom and New York, NY, USA, pp. 229-269.
43. Kalamaras N., H. Michalopoulou, H. R. Byun (2010), Detection of drought events in Greece using daily precipitation, Hydrology Research Apr 2010, 41 (2) 126-133; DOI: 10.2166/nh.2010.001
44. Kaprara, E., Kazakis, N., Simeonidis, K., Coles, S., Zouboulis, A. I., Samaras, P., & Mitrakas, M. (2015). Occurrence of Cr (VI) in drinking water of Greece and relation to the geological background. Journal of hazardous materials, 281, 2-11.
45. Karavitis, C. A., Alexandris, S., Tsesmelis, D.E., Athanasopoulos, G. (2011). Water, Volume 3, pp 787-805, ISSN 2073-4441, doi:10.3390/w3030787
46. Karpouzos, D.K., Kavalieratou, S., & Babajimopoulos, C. (2010). Trend Analysis of Precipitation Data in Pieria Region (Greece), European Water 30: 31-40, E.W. Publications
47. Kanellopoulou E. (2005). Climatology Laboratory Exercises, Athens. (in Greek)
48. Karavitis C. A., Alexandris S., Tsesmelis D. E., & Athanasopoulos G. (2011). Application of the Standardized Precipitation Index (SPI) in Greece Water 2011, 3, 787-805; doi:10.3390/w3030787.
49. Kasimir-Klemedtsson A., Klemedtsson L., Berglund K., Martikainen P., Silvola J., and Oenema O., (1997) "Greenhouse gas emissions from farmed organic soils: a review," Soil Use and Management, no. 13
50. Katsikatsos, G., Fytrolakis, & N., Perdikatsis, V. (1980). Contribution to the genesis of lateritic deposits of the upper Cretaceous transgression in Attica and central Euboea (Greece). Proceedings of International

Symposium in Metallogeny of Mafic and Ultramafic Complexes. The Eastern Mediterranean–Western Asia Area and its Comparison With Similar metallogenic Environments in the World, Athens, 257–265.

51. Katsikatsos, G., Koukis, G., Fytikas, M., Anastopoulos, J., & Kanaris, J. (1981). Geological Map of Greece, Scale 1:50.000, Psachna-Pilion Sheet. Greek Institute of Geology And Mineral Exploration.
52. Kazakis, N., Kantiranis, N., Voudouris, K. S., Mitrakas, M., Kaprara, E., & Pavlou, A. (2015). Geogenic Cr oxidation on the surface of mafic minerals and the hydrogeological conditions influencing hexavalent chromium concentrations in groundwater. Science of the Total Environment, 514, 224-238.
53. Kelepertzis, E., Galanos, E., & Mitsis, I. (2013). Origin, mineral speciation and geochemical baseline mapping of Ni and Cr in agricultural topsoils of Thiva valley (central Greece). Journal of Geochemical Exploration, 125, 56-68.
54. Khan, A.S., A. Ramachandran, N. Usha, S. Punitha, & V. Selvam. (2012). Predicted impact of the sea-level rise at Vellar–Coleroon estuarine region of Tamil Nadu coast in India: mainstreaming adaptation as a coastal zone management option. Ocean and Coastal Management, 69, 327-339.
55. Klein, R. & Nicholls R. (1999). Assessment of coastal vulnerability to climate change. Ambio, 28, 182-187
56. Kontou M., (2011). Public Participation in Environmental Decision-Making Processes. The Asopos case, MA ESST
57. Kostopoulou, E. & Jones, P. D. (2005). Assessment of climate extremes in the Eastern Mediterranean, Meteor. Atmos. Phys., 89, 69–85, doi:10.1007/s00703-005-0122-2.
58. Kostopoulou, E., Giannakopoulos, C., Hatzaki, M., Karali, A., Hadjinicolaou, P., Lelieveld, J., & Lange, M. A. (2014). Spatio-temporal patterns of recent and future climate extremes in the eastern Mediterranean and Middle East region, Nat. Hazards Earth Syst. Sci., 14, 1565-1577, doi:10.5194/nhess-14-1565-2014.
59. Kounis, G. & Vitoriou-Georgouli A. (2003). Hydrogeological survey of Schinos area with implementation of pumping tests.
60. Kovats, R.S., Valentini, R.,. Bouwer, L.M., Georgopoulou, E., Jacob, D., Martin, E., Rounsevell, M. & Soussana, J.-F., (2014). Europe. In: Climate Change 2014: Impacts, Adaptation, and Vulnerability. Part B: Regional Aspects. Contribution of Working Group II to the Fifth Assessment Report of the Intergovernmental Panel on Climate Change [Barros, V.R., C.B. Field, D.J. Dokken, M.D. Mastrandrea, K.J. Mach, T.E. Bilir, M. Chatterjee, K.L. Ebi, Y.O. Estrada, R.C. Genova, B. Girma, E.S. Kissel, A.N. Levy, S. MacCracken, P.R. Mastrandrea, and L.L.White (eds.)]. Cambridge University Press, Cambridge, United Kingdom and New York, NY, USA, pp. 1267-1326.
61. Koutroulis, A. G., Vrohidou, A. E. K., & Tsanis, I. K. (2010). Spatiotemporal Characteristics of Meteorological Drought for the Island of Crete, Journal of Hydrometeorology, 12, 206 - 224
62. Kundzewicz, Z.W., L.J. Mata, N.W. Arnell, P. Döll, P. Kabat, B. Jiménez, K.A. Miller, T. Oki, Z. Sen & I.A. Shiklomanov, (2007). Freshwater resources and their management. Climate Change 2007: Impacts, Adaptation and Vulnerability. Contribution of Working Group II to the Fourth Assessment Report of the Intergovernmental Panel on Climate Change, M.L. Parry, O.F. Canziani, J.P. Palutikof, P.J. van der Linden and C.E. Hanson, Eds., Cambridge University Press, Cambridge, UK, 173-210
63. Lana, X., Serra, C., & Burgueno, A. (2001). Patterns of monthly rainfall shortage and excess in terms of the standardized precipitation index for Catalonia (NE Spain), International Journal Of Climatology, 21, 1669–1691, Wiley InterScience, DOI: 10.1002/joc.697
64. Lioki - Leivada H. & Asimakopoylous D. N. (2010). Applied Statistics Lessons, Symmetria, Athens (in Greek)
65. Lionello, P., et al., (2006). Cyclones in the Mediterranean region: climatology and effects on the environment. In: Lionello, P., Malanotte-Rizzoli, P., Boscolo, R. (Eds.), Mediterranean Climate Variability. Elsevier, Amsterdam, pp. 325–372.
66. Lilli M.A., Moraetis D., Nikolaidis N.P., Karatzas G.P., & Kalogerakis N. (2014). Characterization and mobility of geogenic chromium in soils and riverbed sediments of Asopos basin, Journal of Hazardous Materials, 281, 12–19
67. Lionello, P. (Ed.) (2012). The Climate of the Mediterranean Region: From the Past to the Future, Amsterdam: Elsevier (Netherlands) 9780124160422, 502.

68. Livada I. & Assimakopoulos V.D. (2007). Spatial and temporal analysis of drought in greece using the Standardized Precipitation Index (SPI), Theoretical and Applied Climatology July 2007, Volume 89, Issue 3, 143-153.

69. Lloyd-Hughes, B., & Saunders M.A. (2002). A drought climatology for Europe, International Journal Of Climatology, Volume 22, Pages 1571–1592, Wiley InterScience, 10.1002/joc.846

70. Lu, X.X., Zhang, S. & Xu, J. (2010). Climate change and sediment flux from the Roof of the World. Earth Surface Processes and Landforms, 35(6), 732-735.

71. Luterbacher, J. and E. Xoplaki (2003), "500-Year Winter Temperature and Precipitation Variability over the Mediterranean Area and its Connection to the Large-Scale Atmospheric Circulation", in Bolle, H.-J. (ed.), "Mediterranean Climate. Variability and Trends", Springer Verlag, Berlin, Heidelberg, 133-53.

72. Maheras, P., Tolika, K. , Anagnostopoulou, C. , Vafiadis, M., Patrikas, I. & Floca H. (2004). On the relationship between circulation types and changes in rainfall variability in Greece", International Journal of Climatology, 24, 1695-1712.

73. Mariolopoulos, E.G. (1938). Climate of Greece. Athens Greece (in Greek)

74. Masui, T., Matsumoto, K., Hijioka, Y., Kinoshita, T., Nozawa, T., Ishiwatari, S., Kato, E., Shukla, P.R., Yamagata, Y., Kainuma, M. (2011) An emission pathway to stabilize at 6 W/m2 of radiative forcing. Climatic Change. doi: 10.1007/s10584-011-0150-5

75. McKee, T.B., Doesken, N.J., & Kleist, J. (1993). The relationship of drought frequency and duration to time scales. Preprints Eighth Conf on Applied Climatology Anaheim CA. Amer Meteor Soc, 179 - 184

76. McKenzie, D. (1970). Plate tectonics of the Mediterranean region. Nature 226.

77. McKillup, S. (2006). Statistics Explained: An Introductory Guide for Life Scientists (1st ed.). Cambridge, UK: Cambridge University Press, 32–38.

78. Meier, K. J., Brudney, J. L. & Bohte, J. (2009). Applied Statistics for Public and Nonprofit Administration. Urban Affairs Books. Book 4.

79. Mimikou & Baltas, (2013). Assessment of Climate Change Impacts in Greece: A General Overview, American Journal of Climate Change, Volume 3, 46-56, Scientific Research

80. Mitchell, T.D. & Jones, P.D. (2005). An improved method of constructing a database of monthly climate observations and associated high-resolution grids. International Journal of Climatology 25, 693-712

81. Mitchell, T.D., Hulme, M. & New, M., (2002). Climate data for political areas. Area 34, 109-112

82. Mitchell, T. D., et al, (2003). A comprehensive set of climate scenarios for Europe and the globe. Tyndall Centre Working Paper 55.

83. Molina, M., Aburto, F.N. , Calderon, R.L. , Cazanga, M. , & Escudey, M. , (2009). Trace elementcomposition of selected fertilizers used in Chile: phosphorus fertilizers as asource of long-term soil contamination, J. Soil Contam. 18, 497–511.

84. Moraetis D., Nikolaidis N.P., Karatzas G.P., Dokou Z., Kalogerakis N., Winkel L.H.E., & Palaiogianni-Bellou A., (2012). Origin and mobility of hexavalent chromiumin North-Eastern Attica, Greece, Appl. Geochem. 27 1170–1178.

85. New, M., Hulme, M. & Jones, P.D., (1999). Representing twentieth century space-time climate variability. Part 1: development of a 1961-90 mean monthly terrestrial climatology. Journal of Climate 12, 829-856

86. New, M., Hulme, M. & Jones, P.D., (2000). Representing twentieth century space-time climate variability. Part 2: development of 1901-96 monthly grids of terrestrial surface climate. Journal of Climate 13, 2217-2238

87. New, M., Lister, D., Hulme, M. & Makin, I. (2002). A high-resolution data set of surface climate over global land areas. Climate Research 21

88. Noble, I.R., Huq, S., Anokhin, Y.A., Carmin, J., Goudou, D., Lansigan, F.P., Osman-Elasha, B. & Villamizar, A. (2014). Adaptation needs and options. In: Climate Change 2014: Impacts, Adaptation, and Vulnerability. Part A: Global and Sectoral Aspects. Contribution of Working Group II to the Fifth Assessment Report of the Intergovernmental Panel on Climate Change [Field, C.B., V.R. Barros, D.J. Dokken, K.J. Mach, M.D.

Mastrandrea, T.E. Bilir, M. Chatterjee, K.L. Ebi, Y.O. Estrada, R.C. Genova, B. Girma, E.S. Kissel, A.N. Levy, S. MacCracken, P.R. Mastrandrea, and L.L.White (eds.)]. Cambridge University Press, Cambridge, United Kingdom and New York, NY, USA, 833-868.

89. Oze, C., Fendorf, S., Bird, D.K. , Coleman, R.G., (2004). Chromium geochemistry of serpentine soils, Int. Geol. Rev. 46, 97–126.
90. Pal, J.S., Giorgi, F., & Bi, X., (2004). Consistency of recent summer European precipitation trends an extremes with future regional climate projections. Geophys. Res. Lett. 31, L13202.
91. Panagiotakis, I., Dermatas, D., Vatseris, C., Chrysochoou, M., Papassiopi, N., Xenidis, A., & Vaxevanidou, K. (2015). Forensic investigation of a chromium (VI) groundwater plume in Thiva, Greece. Journal of Hazardous Materials, 281, 27-34.
92. Papanikolaou, D., Mariolakos, I., Lekkas, E., & Lozios, S. (1988). Morphotectonic observations on the Asopos basin and the Coastal zone of Oropos. Contribution to the Neotectonics of Northern Attica, Bull. Geol. Soc. Greece 20 252–267.
93. Pausas, J.G. & .Malak, D. A. (2004). Spatial and temporal patterns of fire and climate change in the eastern Iberian Peninsula (Mediterranean Basin). Ecology, Conservation and Management of Mediterranean Climate Ecosystems of the World, M.
94. Peterson, T.C., & Easterling, D.R., (1994). Creation of homogenous composite climatological reference series. International Journal of Climatology 14: 671–679.
95. Pyrgaki, K., Argyraki, A., Kelepertzis, E. , Paraskevopoulou, V. Botsou, F., Dassenakis, E., Mitsis, I. & Skourtsos, E. , (2016). Occurence Of Hexavalent Chromium In The Ophiolite Related Aquifers Of Loytraki And Schinos Areas, Greece, Bulletin of the Geological Society of Greece, vol. L
96. Repapis, C.C. & Philandras, C.M. (1988). A note on the air temperature trends of the last 100 years as evidenced in the Eastern Mediterranean time series, Theor. Appl. Climatol., 39, 93-107.
97. Riahi, K., Rao, S., Krey, V. Cho, C., Chirkov, V., Fischer, G., Kindermann, G., Nakicenovic, N., & Rafaj., P. (2011). RCP 8.5—A scenario of comparatively high greenhouse gas emissions, Climatic Change 109: 33. doi:10.1007/s10584-011-0149-y
98. Robertson G. P., Paul E. A., Harwood R. R., (2000) Greenhouse Gases in Intensive Agriculture: Contributions of Individual Gases to the Radiative Forcing of the Atmosphere, 289, (New York: American Association for the Advancement of Science).
99. Sales, R.F.M., (2009). Vulnerability and adaptation of coastal communities to climate variability and sea-level rise: their implications for integrated coastal management in Cavite City, Philippines. Ocean and Coastal Management, 52(7), 395-404.
100. Settele, J., Scholes, R., Betts, R., Bunn, S., Leadley, P., Nepstad, D., Overpeck, J.T., & Taboada, M.A. (2014). Terrestrial and inland water systems. In: Climate Change 2014: Impacts, Adaptation, and Vulnerability. Part A: Global and Sectoral Aspects. Contribution of Working Group II to the Fifth Assessment Report of the Intergovernmental Panel on Climate Change [Field, C.B., V.R. Barros, D.J. Dokken, K.J. Mach, M.D. Mastrandrea, T.E. Bilir, M. Chatterjee, K.L. Ebi, Y.O. Estrada, R.C. Genova, B. Girma, E.S. Kissel, A.N. Levy, S. MacCracken, P.R. Mastrandrea, and L.L. White (eds.)]. Cambridge University Press, Cambridge, United Kingdom and New York, NY, USA, pp. 271-359.
101. Skarpelis, N. (2006). Lateritization processes of ultramafic rocks in Cretaceous times: the fossil weathering crusts of mainland Greece. J. Geochem. Explor. 88, 325–328.
102. Smith K.A., Ball T., Conen F., Dobbie K.E., Massheder J., Rey A., "Exchange of greenhouse gases between soil and atmosphere: interactions of soil physical factors and biological processes," European Journal of Soil Science, no. 54 (2003): 779-791.
103. Snedecor, G.W. & Cochran, W. G. (1989), Statistical Methods, Eighth Edition, Iowa State University Press.
104. Spinoni, J., Naumann, G., Vogt J. V., & Barbosa, P. (2015). The biggest drought events in Europe from 1950 to 2012, Journal of Hydrology: Regional Studies, Volume 3, March 2015, Pages 509-524, ISSN 2214-5818, http://dx.doi.org/10.1016/j.ejrh.2015.01.001.

105. Stamatis G., Alexakis D., Gamvroula D., & Migiros G. (2011). Groundwater quality assessment in Oropos – Kalamos basin, Attica, Greece, Environ. Earth Sci. 64 973–988.

106. Taylor, K.E., Stouffer, R.J., & Meehl, G.A. (2012). An Overview of CMIP5 and the experiment design. Bull. Amer. Meteor. Soc., 93, 485-498.

107. Thom, H. C. S. Same methods of climatological analyses. World Meteorological Organization, Geneva, 53p, 1966. (WMO, 199; TP, 103; Technical note. ,81

108. Thomson, A.M., Calvin, K.V., Smith, S.J., Kyle,G. P., Volke, A., Patel, P., Delgado-Arias, S., Bond-Lamberty, B., Wise,M. A., Clarke, L. E., & Edmonds , J. A. (2011). RCP4.5: a pathway for stabilization of radiative forcing by 2100, Climatic Change 109: 77. doi:10.1007/s10584-011-0151-4

109. Tigkas D. (2008). Drought characterization and monitoring in regions of Greece, European Water 23/24, 29-39

110. Vicente-Serrano S.M., Beguería S., & López-Moreno J.I. (2010). A Multi-scalar drought index sensitive to global warming: The Standardized Precipitation Evapotranspiration Index – SPEI. Journal of Climate 23: 1696, DOI: 10.1175/2009JCLI2909.1.

111. Vicente-Serrano, S.M., Zouber, A., Lasanta, T., & Pueyo, Y. (2012). Dryness is accelerating degradation of vulnerable shrublands insemiarid Mediterranean environments. Ecol. Monogr. 82 (4), 407–428

112. Uppala, S., Dee, D., Kobayashi, S., Berrisford, P. & Simmons, A., (2008). Towards a climate adapt assimilation system: status update of ERA Interim, ECMWF Newsletter, 115, 12-18

113. Van Dijk, A.I.J.M. & Keenan, R.J. (2007), Planted forests and water in perspective, Forest Ecology and Management, 251(1-2), 1-9.

114. Van Vuuren, D.P., Den Elzen, M.G.J., Lucas, P.L., Eickhout, B., Strengers, B.J., Van Ruijven, B., Wonink, S., Van Houdt, R.,

115. (2007). Stabilizing greenhouse gas concentrations at low levels: an assessment of reduction strategies and costs. Climate Change 81:119–159

116. Van Vuuren, D.P., Edmonds, J., Kainuma, M. Riahi, K., Thomson, A., Hibbard, K., Hurtt, G. C., Kram, T., Krey, V., Lamarque, J.-F., Masui, T., Meinshausen, M., Nakicenovic , N., Smith, S.J., & Rose, S.K., (2011). The representative concentration pathways: an overview, Climatic Change, 109: 5. doi:10.1007/s10584-011-0148-z

117. Voutsis, N. (2011). Weathering rates of ultrabasic rocks in Euboea Island and controls of the chemical composition of groundwaters and surface waters PhD Thesis National and Kapodistrian University of Athens, Faculty of Geology and Geoenvironment

118. Voutsis, N., Kelepertzis, E., Tziritis, E., & Kelepertsis, A., (2015). Assessing the hydrogeochemistry of groundwaters in ophiolite areas of Euboea Island, Greece, using multivariate statistical methods. Journal of Geochemical Exploration, 159, 79–92

119. WCRP Coupled Model Intercomparison Project – Phase 5: Special Issue of the CLIVAR Exchanges Newsletter, No. 56, Vol. 15, No. 2

120. Wilhite, D.A. & Glantz, M.H. (1985). Understanding the drought phenomenon: the role of definitions. Water International, 10:111–120.

121. World Meteorological Organization (2012), Standardized Precipitation Index User Guide (WMO-No. 1090), Geneva. ISBN 978-92-63-11091-6.

122. World Meteorological Organization (WMO) and Global Water Partnership (GWP), (2016) Handbook of Drought Indicators and Indices (M. Svoboda and B.A. Fuchs). Integrated Drought Management Programme (IDMP), Integrated Drought Management Tools and Guidelines Series 2. Geneva

123. Wong, P.P., Losada, I.J., Gattuso, J.-P., Hinkel, J., Khattabi, A., McInnes, K.L., Saito, Y., & Sallenger, A. (2014). Coastal systems and low-lying areas. In: Climate Change 2014: Impacts, Adaptation, and Vulnerability. Part A: Global and Sectoral Aspects. Contribution of Working Group II to the Fifth Assessment Report of the Intergovernmental Panel on Climate Change [Field, C.B., V.R. Barros, D.J. Dokken, K.J. Mach, M.D. Mastrandrea, T.E. Bilir, M. Chatterjee, K.L. Ebi, Y.O. Estrada, R.C. Genova, B. Girma, E.S. Kissel, A.N. Levy, S.

MacCracken, P.R. Mastrandrea, and L.L. White (eds.)]. Cambridge University Press, Cambridge, United Kingdom and New York, NY, USA, pp. 361-409.

I
Appendix

Precipitation Interpolation Maps (Model Data)

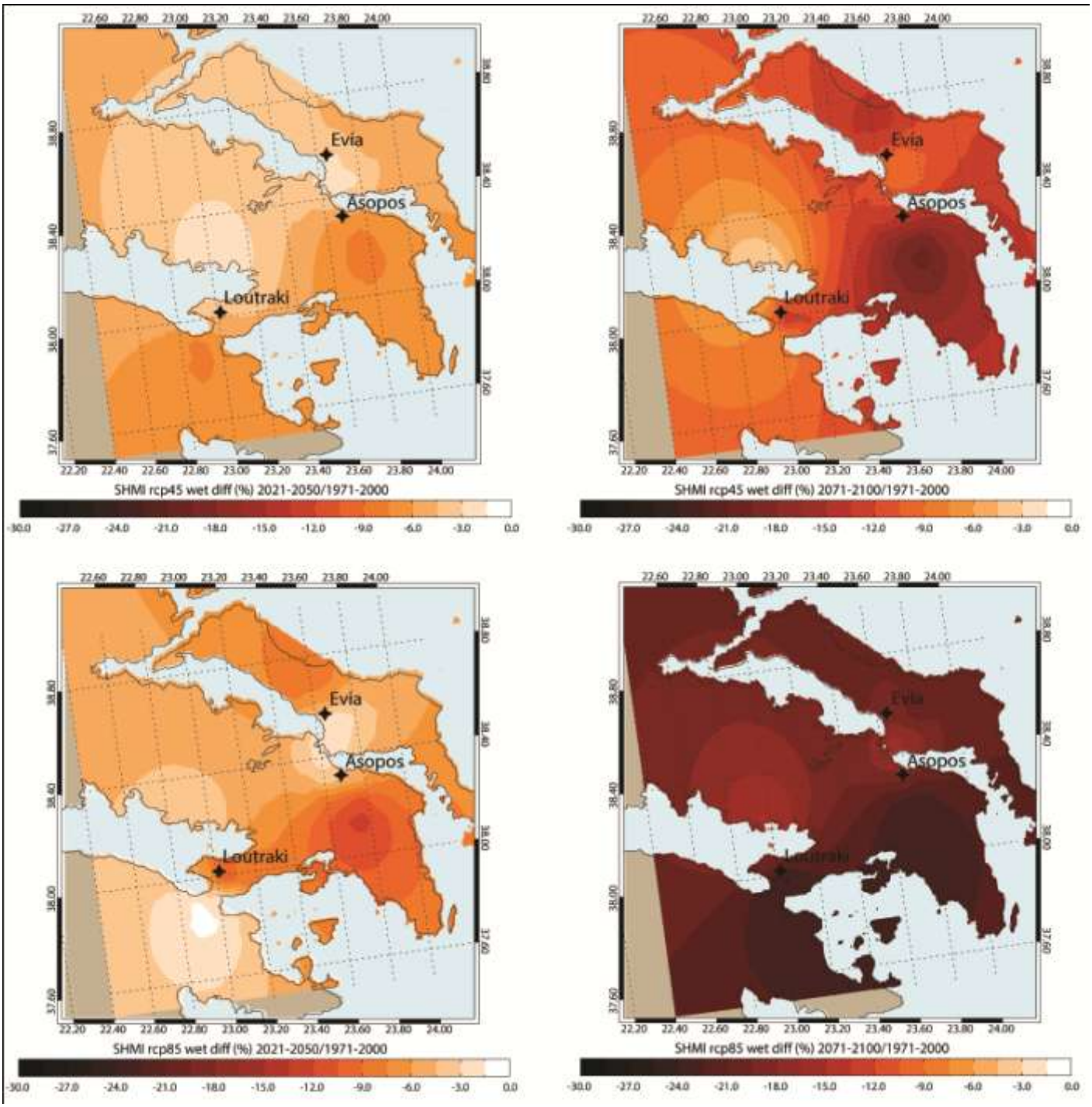

Figure A I. Interpolation maps comparingthe mean's difference from the control period for the near future (upper left) and the remote (upper right) during the wet season for the RCP 4.5 scenario, and the RCP 8.5 (lower left and right) respectively.

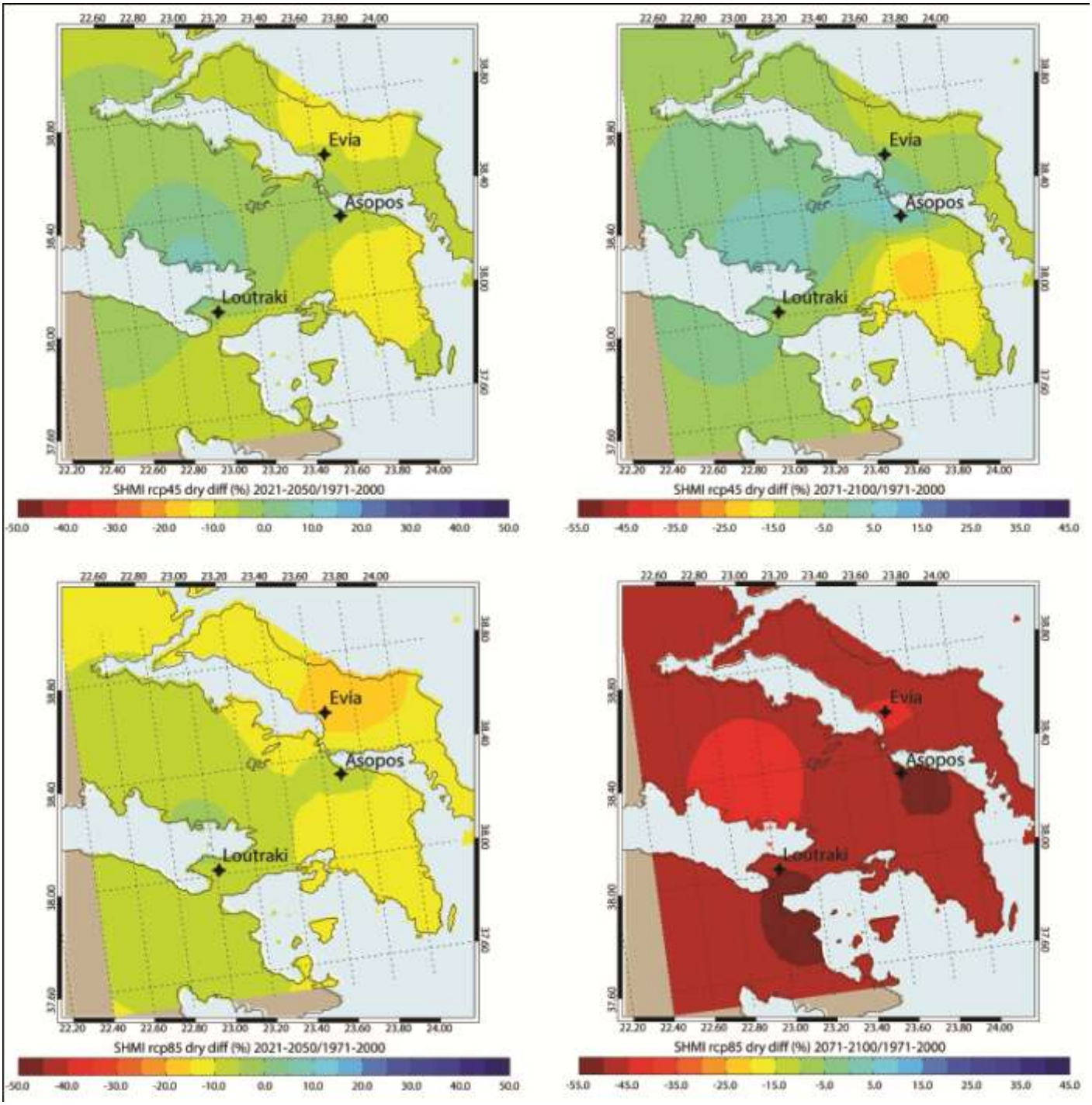

Figure A II. Interpolation maps comparingthe mean's difference from the control period for the near future (upper left) and the remote (upper right) during the dry season for the RCP 4.5 scenario, and the RCP 8.5 (lower left and right) respectively.

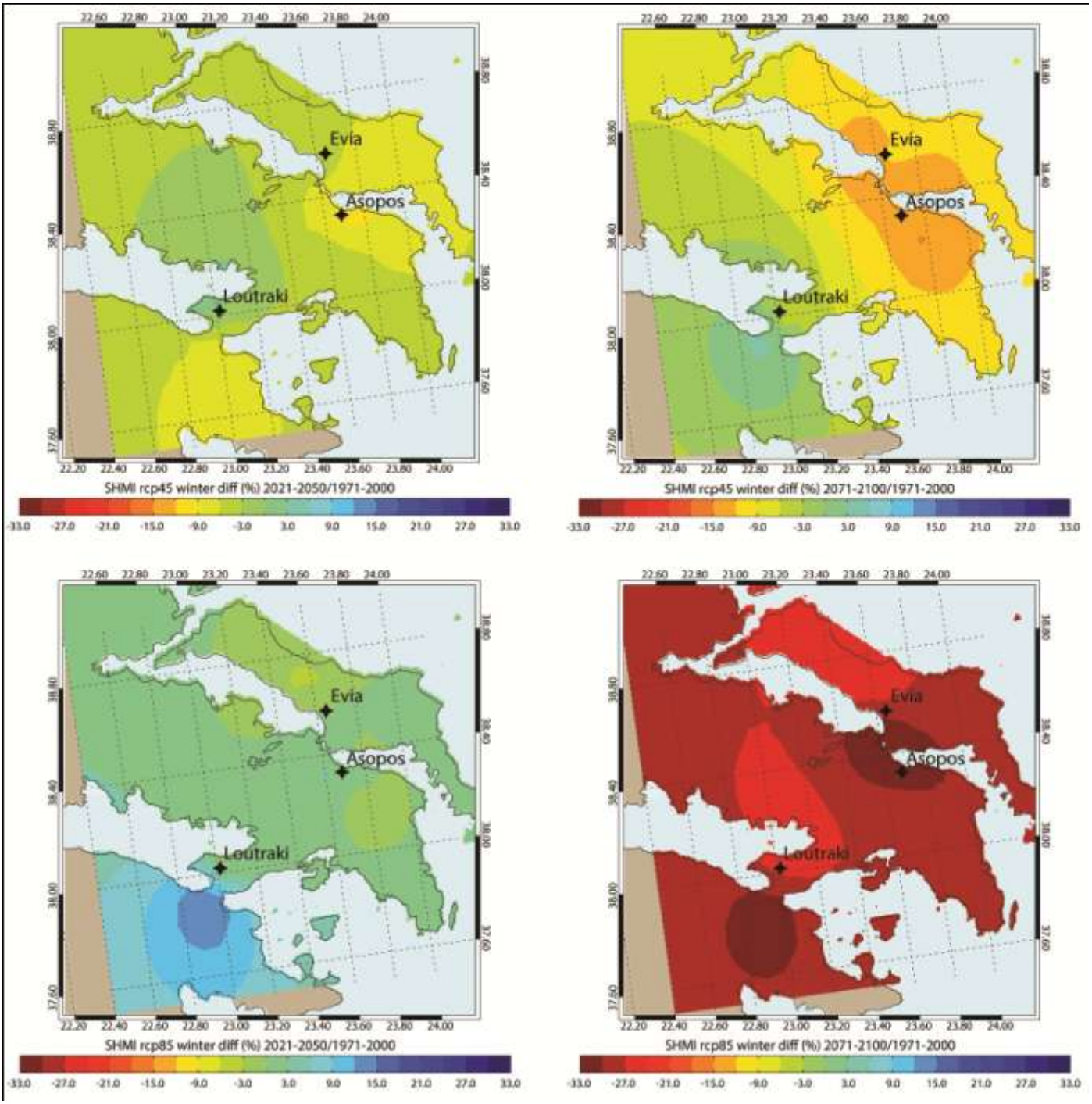

Figure A III. Interpolation Interpolation maps comparingthe mean's difference from the control period for the near future (upper left) and the remote (upper right) during the winter season for the RCP 4.5 scenario, and the RCP 8.5 (lower left and right) respectively.

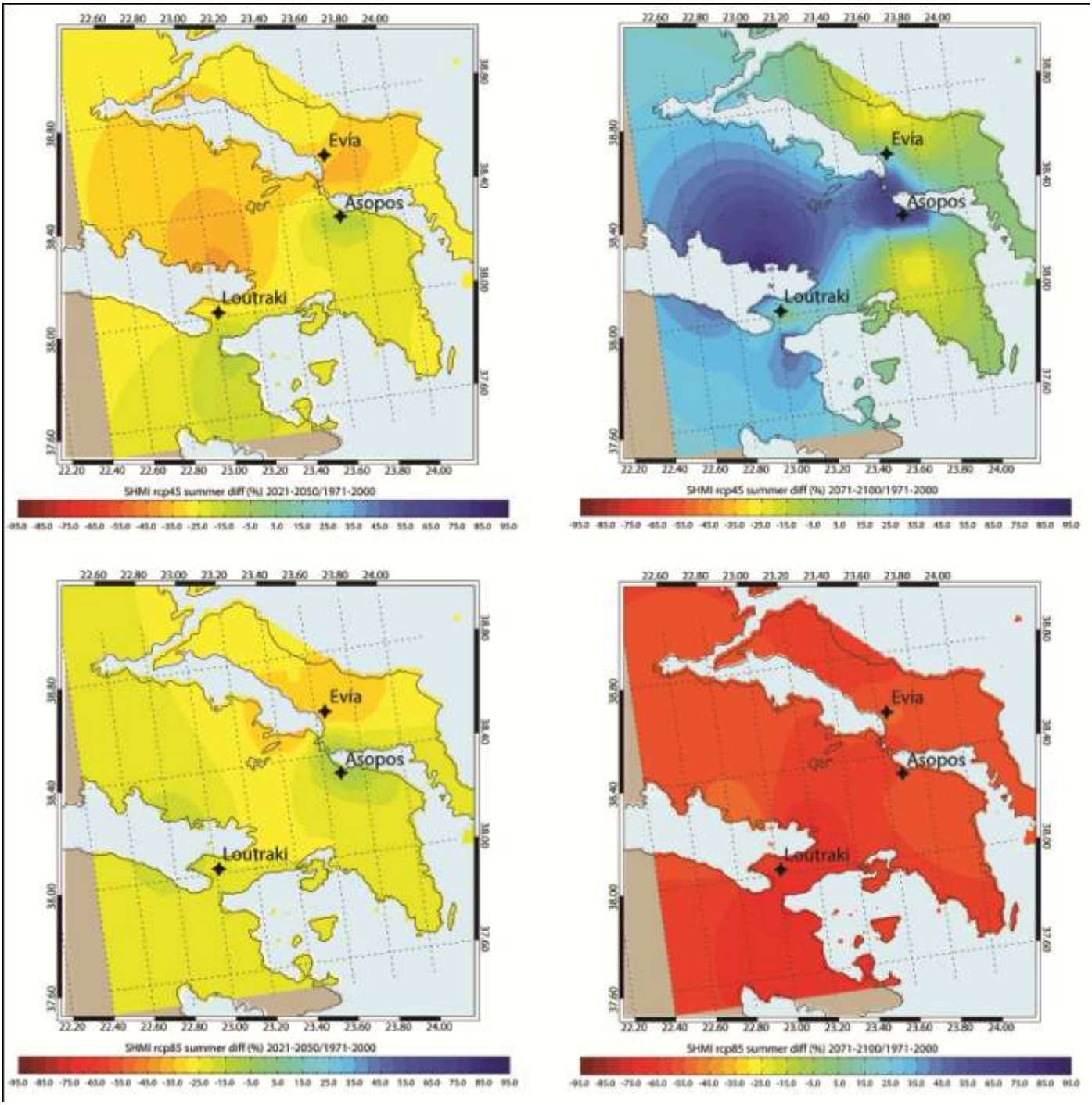

Figure A IV. Interpolation maps comparingthe mean's difference from the control period for the near future (upper left) and the remote (upper right) during the summer season for the RCP 4.5 scenario, and the RCP 8.5 (lower left and right) respectively.

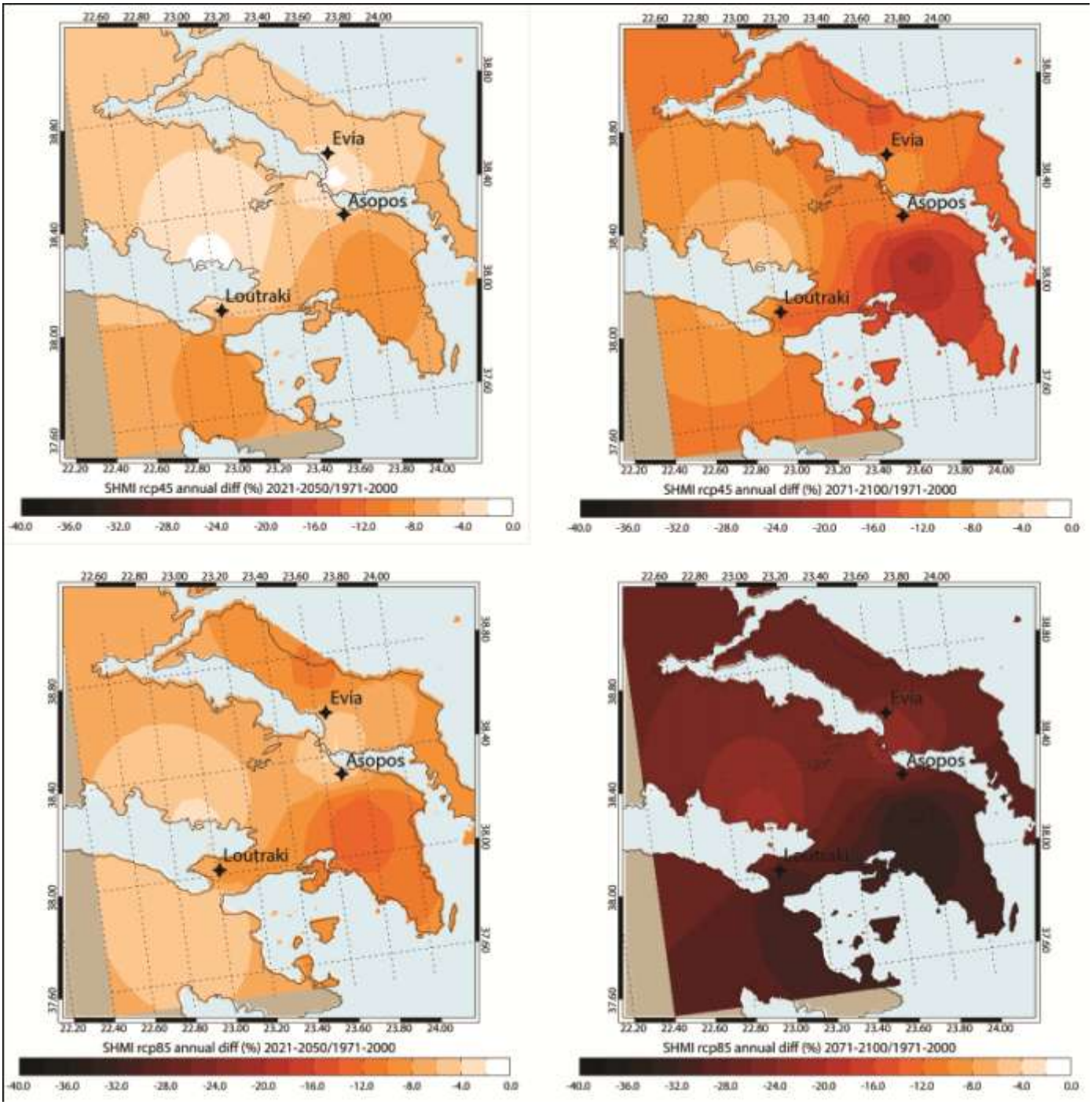

Figure A V. Interpolation maps comparing the mean's difference from the control period for the near future (upper left) and the remote (upper right) during the year for the RCP 4.5 scenario, and the RCP 8.5 (lower left and right) respectively.

SPI Interpolation Maps (Model Data)

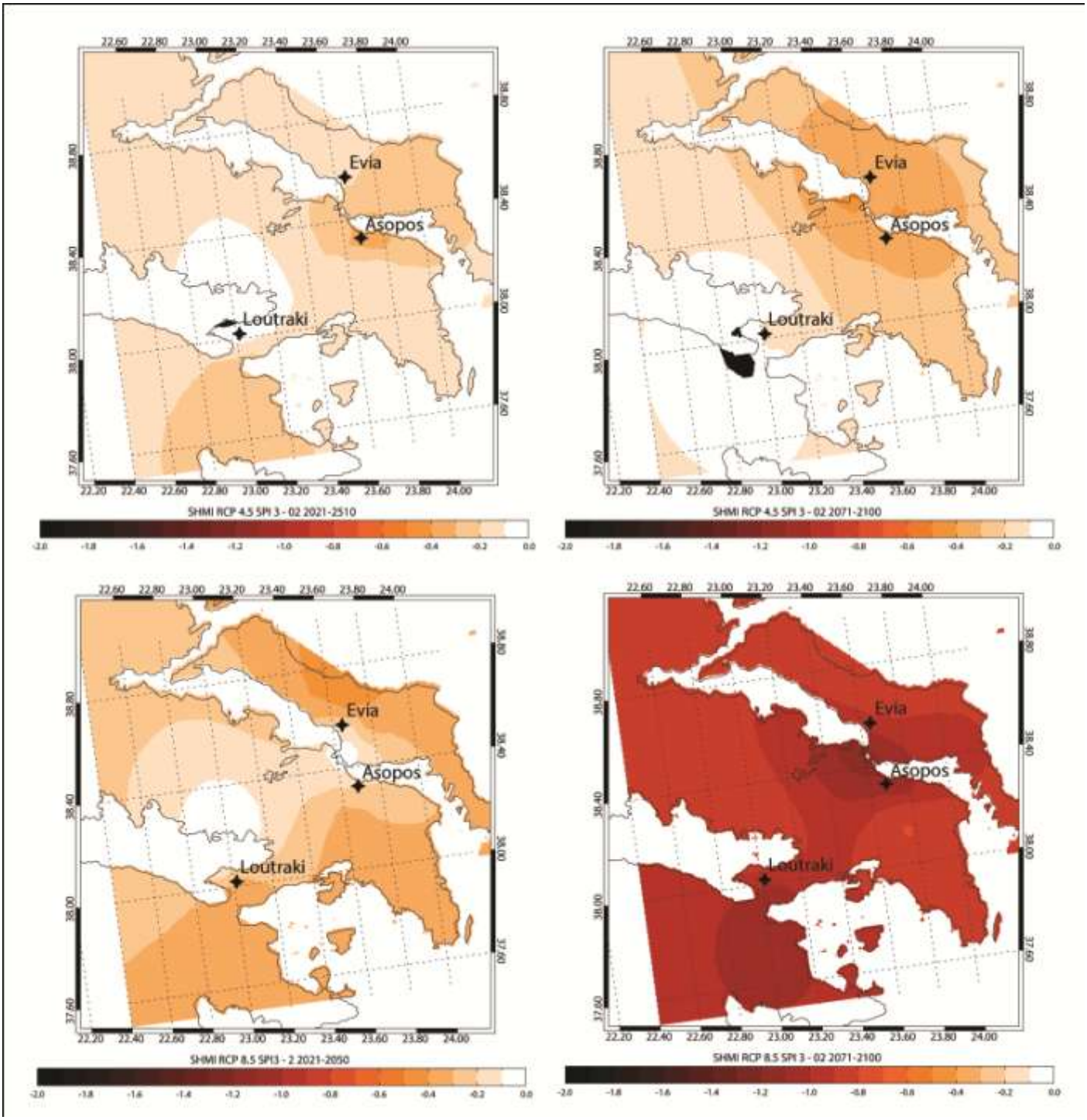

Figure A VI. Interpolation maps displaying 3-month SPI values for February derived from Model data for RCP 4.5 for the near (upper left) and the remote (upper right) future and the RCP 8.5 (lower left and right) respectively.

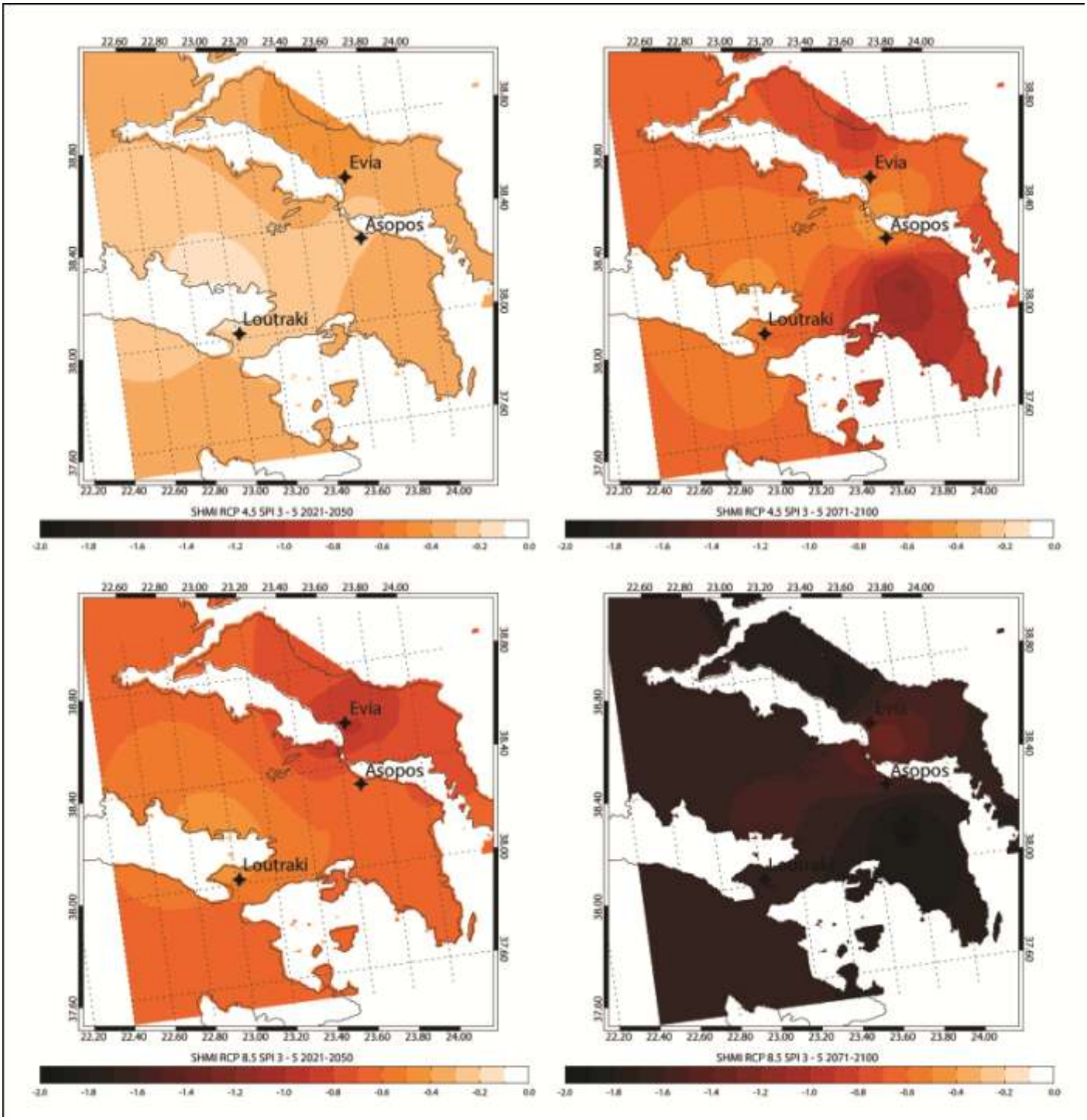

Figure A VII. Interpolation maps displaying 3-month SPI values for May derived from Model data for RCP 4.5 for the near (upper left) and the remote (upper right) future and the RCP 8.5 (lower left and right) respectively.

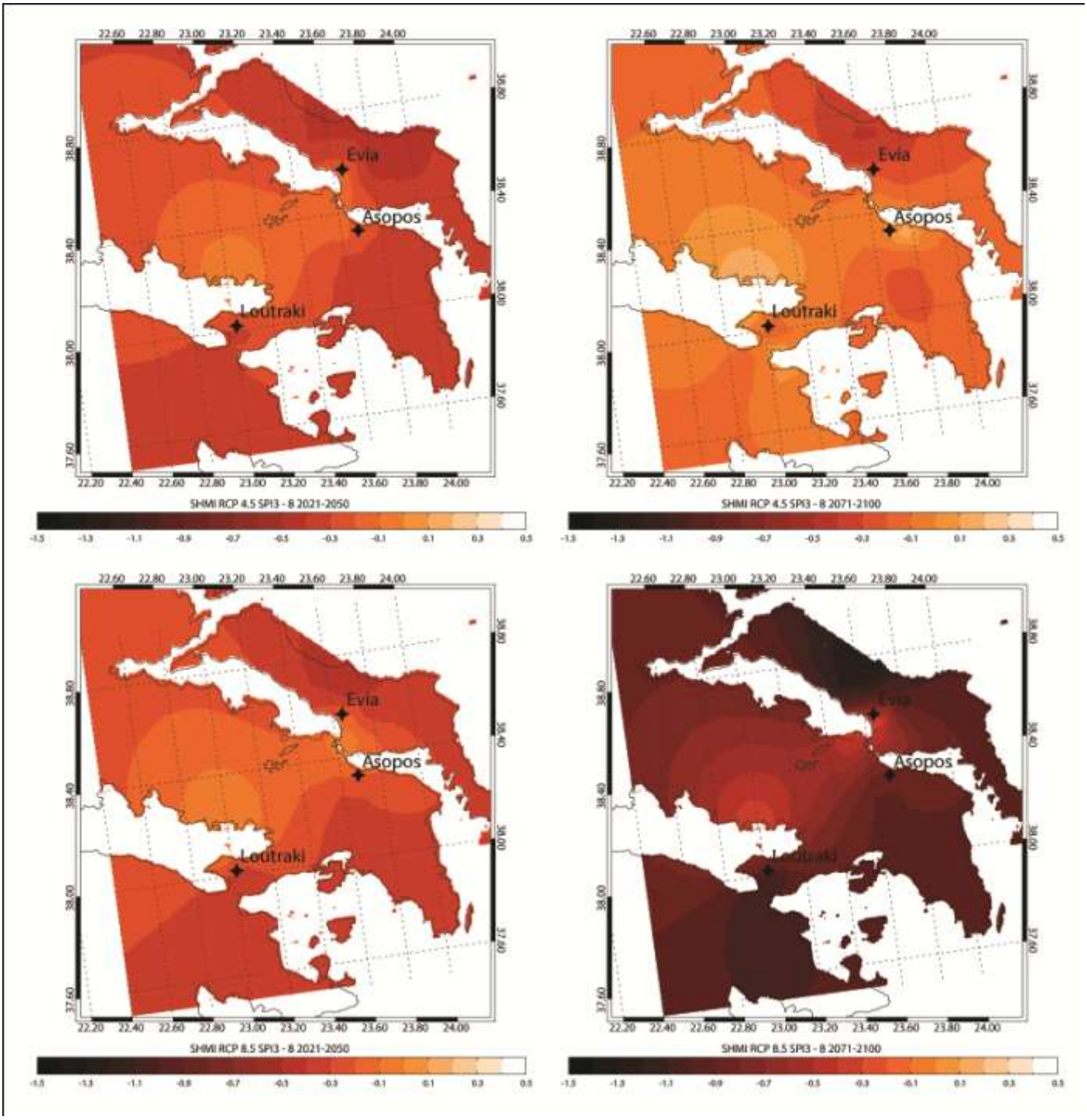

Figure A VIII. Interpolation maps displaying 3-month SPI values for August derived from Model data for RCP 4.5 for the near (upper left) and the remote (upper right) future and the RCP 8.5 (lower left and right) respectively.

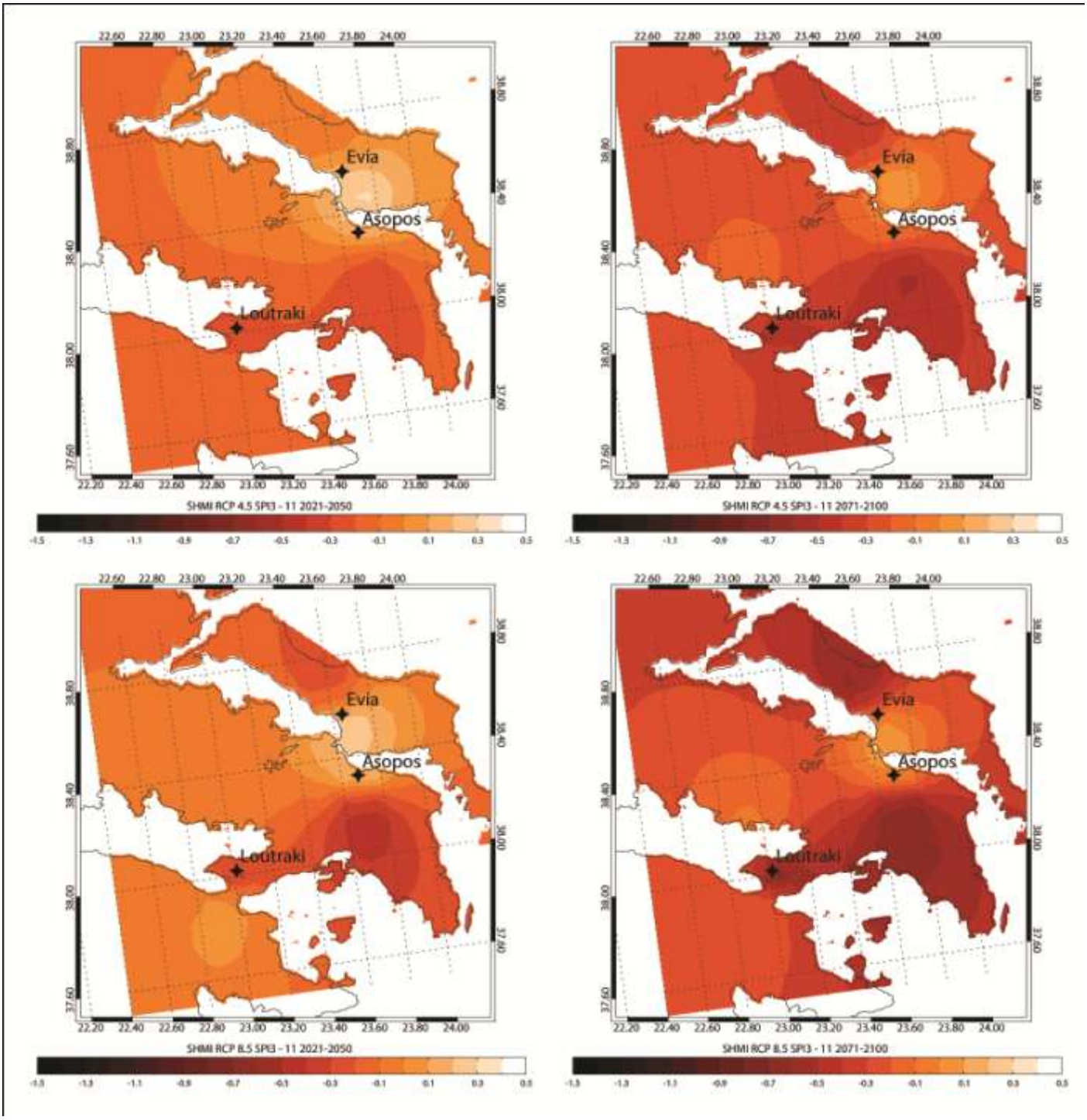

Figure A IX. Interpolation maps displaying 3-month SPI values for November derived from Model data for RCP 4.5 for the near (upper left) and the remote (upper right) future and the RCP 8.5 (lower left and right) respectively.

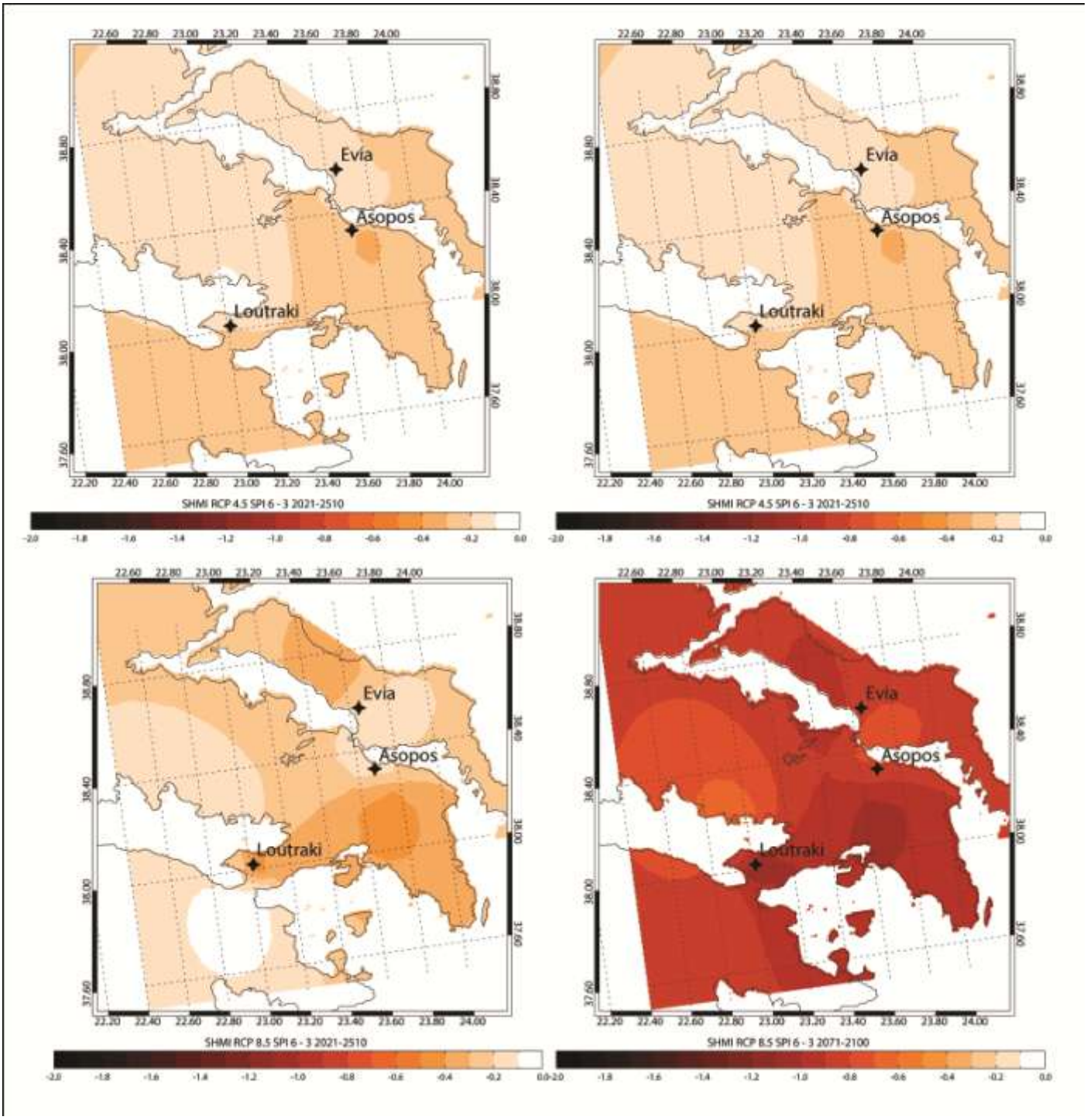

Figure A X. Interpolation maps displaying 6-month SPI values for March derived from Model data for RCP 4.5 for the near (upper left) and the remote (upper right) future and the RCP 8.5 (lower left and right) respectively.

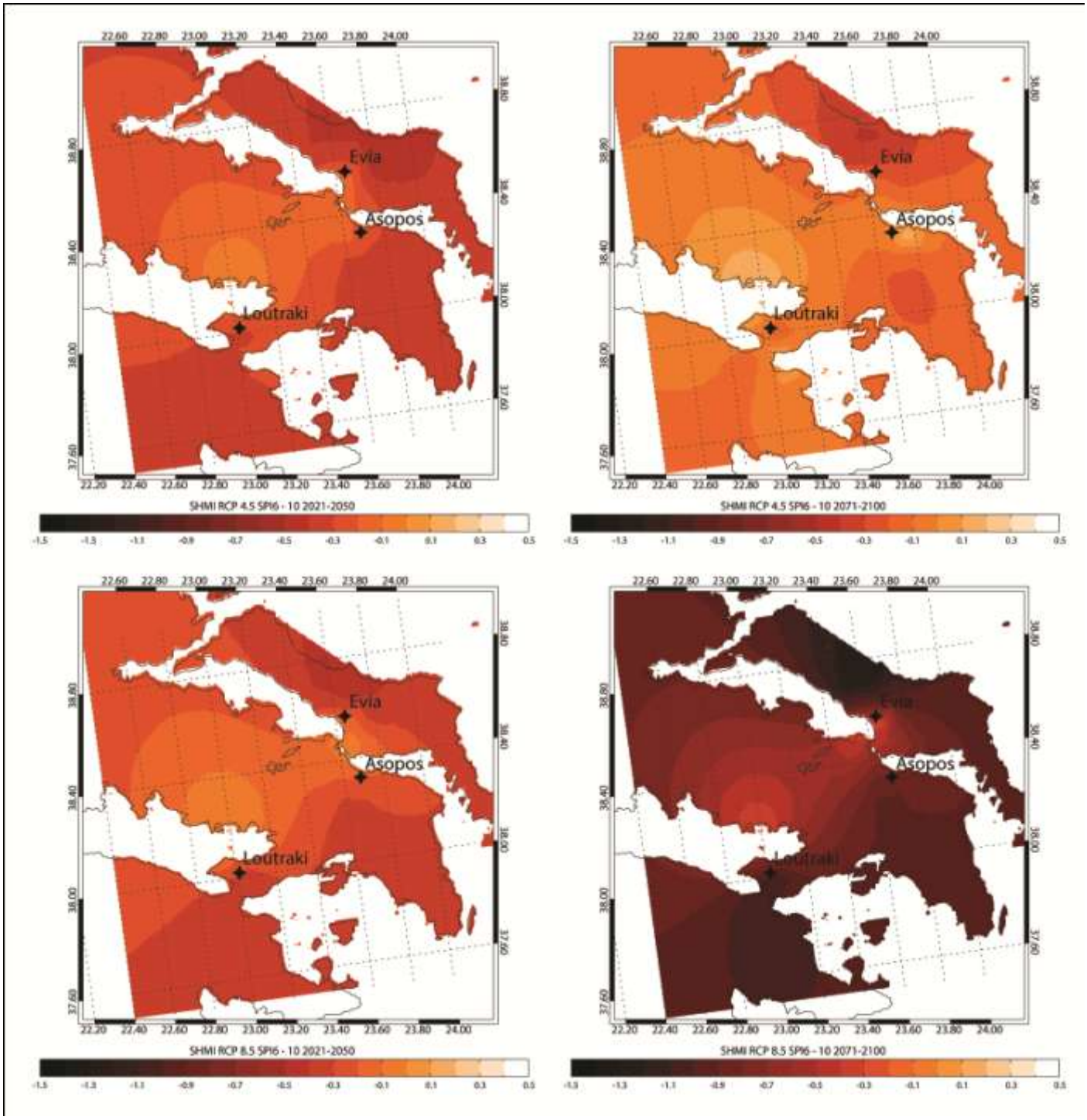

Figure A XI. Interpolation maps displaying 6-month SPI values for October derived from Model data for RCP 4.5 for the near (upper left) and the remote (upper right) future and the RCP 8.5 (lower left and right) respectively.

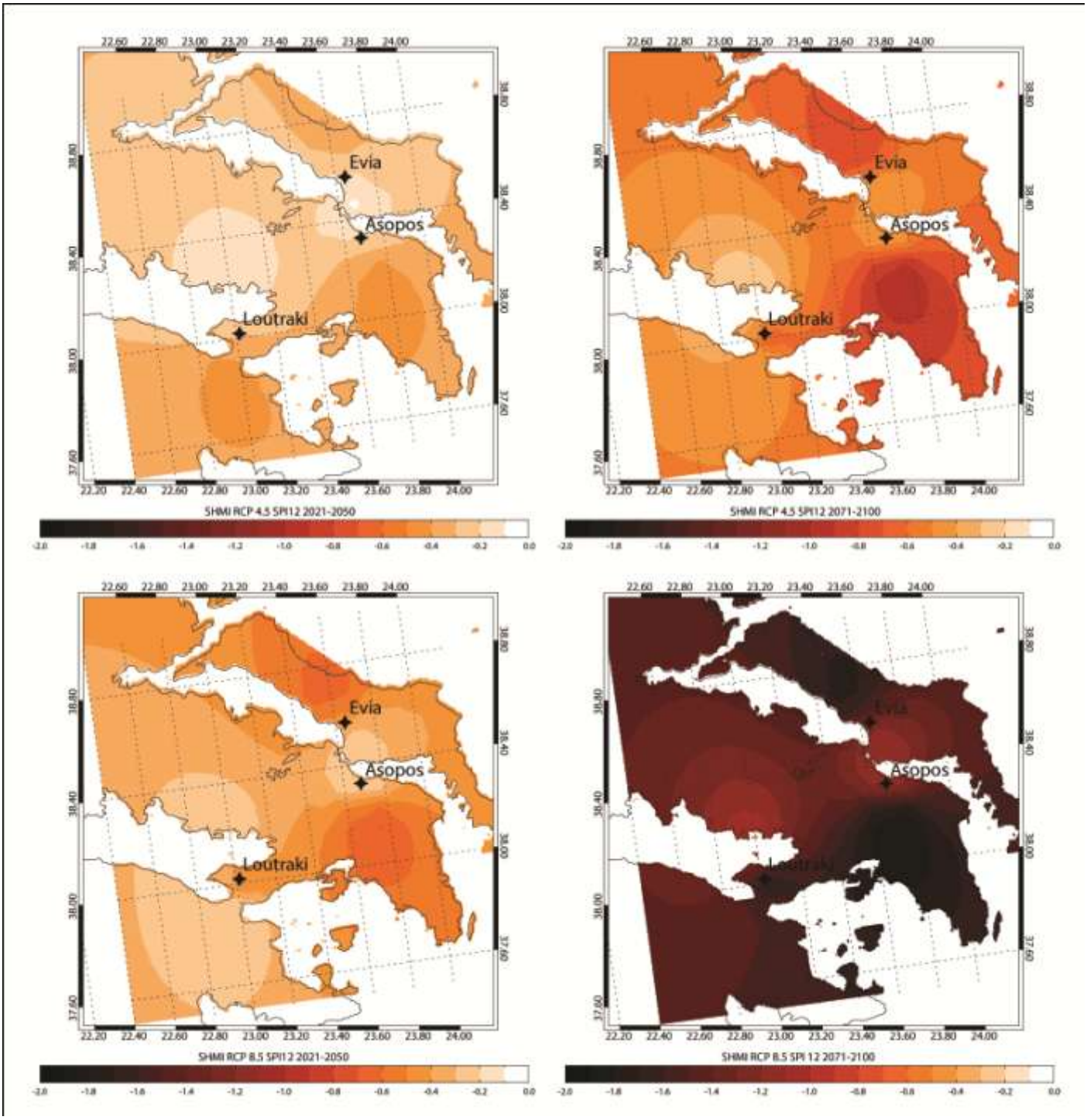

Figure A XII. Interpolation maps displaying 12-month SPI values derived from Model data for RCP 4.5 for the near (upper left) and the remote (upper right) future and the RCP 8.5 (lower left and right) respectively.

II Appendix

Gridded Datasets Correlation Tables

Current Climate - SPI -3 February (Winter) Correlation Table

Table A I. SPI 3 – February – Correlation table (all available datasets) displaying distinctive statistical significance.

	GP1	GP2	GP4	GP5	GP6	GP7	GP8	L3V6	L3V4	L3V5	L3V3	L3V2	L3V1	L2V5	L2V3	L2V2	L2V1	L1V4	L1V3
GP1	1																		
GP2	0.941692	1																	
GP4	0.954136	0.887935	1																
GP5	0.912725	0.926707	0.957884	1															
GP6	0.891518	0.860166	0.96726	0.965885	1														
GP7	0.831659	0.943567	0.798125	0.880838	0.790072	1													
GP8	0.898114	0.92901	0.906995	0.962968	0.918816	0.890629	1												
L3V6	0.839188	0.872761	0.839906	0.856537	0.828145	0.862165	0.828122	1											
L3V4	0.854641	0.862566	0.87393	0.86671	0.867227	0.828476	0.827236	0.834242	1										
L3V5	0.813837	0.86447	0.823848	0.856291	0.826577	0.867118	0.831152	0.99331	0.839788	1									
L3V3	0.885953	0.904963	0.900469	0.906024	0.895235	0.866118	0.868216	0.870485	0.987806	0.86885	1								
L3V2	0.886651	0.907206	0.889732	0.89663	0.8745	0.871592	0.866215	0.860739	0.987921	0.863386	0.992584	1							
L3V1	0.911186	0.913925	0.905599	0.897652	0.878508	0.867593	0.86599	0.883983	0.979939	0.877185	0.990204	0.994723	1						
L2V5	0.911186	0.913925	0.905599	0.897652	0.878508	0.867593	0.86599	0.883983	0.979939	0.877185	0.990204	0.994723	1	1					
L2V3	0.854641	0.862566	0.87393	0.86671	0.867227	0.828476	0.827236	0.834242	1	0.839788	0.987806	0.987921	0.979939	0.979939	1				
L2V2	0.869048	0.853373	0.891104	0.864371	0.880292	0.799954	0.819854	0.823217	0.991941	0.819663	0.981548	0.975119	0.974358	0.974358	0.991941	1			
L2V1	0.885953	0.904963	0.900469	0.906024	0.895235	0.866118	0.868216	0.870485	0.987806	0.86885	1	0.992584	0.990204	0.990204	0.987806	0.981548	1		
L1V4	0.923601	0.872033	0.904799	0.846469	0.849143	0.798351	0.807633	0.865341	0.92855	0.834459	0.942077	0.937218	0.964355	0.964355	0.92855	0.947064	0.942077	1	
L1V3	0.911186	0.913925	0.905599	0.897652	0.878508	0.867593	0.86599	0.883983	0.979939	0.877185	0.990204	0.994723	1	1	0.979939	0.974358	0.990204	0.964355	1

Current Climate - SPI -3 May (Spring) Correlation Table

Table A II. SPI 3 – May – Correlation table (all available datasets) displaying distinctive statistical significance for the correlation between them

	GP1	GP2	GP4	GP5	GP6	GP7	GP8	L3V6	L3V4	L3V5	L3V3	L3V2	L3V1	L2V5	L2V3	L2V2	L2V1	L1V4	L1V3
GP1	1																		
GP2	0.897085	1																	
GP4	0.883023	0.731551	1																
GP5	0.872486	0.853117	0.936128	1															
GP6	0.828898	0.745554	0.933217	0.950952	1														
GP7	0.751058	0.924462	0.631461	0.794034	0.667168	1													
GP8	0.063612	0.011315	0.053156	-0.0609	-0.01631	-0.04254	1												
L3V6	0.78534	0.88115	0.677357	0.778113	0.701126	0.841866	0.043676	1											
L3V4	0.754258	0.804556	0.726932	0.792828	0.788065	0.80525	0.130804	0.872117	1										
L3V5	0.770082	0.880908	0.678831	0.789299	0.714344	0.864721	0.072317	0.984916	0.914568	1									
L3V3	0.792735	0.859276	0.741218	0.816212	0.788859	0.84419	0.107443	0.923914	0.980294	0.946461	1								
L3V2	0.787188	0.856971	0.726595	0.805476	0.764197	0.849524	0.118093	0.937889	0.977397	0.970961	0.980612	1							
L3V1	0.818025	0.871578	0.747059	0.815298	0.77223	0.841605	0.098969	0.958774	0.960004	0.972702	0.978566	0.991211	1						
L2V5	0.818025	0.871578	0.747059	0.815298	0.77223	0.841605	0.098969	0.958774	0.960004	0.972702	0.978566	0.991211	1	1					
L2V3	0.754258	0.804556	0.726932	0.792828	0.788065	0.80525	0.130804	0.872117	1	0.914568	0.980294	0.977397	0.960004	0.960004	1				
L2V2	0.780023	0.791885	0.76211	0.801001	0.818064	0.76617	0.110256	0.866452	0.982856	0.890213	0.971248	0.953828	0.950955	0.950955	0.982856	1			
L2V1	0.792735	0.859276	0.741218	0.816212	0.788859	0.84419	0.107443	0.923914	0.980294	0.946461	1	0.980612	0.978566	0.978566	0.980294	0.971248	1		
L1V4	0.861708	0.854943	0.782238	0.802347	0.769102	0.791681	0.084464	0.905507	0.896031	0.890504	0.931355	0.923536	0.956305	0.956305	0.896031	0.916566	0.931355	1	
L1V3	0.818025	0.871578	0.747059	0.815298	0.77223	0.841605	0.098969	0.958774	0.960004	0.972702	0.978566	0.991211	1	1	0.960004	0.950955	0.978566	0.956305	1

Current Climate - SPI -3 August (Summer) Correlation Table

Table A III. SPI 3 – August – Correlation table (all available datasets)

	GP1	GP2	GP4	GP5	GP6	GP7	GP8	L3V6	L3V4	L3V5	L3V3	L3V2	L3V1	L2V5	L2V3	L2V2	L2V1	L1V4	L1V3
GP1	1																		
GP2	0.852221	1																	
GP4	0.847018	0.667623	1																
GP5	0.810326	0.805352	0.897242	1															
GP6	0.753975	0.696129	0.897591	0.922583	1														
GP7	0.60058	0.849484	0.452657	0.654484	0.509373	1													
GP8	0.723933	0.732148	0.791755	0.844178	0.856404	0.557807	1												
L3V6	0.593896	0.668654	0.480022	0.538606	0.491767	0.546508	0.560698	1											
L3V4	0.601107	0.626056	0.547779	0.556911	0.584876	0.508726	0.627103	0.867425	1										
L3V5	0.545052	0.627054	0.427773	0.48778	0.437658	0.509078	0.534717	0.985875	0.85865	1									
L3V3	0.616855	0.673595	0.544023	0.579491	0.589118	0.556356	0.636361	0.934183	0.974144	0.914365	1								
L3V2	0.598896	0.630827	0.505088	0.530112	0.52366	0.499439	0.581294	0.966704	0.93415	0.964586	0.956528	1							
L3V1	0.617441	0.632685	0.536674	0.557953	0.549609	0.497479	0.584177	0.964693	0.918518	0.948403	0.948049	0.991445	1						
L2V5	0.617441	0.632685	0.536674	0.557953	0.549609	0.497479	0.584177	0.964693	0.918518	0.948403	0.948049	0.991445	1	1					
L2V3	0.601107	0.626056	0.547779	0.556911	0.584876	0.508726	0.627103	0.867425	1	0.85865	0.974144	0.93415	0.918518	0.918518	1				
L2V2	0.616476	0.62492	0.594551	0.598774	0.657513	0.514722	0.645553	0.812297	0.9695	0.780711	0.947836	0.885099	0.885548	0.885548	0.9695	1			
L2V1	0.616855	0.673595	0.544023	0.579491	0.589118	0.556356	0.636361	0.934183	0.974144	0.914365	1	0.956528	0.948049	0.948049	0.974144	0.947836	1		
L1V4	0.695615	0.656611	0.652141	0.636205	0.652725	0.489843	0.638693	0.882234	0.890682	0.83822	0.912477	0.912464	0.935812	0.935812	0.890682	0.909403	0.912477	1	
L1V3	0.617441	0.632685	0.536674	0.557953	0.549609	0.497479	0.584177	0.964693	0.918518	0.948403	0.948049	0.991445	1	1	0.918518	0.885548	0.948049	0.935812	1

Current Climate - SPI - 3 November (Autumn) Correlation Table

Table A IV. SPI 3 – November – Correlation table (all available datasets)

	GP1	GP2	GP4	GP5	GP6	GP7	GP8	L3V6	L3V4	L3V5	L3V3	L3V2	L3V1	L2V5	L2V3	L2V2	L2V1	L1V4	L1V3
GP1	1																		
GP2	0.921858	1																	
GP4	0.924858	0.812603	1																
GP5	0.91957	0.885689	0.967149	1															
GP6	0.81926	0.74952	0.912765	0.935648	1														
GP7	0.806942	0.936582	0.720993	0.810193	0.666193	1													
GP8	0.823318	0.85766	0.865699	0.930927	0.896096	0.821987	1												
L3V6	0.8216	0.896334	0.766963	0.823413	0.747538	0.872668	0.817227	1											
L3V4	0.752445	0.78204	0.736061	0.779428	0.789531	0.762111	0.783519	0.92663	1										
L3V5	0.779215	0.873563	0.737709	0.808232	0.745852	0.865622	0.834576	0.986376	0.931734	1									
L3V3	0.798596	0.835232	0.775498	0.814442	0.791201	0.810724	0.79506	0.967976	0.982459	0.953602	1								
L3V2	0.780483	0.837464	0.746806	0.801007	0.773947	0.818998	0.813278	0.975963	0.976265	0.983926	0.980724	1							
L3V1	0.815618	0.85529	0.772797	0.816063	0.784164	0.815642	0.807525	0.982577	0.968594	0.973254	0.986835	0.991896	1						
L2V5	0.815618	0.85529	0.772797	0.816063	0.784164	0.815642	0.807525	0.982577	0.968594	0.973254	0.986835	0.991896	1	1					
L2V3	0.752445	0.78204	0.736061	0.779428	0.789531	0.762111	0.783519	0.92663	1	0.931734	0.982459	0.976265	0.968594	0.968594	1				
L2V2	0.75436	0.7608	0.747273	0.776724	0.796655	0.724561	0.749077	0.911019	0.984547	0.898431	0.979172	0.953003	0.959776	0.959776	0.984547	1			
L2V1	0.798596	0.835232	0.775498	0.814442	0.791201	0.810724	0.79506	0.967976	0.982459	0.953602	1	0.980724	0.986835	0.986835	0.982459	0.979172	1		
L1V4	0.803073	0.799954	0.757695	0.765282	0.728049	0.734205	0.703168	0.924562	0.893745	0.875539	0.93907	0.908054	0.948044	0.948044	0.893745	0.927952	0.93907	1	
L1V3	0.815618	0.85529	0.772797	0.816063	0.784164	0.815642	0.807525	0.982577	0.968594	0.973254	0.986835	0.991896	1	1	0.968594	0.959776	0.986835	0.948044	1

Current Climate - SPI - 6 March (Wet Season) Correlation Table

Table A V. SPI 6 – March – Correlation table (all available datasets)

	GP1	GP2	GP4	GP5	GP6	GP7	GP8	L3V6	L3V4	L3V5	L3V3	L3V2	L3V1	L2V5	L2V3	L2V2	L2V1	L1V4	L1V3
GP1	1																		
GP2	0.929252	1																	
GP4	0.942649	0.844129	1																
GP5	0.92943	0.91486	0.959041	1															
GP6	0.896924	0.836471	0.960345	0.96439	1														
GP7	0.782977	0.912144	0.702743	0.814535	0.712541	1													
GP8	0.861066	0.899974	0.854502	0.933517	0.895105	0.829461	1												
L3V6	0.785608	0.827628	0.761627	0.793245	0.770009	0.815301	0.776798	1											
L3V4	0.795807	0.81014	0.78188	0.813168	0.818613	0.796016	0.792935	0.75324	1										
L3V5	0.760589	0.821922	0.746055	0.795647	0.769877	0.821407	0.793023	0.991798	0.769919	1									
L3V3	0.8371	0.862379	0.812828	0.847648	0.842968	0.835576	0.826136	0.799079	0.984734	0.804815	1								
L3V2	0.830763	0.86287	0.799992	0.843761	0.824429	0.842754	0.830313	0.792599	0.981602	0.809036	0.987165	1							
L3V1	0.868678	0.87922	0.834255	0.860597	0.845129	0.842841	0.836448	0.832281	0.971116	0.835701	0.986763	0.992313	1						
L2V5	0.868678	0.87922	0.834255	0.860597	0.845129	0.842841	0.836448	0.832281	0.971116	0.835701	0.986763	0.992313	1	1					
L2V3	0.795807	0.81014	0.78188	0.813168	0.818613	0.796016	0.792935	0.75324	1	0.769919	0.984734	0.981602	0.971116	0.971116	1				
L2V2	0.819301	0.807452	0.813041	0.822546	0.844732	0.771104	0.788219	0.74975	0.990817	0.756522	0.980182	0.969196	0.968055	0.968055	0.990817	1			
L2V1	0.8371	0.862379	0.812828	0.847648	0.842968	0.835576	0.826136	0.799079	0.984734	0.804815	1	0.987165	0.986763	0.986763	0.984734	0.980182	1		
L1V4	0.885935	0.838104	0.846849	0.82099	0.821499	0.783034	0.763473	0.824886	0.905796	0.797287	0.935984	0.925553	0.959857	0.959857	0.905796	0.926533	0.935984	1	
L1V3	0.868678	0.87922	0.834255	0.860597	0.845129	0.842841	0.836448	0.832281	0.971116	0.835701	0.986763	0.992313	1	1	0.971116	0.968055	0.986763	0.959857	1

Current Climate - SPI -6 October (Dry Season) Correlation Table

Table A VI. SPI 3 – October – Correlation table (all available datasets) displaying distinctive statistical significance as well.

	GP1	GP2	GP4	GP5	GP6	GP7	GP8	L3V6	L3V4	L3V5	L3V3	L3V2	L3V1	L2V5	L2V3	L2V2	L2V1	L1V4	L1V3
GP1	1																		
GP2	0.931034	1																	
GP4	0.934902	0.875312	1																
GP5	0.933692	0.920538	0.962905	1															
GP6	0.881972	0.85691	0.931724	0.962994	1														
GP7	0.828669	0.957311	0.796568	0.8692	0.80052	1													
GP8	0.835234	0.88675	0.860553	0.922635	0.930536	0.860237	1												
L3V6	0.880312	0.923209	0.869651	0.902556	0.864915	0.889586	0.876724	1											
L3V4	0.808649	0.854567	0.812992	0.857236	0.845171	0.851321	0.857362	0.946899	1										
L3V5	0.842565	0.899884	0.845627	0.886583	0.852481	0.885044	0.883431	0.988941	0.951028	1									
L3V3	0.837612	0.884501	0.834443	0.873569	0.853154	0.865979	0.853561	0.97553	0.98257	0.963178	1								
L3V2	0.848699	0.890562	0.851284	0.889741	0.865484	0.872685	0.883247	0.983957	0.976162	0.990026	0.975816	1							
L3V1	0.8793	0.902865	0.870014	0.900229	0.874268	0.866611	0.873886	0.991708	0.966805	0.981886	0.981332	0.992506	1						
L2V5	0.8793	0.902865	0.870014	0.900229	0.874268	0.866611	0.873886	0.991708	0.966805	0.981886	0.981332	0.992506	1	1					
L2V3	0.808649	0.854567	0.812992	0.857236	0.845171	0.851321	0.857362	0.946899	1	0.951028	0.98257	0.976162	0.966805	0.966805	1				
L2V2	0.813239	0.850939	0.808661	0.843694	0.831273	0.83591	0.827838	0.935367	0.985145	0.921741	0.97785	0.953622	0.956854	0.956854	0.985145	1			
L2V1	0.837612	0.884501	0.834443	0.873569	0.853154	0.865979	0.853561	0.97553	0.98257	0.963178	1	0.975816	0.981332	0.981332	0.98257	0.97785	1		
L1V4	0.901956	0.899527	0.869024	0.876853	0.846591	0.833092	0.82191	0.956784	0.912009	0.918301	0.942836	0.935894	0.96615	0.96615	0.912009	0.935902	0.942836	1	
L1V3	0.8793	0.902865	0.870014	0.900229	0.874268	0.866611	0.873886	0.991708	0.966805	0.981886	0.981332	0.992506	1	1	0.966805	0.956854	0.981332	0.96615	1

Current Climate - SPI -12 Inter - Annual Correlation Table

Table A VII. SPI 12 – Correlation table (all available datasets) showing great statistical significance as expected.

	GP1	GP2	GP4	GP5	GP6	GP7	GP8	L3V6	L3V4	L3V5	L3V3	L3V2	L3V1	L2V5	L2V3	L2V2	L2V1	L1V4	L1V3
GP1	1																		
GP2	0.915684	1																	
GP4	0.914134	0.830291	1																
GP5	0.88396	0.910037	0.936585	1															
GP6	0.812207	0.7864	0.923438	0.947236	1														
GP7	0.759057	0.91079	0.692396	0.82552	0.694344	1													
GP8	0.799025	0.886361	0.828817	0.937938	0.87322	0.842399	1												
L3V6	0.760233	0.819551	0.775536	0.824148	0.778899	0.810223	0.802726	1											
L3V4	0.718957	0.759076	0.775608	0.809204	0.820403	0.764264	0.780297	0.824048	1										
L3V5	0.712752	0.797135	0.742221	0.814856	0.775987	0.801086	0.815898	0.988733	0.838257	1									
L3V3	0.752269	0.803836	0.802852	0.840406	0.832628	0.8008	0.806153	0.875005	0.984815	0.878167	1								
L3V2	0.764993	0.814531	0.807379	0.850703	0.832322	0.804785	0.824501	0.90149	0.976784	0.912019	0.986889	1							
L3V1	0.799698	0.825134	0.832534	0.857142	0.838751	0.798197	0.817077	0.923946	0.960042	0.919744	0.980072	0.992348	1						
L2V5	0.799698	0.825134	0.832534	0.857142	0.838751	0.798197	0.817077	0.923946	0.960042	0.919744	0.980072	0.992348	1	1					
L2V3	0.718957	0.759076	0.775608	0.809204	0.820403	0.764264	0.780297	0.824048	1	0.838257	0.984815	0.976784	0.960042	0.960042	1				
L2V2	0.724004	0.745201	0.794254	0.808678	0.834319	0.750842	0.76084	0.821772	0.990507	0.828231	0.979213	0.96373	0.953992	0.953992	0.990507	1			
L2V1	0.752269	0.803836	0.802852	0.840406	0.832628	0.8008	0.806153	0.875005	0.984815	0.878167	1	0.986889	0.980072	0.980072	0.984815	0.979213	1		
L1V4	0.828259	0.780313	0.831301	0.795568	0.783363	0.739591	0.713909	0.876864	0.876841	0.8313	0.907566	0.907448	0.944399	0.944399	0.876841	0.892704	0.907566	1	
L1V3	0.799698	0.825134	0.832534	0.857142	0.838751	0.798197	0.817077	0.923946	0.960042	0.919744	0.980072	0.992348	1	1	0.960042	0.953992	0.980072	0.944399	1

One Sample T-test for comparing means tables

RCP 4.5 Scenario - Near Future Analysis

Table A VIII. One Sample T-test for comparing means (RCP 4.5 Scenario - Near Future), Model Data Output

One-Sample Test

	Test Value = 0					
	t	df	Sig. (2-tailed)	Mean Difference	Interval of the Lower	Interval of the Upper
SPI12 GP1	-1,328	29,000	0,195	-0,302	-0,768	0,163
SPI12 GP2	-1,128	29,000	0,269	-0,278	-0,782	0,226
SPI12 GP3	-1,601	29,000	0,120	-0,388	-0,885	0,108
SPI12 GP4	-0,459	29,000	0,650	-0,113	-0,615	0,390
SPI12 GP5	-0,430	29,000	0,670	-0,102	-0,588	0,384
SPI12 GP6	-1,877	29,000	0,071	-0,443	-0,927	0,040
SPI12 GP7	-0,472	29,000	0,641	-0,115	-0,612	0,383
SPI12 GP8	-1,453	29,000	0,157	-0,326	-0,784	0,133
SPI12 GP9	-1,073	29,000	0,292	-0,251	-0,729	0,227
SPI12 GP10	-0,931	29,000	0,360	-0,208	-0,666	0,249
SPI12 GP11	-0,339	29,000	0,737	-0,072	-0,503	0,359
SPI12 GP12	-1,168	29,000	0,252	-0,292	-0,804	0,220
SPI12 GP13	-0,968	29,000	0,341	-0,192	-0,599	0,214
SPI12 GP14	-1,203	29,000	0,239	-0,237	-0,641	0,166
SPI12 GP15	-0,339	29,000	0,737	-0,072	-0,503	0,359
SPI12 GP16	-0,479	29,000	0,635	-0,105	-0,552	0,342
SPI12 GP17	-1,904	29,000	0,067	-0,363	-0,753	0,027
SPI12 GP18	-2,476	29,000	0,019	-0,460	-0,839	-0,080
SPI6 - 10 GP1	-0,854	29,000	0,400	-0,166	-0,565	0,232
SPI6 - 10 GP2	-1,113	29,000	0,275	-0,221	-0,628	0,185
SPI6 - 10 GP3	-1,056	29,000	0,300	-0,225	-0,660	0,211
SPI6 - 10 GP4	-0,787	29,000	0,438	-0,181	-0,651	0,289
SPI6 - 10 GP5	-0,521	29,000	0,606	-0,122	-0,599	0,356
SPI6 - 10 GP6	-1,359	29,000	0,185	-0,259	-0,650	0,131
SPI6 - 10 GP7	0,509	29,000	0,614	0,109	-0,328	0,546
SPI6 - 10 GP8	-0,996	29,000	0,327	-0,183	-0,558	0,192
SPI6 - 10 GP9	0,223	29,000	0,825	0,044	-0,361	0,449
SPI6 - 10 GP10	-0,291	29,000	0,773	-0,064	-0,514	0,386
SPI6 - 10 GP11	0,992	29,000	0,330	0,202	-0,215	0,618
SPI6 - 10 GP12	-0,755	29,000	0,456	-0,154	-0,570	0,262
SPI6 - 10 GP13	0,341	29,000	0,735	0,074	-0,371	0,520
SPI6 - 10 GP14	-0,220	29,000	0,827	-0,047	-0,488	0,393
SPI6 - 10 GP15	0,992	29,000	0,330	0,202	-0,215	0,618
SPI6 - 10 GP16	0,543	29,000	0,592	0,113	-0,314	0,541
SPI6 - 10 GP17	-1,188	29,000	0,245	-0,215	-0,585	0,155
SPI6 - 10 GP18	-1,611	29,000	0,118	-0,288	-0,654	0,078
SPI6-3 GP1	-0,958	29,000	0,346	-0,204	-0,639	0,232
SPI6-3 GP2	-0,800	29,000	0,430	-0,179	-0,637	0,279
SPI6-3 GP3	-1,110	29,000	0,276	-0,232	-0,661	0,196
SPI6-3 GP4	-0,331	29,000	0,743	-0,071	-0,512	0,369
SPI6-3 GP5	-0,515	29,000	0,610	-0,110	-0,546	0,326
SPI6-3 GP6	-1,479	29,000	0,150	-0,285	-0,680	0,109
SPI6-3 GP7	-0,547	29,000	0,588	-0,134	-0,633	0,365
SPI6-3 GP8	-0,947	29,000	0,351	-0,199	-0,628	0,231
SPI6-3 GP9	-0,977	29,000	0,337	-0,240	-0,743	0,263
SPI6-3 GP10	-0,880	29,000	0,386	-0,198	-0,657	0,262
SPI6-3 GP11	-0,576	29,000	0,569	-0,145	-0,661	0,371
SPI6-3 GP12	-0,711	29,000	0,483	-0,154	-0,597	0,289
SPI6-3 GP13	-1,185	29,000	0,246	-0,298	-0,813	0,217
SPI6-3 GP14	-1,308	29,000	0,201	-0,324	-0,830	0,183
SPI6-3 GP15	-0,576	29,000	0,569	-0,145	-0,661	0,371
SPI6-3 GP16	-0,541	29,000	0,593	-0,125	-0,600	0,349
SPI6-3 GP17	-1,354	29,000	0,186	-0,271	-0,682	0,139
SPI6-3 GP18	-1,600	29,000	0,120	-0,304	-0,692	0,084
SPI3 - 2 GP1	-0,181	29,000	0,858	-0,039	-0,478	0,400
SPI3 - 2 GP2	0,295	29,000	0,770	0,063	-0,373	0,499
SPI3 - 2 GP3	-1,089	29,000	0,285	-0,255	-0,734	0,224
SPI3 - 2 GP4	0,075	29,000	0,941	0,016	-0,425	0,457
SPI3 - 2 GP5	-0,358	29,000	0,723	-0,075	-0,504	0,354
SPI3 - 2 GP6	-1,133	29,000	0,266	-0,248	-0,695	0,199
SPI3 - 2 GP7	-0,799	29,000	0,431	-0,182	-0,647	0,284
SPI3 - 2 GP8	-0,797	29,000	0,432	-0,156	-0,555	0,244
SPI3 - 2 GP9	-0,910	29,000	0,370	-0,217	-0,706	0,271
SPI3 - 2 GP10	-1,154	29,000	0,258	-0,251	-0,694	0,193
SPI3 - 2 GP11	-1,121	29,000	0,272	-0,253	-0,715	0,209

One-Sample Test

	Test Value = 0					
	t	df	Sig. (2-tailed)	Mean Difference	Interval of the Lower	Interval of the Upper
SPI3 - 2 GP12	-0,522	29,000	0,606	-0,105	-0,517	0,307
SPI3 - 2 GP13	-1,547	29,000	0,133	-0,345	-0,802	0,111
SPI3 - 2 GP14	-1,578	29,000	0,125	-0,373	-0,857	0,111
SPI3 - 2 GP15	-1,121	29,000	0,272	-0,253	-0,715	0,209
SPI3 - 2 GP16	-1,280	29,000	0,211	-0,293	-0,760	0,175
SPI3 - 2 GP17	-0,670	29,000	0,508	-0,128	-0,520	0,264
SPI3 - 2 GP18	-0,730	29,000	0,471	-0,128	-0,489	0,232
SPI3 - 5 GP1	-0,856	29,000	0,399	-0,223	-0,754	0,309
SPI3 - 5 GP2	-0,940	29,000	0,355	-0,249	-0,792	0,293
SPI3 - 5 GP3	-1,304	29,000	0,202	-0,277	-0,712	0,158
SPI3 - 5 GP4	-0,553	29,000	0,584	-0,137	-0,645	0,371
SPI3 - 5 GP5	-0,133	29,000	0,895	-0,034	-0,554	0,486
SPI3 - 5 GP6	-1,532	29,000	0,136	-0,341	-0,796	0,114
SPI3 - 5 GP7	-1,795	29,000	0,083	-0,366	-0,783	0,051
SPI3 - 5 GP8	-1,482	29,000	0,149	-0,422	-1,004	0,160
SPI3 - 5 GP9	-2,061	29,000	0,048	-0,430	-0,856	-0,003
SPI3 - 5 GP10	-1,847	29,000	0,075	-0,374	-0,789	0,040
SPI3 - 5 GP11	-1,217	29,000	0,233	-0,220	-0,590	0,150
SPI3 - 5 GP12	-1,740	29,000	0,092	-0,524	-1,141	0,092
SPI3 - 5 GP13	-1,284	29,000	0,209	-0,226	-0,586	0,134
SPI3 - 5 GP14	-1,729	29,000	0,094	-0,319	-0,696	0,058
SPI3 - 5 GP15	-1,217	29,000	0,233	-0,220	-0,590	0,150
SPI3 - 5 GP16	-1,323	29,000	0,196	-0,235	-0,597	0,128
SPI3 - 5 GP17	-1,335	29,000	0,192	-0,293	-0,743	0,156
SPI3 - 5 GP18	-1,670	29,000	0,106	-0,404	-0,900	0,091
SPI3 - 8 GP1	-1,808	28,000	0,081	-0,353	-0,753	0,047
SPI3 - 8 GP2	-1,486	27,000	0,149	-0,298	-0,709	0,113
SPI3 - 8 GP3	-1,244	29,000	0,224	-0,267	-0,705	0,172
SPI3 - 8 GP4	0,118	29,000	0,907	0,014	-0,229	0,257
SPI3 - 8 GP5	-0,554	29,000	0,584	-0,072	-0,338	0,194
SPI3 - 8 GP6	-1,460	26,000	0,156	-0,363	-0,875	0,148
SPI3 - 8 GP7	-0,557	25,000	0,583	-0,092	-0,435	0,250
SPI3 - 8 GP8	-2,083	28,000	0,046	-0,379	-0,753	-0,006
SPI3 - 8 GP9	-1,258	28,000	0,219	-0,188	-0,493	0,118
SPI3 - 8 GP10	-2,441	28,000	0,021	-0,445	-0,819	-0,072
SPI3 - 8 GP11	-1,407	29,000	0,170	-0,207	-0,507	0,094
SPI3 - 8 GP12	-2,094	28,000	0,045	-0,408	-0,807	-0,009
SPI3 - 8 GP13	-0,725	29,000	0,474	-0,146	-0,557	0,266
SPI3 - 8 GP14	-1,335	29,000	0,192	-0,295	-0,747	0,157
SPI3 - 8 GP15	-1,407	29,000	0,170	-0,207	-0,507	0,094
SPI3 - 8 GP16	-1,717	29,000	0,097	-0,262	-0,575	0,050
SPI3 - 8 GP17	-1,983	29,000	0,057	-0,357	-0,726	0,011
SPI3 - 8 GP18	-1,825	29,000	0,078	-0,323	-0,685	0,039
SPI3 - 11 GP1	-1,248	29,000	0,222	-0,288	-0,760	0,184
SPI3 - 11 GP2	-1,368	29,000	0,182	-0,285	-0,712	0,141
SPI3 - 11 GP3	-0,894	29,000	0,379	-0,192	-0,633	0,248
SPI3 - 11 GP4	-0,722	29,000	0,476	-0,156	-0,599	0,287
SPI3 - 11 GP5	-0,611	29,000	0,546	-0,131	-0,570	0,308
SPI3 - 11 GP6	-0,813	29,000	0,423	-0,161	-0,566	0,244
SPI3 - 11 GP7	1,459	29,000	0,155	0,279	-0,112	0,669
SPI3 - 11 GP8	-0,242	29,000	0,810	-0,055	-0,517	0,408
SPI3 - 11 GP9	0,472	29,000	0,641	0,099	-0,330	0,527
SPI3 - 11 GP10	1,468	29,000	0,153	0,254	-0,100	0,607
SPI3 - 11 GP11	1,263	29,000	0,217	0,259	-0,160	0,678
SPI3 - 11 GP12	-0,082	29,000	0,935	-0,020	-0,518	0,478
SPI3 - 11 GP13	0,701	29,000	0,489	0,132	-0,254	0,518
SPI3 - 11 GP14	0,798	29,000	0,431	0,150	-0,234	0,534
SPI3 - 11 GP15	1,263	29,000	0,217	0,259	-0,160	0,678
SPI3 - 11 GP16	1,746	29,000	0,091	0,335	-0,057	0,727
SPI3 - 11 GP17	-0,895	29,000	0,378	-0,203	-0,668	0,261
SPI3 - 11 GP18	-1,290	29,000	0,207	-0,296	-0,765	0,173

RCP 4.5 Scenario - Remote Future Analysis

Table A IX. One Sample T-test for comparing means (RCP 4.5 Scenario - Remote Future), Model Data Output (statistical significance in red)

One-Sample Test

	Test Value = 0					
	t	df	Sig. (2-tailed)	Mean Difference	Interval of the Lower	Interval of the Upper
SPI12 GP1	-4,800	29	,000	-0,800	-1,141	-0,459
SPI12 GP2	-1,856	29	,074	-0,410	-0,861	0,042
SPI12 GP3	-2,075	29	,047	-0,403	-0,799	-0,006
SPI12 GP4	-,931	29	,360	-0,214	-0,685	0,256
SPI12 GP5	-,770	29	,447	-0,183	-0,670	0,303
SPI12 GP6	-1,934	29	,063	-0,425	-0,874	0,024
SPI12 GP7	-1,731	29	,094	-0,409	-0,891	0,074
SPI12 GP8	-4,250	29	,000	-0,793	-1,175	-0,412
SPI12 GP9	-2,673	29	,012	-0,635	-1,121	-0,149
SPI12 GP10	-1,953	29	,060	-0,404	-0,828	0,019
SPI12 GP11	-2,052	29	,049	-0,433	-0,865	-0,001
SPI12 GP12	-3,572	29	,001	-0,789	-1,241	-0,337
SPI12 GP13	-1,966	29	,059	-0,371	-0,757	0,015
SPI12 GP14	-2,441	29	,021	-0,442	-0,812	-0,072
SPI12 GP15	-2,052	29	,049	-0,433	-0,865	-0,001
SPI12 GP16	-2,039	29	,051	-0,437	-0,875	0,001
SPI12 GP17	-5,166	29	,000	-0,896	-1,251	-0,542
SPI12 GP18	-6,983	29	,000	-1,021	-1,320	-0,722
SPI6 - 10 GP1	-1,095	29	,283	-0,172	-0,494	0,150
SPI6 - 10 GP2	,493	29	,626	0,071	-0,223	0,365
SPI6 - 10 GP3	-,192	29	,849	-0,034	-0,400	0,331
SPI6 - 10 GP4	,977	29	,337	0,187	-0,205	0,579
SPI6 - 10 GP5	1,435	29	,162	0,253	-0,107	0,613
SPI6 - 10 GP6	-,421	29	,677	-0,071	-0,417	0,274
SPI6 - 10 GP7	,452	29	,654	0,080	-0,280	0,439
SPI6 - 10 GP8	-1,422	29	,166	-0,267	-0,651	0,117
SPI6 - 10 GP9	,233	29	,817	0,039	-0,300	0,378
SPI6 - 10 GP10	-,284	29	,779	-0,050	-0,412	0,311
SPI6 - 10 GP11	,880	29	,386	0,145	-0,192	0,483
SPI6 - 10 GP12	-,798	29	,431	-0,157	-0,558	0,244
SPI6 - 10 GP13	,745	29	,462	0,134	-0,234	0,502
SPI6 - 10 GP14	,344	29	,733	0,055	-0,270	0,379
SPI6 - 10 GP15	,880	29	,386	0,145	-0,192	0,483
SPI6 - 10 GP16	,540	29	,593	0,088	-0,244	0,419
SPI6 - 10 GP17	-1,668	29	,106	-0,283	-0,629	0,064
SPI6 - 10 GP18	-2,270	29	,031	-0,381	-0,725	-0,038
SPI6-3 GP1	-3,366	29	,002	-0,688	-1,107	-0,270
SPI6-3 GP2	-1,475	29	,151	-0,375	-0,896	0,145
SPI6-3 GP3	-1,427	29	,164	-0,328	-0,798	0,142
SPI6-3 GP4	-,858	29	,398	-0,218	-0,739	0,302
SPI6-3 GP5	-,557	29	,582	-0,129	-0,603	0,345
SPI6-3 GP6	-1,457	29	,156	-0,355	-0,853	0,143
SPI6-3 GP7	-1,582	29	,125	-0,404	-0,926	0,118
SPI6-3 GP8	-3,010	29	,005	-0,549	-0,921	-0,176
SPI6-3 GP9	-2,428	29	,022	-0,614	-1,132	-0,097
SPI6-3 GP10	-1,723	29	,096	-0,389	-0,851	0,073
SPI6-3 GP11	-1,910	29	,066	-0,456	-0,945	0,032
SPI6-3 GP12	-2,945	29	,006	-0,591	-1,002	-0,181
SPI6-3 GP13	-2,179	29	,038	-0,536	-1,040	-0,033
SPI6-3 GP14	-2,457	29	,020	-0,592	-1,085	-0,099
SPI6-3 GP15	-1,910	29	,066	-0,456	-0,945	0,032
SPI6-3 GP16	-1,895	29	,068	-0,428	-0,889	0,034
SPI6-3 GP17	-3,599	29	,001	-0,738	-1,158	-0,319
SPI6-3 GP18	-4,381	29	,000	-0,786	-1,152	-0,419
SPI3 - 2 GP1	-1,451	29	,157	-0,262	-0,631	0,107
SPI3 - 2 GP2	,145	29	,886	0,029	-0,376	0,433
SPI3 - 2 GP3	-,019	29	,985	-0,004	-0,470	0,461
SPI3 - 2 GP4	-,064	29	,949	-0,012	-0,400	0,375
SPI3 - 2 GP5	-,185	29	,854	-0,033	-0,398	0,332
SPI3 - 2 GP6	,033	29	,974	0,008	-0,507	0,523
SPI3 - 2 GP7	-1,830	29	,078	-0,332	-0,703	0,039
SPI3 - 2 GP8	-2,134	29	,041	-0,350	-0,685	-0,015
SPI3 - 2 GP9	-2,596	29	,015	-0,465	-0,831	-0,099
SPI3 - 2 GP10	-1,876	29	,071	-0,333	-0,695	0,030
SPI3 - 2 GP11	-2,473	29	,019	-0,401	-0,733	-0,069

One-Sample Test

	Test Value = 0					
	t	df	Sig. (2-tailed)	Mean Difference	Interval of the Lower	Interval of the Upper
SPI3 - 2 GP12	-2,325	29	,027	-0,377	-0,709	-0,045
SPI3 - 2 GP13	-2,038	29	,051	-0,350	-0,701	0,001
SPI3 - 2 GP14	-2,235	29	,033	-0,379	-0,727	-0,032
SPI3 - 2 GP15	-2,473	29	,019	-0,401	-0,733	-0,069
SPI3 - 2 GP16	-2,721	29	,011	-0,442	-0,773	-0,110
SPI3 - 2 GP17	-1,877	29	,071	-0,284	-0,593	0,025
SPI3 - 2 GP18	-2,306	29	,028	-0,316	-0,597	-0,036
SPI3 - 5 GP1	-2,538	29	,017	-0,695	-1,255	-0,135
SPI3 - 5 GP2	-1,801	29	,082	-0,479	-1,023	0,065
SPI3 - 5 GP3	-2,557	29	,016	-0,514	-0,926	-0,103
SPI3 - 5 GP4	-1,596	29	,121	-0,434	-0,990	0,122
SPI3 - 5 GP5	-1,591	29	,123	-0,458	-1,047	0,131
SPI3 - 5 GP6	-2,627	29	,014	-0,539	-0,960	-0,119
SPI3 - 5 GP7	-1,997	29	,055	-0,498	-1,009	0,012
SPI3 - 5 GP8	-2,410	29	,023	-0,836	-1,545	-0,127
SPI3 - 5 GP9	-2,115	29	,043	-0,546	-1,075	-0,018
SPI3 - 5 GP10	-2,010	29	,054	-0,502	-1,013	0,009
SPI3 - 5 GP11	-2,013	29	,054	-0,498	-1,004	0,008
SPI3 - 5 GP12	-2,194	29	,036	-0,786	-1,518	-0,053
SPI3 - 5 GP13	-1,632	29	,113	-0,385	-0,868	0,097
SPI3 - 5 GP14	-1,992	29	,056	-0,501	-1,015	0,013
SPI3 - 5 GP15	-2,013	29	,054	-0,498	-1,004	0,008
SPI3 - 5 GP16	-1,864	29	,072	-0,465	-0,975	0,045
SPI3 - 5 GP17	-3,599	29	,001	-1,007	-1,579	-0,435
SPI3 - 5 GP18	-3,668	29	,001	-1,141	-1,777	-0,505
SPI3 - 8 GP1	-1,574	29	,126	-0,284	-0,652	0,085
SPI3 - 8 GP2	,090	28	,929	0,020	-0,444	0,485
SPI3 - 8 GP3	,434	29	,668	0,116	-0,430	0,662
SPI3 - 8 GP4	,766	29	,450	0,153	-0,256	0,562
SPI3 - 8 GP5	,904	29	,373	0,201	-0,254	0,655
SPI3 - 8 GP6	-,634	29	,531	-0,182	-0,769	0,405
SPI3 - 8 GP7	-,637	27	,529	-0,167	-0,704	0,371
SPI3 - 8 GP8	-2,112	29	,043	-0,406	-0,799	-0,013
SPI3 - 8 GP9	-,658	28	,516	-0,158	-0,649	0,334
SPI3 - 8 GP10	-1,206	28	,238	-0,268	-0,722	0,187
SPI3 - 8 GP11	-,140	29	,889	-0,035	-0,550	0,479
SPI3 - 8 GP12	-1,722	29	,096	-0,394	-0,862	0,074
SPI3 - 8 GP13	-,052	29	,959	-0,016	-0,633	0,602
SPI3 - 8 GP14	,704	29	,487	0,187	-0,356	0,731
SPI3 - 8 GP15	-,140	29	,889	-0,035	-0,550	0,479
SPI3 - 8 GP16	-,369	29	,715	-0,088	-0,578	0,401
SPI3 - 8 GP17	-1,113	29	,275	-0,177	-0,502	0,148
SPI3 - 8 GP18	-1,607	29	,119	-0,239	-0,543	0,065
SPI3 - 11 GP1	-3,354	29	,002	-0,563	-0,906	-0,220
SPI3 - 11 GP2	-2,074	29	,047	-0,423	-0,839	-0,006
SPI3 - 11 GP3	-1,734	29	,094	-0,341	-0,742	0,061
SPI3 - 11 GP4	-,996	29	,328	-0,215	-0,656	0,226
SPI3 - 11 GP5	-,678	29	,503	-0,151	-0,607	0,305
SPI3 - 11 GP6	-1,599	29	,121	-0,311	-0,709	0,087
SPI3 - 11 GP7	,414	29	,682	0,067	-0,263	0,396
SPI3 - 11 GP8	-2,093	29	,045	-0,339	-0,671	-0,008
SPI3 - 11 GP9	-1,001	29	,325	-0,182	-0,555	0,190
SPI3 - 11 GP10	,476	29	,638	0,075	-0,248	0,399
SPI3 - 11 GP11	-,275	29	,785	-0,051	-0,428	0,327
SPI3 - 11 GP12	-1,907	29	,066	-0,333	-0,691	0,024
SPI3 - 11 GP13	-,561	29	,579	-0,096	-0,443	0,252
SPI3 - 11 GP14	-,840	29	,408	-0,147	-0,506	0,211
SPI3 - 11 GP15	-,275	29	,785	-0,051	-0,428	0,327
SPI3 - 11 GP16	,091	29	,928	0,017	-0,365	0,399
SPI3 - 11 GP17	-2,326	29	,027	-0,446	-0,838	-0,054
SPI3 - 11 GP18	-2,950	29	,006	-0,510	-0,864	-0,156

RCP 8.5 Scenario - Near Future Analysis

Table A X. One Sample T-test for comparing means (RCP 8.5 Scenario - Near Future), Model Data Output(statistical significance in red)

One-Sample Test

	Test Value = 0					
	t	df	Sig. (2-tailed)	Mean Difference	Interval of the Difference Lower	Interval of the Difference Upper
SPI12 GP1	-2,786	29	,009	-0,626	-1,086	-0,166
SPI12 GP2	-1,597	29	,121	-0,390	-0,889	0,109
SPI12 GP3	-,980	29	,335	-0,212	-0,656	0,231
SPI12 GP4	-,924	29	,363	-0,229	-0,737	0,279
SPI12 GP5	-,750	29	,459	-0,187	-0,698	0,323
SPI12 GP6	-,892	29	,380	-0,195	-0,643	0,252
SPI12 GP7	-1,012	29	,320	-0,281	-0,849	0,287
SPI12 GP8	-2,528	29	,017	-0,637	-1,152	-0,122
SPI12 GP9	-1,556	29	,131	-0,441	-1,020	0,139
SPI12 GP10	-1,167	29	,253	-0,285	-0,784	0,214
SPI12 GP11	-,833	29	,411	-0,208	-0,719	0,303
SPI12 GP12	-2,216	29	,035	-0,638	-1,226	-0,049
SPI12 GP13	-,757	29	,455	-0,167	-0,618	0,284
SPI12 GP14	-1,072	29	,292	-0,218	-0,635	0,198
SPI12 GP15	-,833	29	,411	-0,208	-0,719	0,303
SPI12 GP16	-1,175	29	,249	-0,275	-0,753	0,204
SPI12 GP17	-2,685	29	,012	-0,607	-1,069	-0,145
SPI12 GP18	-3,275	29	,003	-0,716	-1,163	-0,269
SPI6 - 10 GP1	-2,388	29	,024	-0,418	-0,777	-0,060
SPI6 - 10 GP2	-2,354	29	,026	-0,426	-0,796	-0,056
SPI6 - 10 GP3	-2,038	29	,051	-0,377	-0,756	0,001
SPI6 - 10 GP4	-1,598	29	,121	-0,346	-0,789	0,097
SPI6 - 10 GP5	-,964	29	,343	-0,190	-0,592	0,213
SPI6 - 10 GP6	-1,783	29	,085	-0,306	-0,657	0,045
SPI6 - 10 GP7	-1,416	29	,167	-0,298	-0,729	0,132
SPI6 - 10 GP8	-3,113	29	,004	-0,604	-1,001	-0,207
SPI6 - 10 GP9	-1,482	29	,149	-0,259	-0,616	0,098
SPI6 - 10 GP1	-2,255	29	,032	-0,473	-0,902	-0,044
SPI6 - 10 GP1	-,347	29	,731	-0,063	-0,434	0,308
SPI6 - 10 GP1	-2,450	29	,021	-0,459	-0,842	-0,076
SPI6 - 10 GP1	-,855	29	,400	-0,170	-0,576	0,236
SPI6 - 10 GP1	-1,471	29	,152	-0,280	-0,670	0,109
SPI6 - 10 GP1	-,347	29	,731	-0,063	-0,434	0,308
SPI6 - 10 GP1	-1,174	29	,250	-0,220	-0,604	0,163
SPI6 - 10 GP1	-2,870	29	,008	-0,536	-0,917	-0,154
SPI6 - 10 GP1	-3,117	29	,004	-0,584	-0,967	-0,201
SPI6-3 GP1	-2,936	29	,006	-0,588	-0,998	-0,179
SPI6-3 GP2	-1,447	29	,159	-0,287	-0,693	0,119
SPI6-3 GP3	-,428	29	,672	-0,083	-0,480	0,314
SPI6-3 GP4	-,877	29	,388	-0,191	-0,636	0,254
SPI6-3 GP5	-,696	29	,492	-0,129	-0,506	0,249
SPI6-3 GP6	-,185	29	,855	-0,035	-0,420	0,351
SPI6-3 GP7	-,431	29	,669	-0,102	-0,588	0,383
SPI6-3 GP8	-1,662	29	,107	-0,303	-0,676	0,070
SPI6-3 GP9	-1,059	29	,299	-0,256	-0,751	0,239
SPI6-3 GP10	-,474	29	,639	-0,096	-0,512	0,319
SPI6-3 GP11	-,470	29	,642	-0,106	-0,568	0,356
SPI6-3 GP12	-1,724	29	,095	-0,369	-0,808	0,069
SPI6-3 GP13	-,612	29	,545	-0,139	-0,603	0,325
SPI6-3 GP14	-,869	29	,392	-0,181	-0,607	0,245
SPI6-3 GP15	-,470	29	,642	-0,106	-0,568	0,356
SPI6-3 GP16	-,840	29	,408	-0,161	-0,552	0,231
SPI6-3 GP17	-2,043	29	,050	-0,412	-0,824	0,000
SPI6-3 GP18	-2,512	29	,018	-0,477	-0,866	-0,089
SPI3 - 2 GP1	-,491	29	,627	-0,095	-0,492	0,302
SPI3 - 2 GP2	,993	29	,329	0,198	-0,210	0,607
SPI3 - 2 GP3	1,220	29	,232	0,282	-0,190	0,754
SPI3 - 2 GP4	,040	29	,968	0,008	-0,415	0,432
SPI3 - 2 GP5	-,136	29	,893	-0,027	-0,432	0,378
SPI3 - 2 GP6	1,623	29	,115	0,361	-0,094	0,815
SPI3 - 2 GP7	,069	29	,945	0,015	-0,421	0,451
SPI3 - 2 GP8	-,461	29	,648	-0,083	-0,450	0,284
SPI3 - 2 GP9	-,209	29	,836	-0,046	-0,500	0,407
SPI3 - 2 GP10	,145	29	,885	0,029	-0,373	0,430
SPI3 - 2 GP11	,004	29	,997	0,001	-0,476	0,478

One-Sample Test

	Test Value = 0					
	t	df	Sig. (2-tailed)	Mean Difference	Interval of the Difference Lower	Interval of the Difference Upper
SPI3 - 2 GP12	-,585	29	,563	-0,109	-0,488	0,271
SPI3 - 2 GP13	,033	29	,974	0,008	-0,491	0,507
SPI3 - 2 GP14	-,072	29	,943	-0,017	-0,490	0,457
SPI3 - 2 GP15	,004	29	,997	0,001	-0,476	0,478
SPI3 - 2 GP16	-,347	29	,731	-0,072	-0,496	0,352
SPI3 - 2 GP17	,244	29	,809	0,043	-0,314	0,399
SPI3 - 2 GP18	-,116	29	,909	-0,019	-0,353	0,316
SPI3 - 5 GP1	-2,043	29	,050	-0,490	-0,981	0,001
SPI3 - 5 GP2	-2,161	29	,039	-0,496	-0,966	-0,027
SPI3 - 5 GP3	-3,184	29	,003	-0,621	-1,020	-0,222
SPI3 - 5 GP4	-1,930	29	,063	-0,425	-0,876	0,025
SPI3 - 5 GP5	-1,474	29	,151	-0,353	-0,843	0,137
SPI3 - 5 GP6	-3,484	29	,002	-0,658	-1,045	-0,272
SPI3 - 5 GP7	-4,255	29	,000	-0,962	-1,424	-0,500
SPI3 - 5 GP8	-2,735	29	,011	-0,826	-1,444	-0,208
SPI3 - 5 GP9	-3,968	29	,000	-0,924	-1,401	-0,448
SPI3 - 5 GP10	-4,091	29	,000	-0,887	-1,330	-0,443
SPI3 - 5 GP11	-3,271	29	,003	-0,750	-1,219	-0,281
SPI3 - 5 GP12	-2,516	29	,018	-0,803	-1,455	-0,150
SPI3 - 5 GP13	-3,189	29	,003	-0,627	-1,029	-0,225
SPI3 - 5 GP14	-3,209	29	,003	-0,663	-1,085	-0,240
SPI3 - 5 GP15	-3,271	29	,003	-0,750	-1,219	-0,281
SPI3 - 5 GP16	-3,135	29	,004	-0,688	-1,136	-0,239
SPI3 - 5 GP17	-2,459	29	,020	-0,596	-1,091	-0,100
SPI3 - 5 GP18	-2,892	29	,007	-0,707	-1,207	-0,207
SPI3 - 8 GP1	-2,133	29	,042	-0,416	-0,814	-0,017
SPI3 - 8 GP2	-1,063	28	,297	-0,206	-0,602	0,191
SPI3 - 8 GP3	-1,502	29	,144	-0,306	-0,724	0,111
SPI3 - 8 GP4	,029	29	,977	0,004	-0,295	0,303
SPI3 - 8 GP5	-,014	29	,989	-0,002	-0,309	0,305
SPI3 - 8 GP6	-1,657	27	,109	-0,400	-0,895	0,095
SPI3 - 8 GP7	-,396	26	,695	-0,057	-0,352	0,238
SPI3 - 8 GP8	-2,803	29	,009	-0,466	-0,806	-0,126
SPI3 - 8 GP9	-1,240	26	,226	-0,182	-0,485	0,120
SPI3 - 8 GP10	-2,083	29	,046	-0,326	-0,646	-0,006
SPI3 - 8 GP11	-,119	29	,906	-0,021	-0,387	0,345
SPI3 - 8 GP12	-2,346	29	,026	-0,382	-0,714	-0,049
SPI3 - 8 GP13	-1,063	29	,297	-0,217	-0,635	0,201
SPI3 - 8 GP14	-,991	29	,330	-0,216	-0,662	0,230
SPI3 - 8 GP15	-,119	29	,906	-0,021	-0,387	0,345
SPI3 - 8 GP16	-,621	29	,540	-0,109	-0,470	0,251
SPI3 - 8 GP17	-1,955	29	,060	-0,361	-0,738	0,017
SPI3 - 8 GP18	-1,732	29	,094	-0,298	-0,650	0,054
SPI3 - 11 GP1	-2,888	29	,007	-0,460	-0,786	-0,134
SPI3 - 11 GP2	-2,033	29	,051	-0,323	-0,647	0,002
SPI3 - 11 GP3	-,085	29	,933	-0,015	-0,373	0,343
SPI3 - 11 GP4	-,256	29	,800	-0,044	-0,398	0,310
SPI3 - 11 GP5	-,190	29	,851	-0,031	-0,370	0,307
SPI3 - 11 GP6	,267	29	,791	0,045	-0,299	0,389
SPI3 - 11 GP7	1,692	29	,101	0,310	-0,065	0,684
SPI3 - 11 GP8	-1,407	29	,170	-0,230	-0,565	0,104
SPI3 - 11 GP9	,700	29	,489	0,130	-0,250	0,510
SPI3 - 11 GP10	1,332	29	,193	0,241	-0,129	0,612
SPI3 - 11 GP11	,974	29	,338	0,179	-0,197	0,556
SPI3 - 11 GP12	-1,350	29	,187	-0,233	-0,586	0,120
SPI3 - 11 GP13	1,282	29	,210	0,215	-0,128	0,558
SPI3 - 11 GP14	1,022	29	,315	0,173	-0,173	0,520
SPI3 - 11 GP15	,974	29	,338	0,179	-0,197	0,556
SPI3 - 11 GP16	,839	29	,408	0,156	-0,224	0,536
SPI3 - 11 GP17	-2,308	29	,028	-0,409	-0,772	-0,047
SPI3 - 11 GP18	-2,612	29	,014	-0,441	-0,786	-0,096

RCP 8.5 Scenario - Remote Future Analysis

Table A XI. One Sample T-test for comparing means (RCP 8.5 Scenario - Remote Future), Model Data Output (statistical significance in red)

One-Sample Test

	Test Value = 0					
	t	df	Sig. (2-tailed)	Mean Difference	Interval of the Lower	Interval of the Upper
SPI12 GP1	-6,898	29	,000	-1,820	-2,359	-1,280
SPI12 GP2	-5,243	29	,000	-1,530	-2,127	-0,933
SPI12 GP3	-5,622	29	,000	-1,507	-2,055	-0,959
SPI12 GP4	-3,617	29	,001	-1,089	-1,705	-0,473
SPI12 GP5	-3,303	29	,003	-1,022	-1,655	-0,389
SPI12 GP6	-5,340	29	,000	-1,493	-2,064	-0,921
SPI12 GP7	-3,937	29	,000	-1,144	-1,738	-0,550
SPI12 GP8	-5,540	29	,000	-1,632	-2,234	-1,029
SPI12 GP9	-4,642	29	,000	-1,354	-1,951	-0,758
SPI12 GP10	-4,419	29	,000	-1,203	-1,760	-0,646
SPI12 GP11	-3,546	29	,001	-1,119	-1,765	-0,474
SPI12 GP12	-5,634	29	,000	-1,777	-2,422	-1,132
SPI12 GP13	-3,853	29	,001	-1,090	-1,669	-0,512
SPI12 GP14	-4,222	29	,000	-1,170	-1,736	-0,603
SPI12 GP15	-3,546	29	,001	-1,119	-1,765	-0,474
SPI12 GP16	-3,692	29	,001	-1,131	-1,758	-0,505
SPI12 GP17	-6,212	29	,000	-1,833	-2,437	-1,230
SPI12 GP18	-6,616	29	,000	-1,894	-2,480	-1,309
SPI6 - 10 GP1	-4,561	29	,000	-1,018	-1,474	-0,561
SPI6 - 10 GP2	-3,047	29	,005	-0,683	-1,142	-0,225
SPI6 - 10 GP3	-2,999	29	,006	-0,767	-1,290	-0,244
SPI6 - 10 GP4	-1,785	29	,085	-0,468	-1,004	0,068
SPI6 - 10 GP5	-1,361	29	,184	-0,370	-0,926	0,186
SPI6 - 10 GP6	-2,721	29	,011	-0,633	-1,110	-0,157
SPI6 - 10 GP7	-1,731	29	,094	-0,433	-0,943	0,078
SPI6 - 10 GP8	-4,227	29	,000	-1,085	-1,610	-0,560
SPI6 - 10 GP9	-1,889	29	,069	-0,428	-0,891	0,035
SPI6 - 10 GP10	-3,054	29	,005	-0,825	-1,377	-0,273
SPI6 - 10 GP11	-1,545	29	,133	-0,395	-0,917	0,128
SPI6 - 10 GP12	-3,751	29	,001	-0,950	-1,468	-0,432
SPI6 - 10 GP13	-2,002	29	,055	-0,520	-1,051	0,011
SPI6 - 10 GP14	-2,560	29	,016	-0,651	-1,171	-0,131
SPI6 - 10 GP15	-1,545	29	,133	-0,395	-0,917	0,128
SPI6 - 10 GP16	-1,970	29	,058	-0,516	-1,053	0,020
SPI6 - 10 GP17	-4,972	29	,000	-1,095	-1,545	-0,645
SPI6 - 10 GP18	-5,523	29	,000	-1,221	-1,674	-0,769
SPI6-3 GP1	-4,508	29	,000	-1,172	-1,704	-0,641
SPI6-3 GP2	-3,678	29	,001	-0,963	-1,499	-0,428
SPI6-3 GP3	-4,080	29	,000	-0,943	-1,415	-0,470
SPI6-3 GP4	-2,616	29	,014	-0,734	-1,307	-0,160
SPI6-3 GP5	-2,371	29	,025	-0,603	-1,123	-0,083
SPI6-3 GP6	-3,918	29	,000	-0,873	-1,329	-0,417
SPI6-3 GP7	-3,161	29	,004	-0,819	-1,349	-0,289
SPI6-3 GP8	-3,368	29	,002	-0,813	-1,307	-0,319
SPI6-3 GP9	-3,480	29	,002	-0,977	-1,551	-0,403
SPI6-3 GP10	-3,577	29	,001	-0,797	-1,252	-0,341
SPI6-3 GP11	-2,395	29	,023	-0,727	-1,348	-0,106
SPI6-3 GP12	-3,559	29	,001	-0,966	-1,522	-0,411
SPI6-3 GP13	-2,937	29	,006	-0,806	-1,368	-0,245
SPI6-3 GP14	-3,235	29	,003	-0,843	-1,376	-0,310
SPI6-3 GP15	-2,395	29	,023	-0,727	-1,348	-0,106
SPI6-3 GP16	-2,570	29	,016	-0,691	-1,242	-0,141
SPI6-3 GP17	-3,790	29	,001	-1,026	-1,579	-0,472
SPI6-3 GP18	-3,959	29	,000	-1,006	-1,526	-0,486
SPI3 - 2 GP1	-3,995	29	,000	-0,981	-1,483	-0,479
SPI3 - 2 GP2	-4,037	29	,000	-0,908	-1,368	-0,448
SPI3 - 2 GP3	-4,706	29	,000	-1,106	-1,586	-0,625
SPI3 - 2 GP4	-3,467	29	,002	-0,776	-1,233	-0,318
SPI3 - 2 GP5	-3,892	29	,001	-0,833	-1,271	-0,395
SPI3 - 2 GP6	-4,787	29	,000	-1,058	-1,509	-0,606
SPI3 - 2 GP7	-5,124	29	,000	-0,982	-1,374	-0,590
SPI3 - 2 GP8	-4,090	29	,000	-0,844	-1,265	-0,422
SPI3 - 2 GP9	-5,213	29	,000	-1,153	-1,606	-0,701
SPI3 - 2 GP10	-4,873	29	,000	-0,920	-1,306	-0,534
SPI3 - 2 GP11	-4,992	29	,000	-1,149	-1,619	-0,678

One-Sample Test

	Test Value = 0					
	t	df	Sig. (2-tailed)	Mean Difference	Interval of the Lower	Interval of the Upper
SPI3 - 2 GP12	-4,030	29	,000	-0,868	-1,309	-0,428
SPI3 - 2 GP13	-4,543	29	,000	-1,075	-1,559	-0,591
SPI3 - 2 GP14	-4,516	29	,000	-1,078	-1,566	-0,590
SPI3 - 2 GP15	-4,992	29	,000	-1,149	-1,619	-0,678
SPI3 - 2 GP16	-4,700	29	,000	-1,050	-1,507	-0,593
SPI3 - 2 GP17	-3,834	29	,001	-0,874	-1,340	-0,408
SPI3 - 2 GP18	-3,829	29	,001	-0,784	-1,203	-0,365
SPI3 - 5 GP1	-6,369	29	,000	-1,759	-2,324	-1,194
SPI3 - 5 GP2	-5,927	29	,000	-1,658	-2,230	-1,086
SPI3 - 5 GP3	-6,687	29	,000	-1,624	-2,121	-1,127
SPI3 - 5 GP4	-4,842	29	,000	-1,522	-2,165	-0,879
SPI3 - 5 GP5	-4,714	29	,000	-1,609	-2,308	-0,911
SPI3 - 5 GP6	-6,990	29	,000	-1,628	-2,104	-1,152
SPI3 - 5 GP7	-4,656	29	,000	-1,328	-1,911	-0,745
SPI3 - 5 GP8	-5,594	29	,000	-1,682	-2,297	-1,067
SPI3 - 5 GP9	-5,354	29	,000	-1,489	-2,058	-0,920
SPI3 - 5 GP10	-5,249	29	,000	-1,370	-1,903	-0,836
SPI3 - 5 GP11	-5,242	29	,000	-1,461	-2,031	-0,891
SPI3 - 5 GP12	-6,250	29	,000	-1,839	-2,440	-1,237
SPI3 - 5 GP13	-5,318	29	,000	-1,513	-2,095	-0,931
SPI3 - 5 GP14	-5,938	29	,000	-1,601	-2,153	-1,050
SPI3 - 5 GP15	-5,242	29	,000	-1,461	-2,031	-0,891
SPI3 - 5 GP16	-5,282	29	,000	-1,375	-1,907	-0,843
SPI3 - 5 GP17	-6,147	29	,000	-1,815	-2,419	-1,211
SPI3 - 5 GP18	-6,094	29	,000	-1,951	-2,605	-1,296
SPI3 - 8 GP1	-6,770	28	,000	-1,117	-1,455	-0,779
SPI3 - 8 GP2	-4,705	25	,000	-0,920	-1,323	-0,518
SPI3 - 8 GP3	-7,114	29	,000	-0,999	-1,286	-0,712
SPI3 - 8 GP4	-3,248	29	,003	-0,385	-0,627	-0,143
SPI3 - 8 GP5	-2,176	29	,038	-0,325	-0,630	-0,020
SPI3 - 8 GP6	-5,919	25	,000	-1,091	-1,471	-0,711
SPI3 - 8 GP7	-,524	18	,607	-0,105	-0,524	0,315
SPI3 - 8 GP8	-5,581	27	,000	-1,174	-1,606	-0,742
SPI3 - 8 GP9	-1,762	21	,093	-0,325	-0,709	0,059
SPI3 - 8 GP10	-3,595	24	,001	-0,791	-1,246	-0,337
SPI3 - 8 GP11	-5,076	29	,000	-0,663	-0,931	-0,396
SPI3 - 8 GP12	-5,240	27	,000	-1,247	-1,736	-0,759
SPI3 - 8 GP13	-4,828	29	,000	-0,870	-1,238	-0,501
SPI3 - 8 GP14	-4,809	29	,000	-0,865	-1,233	-0,497
SPI3 - 8 GP15	-5,076	29	,000	-0,663	-0,931	-0,396
SPI3 - 8 GP16	-4,027	29	,000	-0,647	-0,976	-0,318
SPI3 - 8 GP17	-6,225	28	,000	-0,952	-1,265	-0,639
SPI3 - 8 GP18	-6,189	28	,000	-0,897	-1,194	-0,600
SPI3 - 11 GP1	-3,205	29	,003	-0,822	-1,347	-0,298
SPI3 - 11 GP2	-1,899	29	,068	-0,516	-1,071	0,040
SPI3 - 11 GP3	-1,178	29	,248	-0,304	-0,832	0,224
SPI3 - 11 GP4	-,681	29	,501	-0,180	-0,721	0,361
SPI3 - 11 GP5	-,228	29	,822	-0,061	-0,613	0,490
SPI3 - 11 GP6	-,765	29	,451	-0,201	-0,738	0,336
SPI3 - 11 GP7	,240	29	,812	0,058	-0,439	0,555
SPI3 - 11 GP8	-1,866	29	,072	-0,495	-1,037	0,048
SPI3 - 11 GP9	-,388	29	,701	-0,104	-0,651	0,444
SPI3 - 11 GP10	-,136	29	,893	-0,032	-0,509	0,446
SPI3 - 11 GP11	,215	29	,831	0,062	-0,525	0,648
SPI3 - 11 GP12	-2,032	29	,051	-0,620	-1,243	0,004
SPI3 - 11 GP13	,065	29	,949	0,017	-0,509	0,542
SPI3 - 11 GP14	-,117	29	,908	-0,031	-0,576	0,514
SPI3 - 11 GP15	,215	29	,831	0,062	-0,525	0,648
SPI3 - 11 GP16	,041	29	,967	0,012	-0,583	0,607
SPI3 - 11 GP17	-2,224	29	,034	-0,609	-1,169	-0,049
SPI3 - 11 GP18	-2,665	29	,012	-0,700	-1,237	-0,163

Color tables displaying SPI values calculated by SMHI Model Data (1971 – 2100) under RCP 8.5 and RCP 4.5 climate change scenarios

Table A XII. SPI 3 – February – Tables displaying model data values (RCP4.5)

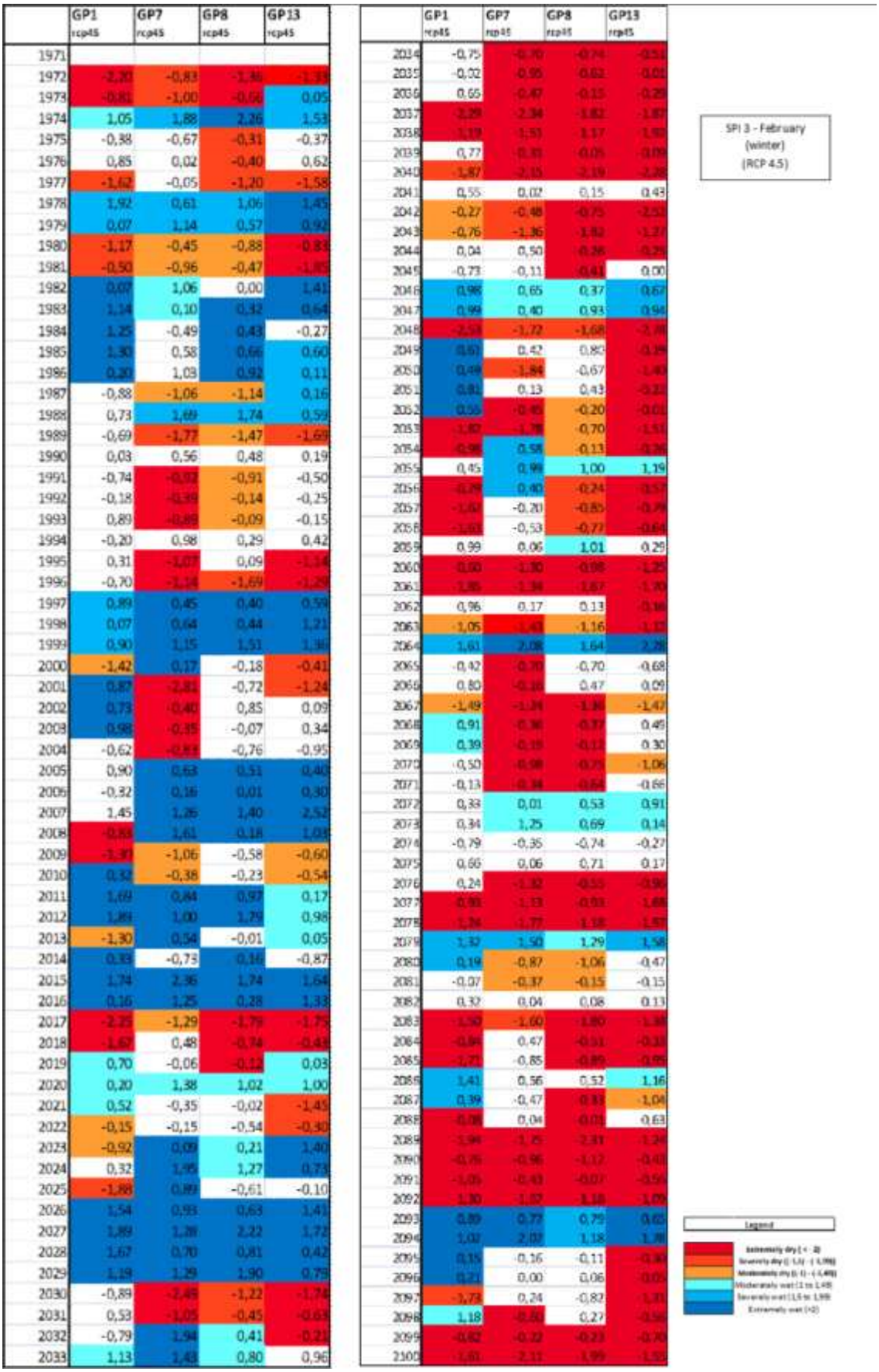

Table A XIII. SPI 3 – May – Tables displaying model data values (RCP4.5)

	GP1 rcp45	GP7 rcp45	GP8 rcp45	GP13 rcp45
1971	-0,34	-0,10	-0,38	-0,17
1972	-0,81	0,54	-0,45	0,65
1973	-0,33	-0,80	-1,51	-0,58
1974	1,57	2,19	2,53	1,94
1975	0,99	1,05	0,59	1,49
1976	0,05	0,88	0,63	0,80
1977	-0,27	-0,41	-0,02	-0,22
1978	-0,57	0,10	0,14	0,35
1979	-0,56	-0,67	-0,97	-0,57
1980	-0,86	0,89	-0,25	0,39
1981	0,30	-0,44	0,36	-0,17
1982	1,08	0,74	0,19	0,76
1983	1,90	-0,32	0,97	-0,61
1984	1,38	1,60	0,80	1,56
1985	1,21	0,21	1,19	0,63
1986	-0,32	-0,63	0,05	-0,59
1987	0,74	1,18	0,28	0,54
1988	0,12	-1,52	0,06	-1,04
1989	-0,07	-1,08	-0,48	-1,28
1990	0,68	0,15	0,43	0,80
1991	0,31	0,04	0,00	-0,35
1992	-0,78	-0,69	-0,67	-1,07
1993	-0,19	0,93	0,49	0,48
1994	-1,54	-2,34	-2,83	-2,01
1995	-2,20	-1,90	-2,75	-2,18
1996	0,37	0,32	1,70	0,29
1997	-0,23	0,68	0,21	0,76
1998	0,94	0,49	0,33	1,14
1999	-2,49	-0,59	-1,10	-0,83
2000	-0,05	-0,38	0,02	-0,77
2001	0,61	0,09	1,03	0,14
2002	0,86	0,55	1,44	0,05
2003	-0,13	-1,65	-0,87	-0,41
2004	1,51	-0,20	0,68	0,63
2005	-0,11	0,51	0,78	0,99
2006	-1,23	-1,50	-1,70	-0,08
2007	-1,07	1,07	0,82	2,06
2008	-1,00	-1,20	-0,93	-0,88
2009	-2,73	-2,67	-3,26	-2,66
2010	-0,46	-0,75	-0,72	-0,12
2011	-0,11	0,19	0,50	-0,69
2012	-1,09	-0,82	-0,82	-1,23
2013	-3,46	-3,85	-4,50	-4,13
2014	-0,23	-0,29	-0,94	-0,06
2015	0,08	-1,08	0,36	-0,45
2016	-2,47	-2,32	-2,06	-1,30
2017	-1,23	-2,13	-1,24	-0,98
2018	-0,28	-0,48	-0,54	-0,76
2019	0,06	-1,07	-0,61	0,03
2020	-2,16	-2,72	-2,94	-2,40
2021	1,04	-0,28	-0,17	0,12
2022	-2,51	-1,12	-3,08	-1,93
2023	0,49	-0,83	-0,08	-0,45
2024	-0,57	-1,03	-1,42	-0,67
2025	-0,33	-0,89	-1,35	0,04
2026	0,68	-0,38	0,07	-0,39
2027	-1,64	-0,09	-2,00	-0,64
2028	-0,51	-1,05	-1,42	-0,76
2029	1,52	0,70	1,64	0,94
2030	-0,70	-0,07	0,08	-0,52
2031	1,35	1,06	1,66	1,17
2032	2,10	-0,11	1,92	-0,28
2033	-0,87	-1,87	-2,15	-1,01

	GP1 rcp45	GP7 rcp45	GP8 rcp45	GP13 rcp45
2034	-1,20	-0,52	-0,76	-0,51
2035	-1,58	-3,40	-2,65	-2,77
2036	-0,69	-1,03	-2,00	-0,19
2037	-1,78	-2,36	-2,30	-1,69
2038	-1,62	-0,98	-1,73	-1,29
2039	-0,69	-0,84	-0,42	-0,96
2040	-3,25	-1,65	-2,26	-0,52
2041	0,60	-0,84	-0,68	0,10
2042	-0,29	-0,52	0,62	-1,43
2043	0,58	0,88	-0,50	0,89
2044	-0,75	-0,44	-1,05	-0,58
2045	1,34	0,77	1,56	1,12
2046	1,63	0,52	1,22	0,08
2047	0,89	0,07	0,55	0,53
2048	-3,24	-1,92	-3,15	-0,86
2049	0,62	0,73	1,38	0,52
2050	-0,46	-0,30	0,31	-0,48
2051	1,16	1,29	0,73	1,47
2052	-1,07	-0,62	-2,17	-0,76
2053	0,71	-0,57	0,00	0,19
2054	-1,89	-0,25	-0,93	-0,79
2055	-0,77	-2,09	-1,90	-1,67
2056	1,09	-0,31	0,23	0,15
2057	-1,82	-2,19	-1,35	-2,44
2058	-0,83	-1,00	-1,76	-1,00
2059	-0,24	-0,08	-0,19	-0,60
2060	0,16	-0,04	0,28	0,33
2061	0,00	0,45	0,96	0,15
2062	-0,24	-0,69	-0,03	-0,46
2063	0,87	-0,15	0,25	0,34
2064	-0,36	-0,03	-0,92	-0,12
2065	-1,61	-1,41	-1,39	-1,27
2066	-0,53	-1,30	-1,33	-1,16
2067	0,04	0,09	-0,29	0,43
2068	-0,42	-1,36	0,29	-0,68
2069	-0,42	-0,39	0,65	-0,63
2070	-0,18	0,80	1,07	0,84
2071	-0,85	0,61	0,09	0,46
2072	1,65	2,77	2,90	2,52
2073	-0,08	-0,56	0,58	-0,39
2074	-4,50	-3,36	-5,27	-3,49
2075	-0,40	0,53	-1,21	-0,03
2076	1,20	0,11	0,70	0,32
2077	-2,39	-0,29	-2,73	-0,25
2078	-1,56	-2,93	-1,88	-1,80
2079	-1,15	-0,52	-0,99	-0,44
2080	-1,83	-1,20	-2,16	-0,30
2081	0,99	1,57	1,26	1,47
2082	0,70	0,57	1,26	1,53
2083	-0,70	-1,18	-1,11	-1,27
2084	-2,75	-0,99	-3,17	-1,76
2085	-0,25	0,31	-1,54	-0,17
2086	-0,54	-0,63	-0,66	-0,37
2087	-2,02	-1,48	-2,49	-1,97
2088	0,35	-0,25	0,40	-0,04
2089	-2,25	-1,36	-2,83	-1,44
2090	-1,51	-0,74	-1,98	-0,46
2091	-2,21	-2,33	-2,39	-2,84
2092	-0,89	-0,65	-2,40	-0,41
2093	0,60	0,44	0,06	0,20
2094	-0,70	-0,37	1,16	-0,55
2095	0,51	-0,68	0,52	-0,35
2096	-3,11	-2,66	-3,96	-1,57
2097	-0,07	1,51	1,65	1,46
2098	0,58	-1,76	-0,29	-0,72
2099	0,61	1,34	1,20	0,19
2100	1,71	0,35	1,36	0,94

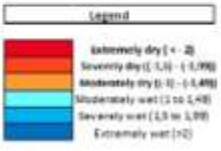

Table A XIV. SPI 3 – August – Tables displaying model data values (RCP4.5)

	GP1 rcp45	GP7 rcp45	GP8 rcp45	GP13 rcp45
1971	-1,79	-0,29	-1,83	-1,06
1972	0,23	-0,12	-0,19	-0,42
1973	0,10	0,78	-0,10	-0,01
1974	0,31	-0,68	0,21	0,71
1975	-0,72	0,35	0,06	0,22
1976	0,00	0,38	0,50	-0,44
1977	0,05	-0,65	-0,99	-0,85
1978	0,83	-0,34	0,63	-0,55
1979	0,70	0,38	0,66	1,40
1980	-0,31	0,00	0,11	-0,52
1981	-0,48	-0,33	-0,60	0,65
1982	1,46	1,54	0,85	1,21
1983	-1,60	-1,44	-1,16	-1,12
1984	-1,54	-0,64	-1,25	-1,05
1985	0,53	0,24	0,69	0,70
1986	0,50	-0,95	0,43	-0,33
1987	-1,09	-1,16	-1,41	-1,83
1988	-0,43	0,21	-0,23	-0,38
1989	1,95	2,23	2,30	2,39
1990	0,19	-0,74	0,01	0,15
1991	0,22	1,23	-0,23	0,94
1992	-1,90	-0,37	-1,95	-1,03
1993	0,40	0,26	1,10	0,69
1994	0,57	0,14	0,04	-0,11
1995	0,60	-0,31	0,04	-0,21
1996	0,06	0,77	1,23	0,59
1997	-0,51	0,31	-0,69	-0,53
1998	2,32	1,67	1,84	1,26
1999	-1,06	1,01	0,67	0,85
2000	0,44	-0,35	-0,39	0,25
2001	-1,88	-1,09	-1,46	-0,80
2002	-0,24	0,50	-0,59	-0,60
2003	1,12	0,40	0,74	1,07
2004	0,14	0,54	1,31	0,69
2005	0,88	-0,12	0,75	-0,09
2006	0,35	-1,44	-0,95	-0,51
2007	-0,79	-0,42	0,45	-1,08
2008	0,84	0,19	0,32	-0,34
2009	-0,42	-1,33	-0,52	-1,30
2010	-0,28	-0,24	-0,22	1,08
2011	-0,04	-0,92	-0,19	-0,42
2012	0,56	-0,23	-0,13	-0,47
2013	0,60	0,99	0,83	0,42
2014	-0,18	-1,63	-1,05	-1,89
2015	0,53	0,99	0,36	0,45
2016	0,88	0,18	0,03	1,21
2017	0,72	0,05	-0,36	-0,65
2018	-0,89	0,94	0,32	0,35
2019	-1,09	0,00	-2,05	-1,83
2020	0,04	-0,68	0,08	-0,21
2021	-0,21	-0,35	-1,77	-1,33
2022	-1,28	-1,32	-1,28	-0,02
2023	0,21	-0,16	-0,15	-1,24
2024	-0,87	-1,23	-0,96	-1,83
2025	-1,00	-0,20	-1,40	-1,24
2026	-1,25	-0,68	-1,56	-0,30
2027	0,03	-0,47	-0,46	0,51
2028	0,44	1,36	1,36	1,36
2029	-0,85	-0,28	-0,90	-0,84
2030	-0,85	-0,55	-1,41	-0,22
2031	0,05	1,46	-0,21	2,09
2032	0,35	0,87	0,14	1,16
2033	2,14	1,30	0,75	1,57

	GP1 rcp45	GP7 rcp45	GP8 rcp45	GP13 rcp45
2034	-0,93	0,76	0,31	0,42
2035	-1,39	-1,81	0,31	0,10
2036	-1,98	0,00	-1,52	-1,83
2037	-1,39	0,06	1,50	0,36
2038	-0,71	-0,01	-1,01	0,46
2039	-2,61	0,00	-2,52	-1,20
2040	0,00	0,00	0,00	-1,83
2041	-0,23	-0,34	0,24	-0,73
2042	1,77	0,75	0,92	1,97
2043	0,03	-0,69	0,09	0,68
2044	-1,27	0,20	-0,66	-0,04
2045	0,08	-0,12	0,91	0,44
2046	-0,67	-0,49	-0,03	0,10
2047	0,53	0,58	-0,25	0,58
2048	0,42	0,20	-0,83	-0,52
2049	-0,43	-1,23	0,07	-1,07
2050	-1,15	0,00	-0,71	-1,01
2051	-1,43	-0,02	-0,85	-1,30
2052	0,79	2,19	0,18	-0,40
2053	-0,09	0,10	-0,43	0,23
2054	-2,58	0,00	-1,79	-1,83
2055	-1,30	-0,59	-1,05	-0,90
2056	-1,96	-0,63	-1,93	-1,83
2057	0,70	0,60	0,06	0,44
2058	-0,09	1,01	1,34	1,04
2059	-0,28	0,05	-0,38	-0,57
2060	-0,96	0,38	-0,65	0,07
2061	-0,82	1,59	-0,31	1,75
2062	-0,83	-0,23	-1,35	-1,05
2063	1,44	0,37	0,39	-1,00
2064	-0,83	0,00	-1,42	-1,01
2065	-0,48	1,05	0,48	0,80
2066	-0,52	0,16	0,05	-1,83
2067	-1,30	0,00	-0,91	-1,04
2068	0,62	-0,97	0,10	0,10
2069	-1,48	-1,63	-1,28	-1,74
2070	-0,66	-0,61	-0,13	-0,66
2071	-0,96	-1,63	-1,62	-1,57
2072	-0,82	-1,63	-2,24	-1,83
2073	-1,03	-0,97	-1,31	-1,35
2074	-0,97	-0,46	-0,51	-0,01
2075	-0,28	-0,82	-0,39	-0,33
2076	0,47	1,08	0,56	1,51
2077	-1,39	-0,36	-1,57	-0,90
2078	0,40	0,44	0,79	1,26
2079	-0,60	-0,50	-0,80	0,50
2080	-1,38	0,00	-1,33	-1,83
2081	-0,42	0,33	-1,21	-0,42
2082	0,35	0,61	0,50	0,09
2083	-0,17	-1,15	-0,57	-0,07
2084	-0,72	-1,01	-0,67	-1,30
2085	0,05	-0,71	-0,41	-0,20
2086	-0,84	-1,32	-1,16	-1,83
2087	1,10	-0,48	0,50	0,16
2088	-0,67	0,04	-0,15	-0,74
2089	-0,42	0,00	0,13	-1,20
2090	0,74	1,96	0,76	1,49
2091	0,71	1,45	0,25	2,32
2092	0,53	-1,44	0,42	1,35
2093	-1,24	-1,44	-1,02	-0,48
2094	1,55	1,18	0,99	1,28
2095	0,53	-0,15	-1,53	-0,89
2096	-1,65	-1,81	-2,05	-1,74
2097	1,39	0,03	0,97	1,23
2098	-0,94	-0,88	-1,38	-1,08
2099	-1,04	0,06	-0,39	-0,07
2100	2,66	4,81	2,21	6,18

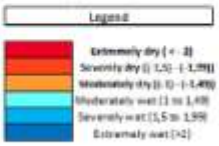

Table A XV. SPI 3 – November – Tables displaying model data values (RCP4.5)

	GP1 rcp45	GP7 rcp45	GP8 rcp45	GP13 rcp45
1971	-0,03	-0,76	-0,29	-0,21
1972	-1,89	-0,50	-1,23	-1,00
1973	0,67	0,19	0,19	-0,13
1974	-0,57	-0,73	-0,76	-0,78
1975	1,37	1,44	0,99	1,64
1976	1,35	-0,10	0,35	0,25
1977	0,03	-1,12	-0,76	-0,28
1978	1,83	0,70	1,69	0,73
1979	0,06	1,65	1,46	1,22
1980	2,31	1,29	1,58	1,54
1981	0,04	1,75	0,41	1,14
1982	-1,13	0,28	-1,05	-0,15
1983	0,25	-1,02	0,37	-0,55
1984	-0,84	-0,16	0,00	-0,48
1985	-0,09	-1,37	-0,38	-1,86
1986	-1,74	-1,04	-1,82	-1,23
1987	-0,06	-0,54	0,52	-0,66
1988	0,50	0,19	-0,56	-0,17
1989	0,51	-1,05	-0,36	-1,48
1990	0,62	0,01	0,55	0,02
1991	0,05	-0,40	-0,67	1,48
1992	-0,31	0,14	1,16	-0,01
1993	-0,68	-0,32	-1,24	-0,34
1994	-2,90	-2,17	-2,73	-2,11
1995	-0,51	1,20	0,35	0,59
1996	0,13	0,47	0,50	-0,24
1997	-0,32	1,32	-0,07	1,27
1998	0,20	0,31	1,47	0,38
1999	0,72	0,04	0,36	0,63
2000	0,17	0,87	-0,05	1,08
2001	-0,99	-0,70	-0,85	-0,85
2002	-0,08	0,66	1,13	0,65
2003	-0,44	-0,35	1,10	0,22
2004	-2,36	-0,85	-1,71	-2,06
2005	-1,13	-0,59	-0,98	-0,23
2006	-0,07	-1,26	-0,53	-1,11
2007	-0,81	1,17	0,23	1,05
2008	-1,47	-0,69	-1,06	-1,05
2009	0,81	0,50	1,54	0,40
2010	0,38	0,49	0,20	-0,16
2011	-0,77	-0,11	-0,98	-0,42
2012	-0,24	-0,63	0,20	-0,51
2013	1,06	0,10	0,17	0,54
2014	0,71	1,01	1,20	1,32
2015	1,14	1,18	0,79	1,23
2016	-0,22	-0,27	-0,38	-0,71
2017	-0,94	-1,03	-1,40	-1,91
2018	-0,81	-0,52	-0,76	-0,44
2019	0,80	-0,05	0,57	0,75
2020	0,81	-0,34	-0,55	0,35
2021	-0,42	-0,47	0,18	-0,63
2022	-1,03	1,39	1,08	1,24
2023	-2,26	-1,22	-2,22	-1,72
2024	-1,70	-1,29	-1,50	-1,02
2025	-3,99	-1,84	-3,65	-1,78
2026	-0,09	0,99	0,61	0,90
2027	0,64	0,51	-0,43	0,82
2028	-1,04	0,54	-0,80	-0,13
2029	1,13	0,34	0,39	0,53
2030	0,92	0,16	1,16	0,40
2031	-0,49	0,24	-0,41	-0,63
2032	1,54	0,64	2,08	0,35
2033	1,32	1,74	1,79	1,66

	GP1 rcp45	GP7 rcp45	GP8 rcp45	GP13 rcp45
2034	-0,94	1,52	0,81	1,26
2035	-1,16	-1,15	-1,23	-0,94
2036	-0,07	0,10	-0,17	0,26
2037	-0,53	-2,08	-0,86	-0,95
2038	-0,05	1,31	0,21	0,18
2039	-1,02	0,42	-1,00	-0,74
2040	0,69	0,08	0,85	-0,30
2041	1,39	0,70	0,93	0,91
2042	-0,10	0,24	-0,56	0,91
2043	-1,18	-0,11	-0,78	-0,25
2044	-0,39	0,64	0,82	-0,01
2045	1,40	2,28	1,32	2,67
2046	-0,11	0,25	-0,77	0,62
2047	0,88	1,43	0,57	0,92
2048	0,86	-0,32	0,21	-0,29
2049	-1,98	-0,14	-1,06	-1,32
2050	-0,90	1,46	1,21	1,05
2051	-2,95	-0,56	1,83	-1,24
2052	-2,14	-0,65	1,01	0,95
2053	-0,27	-0,46	0,60	0,44
2054	0,70	0,66	1,38	2,07
2055	-0,71	-0,73	-1,67	-0,69
2056	-0,56	0,46	0,22	-0,25
2057	0,73	0,84	0,35	0,81
2058	1,07	1,80	1,49	1,83
2059	0,50	1,06	0,36	0,87
2060	-0,88	0,07	-1,00	0,22
2061	-0,09	-0,42	-1,20	0,46
2062	-1,45	-1,61	-0,92	-1,74
2063	0,58	0,18	0,80	0,21
2064	-0,86	-0,21	-0,81	-0,72
2065	-1,13	-0,22	0,01	0,10
2066	-1,68	-1,50	-1,54	-1,52
2067	-0,40	0,43	0,12	0,44
2068	-0,22	0,67	0,18	1,68
2069	1,22	1,30	1,23	1,95
2070	0,91	0,98	1,05	1,19
2071	1,07	1,14	1,55	1,82
2072	-0,68	2,04	0,21	1,38
2073	-0,63	0,70	-0,54	-0,13
2074	-0,49	-0,33	-0,60	-1,10
2075	-0,47	-1,24	0,01	0,66
2076	-2,33	-0,91	-1,27	-1,88
2077	-1,47	-1,26	1,87	-1,88
2078	0,64	-0,32	0,12	0,07
2079	-1,65	-0,46	1,83	-1,16
2080	-0,98	-0,18	-0,80	-0,75
2081	-1,02	0,73	0,25	0,57
2082	0,37	0,80	-0,29	0,80
2083	-0,59	1,22	1,30	0,44
2084	-0,24	-0,09	0,25	0,06
2085	1,41	1,63	0,01	2,27
2086	1,06	0,70	0,64	0,34
2087	-0,92	0,41	-0,87	-0,24
2088	-0,81	0,89	0,17	-0,17
2089	-0,05	-0,71	-0,07	-0,04
2090	-0,98	-1,05	-0,58	-0,73
2091	-1,32	0,29	-0,23	0,14
2092	-0,28	0,22	0,38	-0,06
2093	-1,80	-0,85	2,51	-0,86
2094	-1,81	0,18	1,43	-1,05
2095	-0,23	-0,83	0,15	-0,65
2096	-1,23	-0,43	-1,10	-0,25
2097	-0,56	0,35	0,04	-0,11
2098	0,47	1,05	0,02	1,05
2099	-1,79	-0,75	-0,86	-0,66
2100	-0,38	-0,59	-0,41	0,31

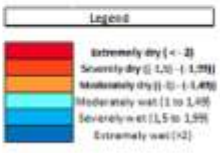

Table A XVI. SPI 6 – March – Tables displaying model data values (RCP4.5)

	GP1 rcp45	GP7 rcp45	GP8 rcp45	GP13 rcp45
1971				
1972	-1,47	-0,79	-1,65	-0,54
1973	-1,52	-1,17	-1,17	-0,54
1974	0,77	1,12	1,53	0,76
1975	-0,75	-0,21	-0,27	0,55
1976	1,74	1,05	0,64	1,73
1977	-0,03	-0,56	-0,83	-1,29
1978	1,18	-0,35	0,21	0,88
1979	1,60	1,26	1,70	0,87
1980	-0,73	1,39	0,36	0,57
1981	1,60	0,27	0,93	0,18
1982	0,09	1,99	0,38	1,85
1983	0,52	-0,30	-0,37	-0,08
1984	1,39	-0,19	0,73	0,02
1985	0,81	0,59	0,94	0,49
1986	-0,09	-0,27	0,17	-1,25
1987	-1,13	-1,11	-1,63	-0,46
1988	0,10	0,65	0,95	-0,23
1989	-0,13	-1,62	-1,46	-1,81
1990	0,09	-0,63	-0,25	-1,08
1991	-0,09	-0,49	-0,34	-0,59
1992	-0,10	-0,75	-0,49	0,76
1993	0,21	-0,45	0,79	-0,44
1994	-1,14	0,00	-0,75	-0,44
1995	-1,84	-2,65	-1,76	-2,72
1996	-0,35	0,37	-0,70	-0,12
1997	0,70	1,16	0,85	0,86
1998	-0,88	0,91	-0,19	1,25
1999	0,27	0,64	1,40	0,74
2000	-0,12	0,23	0,49	0,08
2001	0,48	-0,92	-0,46	0,02
2002	-0,09	-0,56	0,33	-0,70
2003	-0,15	-0,57	-0,57	-0,29
2004	-0,71	-1,61	-0,12	-1,07
2005	-0,42	0,31	-0,34	0,09
2006	-1,08	-0,67	-0,68	0,06
2007	0,68	0,58	0,88	1,80
2008	-1,45	1,39	-0,01	0,75
2009	-2,86	-2,03	-1,90	-1,81
2010	0,98	-0,19	0,88	0,01
2011	1,21	0,73	0,57	-0,34
2012	0,26	0,32	0,54	0,02
2013	-1,33	-0,55	-0,21	-0,98
2014	1,25	-0,48	0,13	-0,18
2015	1,65	2,20	1,69	1,97
2016	0,46	1,23	0,26	1,35
2017	-1,64	-1,66	-1,70	-1,87
2018	-1,96	-0,51	-1,46	-1,78
2019	0,07	-0,79	-0,73	-0,38
2020	0,52	0,62	0,70	0,82
2021	1,20	-0,44	-0,28	-0,32
2022	-1,05	-1,13	-1,40	-1,36
2023	-1,05	0,68	0,86	1,55
2024	-1,14	0,67	-0,02	-0,44
2025	-1,68	0,06	-0,92	-0,33
2026	-0,58	-0,64	-1,09	-0,06
2027	0,76	0,67	1,17	1,27
2028	1,21	0,43	0,10	0,35
2029	0,60	1,51	1,59	0,89
2030	-0,13	-2,25	-0,92	-1,56
2031	0,73	-0,46	0,36	-0,11
2032	-0,12	1,57	0,56	-0,70
2033	1,76	1,18	1,65	0,62

	GP1 rcp45	GP7 rcp45	GP8 rcp45	GP13 rcp45
2034	0,49	1,02	1,00	0,99
2035	0,11	2,78	1,41	2,66
2036	-1,13	-2,19	-1,82	-1,73
2037	-2,03	-2,08	-1,69	-1,42
2038	-2,83	-2,93	-2,64	-2,97
2039	0,36	0,60	-0,17	0,34
2040	-2,21	-1,66	-2,13	-2,80
2041	0,68	0,37	0,29	0,27
2042	0,31	-0,84	-0,44	-2,27
2043	-0,40	-0,69	-1,56	0,02
2044	-1,13	-0,92	-0,96	-0,89
2045	-0,15	0,24	0,61	0,12
2046	1,93	2,17	1,01	2,57
2047	0,39	0,27	0,32	0,80
2048	-1,02	-0,19	-0,85	-0,65
2049	0,69	0,53	0,42	0,98
2050	-0,67	-1,14	-0,42	-1,67
2051	0,51	1,33	1,31	1,32
2052	-1,20	-0,90	-1,29	-1,08
2053	-3,22	-2,46	-1,75	-2,28
2054	-1,05	-0,16	-0,62	-0,28
2055	1,01	0,82	1,51	2,12
2056	-0,68	-0,53	-1,19	-1,16
2057	-1,75	-0,47	-0,70	-1,48
2058	-0,70	0,01	-0,46	-0,14
2059	1,09	0,84	1,38	1,05
2060	0,23	0,15	-0,11	0,30
2061	-1,64	-0,86	-1,28	-1,19
2062	0,11	-0,83	-0,91	-0,39
2063	-1,90	-1,93	-1,84	-1,21
2064	0,98	1,38	1,17	1,43
2065	-0,80	-0,82	-0,66	-1,18
2066	-0,50	-1,17	-0,61	-1,09
2067	-2,24	-1,73	-1,80	-1,88
2068	0,48	-0,26	-0,10	0,53
2069	-0,08	0,19	0,09	1,36
2070	0,64	0,54	0,56	1,19
2071	0,11	0,24	-0,08	0,23
2072	1,23	1,65	1,49	2,46
2073	0,05	2,24	0,69	1,14
2074	-1,57	-0,25	-1,19	-0,89
2075	0,20	-0,50	0,25	0,61
2076	-0,35	-2,34	-1,16	-1,79
2077	-2,58	-2,03	-1,73	-2,58
2078	-2,24	-3,67	-2,69	-3,61
2079	0,89	0,79	0,87	1,04
2080	-1,19	-1,35	-1,84	-1,51
2081	-0,22	0,28	-0,21	0,31
2082	-0,74	-0,51	-0,72	-0,36
2083	-0,59	-0,73	-1,33	-0,32
2084	-1,37	1,07	0,45	-0,39
2085	-1,00	-0,38	-0,58	-0,96
2086	1,98	1,50	0,37	2,48
2087	0,52	-0,44	-0,19	-0,99
2088	-0,77	0,43	-0,18	0,29
2089	-2,27	-0,93	-1,69	-1,47
2090	-1,14	-1,83	-1,53	-0,85
2091	-2,11	-1,61	-1,10	-1,78
2092	-1,88	-1,71	-1,25	-1,69
2093	0,25	0,64	0,70	0,15
2094	-0,22	-1,19	0,18	0,75
2095	-0,70	-0,62	-0,50	-1,06
2096	-0,88	-1,17	-0,80	-0,93
2097	-1,67	1,00	0,00	0,06
2098	0,29	-0,64	-0,23	-0,95
2099	-0,43	0,45	-0,12	0,04
2100	-2,24	-2,87	-2,35	-2,46

SPI 6 – March (wet season) (RCP 4.5)

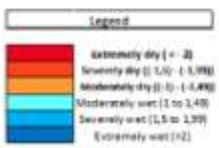

Table A XVII. SPI 10 – October – Tables displaying model data values (RCP4.5)

	GP1 rcp45	GP7 rcp45	GP8 rcp45	GP13 rcp45
1971	-0,47	-0,24	-0,65	0,29
1972	-0,09	0,53	0,12	0,04
1973	1,17	0,86	0,31	0,49
1974	-0,05	-0,08	-0,58	-0,31
1975	0,82	0,70	0,04	0,78
1976	1,17	0,57	0,77	0,23
1977	0,61	-0,04	-0,29	0,53
1978	-0,68	-0,21	-0,37	-0,39
1979	0,77	1,49	1,78	1,70
1980	0,81	1,49	0,60	1,58
1981	-0,41	-0,57	0,11	-0,04
1982	0,18	0,84	-0,05	0,34
1983	0,72	-1,32	0,71	1,28
1984	1,74	-1,27	-1,71	-1,32
1985	1,38	-0,96	0,97	-0,18
1986	-0,55	-1,09	-0,48	-0,80
1987	-0,76	0,34	-0,18	-0,17
1988	0,01	-0,53	-0,55	-0,48
1989	1,58	0,39	1,37	0,10
1990	0,34	0,62	0,39	0,68
1991	-1,27	-0,86	-1,42	-0,47
1992	-0,58	-0,45	-0,32	-0,18
1993	-0,26	-0,53	-0,25	-0,84
1994	-1,65	-2,54	-1,60	-2,34
1995	0,16	-0,16	0,10	-0,05
1996	-0,74	0,72	0,79	-0,53
1997	-0,75	-0,23	-0,65	-0,29
1998	2,41	2,31	2,87	2,52
1999	-0,06	1,07	0,74	1,46
2000	-0,18	-0,57	-0,67	-0,57
2001	0,05	-0,27	0,01	-0,18
2002	0,28	0,59	1,16	0,76
2003	0,27	0,60	1,51	0,85
2004	-1,04	-0,91	-0,06	-0,77
2005	-0,07	-0,10	0,06	0,10
2006	0,20	-0,97	-0,81	-0,74
2007	-0,95	1,51	0,48	2,05
2008	-0,53	-0,07	-0,32	-0,68
2009	0,78	0,82	1,30	0,53
2010	-0,48	0,87	-0,40	0,17
2011	-0,11	0,23	-0,47	-0,16
2012	0,05	0,03	0,36	-0,05
2013	-0,36	-0,17	-0,19	-0,92
2014	-0,07	-0,09	-0,17	-0,10
2015	1,22	0,36	0,21	0,87
2016	-0,28	-1,19	-0,90	-0,77
2017	-0,53	-1,67	-0,95	-1,98
2018	-0,23	0,20	0,04	-0,56
2019	0,35	-0,55	-0,22	-0,34
2020	-1,29	-2,83	-1,36	-1,94
2021	0,09	0,29	0,33	-0,38
2022	-1,81	-0,70	-1,92	-0,37
2023	-0,36	0,04	-0,48	-0,09
2024	-2,89	-1,95	-2,64	-2,35
2025	-2,34	-2,41	-3,02	-3,02
2026	-0,16	1,52	0,46	1,23
2027	0,78	1,61	-0,26	1,36
2028	-0,47	1,35	0,25	0,66
2029	1,23	1,08	0,70	1,19
2030	0,38	-0,58	0,27	-0,52
2031	-0,59	-0,17	-0,42	-0,29
2032	1,32	0,78	1,46	0,83
2033	1,37	1,88	1,10	2,05

	GP1 rcp45	GP7 rcp45	GP8 rcp45	GP13 rcp45
2034	-1,62	-1,30	-1,10	-0,66
2035	-0,99	-0,88	-0,46	-0,74
2036	0,69	0,95	0,21	1,43
2037	0,87	-1,81	0,70	-1,07
2038	0,61	1,44	-0,29	0,57
2039	-0,71	-1,35	-0,91	-1,22
2040	-0,49	-1,43	-0,52	-1,21
2041	0,40	0,32	0,14	1,06
2042	1,01	0,64	0,32	1,78
2043	-0,15	0,64	-0,52	0,63
2044	-0,11	0,90	0,87	0,43
2045	-0,15	0,24	0,44	0,72
2046	0,33	0,74	0,15	0,69
2047	0,91	1,40	0,50	1,29
2048	-0,27	-0,34	-0,91	-0,71
2049	-0,65	0,64	0,34	0,43
2050	-1,21	-0,30	-0,27	-0,58
2051	-2,94	-1,29	-2,13	-2,09
2052	-1,20	0,18	-0,84	-0,71
2053	-1,01	-1,14	-1,54	-1,08
2054	-0,18	0,79	0,31	2,11
2055	-1,37	-0,84	-1,70	-0,94
2056	-0,81	0,39	-0,71	-0,77
2057	1,13	1,02	0,47	1,09
2058	0,18	0,95	0,93	1,26
2059	0,37	0,86	-0,17	-0,05
2060	-0,51	-0,15	-1,17	0,14
2061	-1,05	-0,08	-1,28	0,06
2062	0,06	0,19	0,49	-0,12
2063	-0,33	-0,95	-0,74	-1,48
2064	-0,96	-0,77	-1,59	-1,38
2065	-1,96	0,04	0,09	0,22
2066	-0,86	-1,25	-0,75	-1,58
2067	-1,33	0,27	-0,50	-0,07
2068	0,63	0,41	0,41	0,68
2069	0,19	-0,31	-0,26	0,19
2070	0,59	1,48	1,24	1,82
2071	1,12	1,36	1,26	2,19
2072	-1,59	-1,98	-2,51	-2,13
2073	0,20	0,91	-0,39	0,07
2074	-1,08	-0,55	-1,28	-0,64
2075	-0,03	-0,95	0,12	-0,22
2076	-0,64	0,19	-0,21	-0,17
2077	-1,69	0,43	-1,67	-0,20
2078	0,02	-0,64	0,15	0,47
2079	-0,59	-0,47	-1,20	-0,74
2080	-1,27	-1,35	-2,19	-1,65
2081	-0,31	0,72	0,60	0,69
2082	-0,12	0,00	-0,48	0,11
2083	0,24	0,28	0,83	0,61
2084	0,13	0,44	0,39	0,45
2085	0,92	0,93	-0,53	1,49
2086	0,88	0,71	0,32	0,58
2087	0,50	1,07	-0,23	0,41
2088	-0,09	0,23	-0,08	-0,42
2089	-1,31	-1,16	-0,64	-1,32
2090	0,08	-0,52	-0,16	-0,39
2091	-1,58	0,73	-0,19	0,62
2092	-0,65	-0,32	0,11	0,09
2093	-1,36	-0,16	-2,28	-0,20
2094	0,25	0,65	0,59	0,25
2095	0,81	0,20	0,72	0,41
2096	-0,76	-1,26	-1,76	-0,62
2097	0,97	1,09	0,99	1,08
2098	0,75	0,62	-0,07	0,79
2099	-0,33	1,51	0,57	0,67
2100	1,15	2,26	1,18	2,50

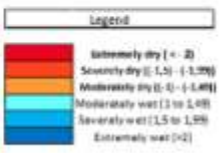

Table A XVIII. SPI 12 – Tables displaying model data values (RCP4.5)

	GP1 rcp45	GP7 rcp45	GP8 rcp45	GP13 rcp45
1971	-0,46	-0,63	-0,95	-0,45
1972	-2,35	-1,38	-2,05	-1,02
1973	0,64	-0,07	0,40	0,16
1974	0,11	1,76	1,24	1,31
1975	1,18	0,97	0,56	1,41
1976	0,69	0,01	-0,21	0,43
1977	-0,09	-0,28	-0,66	-0,37
1978	1,50	1,01	1,59	0,95
1979	-0,20	0,66	0,64	0,60
1980	1,22	1,01	0,80	0,80
1981	-0,68	0,88	-0,45	0,29
1982	0,33	0,89	-0,21	0,86
1983	1,17	-0,93	0,41	-0,72
1984	1,01	0,25	0,26	0,57
1985	1,11	0,18	0,97	-0,14
1986	-2,03	-0,94	-1,05	-0,77
1987	-0,07	0,84	0,30	-0,16
1988	0,36	-0,66	-0,01	-0,90
1989	0,30	-1,51	-0,06	-1,88
1990	0,44	-0,01	0,38	0,36
1991	0,15	-0,40	-0,61	0,82
1992	-0,97	-1,08	-0,10	-1,13
1993	-0,25	0,44	-0,09	0,21
1994	-2,02	-2,23	-2,40	-2,07
1995	-1,35	-0,83	-1,27	-1,57
1996	0,18	-0,40	0,64	-0,62
1997	-0,34	1,61	0,00	1,47
1998	1,47	1,18	2,57	1,63
1999	-0,50	0,63	0,47	0,56
2000	-0,55	-0,83	-1,15	-0,50
2001	0,40	-1,20	0,05	-0,72
2002	0,38	0,14	0,98	0,27
2003	-0,32	-1,61	0,27	-0,29
2004	-0,52	-0,94	-0,43	-0,83
2005	-0,40	0,32	-0,42	0,57
2006	-0,72	-1,56	-1,48	-0,62
2007	-0,70	1,89	1,14	2,64
2008	-1,61	-0,22	-1,27	-0,48
2009	-0,35	-1,15	0,00	-0,79
2010	0,19	-0,32	0,06	-0,70
2011	0,34	0,93	0,03	-0,06
2012	-0,13	-1,36	-0,05	-1,19
2013	-0,76	-0,80	-0,97	-0,73
2014	1,18	0,73	1,01	0,72
2015	1,77	2,28	1,87	1,64
2016	-1,71	-1,31	-1,89	-0,60
2017	-2,22	-1,57	-2,64	-2,38
2018	-1,32	-0,09	-0,61	-0,55
2019	0,05	-2,43	-1,39	-0,52
2020	0,38	0,65	-0,03	0,17
2021	0,46	-0,40	-0,03	-0,88
2022	-3,01	-1,08	-1,86	-0,85
2023	-1,53	-0,22	-0,99	0,21
2024	-1,06	0,99	-0,24	-0,12
2025	-2,39	-1,39	-2,97	-0,54
2026	1,14	1,54	1,65	1,52
2027	0,14	0,12	-0,97	0,03
2028	0,90	0,84	1,17	0,31
2029	1,06	0,21	0,42	0,28
2030	-0,57	-1,52	-0,42	-1,13
2031	0,64	0,45	0,44	0,23
2032	1,68	2,02	2,37	0,32
2033	1,43	0,91	0,85	0,80

	GP1 rcp45	GP7 rcp45	GP8 rcp45	GP13 rcp45
2034	1,48	0,85	0,13	0,96
2035	0,15	1,27	0,06	1,13
2036	-0,91	-1,46	-1,36	-0,76
2037	1,67	-4,44	-2,20	2,90
2038	1,45	-0,62	2,17	1,71
2039	1,04	-0,63	-1,21	1,36
2040	-1,46	-1,32	-1,21	-0,97
2041	1,38	-0,16	0,09	0,10
2042	-0,10	-1,26	-0,61	-0,84
2043	-0,54	0,46	-1,15	0,31
2044	-1,29	-0,34	-0,98	-1,11
2045	1,16	2,04	1,44	2,27
2046	1,24	1,02	0,91	1,17
2047	0,67	-0,23	-0,25	0,38
2048	0,27	-1,74	-1,41	-1,73
2049	-1,15	0,36	0,28	-0,63
2050	-0,89	-0,16	0,27	-0,27
2051	-0,79	0,27	-0,74	-0,12
2052	-1,73	-0,99	-1,50	-0,92
2053	-0,84	-1,68	-1,09	-0,69
2054	0,34	0,77	0,76	1,33
2055	-0,79	-0,16	-1,29	-0,43
2056	-1,07	-1,11	-1,13	-1,36
2057	-0,92	0,29	-0,43	-0,18
2058	0,11	0,22	0,65	0,43
2059	0,15	0,20	-0,11	0,15
2060	-1,32	-0,59	-1,57	-0,32
2061	0,11	-0,57	-0,57	-0,06
2062	-1,40	-1,26	-1,46	-1,44
2063	0,72	-0,30	0,34	0,33
2064	-0,28	1,02	-0,18	0,25
2065	-1,61	-1,70	-0,85	-1,09
2066	-1,20	-1,81	-1,44	-1,78
2067	-0,71	-0,67	-1,36	0,08
2068	-0,48	-0,60	-0,36	0,62
2069	0,42	0,20	0,38	1,08
2070	0,60	0,60	0,90	0,88
2071	-0,28	0,28	0,30	0,83
2072	0,28	1,50	1,42	2,64
2073	0,22	0,22	0,55	0,46
2074	-1,86	-1,19	-1,66	-1,64
2075	-0,92	-1,99	-1,36	-0,87
2076	-0,25	-1,43	-0,47	-1,15
2077	2,59	-1,58	-2,86	-1,93
2078	-0,95	-2,33	-1,38	-1,27
2079	-0,70	0,03	-1,04	-0,22
2080	-1,47	-1,38	-1,92	-0,74
2081	0,15	1,51	0,52	0,96
2082	-0,10	-0,11	-0,49	0,69
2083	1,58	0,33	-0,28	-0,58
2084	1,51	-1,20	-1,61	-1,24
2085	0,91	0,95	-0,79	1,43
2086	0,19	0,04	-0,54	-0,09
2087	-0,98	-0,50	-1,24	-1,19
2088	-0,98	-0,22	-0,50	-0,55
2089	-1,29	-2,31	-2,13	-1,28
2090	-1,63	-1,25	-1,49	-1,05
2091	-2,14	-1,31	-1,16	-0,98
2092	-1,39	-0,74	-0,87	-0,47
2093	-0,74	0,23	-1,09	-0,45
2094	-0,12	0,74	0,65	0,30
2095	-0,02	-0,61	-0,01	-0,67
2096	-2,76	-2,43	-3,03	-1,66
2097	-0,28	1,48	0,81	0,65
2098	0,34	-0,75	-0,89	-0,52
2099	-1,25	-0,25	-0,39	-0,83
2100	0,43	0,01	0,21	1,03

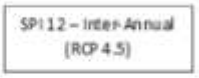

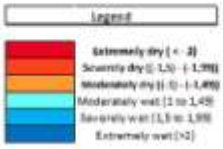

Table A XIX. SPI 3 – February – Tables displaying model data values (RCP 8.5)

	GP1 rcp85	GP7 rcp85	GP8 rcp85	GP13 rcp85
1971				
1972	-2,20	-0,83	-1,36	-1,33
1973	-0,81	-1,00	-0,66	0,05
1974	1,05	1,88	2,26	1,53
1975	-0,38	-0,67	-0,31	-0,37
1976	0,85	0,02	-0,40	0,62
1977	-1,62	-0,05	-1,20	-1,58
1978	1,92	0,61	1,06	1,45
1979	0,07	1,14	0,57	0,92
1980	-1,17	-0,45	-0,88	-0,83
1981	-0,50	-0,96	-0,47	-1,85
1982	0,07	1,06	0,00	1,41
1983	1,14	0,10	0,32	0,64
1984	1,25	-0,49	0,43	-0,27
1985	1,30	0,58	0,66	0,60
1986	0,20	1,03	0,92	0,11
1987	-0,88	-1,06	-1,14	0,16
1988	0,73	1,69	1,74	0,59
1989	-0,69	-1,77	-1,47	-1,69
1990	0,03	0,56	0,48	0,19
1991	-0,74	-0,92	-0,91	-0,50
1992	-0,18	-0,39	-0,14	-0,25
1993	0,89	-0,89	-0,09	-0,15
1994	-0,20	0,98	0,29	0,42
1995	0,31	-1,07	0,09	-1,14
1996	-0,70	-1,14	-1,69	-1,29
1997	0,89	0,45	0,40	0,59
1998	0,07	0,64	0,44	1,21
1999	0,90	1,15	1,51	1,36
2000	-1,42	0,17	-0,18	-0,41
2001	0,87	-2,81	-0,72	-1,24
2002	0,73	-0,40	0,85	0,09
2003	0,98	-0,35	-0,07	0,34
2004	-0,62	-0,83	-0,76	-0,95
2005	0,90	0,63	0,51	0,40
2006	-0,45	-0,25	-0,43	-0,41
2007	2,66	1,64	1,75	2,35
2008	0,41	0,28	-0,25	0,36
2009	-0,20	0,89	0,18	-0,35
2010	-0,01	0,63	0,01	-0,46
2011	0,77	1,71	1,39	0,95
2012	-0,24	0,26	-0,22	-0,08
2013	-0,08	-0,01	0,09	0,06
2014	-0,86	-1,67	-1,17	-1,05
2015	-1,95	-1,73	-2,08	-1,76
2016	0,24	0,83	-0,10	0,10
2017	-0,86	-0,93	-1,12	-0,80
2018	1,47	0,63	0,93	0,42
2019	-0,77	-1,83	-1,48	-1,02
2020	0,42	1,29	0,57	0,72
2021	1,49	2,03	1,46	1,57
2022	1,98	1,29	1,72	1,25
2023	1,30	1,43	1,42	0,12
2024	0,82	0,24	-0,09	0,06
2025	-0,05	0,19	-0,18	0,35
2026	-0,05	-0,06	-0,67	-0,50
2027	-0,59	0,43	0,47	-0,12
2028	0,38	0,30	0,21	0,39
2029	-1,29	-0,93	-1,65	-1,05
2030	0,05	0,56	0,37	3,15
2031	1,12	1,02	0,67	1,30
2032	0,75	-0,33	0,26	0,52
2033	-0,35	-1,09	-0,55	-0,50

	GP1 rcp85	GP7 rcp85	GP8 rcp85	GP13 rcp85
2034	-2,50	-2,40	-1,71	-2,46
2035	-0,94	-0,10	-0,27	-0,33
2036	-0,85	-0,04	-1,16	-0,46
2037	-1,57	-1,89	-1,58	-2,53
2038	0,26	0,55	0,13	1,25
2039	-0,44	-1,93	-0,91	-1,80
2040	-0,02	1,07	0,24	0,61
2041	-0,27	-1,11	0,24	-1,22
2042	0,64	0,42	0,46	0,77
2043	-0,72	0,49	-0,34	-0,60
2044	-0,38	-0,32	0,50	0,25
2045	-2,63	-2,09	-1,97	-1,74
2046	-0,07	-1,19	-0,77	-1,31
2047	-0,41	-0,49	-0,60	-0,15
2048	-0,18	1,34	0,58	1,23
2049	0,57	0,62	0,59	-0,44
2050	1,11	2,11	1,65	2,64
2051	1,83	0,31	1,08	0,44
2052	0,10	0,30	-0,09	0,68
2053	0,24	-0,09	0,08	0,67
2054	0,22	0,85	0,57	0,26
2055	0,50	-0,74	-0,85	-0,09
2056	0,04	-0,59	-0,55	-0,92
2057	-0,18	-0,67	-0,79	-1,12
2058	-1,91	0,05	-0,64	-0,02
2059	0,89	2,41	2,30	2,42
2060	-1,44	-0,17	-0,75	-1,09
2061	-0,64	-1,10	-0,61	-1,28
2062	-0,09	0,26	0,39	0,27
2063	0,40	0,39	0,14	0,04
2064	-0,28	-0,32	0,09	-0,58
2065	-0,03	0,69	-0,16	-0,13
2066	2,38	2,39	2,21	2,58
2067	1,41	0,98	0,89	0,48
2068	-0,79	-0,97	-1,47	-0,67
2069	-1,37	0,12	-0,35	-0,63
2070	0,56	2,13	0,73	1,39
2071	-0,44	-1,27	-0,65	-1,72
2072	-0,80	-0,69	-0,21	-1,26
2073	-2,95	-2,26	-2,90	-2,08
2074	-1,27	-1,32	-1,40	-1,61
2075	0,41	-1,48	-0,48	-0,83
2076	-0,04	-1,14	-0,33	-1,60
2077	1,29	0,66	0,90	1,72
2078	-1,32	-1,31	-1,09	-0,96
2079	-1,16	-1,47	-0,76	-2,10
2080	-3,08	-1,46	-2,04	-1,97
2081	0,61	0,32	0,36	1,26
2082	-0,17	-1,32	-0,91	-1,65
2083	-2,59	-1,89	-2,60	-2,32
2084	-0,10	-1,27	-0,61	-0,87
2085	-0,72	-0,77	-0,34	-0,94
2086	-1,55	-1,94	-1,71	-1,70
2087	-3,03	-0,96	-1,58	-1,75
2088	-3,07	-3,20	-2,69	-3,50
2089	-1,17	-0,27	-1,02	-0,99
2090	-0,66	-0,46	-0,79	-0,73
2091	-0,29	-1,72	-1,13	-1,80
2092	0,91	1,90	1,46	1,37
2093	-2,21	-1,97	-1,90	-3,13
2094	0,19	-0,80	0,11	-0,40
2095	-1,36	-0,83	-0,45	-0,88
2096	-1,65	-1,49	-0,94	-1,72
2097	0,46	0,84	1,39	1,08
2098	1,28	0,84	0,79	1,26
2099	-1,83	-1,18	-1,78	-1,12
2100	-3,12	-1,55	-2,02	-2,07

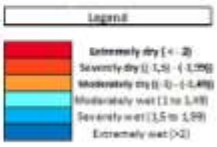

Table A XX. SPI 3 – May – Tables displaying model data values (RCP 8.5)

	GP1 rcp85	GP7 rcp85	GP8 rcp85	GP13 rcp85
1971	-0,34	-0,10	-0,35	-0,17
1972	-0,81	0,54	-0,45	0,65
1973	-0,33	-0,80	-1,51	-0,58
1974	1,57	2,19	2,53	1,94
1975	0,99	1,05	0,59	1,49
1976	0,05	0,88	0,63	0,80
1977	-0,27	-0,41	-0,02	-0,22
1978	-0,57	0,10	0,14	0,35
1979	-0,56	-0,67	-0,97	-0,57
1980	-0,86	0,89	-0,25	0,39
1981	0,30	-0,44	0,36	-0,17
1982	1,08	0,74	0,19	0,76
1983	1,90	-0,32	0,97	-0,61
1984	1,38	1,60	0,80	1,56
1985	1,21	0,21	1,19	0,63
1986	-0,32	-0,63	0,05	-0,59
1987	0,74	1,18	0,28	0,54
1988	0,12	-1,52	0,06	-1,04
1989	-0,07	-1,08	-0,48	-1,28
1990	0,68	0,15	0,43	0,80
1991	0,31	0,04	0,00	-0,35
1992	-0,78	-0,69	-0,67	-1,07
1993	-0,19	0,93	0,49	0,48
1994	-1,54	-2,34	-2,83	-2,01
1995	-2,20	-1,90	-2,75	-2,18
1996	0,37	0,32	1,70	0,29
1997	-0,23	0,68	0,21	0,76
1998	0,94	0,49	0,33	1,14
1999	-2,49	-0,59	-1,10	-0,83
2000	-0,09	-0,38	0,02	-0,77
2001	0,61	0,09	1,03	0,14
2002	0,86	0,55	1,44	0,05
2003	-0,13	-1,65	-0,87	-0,41
2004	1,51	-0,20	0,68	0,63
2005	-0,11	0,51	-0,78	0,99
2006	0,08	-0,88	-0,62	-0,08
2007	1,49	0,81	1,82	0,63
2008	-0,65	-0,53	-1,61	-0,13
2009	0,95	1,65	1,17	0,80
2010	-1,74	-2,57	-1,99	-2,86
2011	0,38	1,72	1,48	0,77
2012	2,12	0,51	0,65	0,52
2013	-0,23	-0,92	-0,43	-0,51
2014	-0,40	0,32	0,41	0,49
2015	0,39	-0,03	1,41	0,50
2016	-1,25	-1,10	-1,49	-1,16
2017	-1,80	-1,61	-2,09	-1,35
2018	-2,82	-2,22	-2,81	-2,11
2019	1,34	0,65	2,15	0,47
2020	1,83	-0,89	1,62	0,09
2021	1,02	-0,24	0,72	0,28
2022	0,09	0,74	0,72	0,65
2023	0,06	0,97	0,65	0,50
2024	1,07	0,36	1,09	0,64
2025	-1,12	-2,90	-1,30	-1,97
2026	1,40	0,27	1,71	0,58
2027	-0,22	-0,29	0,69	-0,28
2028	-2,21	-2,07	-3,36	-1,69
2029	-0,58	-0,81	-0,83	-0,69
2030	0,18	-1,13	0,05	-0,76
2031	0,61	-0,45	0,25	-0,37
2032	-1,97	-0,79	-1,79	-0,32
2033	0,51	0,80	0,62	0,83

	GP1 rcp85	GP7 rcp85	GP8 rcp85	GP13 rcp85
2034	-0,21	-1,35	-1,26	-0,84
2035	-1,16	-2,53	-1,28	-2,69
2036	0,62	-0,86	0,38	0,07
2037	0,33	-1,78	0,09	-0,62
2038	-3,17	-2,39	-3,68	-2,31
2039	-0,91	-1,80	-1,97	-1,36
2040	1,20	-2,17	1,51	1,64
2041	-1,55	-1,65	-2,07	-1,29
2042	0,35	0,05	0,09	0,55
2043	-2,01	-2,25	-3,73	-1,64
2044	-1,69	-2,22	-2,92	-1,62
2045	-3,90	-3,10	-4,35	-2,55
2046	0,56	-1,07	0,59	-0,79
2047	-0,39	-0,24	-2,00	-0,23
2048	-0,59	-1,92	-1,00	-0,89
2049	0,48	-0,82	-1,18	-0,38
2050	-1,51	-1,09	-1,04	-1,30
2051	0,79	0,05	1,14	0,78
2052	-1,32	-1,00	-1,63	-0,24
2053	-2,07	-1,30	-2,85	-0,98
2054	0,59	-0,95	-0,42	-0,42
2055	0,64	1,02	0,70	1,18
2056	-3,06	-2,99	-4,16	-1,94
2057	-0,71	-0,43	-0,89	-0,15
2058	-1,58	-2,84	-1,92	-2,13
2059	-1,53	-2,30	-1,46	-2,18
2060	-1,10	-1,25	-1,40	-1,23
2061	-0,23	0,68	0,77	0,61
2062	-0,09	1,47	0,78	0,84
2063	1,83	2,95	1,94	1,52
2064	-4,28	-2,71	-4,60	-2,90
2065	-0,48	0,23	-0,10	-0,37
2066	-1,06	-0,61	-2,28	-0,32
2067	-0,07	0,01	-0,18	0,20
2068	1,34	0,89	1,06	1,30
2069	-1,11	-1,03	-1,90	-2,04
2070	-0,82	-0,10	-0,28	-0,48
2071	-1,89	-0,71	-1,72	-1,09
2072	-0,48	0,74	-0,80	-0,14
2073	-0,65	-0,62	-0,79	-0,66
2074	-2,54	-1,82	-1,14	-1,64
2075	-1,40	-1,86	-1,10	-1,82
2076	1,78	1,05	2,42	1,83
2077	0,24	0,68	0,78	0,39
2078	-2,07	-0,92	-1,36	-1,26
2079	-1,49	-1,56	-2,19	-1,87
2080	-2,97	-3,12	-2,62	-3,19
2081	-3,91	-3,49	-3,81	-4,31
2082	0,70	0,43	0,35	0,22
2083	-1,36	-1,37	-2,39	-1,47
2084	-0,51	-0,34	-0,29	-0,02
2085	-2,87	-2,76	-2,70	-2,09
2086	-3,66	-4,33	-3,62	-3,55
2087	-2,22	-2,50	-2,48	-3,28
2088	-2,28	-1,07	-1,77	-1,56
2089	0,18	-0,14	-0,55	-0,19
2090	-2,66	-1,07	-2,74	-2,34
2091	-2,82	-0,81	-3,10	-1,80
2092	-2,42	-0,41	-0,29	-1,07
2093	-4,83	-2,70	-4,71	-3,16
2094	-2,96	-1,26	-2,73	-1,67
2095	-1,75	-1,47	-2,55	-0,99
2096	-0,51	-0,74	-0,41	-0,62
2097	-1,49	0,18	-0,81	0,06
2098	0,31	0,80	0,62	0,09
2099	-2,85	-3,09	-4,08	-4,97
2100	-3,41	-3,56	-3,94	-3,78

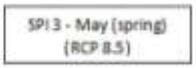

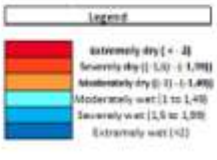

Table A XXI. SPI 3 – August – Tables displaying model data values (RCP 8.5)

	GP1 rcp85	GP7 rcp85	GP8 rcp85	GP13 rcp85
1971	-0,34	-0,29	-1,83	-1,06
1972	-0,81	-0,12	-0,19	-0,42
1973	-0,33	0,78	-0,10	-0,01
1974	1,57	-0,68	0,21	0,71
1975	0,99	0,35	0,06	0,22
1976	0,05	0,38	0,50	-0,44
1977	-0,27	-0,65	-0,99	-0,85
1978	-0,57	-0,34	0,63	-0,55
1979	-0,56	0,38	0,66	1,40
1980	-0,86	0,00	0,11	-0,52
1981	0,30	-0,33	-0,60	0,65
1982	1,08	1,54	0,85	1,21
1983	1,90	-1,44	-1,16	-1,12
1984	1,38	-0,64	-1,25	-1,05
1985	1,21	0,24	0,69	0,70
1986	-0,32	-0,95	0,43	-0,33
1987	0,74	-1,16	-1,41	-1,83
1988	0,12	0,21	-0,23	-0,38
1989	-0,07	2,23	2,30	2,39
1990	0,68	-0,74	0,01	0,15
1991	0,31	1,23	-0,23	0,94
1992	-0,78	-0,37	-1,95	-1,09
1993	-0,19	0,26	1,10	0,69
1994	-1,54	0,14	0,04	-0,11
1995	-2,20	-0,31	0,04	-0,21
1996	0,37	0,77	1,23	0,59
1997	-0,23	0,31	-0,69	-0,53
1998	0,94	1,67	1,84	1,26
1999	-2,49	1,01	0,67	0,85
2000	-0,08	-0,35	-0,39	0,25
2001	0,61	-1,09	-1,46	-0,80
2002	0,86	0,50	-0,59	-0,60
2003	-0,13	0,40	0,74	1,07
2004	1,51	0,54	1,31	0,69
2005	-0,11	-0,12	0,75	-0,09
2006	0,08	0,08	0,89	0,75
2007	1,49	0,00	-1,97	-1,48
2008	-0,65	0,00	-4,35	-1,83
2009	0,95	1,40	0,40	1,17
2010	-1,74	-0,23	-0,38	0,13
2011	0,38	1,02	-0,81	1,02
2012	2,12	1,24	0,58	2,07
2013	-0,23	0,04	-0,17	-0,15
2014	-0,40	0,28	0,01	-0,06
2015	0,39	0,00	-1,31	-1,05
2016	-1,25	1,44	1,52	1,87
2017	-1,80	0,76	-0,46	0,17
2018	-2,82	0,67	0,54	-0,09
2019	1,34	0,00	-1,22	0,25
2020	1,83	0,15	-1,39	-0,44
2021	1,02	-1,32	0,01	-0,56
2022	0,09	-0,49	-0,28	1,40
2023	0,06	0,36	-0,97	0,92
2024	1,07	0,20	-0,32	1,09
2025	-1,12	0,00	-0,90	-1,83
2026	1,40	-1,23	-1,93	-1,83
2027	-0,22	-0,29	0,10	-0,27
2028	-2,21	0,24	-0,71	-0,16
2029	-0,58	0,62	0,11	0,36
2030	0,18	0,14	-1,67	-0,75
2031	0,61	0,23	0,03	0,52
2032	-1,97	-0,93	-0,41	0,76
2033	0,51	0,75	1,72	1,02

	GP1 rcp85	GP7 rcp85	GP8 rcp85	GP13 rcp85
2034	-0,21	0,39	0,16	1,25
2035	-1,16	1,86	0,65	1,76
2036	0,62	-0,67	-1,17	-0,37
2037	0,33	0,01	0,25	-0,56
2038	-3,17	0,00	-1,75	-1,83
2039	-0,91	-0,10	-0,30	-0,58
2040	1,20	0,71	-1,34	0,97
2041	-3,33	-0,38	-0,29	-0,99
2042	0,35	0,31	1,37	0,73
2043	-2,01	1,20	-0,43	0,81
2044	-1,69	0,00	-2,25	-1,83
2045	-3,90	0,23	-1,55	-1,83
2046	0,56	-0,79	-0,49	-0,92
2047	-0,39	-0,81	-0,55	-0,79
2048	-0,59	-0,39	1,07	-1,34
2049	0,48	-0,97	-0,37	-0,25
2050	-1,51	-0,41	0,39	-1,41
2051	0,79	-0,30	-0,97	-1,76
2052	-1,82	-1,81	-1,96	-1,83
2053	-2,07	0,00	-0,87	-1,83
2054	0,59	0,00	-0,85	-1,83
2055	0,64	0,25	0,38	1,06
2056	-3,09	-0,24	-0,93	-0,69
2057	-0,71	0,86	0,39	0,60
2058	-1,58	-0,06	0,57	-0,85
2059	-1,53	0,00	-3,44	-1,83
2060	-1,10	-0,79	-0,79	-0,92
2061	-0,23	0,00	-2,57	-1,83
2062	-0,09	0,00	-2,75	-1,83
2063	1,83	1,45	-0,01	2,34
2064	-4,28	-0,39	-0,99	-1,05
2065	-0,48	0,00	-2,10	-1,83
2066	-1,06	2,82	1,24	3,02
2067	-0,07	0,57	-0,26	-0,47
2068	1,34	0,67	0,95	0,74
2069	-1,11	0,14	0,23	2,49
2070	-0,82	-1,15	-1,30	-0,32
2071	-1,89	0,00	-1,58	-1,67
2072	-0,48	0,10	0,31	0,08
2073	-0,65	1,45	1,29	0,77
2074	-2,54	-0,54	-1,68	-1,83
2075	-1,46	0,00	-1,94	-1,83
2076	1,78	0,43	-1,49	-0,23
2077	0,24	0,00	-1,11	-1,11
2078	-2,07	2,30	-0,03	1,76
2079	-1,48	0,00	0,00	-1,83
2080	-2,97	0,75	-1,97	-1,57
2081	-3,97	0,49	0,06	-0,15
2082	0,70	-1,00	-2,45	-1,24
2083	-1,38	0,00	0,00	-1,83
2084	-0,51	-1,09	-1,94	-1,57
2085	-2,87	-0,18	-2,02	-0,82
2086	-3,66	0,00	-1,18	-1,83
2087	-2,22	-0,20	-0,17	-1,83
2088	-2,28	-0,12	-0,22	-0,52
2089	0,18	0,00	-2,80	-1,83
2090	-2,66	-0,95	-2,54	-0,44
2091	-2,82	0,00	-1,90	0,06
2092	-2,42	-0,45	-0,09	-0,17
2093	-4,83	0,00	-2,51	-1,83
2094	-2,96	0,15	-0,42	-0,48
2095	-1,75	0,00	-1,85	-0,92
2096	-0,51	-1,44	-0,98	-1,83
2097	-1,48	0,73	0,67	0,79
2098	0,31	0,26	-0,38	0,17
2099	-2,85	-0,01	-1,06	-0,33
2100	-3,41	0,00	-2,75	-1,83

SPI 3 - August (summer) (RCP 8.5)

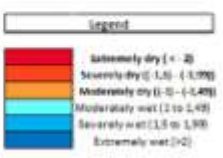

Table A XXII. 3 – November – Tables displaying model data values (RCP 8.5)

	GP1 rcp85	GP7 rcp85	GP8 rcp85	GP13 rcp85
1971	-0,03	-0,76	-0,29	-0,21
1972	-1,89	-0,50	-1,23	-1,00
1973	0,67	0,19	0,19	-0,13
1974	-0,57	-0,73	-0,76	-0,78
1975	1,37	1,44	0,99	1,64
1976	1,35	-0,10	0,35	0,25
1977	0,03	-1,12	-0,76	-0,28
1978	1,83	0,70	1,69	0,73
1979	0,06	1,65	1,46	1,22
1980	2,31	1,29	1,58	1,54
1981	0,04	1,75	0,41	1,14
1982	-1,13	0,20	-1,05	-0,15
1983	0,25	-1,02	0,37	-0,55
1984	-0,84	-0,16	0,00	-0,48
1985	-0,09	-1,37	-0,38	-1,36
1986	-1,74	-1,04	-1,82	-1,23
1987	-0,06	-0,54	0,52	-0,66
1988	0,50	0,19	-0,56	-0,13
1989	0,51	-1,05	-0,36	-1,48
1990	0,62	0,01	0,55	0,02
1991	0,05	-0,40	-0,67	1,48
1992	-0,31	0,14	1,16	-0,01
1993	-0,68	-0,32	-1,24	-0,34
1994	-2,99	-2,17	-2,73	-2,13
1995	-0,51	1,20	0,35	0,59
1996	0,13	0,47	0,50	-0,24
1997	-0,32	1,32	-0,07	1,27
1998	0,20	0,31	1,47	0,38
1999	0,72	0,04	0,36	0,63
2000	0,17	0,87	-0,05	1,08
2001	-0,99	-0,70	-0,85	-0,85
2002	-0,03	0,66	1,13	0,65
2003	-0,44	-0,35	1,10	0,22
2004	-2,36	-0,85	-1,71	-2,06
2005	-1,13	-0,59	-0,98	-0,23
2006	-1,50	-0,95	-1,19	-1,35
2007	-0,10	-0,68	-0,47	-0,31
2008	0,75	0,84	1,58	0,39
2009	-2,86	-1,34	-2,34	-1,48
2010	1,50	1,32	1,51	1,50
2011	0,86	0,18	0,86	0,83
2012	-0,42	-0,14	-0,31	-0,35
2013	-1,56	-0,47	-0,98	-0,88
2014	-1,13	-0,52	-1,21	-0,37
2015	-0,09	0,20	0,01	-0,77
2016	-2,84	-0,89	-2,15	-1,49
2017	-0,36	-0,49	-0,95	-0,04
2018	0,18	-0,36	-0,48	-0,88
2019	-0,20	-0,36	1,00	-0,52
2020	0,16	0,26	1,35	0,18
2021	-0,45	1,01	0,41	1,43
2022	0,66	2,51	1,26	2,03
2023	-1,42	-0,81	-0,99	-1,18
2024	0,09	1,56	0,41	0,80
2025	-0,66	0,58	1,03	0,88
2026	-0,66	1,46	0,05	0,05
2027	-0,68	-0,97	-1,05	-0,20
2028	-0,35	2,23	0,53	1,20
2029	0,67	-0,25	-0,05	-0,26
2030	-1,42	1,01	0,25	0,36
2031	-0,05	-0,61	-0,72	-0,28
2032	0,31	-0,37	-0,36	-0,08
2033	0,21	0,58	0,24	0,22

	GP1 rcp85	GP7 rcp85	GP8 rcp85	GP13 rcp85
2034	-1,48	0,32	-1,18	-0,15
2035	-0,40	1,01	0,16	1,23
2036	0,04	0,56	0,22	1,16
2037	-0,18	-0,69	-0,33	-0,53
2038	-0,40	0,39	0,96	0,25
2039	0,67	0,28	0,30	0,96
2040	-0,17	-1,05	-1,19	-0,86
2041	0,50	1,33	0,90	1,11
2042	0,29	0,72	0,73	0,59
2043	-1,82	-1,39	-2,35	-1,78
2044	-2,18	-1,03	-1,87	-1,27
2045	-0,91	-0,54	-1,31	-0,79
2046	1,07	0,63	0,06	1,55
2047	-1,66	-0,38	-0,50	-0,57
2048	-1,76	-0,43	-1,26	-0,22
2049	-1,51	0,41	-0,81	0,24
2050	-0,12	1,25	-0,45	0,55
2051	1,06	-0,24	0,47	0,10
2052	-1,43	-0,48	-1,60	-0,73
2053	-0,90	-0,39	-0,56	-0,26
2054	-1,86	0,38	-1,37	1,02
2055	-1,80	-1,32	-1,64	-1,85
2056	1,17	0,79	0,99	0,98
2057	1,74	0,50	2,09	0,59
2058	-2,86	-1,42	-3,11	-1,04
2059	1,19	0,54	1,55	1,12
2060	-3,23	-0,61	-2,27	-1,24
2061	-1,50	-1,14	-1,74	-1,24
2062	0,78	0,43	0,75	1,14
2063	0,31	1,09	0,09	0,72
2064	-0,61	-0,13	0,15	-0,01
2065	-0,85	0,24	-1,23	-0,26
2066	-0,25	0,51	0,16	0,68
2067	-0,12	0,57	-0,30	0,18
2068	0,00	0,80	0,83	0,97
2069	-0,92	-0,75	-0,30	-0,78
2070	0,59	0,16	-0,11	0,26
2071	0,31	1,40	1,95	0,57
2072	-0,79	-0,83	-2,00	-0,76
2073	0,15	1,24	0,43	1,51
2074	-0,35	-1,20	1,19	-1,67
2075	-0,94	-0,91	-1,06	-1,40
2076	1,11	1,68	1,15	1,71
2077	-2,62	2,39	2,46	2,41
2078	-0,36	1,23	-0,01	1,04
2079	-2,18	0,86	-1,83	-1,19
2080	-1,17	-0,74	-1,05	-0,90
2081	-2,07	-1,54	-1,33	-1,79
2082	-0,99	0,40	-0,15	0,57
2083	0,64	2,16	0,78	2,35
2084	0,87	2,78	2,40	2,96
2085	-1,75	-1,71	-2,25	-1,28
2086	1,67	0,88	1,02	0,48
2087	-1,51	-0,74	-1,81	-0,81
2088	1,09	1,96	0,82	1,98
2089	-1,44	-0,50	-1,07	-0,52
2090	-0,70	1,13	-0,35	1,87
2091	-2,73	-0,93	-1,76	-1,12
2092	-0,71	0,42	-0,28	0,18
2093	-0,49	-0,85	-1,26	-0,18
2094	1,97	1,15	2,04	1,98
2095	-3,77	-1,99	-2,84	-1,40
2096	-0,56	0,42	-0,07	0,76
2097	-1,45	0,07	-1,40	0,09
2098	-0,84	0,11	-0,66	0,41
2099	1,58	1,29	1,38	1,41
2100	-3,37	-0,89	-2,30	-1,63

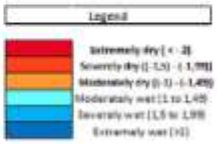

Table A XXIII. SPI 6 – March – Tables displaying model data values (RCP 8.5)

	GP1 rcp85	GP7 rcp85	GP8 rcp85	GP13 rcp85
1971				
1972	-1,47	-0,79	-1,65	-0,54
1973	-1,52	-1,17	-1,17	-0,54
1974	0,77	1,12	1,53	0,76
1975	-0,75	-0,21	-0,27	0,55
1976	1,74	1,05	0,64	1,73
1977	-0,03	-0,56	-0,83	-1,29
1978	1,18	-0,35	0,21	0,88
1979	1,60	1,26	1,70	0,87
1980	-0,73	1,39	0,36	0,57
1981	1,60	0,27	0,93	0,18
1982	0,09	1,99	0,38	1,85
1983	0,52	-0,30	-0,37	-0,08
1984	1,39	-0,19	0,73	0,02
1985	0,81	0,59	0,94	0,49
1986	-0,09	-0,27	0,17	-1,25
1987	-1,13	-1,11	-1,63	-0,46
1988	0,10	0,65	0,95	-0,23
1989	-0,13	-1,62	-1,46	-1,81
1990	0,09	-0,63	-0,25	-1,08
1991	-0,09	-0,49	-0,34	-0,59
1992	-0,10	-0,75	-0,89	0,76
1993	0,21	-0,45	0,79	-0,44
1994	-1,14	0,00	-0,75	-0,44
1995	-1,84	-2,65	-1,76	-2,72
1996	-0,55	0,37	-0,70	-0,12
1997	0,70	1,16	0,85	0,86
1998	-0,88	0,91	-0,19	1,25
1999	0,27	0,64	1,40	0,74
2000	-0,12	0,23	0,49	0,03
2001	0,48	-0,92	-0,46	0,02
2002	-0,09	-0,56	0,33	-0,76
2003	-0,15	-0,57	-0,57	-0,29
2004	-0,71	-1,61	-0,12	-1,07
2005	-0,42	0,31	-0,34	0,09
2006	-0,89	-0,84	-0,75	-0,83
2007	0,92	0,54	0,54	1,01
2008	0,22	-0,14	-0,49	0,17
2009	-0,25	0,86	-0,17	-0,44
2010	-1,81	-0,64	-1,24	-1,80
2011	0,94	1,70	1,37	1,13
2012	1,39	0,79	0,71	0,95
2013	-0,49	-0,57	-0,24	-0,71
2014	-1,98	-1,89	-1,46	-1,73
2015	-2,36	-2,14	-1,93	-1,78
2016	0,06	0,62	-0,04	-0,68
2017	-2,50	-1,67	-1,92	-1,96
2018	0,10	-0,54	-0,37	-0,56
2019	-0,41	-1,50	-0,80	-1,29
2020	0,14	0,52	0,95	0,06
2021	1,43	1,79	1,73	1,37
2022	0,76	1,37	1,22	1,60
2023	1,17	2,48	1,47	1,47
2024	-0,57	-0,77	-0,84	-1,02
2025	-0,16	0,87	-0,08	0,40
2026	-1,94	-1,09	-1,70	-1,14
2027	-1,46	0,95	-0,05	-0,58
2028	-1,90	-1,24	-1,26	-0,85
2029	-1,94	0,70	-1,08	-0,90
2030	0,10	-0,04	0,06	2,04
2031	0,19	1,28	0,96	0,99
2032	-0,11	-1,13	-0,52	-0,35
2033	0,04	-0,83	-0,36	-0,25

	GP1 rcp85	GP7 rcp85	GP8 rcp85	GP13 rcp85
2034	-1,29	-1,39	-0,78	-1,64
2035	-2,07	-0,43	-0,95	-0,94
2036	-1,17	0,20	-0,87	0,23
2037	-0,62	1,10	-0,63	-0,36
2038	-0,65	-0,94	-0,52	0,09
2039	-0,22	-1,30	0,01	-1,48
2040	0,79	1,73	0,94	1,43
2041	-0,79	-1,99	-0,83	-1,90
2042	0,72	1,02	0,98	1,14
2043	-0,91	0,23	-0,44	-0,54
2044	-1,29	1,46	-1,58	-0,99
2045	-3,65	-2,85	-2,72	-2,68
2046	-0,34	-1,54	-1,05	-1,83
2047	0,55	-0,13	-0,43	0,92
2048	-1,36	0,42	0,01	0,25
2049	-0,68	0,05	-0,37	-0,43
2050	0,17	1,67	0,62	1,86
2051	1,36	1,19	0,87	0,94
2052	0,32	-0,26	-0,23	0,28
2053	-1,66	-1,12	-1,42	-0,55
2054	-0,13	0,09	-0,12	-0,23
2055	-0,98	-0,80	-1,66	0,30
2056	-1,48	1,92	-1,87	-2,35
2057	0,86	-0,12	0,17	-0,07
2058	0,16	-0,39	0,44	-0,10
2059	-0,91	0,96	0,57	0,99
2060	0,17	-0,08	0,78	-0,04
2061	-1,87	-0,81	-0,86	-1,61
2062	-0,68	0,28	-0,06	0,16
2063	1,31	1,79	0,82	1,35
2064	-0,97	-0,49	-0,66	-0,83
2065	0,10	0,82	0,59	0,09
2066	0,55	1,39	0,68	1,12
2067	0,97	0,97	0,84	0,92
2068	-0,05	-0,14	-0,58	-0,17
2069	-0,97	0,24	0,21	-0,08
2070	-0,20	1,54	0,67	0,69
2071	-0,02	-0,65	-0,43	-1,13
2072	-0,24	0,88	1,36	-0,31
2073	-2,00	-1,86	-2,51	-1,94
2074	-1,23	-0,28	-0,43	0,08
2075	-0,42	-2,24	-0,06	-2,07
2076	0,54	-1,78	-0,76	-2,20
2077	1,82	1,55	1,45	2,22
2078	-3,42	-3,00	-2,80	-2,63
2079	-1,49	-0,29	-0,77	-0,83
2080	-3,73	-1,93	-2,33	-2,96
2081	-0,90	-0,94	-0,96	-0,17
2082	-1,14	-2,08	-1,24	-2,30
2083	-2,35	-1,08	-1,51	-1,11
2084	0,53	0,73	-0,01	1,48
2085	0,36	1,32	0,98	1,27
2086	-2,67	-3,37	-2,87	-2,83
2087	-3,04	-0,45	-1,74	-1,16
2088	-3,40	-3,40	-3,28	-3,58
2089	0,58	1,47	0,36	1,30
2090	-1,85	-0,72	-1,42	-1,38
2091	-1,12	-0,76	-1,33	0,30
2092	-1,15	0,79	0,13	0,00
2093	-2,31	-1,45	-1,61	-2,18
2094	-0,81	-1,65	-1,00	-0,87
2095	1,19	0,17	1,32	1,24
2096	-2,75	-2,52	-1,91	-2,03
2097	-0,44	-0,39	0,65	-0,18
2098	0,64	1,00	0,58	1,10
2099	-2,10	-1,45	-1,98	-1,03
2100	-0,23	-0,42	-0,25	-0,31

SPI 6 – March (wet season) (RCP 8.5)

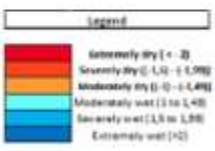

Table A XXIV. SPI 6 – October – Tables displaying model data values (RCP 8.5)

	GP1 rcp85	GP7 rcp85	GP8 rcp85	GP13 rcp85
1971	-0,47	-0,24	-0,65	0,29
1972	-0,09	0,53	0,12	0,04
1973	1,17	0,86	0,31	0,49
1974	-0,05	-0,08	-0,58	-0,31
1975	0,82	0,70	0,04	0,78
1976	1,17	0,57	0,77	0,23
1977	0,61	-0,04	-0,29	0,53
1978	-0,68	-0,21	-0,37	-0,39
1979	0,77	1,49	1,78	1,70
1980	0,81	1,49	0,69	1,58
1981	-0,41	-0,57	-0,11	-0,04
1982	0,18	0,84	-0,05	0,34
1983	-0,72	-1,32	-0,71	-1,28
1984	-1,74	-1,27	-1,73	-1,32
1985	1,38	-0,96	0,97	-0,18
1986	-0,55	-1,09	-0,48	-0,80
1987	-0,76	0,34	-0,18	-0,17
1988	0,01	-0,53	-0,55	-0,48
1989	1,58	0,39	1,37	0,10
1990	0,34	0,62	0,39	0,68
1991	-1,27	-0,86	-1,42	-0,47
1992	-0,58	-0,45	-0,32	-0,18
1993	-0,26	-0,53	-0,25	-0,84
1994	-1,65	-2,54	-1,60	-2,34
1995	0,16	-0,16	0,10	-0,05
1996	-0,74	0,72	0,79	-0,53
1997	-0,75	-0,23	-0,65	-0,25
1998	2,41	2,31	2,87	2,52
1999	-0,06	1,07	0,74	1,46
2000	-0,18	-0,57	-0,67	-0,57
2001	0,05	-0,27	0,01	-0,18
2002	0,28	0,59	1,16	0,76
2003	0,27	0,60	1,51	0,85
2004	-1,04	-0,91	-0,06	-0,77
2005	-0,07	-0,10	0,06	0,10
2006	-0,77	-1,21	-0,69	-1,12
2007	-0,49	-0,12	-0,63	-0,35
2008	0,29	0,42	0,85	0,07
2009	-0,09	0,76	-0,36	0,38
2010	0,30	0,93	0,48	1,03
2011	0,20	1,47	0,87	0,66
2012	-1,45	-1,21	-1,05	-0,48
2013	-0,63	0,20	-0,17	-0,65
2014	-0,10	-0,02	-0,81	0,68
2015	-0,16	0,59	0,51	-0,29
2016	-0,47	-0,94	-0,10	-0,44
2017	-1,41	-0,50	-1,38	-0,60
2018	-0,15	-1,24	-0,58	-1,25
2019	-0,56	-0,61	-0,56	-0,57
2020	0,42	-0,22	1,02	0,34
2021	-0,06	-1,22	-0,34	-0,78
2022	-1,39	-1,23	-0,53	-0,59
2023	-0,68	0,32	-0,51	-0,12
2024	0,20	1,34	0,18	0,81
2025	0,50	1,28	1,31	1,63
2026	0,64	0,71	0,52	0,26
2027	0,71	0,44	0,66	1,07
2028	0,47	1,28	-0,18	1,45
2029	0,22	-1,32	-0,64	-0,92
2030	-1,05	-0,25	-0,95	-0,05
2031	-1,30	-1,04	-1,49	-0,96
2032	-0,44	-0,12	-0,56	-0,12
2033	1,08	1,16	1,15	1,14

	GP1 rcp85	GP7 rcp85	GP8 rcp85	GP13 rcp85
2034	-0,76	-1,74	-1,21	-0,82
2035	-0,31	1,17	0,31	1,16
2036	-1,30	-1,42	-1,25	-1,37
2037	0,43	-1,41	-0,39	-1,21
2038	-0,98	-0,39	-0,85	-1,51
2039	0,37	-0,13	-0,49	0,81
2040	-0,43	-0,10	-1,63	-0,15
2041	-0,03	0,98	-0,15	0,53
2042	0,54	-0,07	0,91	0,11
2043	-1,46	-0,58	-1,86	-1,16
2044	-2,43	-1,96	-2,90	-1,62
2045	-1,76	-1,47	-2,55	-1,35
2046	0,85	0,79	0,35	1,71
2047	-1,31	-0,99	-1,63	-0,41
2048	-2,47	-2,28	-2,89	-2,36
2049	-0,44	-1,96	-0,93	-0,96
2050	0,05	1,27	-0,18	0,66
2051	0,86	0,06	0,38	0,50
2052	-1,30	-1,03	-2,21	-1,16
2053	0,10	0,64	0,05	0,83
2054	-0,12	1,38	0,07	2,00
2055	0,59	1,45	0,78	1,44
2056	-0,17	-1,14	-0,42	-1,22
2057	0,81	0,75	0,97	0,20
2058	-2,87	-1,78	-1,89	-1,75
2059	0,65	-0,68	0,49	0,13
2060	-2,00	-0,63	-1,88	-1,08
2061	-1,82	-1,46	-2,52	-1,18
2062	0,96	0,40	0,56	1,49
2063	0,76	2,05	0,42	1,48
2064	-1,89	-2,05	-1,27	-2,41
2065	-1,69	-0,52	-2,06	-0,51
2066	-0,72	0,23	-0,61	0,00
2067	0,00	-0,45	-0,52	-0,09
2068	0,14	0,74	0,60	1,13
2069	0,19	-0,14	0,28	0,61
2070	-0,31	-0,16	-0,86	0,56
2071	-0,35	-0,24	-0,59	-1,10
2072	-1,39	-1,92	-1,56	-2,13
2073	0,03	0,26	0,20	0,28
2074	-0,27	-1,55	0,82	-1,50
2075	-0,71	-0,85	-0,76	-0,85
2076	1,36	1,75	0,84	1,73
2077	-1,88	-1,98	-1,87	-2,06
2078	-0,30	1,23	0,13	0,33
2079	-1,87	-0,70	-2,48	-1,11
2080	-1,89	-1,40	-1,70	-1,58
2081	-1,16	-1,24	-0,70	-2,19
2082	-0,28	0,45	0,00	1,04
2083	1,32	1,69	-0,83	0,96
2084	-0,31	1,31	-0,47	1,40
2085	-2,11	-1,44	-1,84	-1,70
2086	-1,65	0,13	-1,55	0,09
2087	-0,55	-0,58	-1,58	-0,64
2088	0,87	2,53	0,86	1,92
2089	-1,15	-0,46	-1,83	-0,39
2090	-2,49	-1,89	-4,52	-1,88
2091	-1,74	-1,29	-1,57	-1,32
2092	-1,22	-1,55	-1,28	-1,09
2093	-1,80	-1,43	-2,77	-1,64
2094	1,41	0,84	1,38	2,25
2095	-3,96	-2,23	-3,06	-1,60
2096	-0,73	-0,81	-0,45	-1,35
2097	-1,52	-0,38	-1,02	-0,29
2098	-0,07	0,98	-0,14	1,12
2099	-0,04	0,67	-0,45	0,82
2100	-3,45	-3,07	-4,27	-3,44

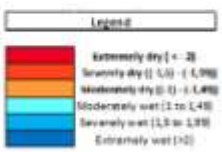

Table A XXV. SPI 12 – Tables displaying model data values (RCP 8.5)

	GP1 rcp85	GP7 rcp85	GP8 rcp85	GP13 rcp85
1971	-0,46	-0,63	-0,95	-0,45
1972	-2,35	-1,38	-2,09	-1,02
1973	0,64	-0,07	0,40	0,16
1974	0,11	1,76	1,24	1,91
1975	1,18	0,97	0,56	1,41
1976	0,69	0,01	-0,21	0,48
1977	-0,09	-0,28	-0,66	-0,37
1978	1,50	1,01	1,59	0,95
1979	-0,20	0,66	0,64	0,63
1980	1,22	1,01	0,80	0,80
1981	-0,68	0,88	-0,45	0,29
1982	0,33	0,89	-0,21	0,86
1983	1,17	-0,93	0,41	-0,72
1984	1,01	0,25	0,26	0,57
1985	1,11	0,18	0,97	-0,13
1986	-2,03	-0,94	-1,05	-0,77
1987	-0,07	0,84	0,30	-0,15
1988	0,36	-0,66	-0,01	-0,93
1989	0,30	-1,51	-0,06	-1,88
1990	0,44	-0,01	0,38	0,36
1991	0,15	-0,40	-0,61	0,82
1992	-0,97	-1,03	-0,10	-1,13
1993	-0,25	0,44	-0,09	0,21
1994	-2,02	-2,23	-2,40	-2,07
1995	-1,35	-0,83	-1,27	-1,57
1996	0,18	-0,40	0,64	-0,66
1997	-0,34	1,61	0,00	1,47
1998	1,47	1,18	2,57	1,63
1999	-0,50	0,63	0,47	0,56
2000	-0,55	-0,83	-1,15	-0,50
2001	0,40	-1,20	0,05	-0,72
2002	0,38	0,14	0,98	0,27
2003	-0,32	-1,61	0,27	-0,29
2004	-0,52	-0,94	-0,43	-0,83
2005	-0,40	0,32	-0,42	0,57
2006	0,22	-0,89	-0,52	0,01
2007	1,09	0,12	0,56	0,28
2008	-0,58	0,91	0,01	0,25
2009	0,08	1,08	0,26	-0,12
2010	0,32	1,27	0,71	0,21
2011	1,17	1,69	1,53	1,36
2012	-0,06	-0,71	-1,02	-0,40
2013	-1,58	-1,22	-1,10	-1,26
2014	-1,18	-0,91	-1,22	-0,49
2015	-1,01	0,27	-0,22	-0,89
2016	-1,53	-1,68	-1,63	-2,01
2017	-0,96	-1,54	-1,95	-0,70
2018	-0,81	-1,48	-1,21	-1,79
2019	0,27	-0,25	0,94	-0,57
2020	1,00	1,11	1,85	1,05
2021	1,10	0,81	0,91	0,90
2022	1,14	3,47	2,28	2,58
2023	-0,16	0,38	0,12	-0,40
2024	0,87	1,34	0,32	1,14
2025	-1,38	-1,11	-0,45	-0,72
2026	-0,08	1,55	0,68	-0,20
2027	-0,11	-1,25	-0,28	-0,03
2028	-2,87	0,88	-1,75	-0,49
2029	-0,44	-1,93	-1,76	-1,39
2030	-1,02	0,70	0,08	1,54
2031	1,40	0,38	0,60	0,92
2032	-1,12	-1,42	-1,39	-0,65
2033	0,54	-0,03	0,54	0,15

	GP1 rcp85	GP7 rcp85	GP8 rcp85	GP13 rcp85
2034	-2,10	-1,30	-2,18	-1,40
2035	-0,90	0,34	-0,51	0,09
2036	-1,04	0,64	-1,16	-0,03
2037	-0,97	2,01	-0,93	-1,76
2038	-1,08	0,94	-0,73	-0,14
2039	-0,49	1,21	-1,09	-0,37
2040	0,53	1,48	0,20	0,57
2041	-0,26	0,01	0,01	0,05
2042	0,34	0,56	0,30	0,29
2043	-2,22	-1,92	-2,95	-1,46
2044	-2,68	-2,48	-3,16	-1,59
2045	-3,43	-4,04	-4,49	-3,93
2046	0,72	0,01	0,01	0,73
2047	-1,66	0,15	-1,18	-0,06
2048	-1,31	-1,68	-1,56	-1,01
2049	-0,29	1,06	0,12	0,41
2050	-0,04	1,07	0,22	0,63
2051	0,93	0,64	0,38	0,46
2052	-1,86	-1,77	-2,33	-0,89
2053	-0,95	-1,06	-1,21	0,05
2054	-0,40	0,72	-0,66	0,71
2055	-0,85	-1,27	-1,54	-0,56
2056	0,03	0,82	-0,91	-0,63
2057	0,19	-0,78	0,40	-0,73
2058	-1,74	-0,35	-0,44	0,05
2059	0,11	0,27	0,72	0,56
2060	-3,85	-2,15	-3,55	-2,86
2061	-1,97	-1,19	-1,45	-1,25
2062	0,40	1,85	1,07	1,60
2063	1,02	2,13	0,45	0,77
2064	-1,28	-0,61	-0,74	-0,92
2065	-0,62	0,55	-0,98	-0,41
2066	0,79	2,28	1,27	1,87
2067	-0,43	-0,14	-1,62	-0,33
2068	0,37	1,30	0,94	1,15
2069	-1,27	-1,09	-1,08	-0,84
2070	-0,05	0,66	0,42	0,01
2071	-1,61	0,33	-0,16	-1,30
2072	-1,15	-0,63	-1,53	-1,07
2073	-1,59	-0,27	-0,91	-0,21
2074	-1,84	-1,22	-0,60	-3,14
2075	-1,05	-2,46	-1,74	-2,26
2076	1,71	1,38	1,67	2,21
2077	-1,76	-0,98	-1,51	-0,79
2078	-1,80	-0,04	-1,26	-0,24
2079	-1,26	-2,22	-3,09	-2,80
2080	-2,52	-2,33	-2,69	-1,86
2081	-2,73	-2,83	-2,64	-2,34
2082	-1,00	-0,02	-0,35	-0,29
2083	-1,54	-0,26	-2,25	0,25
2084	0,45	1,74	1,20	1,62
2085	-3,77	-3,83	-3,35	-2,98
2086	-1,43	-1,46	-1,32	-1,52
2087	-3,62	-3,37	-3,89	-3,43
2088	-1,22	0,56	-1,65	0,01
2089	-1,97	-2,14	-2,80	-1,75
2090	-1,61	0,14	-1,89	0,44
2091	-2,71	-1,26	-2,28	-1,54
2092	-1,23	0,47	-0,23	-0,34
2093	-2,96	-1,21	-3,91	-2,81
2094	0,47	0,08	0,91	0,85
2095	-4,29	-3,64	-4,53	-2,88
2096	-1,34	-1,24	-0,85	-1,41
2097	-1,04	1,01	0,36	0,99
2098	-0,30	0,12	-0,55	0,33
2099	-0,83	-0,84	-1,35	-0,90
2100	-4,93	-3,30	-4,08	-3,66

SPI 12 – Inter-Annual (RCP 8.5)